NASA

Technical Memorandum 80642

(E80-10087) [EARTH SURVEY APPLICATIONS DIVISION: RESEARCH LEADING TO THE EFFECTIVE USE OF SPACE TECHNOLOGY IN APPLICATIONS RELATING TO THE EARTH'S SURFACE AND INTERIOR] Annual Report, 1979 (NASA) 322 p G3/43

N80-20723
THRU
N80-20785
Unclas
00087

Earth Survey Applications Division Research Report - 1979

Edited by Lloyd Carpenter

JANUARY 1980

National Aeronautics and
Space Administration

Goddard Space Flight Center
Greenbelt, Maryland 20771

EARTH SURVEY
APPLICATIONS DIVISION
RESEARCH REPORT - 1979

EDITED BY

LLOYD CARPENTER

JANUARY 1980

GODDARD SPACE FLIGHT CENTER
GREENBELT, MARYLAND

CONTENTS

EARTH SURVEY APPLICATIONS DIVISION

CODE 920

LIST OF RESEARCHERS

Louis S. Walter, Chief

Ph.D., 1960, Penn. State U.
Geochemistry

(Betty Wilson and Robin Mohr, Secretaries)

GEODYNAMICS BRANCH

Code 921

David Smith, Branch Head
Ph.D., 1966, University of London
Mathematics

(Beatrice Boccucci, Secretary)

Lloyd Carpenter, *B.S., 1951, U. of Missouri, Mathematics*
Robert Cheney, *M.S., 1974, U. of Rhode Island, Oceanography*
Stephen Cohen, *Ph.D., 1973, U. of Maryland, Physics*
Theodore Felsentreger, *M.A., 1961, U. of Maryland, Mathematics*
Michael Graber, *Ph.D., 1970, Princeton U., Physics*
Werner Kahn, *M.S., 1955, U. of Illinois, Mathematics*
Ronald Kolenkiewicz, *M.S., 1965, Catholic U., Space Science and Applied Physics*
Francis Lerch, *M.S., 1950, U. of Delaware, Mathematics*
Han-Shou Liu, *Ph.D., 1963, Cornell U., Physics*
James Marsh, *M.S., 1963, West Virginia U., Physics*
David McAdoo, *Ph.D., 1976, Cornell U., Geophysics*
Patrick McClain, *M.S., 1959, Howard U., Mathematics*
Barbara Putney, *B.S., 1960, Brooklyn College, Mathematics*
David Rubincam, *Ph.D., 1973, U. of Maryland, Physics*
Braulio Sanchez, *Ph.D., 1975, U. of Texas, Aerospace Engineering*
Frederick Schamann, *B.S., 1967, City College of New York, Mathematics*
George Wyatt, *B.S., 1962, North Carolina State College, Mathematics*

GEOPHYSICS BRANCH

Code 922

Gilbert Mead, Branch Head
Ph.D., 1962, U. of California, Berkeley
Physics

(Barbara Lueders, Secretary)

Richard J. Allenby, *Ph.D., 1952, U. of Toronto, Geophysics*
Herbert Frey, *Ph.D., 1977, U. of Maryland, Astronomy*
Robert A. Langel, *Ph.D., 1973, U. of Maryland, Physics*
Paul D. Lowman, Jr., *Ph.D., 1963, U. of Colorado, Geology*
Chopo Ma, *Ph.D., 1978, U. of Maryland, Physics*
James Ryan, *M.S., 1968, George Washington U., Mathematics*
Patrick T. Taylor, *Ph.D., 1965, Stanford U., Geophysics*
Herman H. Thomas, *Ph.D., 1973, U. of Pennsylvania, Geochemistry*
William J. Webster, Jr., *Ph.D., 1970, Case Western Reserve U., Astronomy*

EARTH RESOURCES BRANCH

Code 923

Charles Schnetzler, Branch Head
Ph.D., 1962, MIT, Geochemistry

(Bobbie Wilmer, Secretary)

John Barker, *Ph.D., 1967, Chicago U., Nuclear Chemistry*
Robert Belcher, *Ph.D., 1979, U. of Texas, Geology*
Emmett Chappelle, *M.S., 1954, U. of Washington, Biochemistry*
Jerrold Christenson, *M.S., 1975, San Diego State U., Geography (resigned 5/79)*
Donald Deering, *Ph.D., 1978, Texas A & M U., Range Sciences*
Michael Forman, *M.S., 1965, Lowell Tech. Inst., Physics*
Brent Holben, *M.S., 1975, Colorado State U., Agricultural Sciences*
James Irons, *M.S., 1978, Penn State U., Agronomy*
George Jacobs, *Ph.D., 1955, U. of Mississippi, Biology (retired 9/79)*
Daniel Kimes, *Ph.D., 1979, Colorado State U., Natural Resources*
Charles W. Kouns, *M.S., 1966, George Washington U., Geology*

Mark Labovitz, *Ph.D., 1978, Penn State U., Geostatistics*
Brian Markham, *M.S., 1978, Cornell U., Civil Engineering*
Edward Masuoka, *M.S., 1978, U. of Tennessee, Geology*
Kenneth Meehan, *Ph.D., 1978, Idaho U., Geology*
Ross Nelson, *M.S., 1979, Purdue U., Forestry*
John Schutt, *Ph.D., 1954, Rochester U., Physical Chemistry*
Alicia Watson Siegrist, *M.S., 1977, Penn State U., Geology*
David Toll, *M.S., 1978, Colorado State U., Natural Resources*
Compton J. Tucker, *Ph.D., 1975, Colorado State U., Remote Sensing*
Jean Welker, *B.A., 1975, Hofstra College, Physics (transferred 2/79)*
Steven Wharton, *M.S., 1979, Penn State U., Forestry/Computer Sciences*
Darrell Williams, *M.S., 1975, Penn State U., Forestry*
Frank Wood, *Technician*

Postdoctoral Associates

Christopher O. Justice, *Ph.D., 1978, U. of Reading, England, Geography*
John R.G. Townshend, *Ph.D., 1974, U. of London, England, Geography*

INTRODUCTION

by

Louis S. Walter

This is the second Annual Research Report of the staff of the Earth Survey Applications Division. The material was written and compiled in December 1979 and represents the status of our work as of that date. The report emphasizes accomplishments rather than plans; however, there is some discussion of a few developing efforts. In this, the second Report, specific authors have been identified with each section. Their contributions have been coordinated by nine section (discipline) editors who are also identified in the corresponding chapter introduction. It is expected that future Annual Research Reports will be published at the beginning of future calendar years. Critical or constructive comments and inquiries may be addressed to the individual authors, section editors, or to the Chief, Earth Survey Applications Division.

Acknowledgments

The dedication of the Division's research staff and the section editors was critical to the timely production of this Report. An all-out effort of the secretarial staff (which was short-handed at the time of preparation of the report) was also necessary. The greatest individual effort, however, was contributed by Lloyd Carpenter who performed the complex job of coordinator and editor with tact, dedication, and with conscientious hard work.

CHAPTER 1

GEOLOGY

edited by

Kenneth T. Meehan

OVERVIEW

The overall objective of the geology research effort within the Earth Survey Applications Division is to develop and evaluate methods for the application of satellite data to geologic problems, and to understand the relationships between satellite and pertinent ground data. In conforming with this objective and the mission and research goals of NASA, substantial effort is being applied to the development of new digital image processing and statistical analysis techniques. These techniques are being designed to analyze separately and in combination satellite, aircraft, and ground derived data. Information obtained by these techniques will assist in design and improvement of future orbital sensor systems capable of providing optimal data for geologic, geobotanical, and geophysical studies.

To meet the goals and directions of NASA within the framework of non-renewable resources, research by the geology group at GSFC has taken two primary directions. The first is a geobotanical research effort that will investigate the utility of remote sensing of geobotanical indicators for mineral and petroleum exploration. Current research in this effort is divided into laboratory and field studies. Laboratory work will investigate the relationships between plant morphology, composition and reflectance spectra, and underlying or growing substrate. This work is being carried out primarily on contract to Barringer Research Inc. and Imperial College in London, England. Field work will be carried out locally in a mineralized study area in Mineral, Virginia. Here, botanical sampling and data analaysis procedures will be developed to determine the distinquishability of anomalous areas within a continuous forest canopy and low relief terrane. Ultimately, guidelines for effective sensors to be used in geobotanical exploration will be developed.

The second direction is a geologic/geophysical resource assessment effort that is investigating both the utility of geopotential data in development of crustal models, and the applicability of combined satellite and ground data to the analaysis and understanding of major tectonic features and their related economic resources. This effort focuses on the Rio Grande rift, a geologic feature extending south from central Colorado through New Mexico into west Texas northern Mexico. Work in this area will attempt to develop modeling and multisource data analysis techniques that enable better estimation of crustal composition and structure in three dimensions.

A. GEOBOTANICAL EXPLORATION

by

M. Labovitz, E. Masuoka, A. Siegrist

OBJECTIVES

The objectives of our geobotanical research are to investigate the utility of remote sensing of geobotanical indicators for mineral and petroleum exploration and to develop new remote sensing geobotanical exploration techniques, including recommendations for future satellite systems having a geobotanical mission.

BACKGROUND

The use of the type or vigor of vegetation as a guide to subsurface mineral or petroleum deposits has been an accepted exploration tool for centuries. However, the possibility of using remote-sensing techniques to detect the changes in vegetation caused by nearby mineralization has just recently received attention. Satellite remote sensing enables investigators to analyze large segments of the Earth's surface repeatedly at different seasons and under different conditions, and an increasing awareness of potential mineral and energy shortages has stimulated the development of new exploration techniques. Since over two-thirds of the Earth's land surface is covered with vegetation, the need to establish a research program for the development and evaluation of geobotanical exploration techniques is essential.

During C.Y. 1979 the long range research effort in geobotanical exploration begun in 1978, proceeded. The effort during 1979 was designed to: (1) provide laboratory controlled experiments to test the effects of high concentrations of trace metals upon the physiology and optical properties of plants. These experiments are designed to provide the underlying theory and direction for field studies; (2) foster communications between researchers in the field, by sponsoring workshops which will hopefully lead to cooperative and complementary efforts; and (3) design and initiate a pilot field study in Mineral, VA to demonstrate the utility of remotely sensed data in geobotanical exploration.

RECENT ACCOMPLISHMENTS

Laboratory studies are being conducted by Drs J. Barber and D. Horler, Department of Botany, Imperial College, London. This work is funded as an AN with Barringer Researcher Associates of Golden, CO. Preliminary research reports received from Barber and Horler, demonstrate in the laboratory the potential utility of Thematic Mapper, bands 4, 5, and 6 (.89 μm, 1.66 μm, and 2.22 μm) for the detection of metal stressed vegetation. This work has been carried out in selected field sites and their preliminary results are in agreement with laboratory studies.

The 2nd Annual GSFC Geobotanical meeting was held in May which brought together researchers who were or had been engaged in geobotanical research. There were 36 participants representing industry, academia and government. The objective of this meeting was to continue communications between researchers in the field, to provide a forum for presenting current research in the field of geobotany and to solicit from the participants their views on significant directions for future research including the requirements for future sensors.

As part of the overall geobotanical research plan, a field site study was designed and initiated by Goddard personnel. The field site is in the Mineral, VA Sulfide District. The area was chosen because it possesses several very desireable properties: (1) The district has been previously mined for its economic concentrations of Pb, Zn, Cu, and Fe (Young, 1956). (2) Previous work has demonstrated that these trace metals plus Cd are present in the vegetation in anomalous concentrations (Leavitt, 1971). (3) The area has low relief. Arden and Westra (1977), demonstrated that topographic effects complicate the detection of mineral stressed vegetation by remote sensing techniques. (4) The geology of the area is known. Thus, we avoid much of the expense of collecting this data. (5) The test site has a complete canopy cover. (6) It is accessible year round and is only 110 miles from GSFC. Thus, it is an ideal site for testing hypotheses about the relationship between remote sensing and changes in vegetation caused in mineralization.

Initial collection of vegetation samples for geochemical analysis of trace metal concentrations has been completed for this site. This will provide the researchers with information about the specific distribution of trace metal concentrations within the vegetation.

Additional ground truth data over the area including soils, geophysics and geochemistry is presently being compiled.

SIGNIFICANCE

Directed by experiments performed in the laboratory and in natural sites, the geobotanical research program is identifying portions of the spectrum where mineralization or metal stress in the vegetation can be observed. Then through field studies, the information obtained in the laboratory is being tested under the more complex situations observed in nature. The techniques developed from this research may provide a means of remotely detecting mineralization within vast tracts of heavily vegetated areas not readily studied by other means.

FUTURE EMPHASIS

Work in the laboratory will be continued, (funded by GSFC RTOP 923-677-42-02) in order to refine the results produced during C.Y. 1979. The researchers will concentrate on reflectance in the infrared and emissivity in the thermal infrared portions of the electromagnetic spectrum.

Field studies in Mineral, VA will continue to determine the spectral and temporal parameters necessary to perform geobotanical exploration with remote sensing methods.

A geobotanical steering panel, composed of active researchers from private industry, government agencies and universities, will be established to provide guidance for NASA's geobotanical research program.

The geographic information system (GIS) at GSFC will be used to input geologic, geophysical and remote sensing data into the SACC computer and to create a spatially referenced multivariable data set for the Mineral, VA test site. Statistical analyses will be performed on this data set by the SAS and BMD statistical packages and the results of these analyses will be displayed as GIS produced maps and figures, which highlight the important relationships between different ground based data types and the areas classified as mineralized from the remote sensing data.

REFERENCES AND PUBLICATIONS

Arden, D.D. Jr., and Raymon N. Westra. 1977. Geological Vegetative Relationships (Botanical). Final Report on NASA Contract NAS8-30884.

Barber J. and D.N.H. Horler. 1979. Fundamental relationships between plant spectra and geobotanical stress phenomena. Six months report on NASA contract NAS5-25738.

Leavitt, S.W. 1977. Soil-Plant Relationships of Nutrient and Non-Nutrient Metals in Louisa Co., Virginia. unpublished M.S. thesis. University of Virginia.

Young, R.S. 1956. Sulfides in Virginia. Virginia, Minerals. Vol. 2, No. 1. p. 1-7.

B. GEOLOGICAL/GEOPHYSICAL RESOURCE ASSESSMENT

by

R.C. Belcher, V. Gornitz, E.J. Masuoka and K.T. Meehan

OBJECTIVES

The objectives of the geological/geophysical resource assessment are the following: (1) to determine and understand the utility of geopotential data in development of crustal models; (2) to investigate the applicability of combined satellite and ground data to the analysis and understanding of major tectonic features and their related economic resources; (3) to determine those data types that are most capable of explaining geological relationships between mineralization, volcanism, and fracture/strain patterns, and understand why these data types explain the relationships; (4) to develop processing and interpretive techniques for modeling crustal features with highly diverse data types; (5) to evaluate and understand the performance of satellite data in analyses of major geologic features; and (6) to determine characteristics of future sensor systems that will provide optimal geologic/geophysical information for the analyses of major geologic features.

BACKGROUND

Recent quantitative analyses of localized and geologically simple areas have demonstrated that lithologic classification results utilizing combined satellite (spectral) and ground data are superior to classification results from satellite spectral data alone. These results suggest that similar analyses of larger geologic features will produce optimum results if both satellite and ground data are analyzed. However, this study will thematically classify by tectonic regime rather than lithology.

The first part of this effort consists of compiling, modifying, and testing (prediction accuracy vs known geology) numerous multivariate quantitative techniques on an area that contains abundant ground truth and that is being studied by numerous geologists from other organizations. Cause and effect relationships between satellite and ground data are being studied in hopes of decreasing both the dependency on large amounts of ground data and the dimensionality of the requisite data base.

The Rio Grande Rift was the selected test site for the first part of this study because of the large amount of available ground data and because its large areal extent affords an opportunity to perform the following:

1) evaluate the utility of relatively coarse orbital geopotential data to define and model intraplate rift zones.

2) evaluate the large feature with reguard to the fundamentally different types of mineral deposits found along its extent.

3) evaluate the feature in a significant statistical way with abundant data from several different data types.

The rift is a tensional geologic structure extending southward from Colorado through New Mexico into northern Mexico and west Texas, and exhibits unexplained variations in tectonic pattern, volcanism, heat flow, seismicity, and mineralization. These multiple, unexplained problems require an analytic approach using suitable data this is, therefore, multisource. These data and their anticipated usefulness are as follows:

1) lineament patterns used in conjunction with upper crustal lithology (derived through gravity, magnetic and spectral data) to assess multiple tectonic patterns along the rift.

2) crude extrusive/intrusive lithology estimates obtained through spectral (including radar) data, surface geochemistry (stream sediment and bulk rock) and age dates, to delineate the spatial and temporal transition of igneous activity along the rift.

3) heat flow patterns associated with major thermal regimes as indicated through well water samples, and values from the heat flow data base.

4) seismic events correlated with lineament (topographic, aeromagnetic, and gravity) patterns and recognized faults to assess characteristics of tectonically active areas within the rift.

5) mineral deposit types (characterized using USGS Computer Resources Information Bank--CRIB--data) and their spatial/temporal relationship to structural features that relate to genesis of the rift.

This area has been well-studied in the past and is the subject of many present investigations by universities, state and federal surveys, and private companies. Because of this interest, large quantities of data have been compiled that, for the most part, have been qualitatively interpreted. Quantitative interpretations of these data by multivariate analytic techniques of pattern recognition, spatial analysis, and image processing have not been attempted.

After the data set relationships are understood and satisfactory prediction accuracies have been obtained, the procedures and relationships developed during the first part of the study will be applied to areas containing moderate or limited amounts of acquired geologic data. Such areas might include those with limited access due to political, climatic or physiographic reasons. Tenative study areas for the second part are the East African rift and the Baikal rift in southeastern Siberia.

RECENT ACCOMPLISHMENTS

The satellite and ground based data sets that have been acquired or compiled during this first year of the effort are the following: Computer Resource Information Bank (CRIB) of the USGS; ground based digital gravity; lead isotope age dates; radiometric age dates;

Rock Analysis Storage System (RASS) composed of geochemical data from the USGS; heat flow; Water resources Storage System (WATSTORE) composed of water chemistry and temperature from the USGS; seismic events; orbital multispectral data (LANDSAT); digitized lineaments; orbital magnetic data (POGO and MAGSAT); Heat Capacity Mapping Mission Satellite data (HCMM--in process of being acquired) and GEM10B satellite gravity data.

The ground based gravity data set acquired from researchers at USGS-Denver and University of Texas at El Paso has been gridded to a cell size of 15 minutes latitude and longitude. Station elevation, free air gravity, and Bouger gravity for the Rio Grande rift have been plotted (Figs. 1B-1, 1B-2, 1B-3). Interpretation of the Bouger gravity map suggests that the earth's crust north of the Las Cruces, New Mexico-El Paso, Texas area is thicker than that to the south; and that to the north the rift is a shallow crustal feature represented by a linear 20 mgal high, whereas to the south the rift is a deeper crustal feature represented by a linear 30 to 40 mgal low.

The heat flow data set acquired from the USGS has been plotted (Fig. 1B-4). The map shows distinct heat flow highs (greater than 3 heat flow units) in southwestern Colorado (San Juan Mountains), south central Colorado and southwestern New Mexico (Deming-Las Cruces area). The heat flow highs in Colorado are not associated with the rift, whereas the high in New Mexico is associated with an area of shallow crust (approximately 27 km thick), and the juncture of the Rio Grande rift with the Texas Lineament, a major tectonic boundary for the last 600 million years.

Lineaments have been interpreted from Landsat scenes covering the Rio Grande rift and are in the process of being checked for reproductiveness. The preliminary lineament map indicates that there are several narrow zones of lineaments cutting across the rift, and that certain parts of the rift exhibit distinct lineament patterns. One such region is south of the Las Cruces, New Mexico-El Paso, Texas area where a distinct northwest lineament trend parallel to the Texas Lineament predominates; north of this area the northwest trend is absent. Abrupt changes such as these indicate that textural analysis of lineament patterns will identify different tectonic features within the rift area and will clarify the areal extent of the rift structure.

The locations of individual mineral deposits in the CRIB data set have been plotted at the same scale as the previously mentioned data (Fig. 1B-5). Spatial analysis of specific mineral types, and their correlation to lineament trends, heat flow anomalies, and gravity anomalies have just begun.

A thorough literature survey of Tertiary volcanism related to the Rio Grande rift area conducted by Vivian Gornitz (Goddard Institute of Space Studies) determined the following: a) igneous activity clearly preceded rifting throughout the area, b) early volcanism (40-30 mybp) was composed predominantly of calcalkaline andesites, c) a transitional period of volcanism occurred between 30 and 20 mybp that was characterized by explosive silicic ash-flow tuffs and

basaltic andesites, d) a magmatic lull occurred between 20 and 15 mybp, which was followed by basaltic volcanism that lasted into recent times, and e) distinct unexplained geochemical differences exist in comtemporaneous extrusives along the rift. The early and transitional volcanism in west Texas was alkalic whereas comtemporaneous volcanism in New Mexico and Colorado was calcalkalic. During the recent episode of basaltic volcanism both alkalic and tholeiitic basalts erupted in the northern rift while only aklalic basalts erupted in the southern part. For the last 3 to 4 million years, most of the volcanism has not been related to the Rio Grande rift, but to the northeast trending Jemez Lineament which cuts across the rift north of Albuquerque, New Mexico.

A geographic information system (GIS) has been modified and put up in a load module form on our computational facilities. The GIS facilitates the storage, manipulation and display of spatially referenced data. In this study the GIS will be an important tool in the display and statistical analysis of geophysical, geochemical and remote sensing data because of its substantial graphics capability (Fig. 1B-6, 1B-7) and its interactive interfaces with statistical and image processing systems.

Quantitative techniques to be used in conjunction with GIS that have been acquired and modified during the last year basically belong to one of the following types: (1) non-parametric multivariate spatial analytic techniques of nominal and ordinal scale data; (2) parametric multivariate spatial analytic techniques of ratio and interval scale data; and (3) textural analysis techniques for suitable data. The textural analysis algorithms are being modified to accept lineament (as well as spectral) data in order to quantitatively study distinct lineament patterns and their spatial distribution.

In summary, contours of the POGO satellite magnetic data are sharply deflected along the Rio Grande rift in Colorado and northern New Mexico, and show a steep southerly gradient in southwestern New Mexico and west Texas (Fig. 1B-8). Analysis of the gravity data suggests that the rift north of the Las Cruces, New Mexico-El Paso, Texas area is different from that to the south. There is a distinct difference in lineament patterns north and south of this area, and a high heat flow anomaly also occurs in this area of southwestern New Mexico. The "boundary" appears to separate the early and transitional stages of volcanism in New Mexico and Colorado from the contemporaneous but yet distinctly different volcanism of west Texas. Analysis of the CRIB data which has just started, will determine if a "mineralization boundary" also occurs along the same line, and perhaps elsewhere along the rift. The cross-cutting Jemez lineament which has both controlled recent volcanism and apparently limited the southern extent of tholeiitic basalts, is a distinct feature on the lineament map but is not present on the Bouger gravity map.

SIGNIFICANCE

The ever increasing scarcity of natural resources, the continuously escalating costs of exploration, and the political and logistical problems confronting acquisition of ground data for international

exploration, point to the need for a set of analysis procedures that ideally would utilize satellite-derived data and require a minimum of ground data. The development of such analytic procedures would provide an effective low cost method of regional exploration that would identify local areas most likely to be economically important. During the development and testing of these procedures the relationships between satellite and ground data will be thoroughly studied, and requirements for optimum sensor development established.

FUTURE EMPHASIS

The correlations and cause-and-effect relationships between satellite derived and ground data will continue to be thoroughly studied. To achieve an understanding of these relationships future emphasis will be in the following areas:

1) Crustal Modeling--two and three dimensional theoretical modeling of gravity and magnetics will be conducted to determine a crustal configuration for the rift and surrounding area which produces results that closely approximate the measured gravity and magnetic data.

2) Spatial Analysis--ground gravity, heat flow, and lineament patterns will be spatially correlated to determine and understand what geological relationships exist between them. These same data sets will also be spatially correlated with occurrences of mineralization for the same reasons.

3) Lineament Analysis--after dataset reproductiveness has been verified the lineaments will be digitized. Statistically distinct lineament patterns (tectonic units) will be identified through the use of textural analysis, and these will be spatially correlated with known tectonic features. Chronologically distinct lineament sets (Precambrian, Paleozoic, Early Tertiary, etc.) will be identified by use of stress/strain relationships. Each set will be correlated with mineralization and geochemical trends and boundaries to understand what relationships exist between lineament patterns, and mineralization type and volcanism.

4) Trend Analysis--mineralization and geochemical data sets will be statistically analyzed to determine whether geologically meaningful trends or boundaries exist within them.

5) Areal Analysis--several areas of economic mineralization occur within or adjacent to the Rio Grande rift. Those portions of the acquired data sets which lie within each mineralized area will be analyzed to understand the geologic relationships between data types for each area. The results from the different areas will be compared to determine whether or not the relationships between data types vary along the rift, and to understand why.

6) Sensor Characteristics--free air gravity and aeromagnetic data will be gridded to various cell sizes and upward continued to satellite altitudes to determine the relationships between ground resolution and geologically meaningful information.

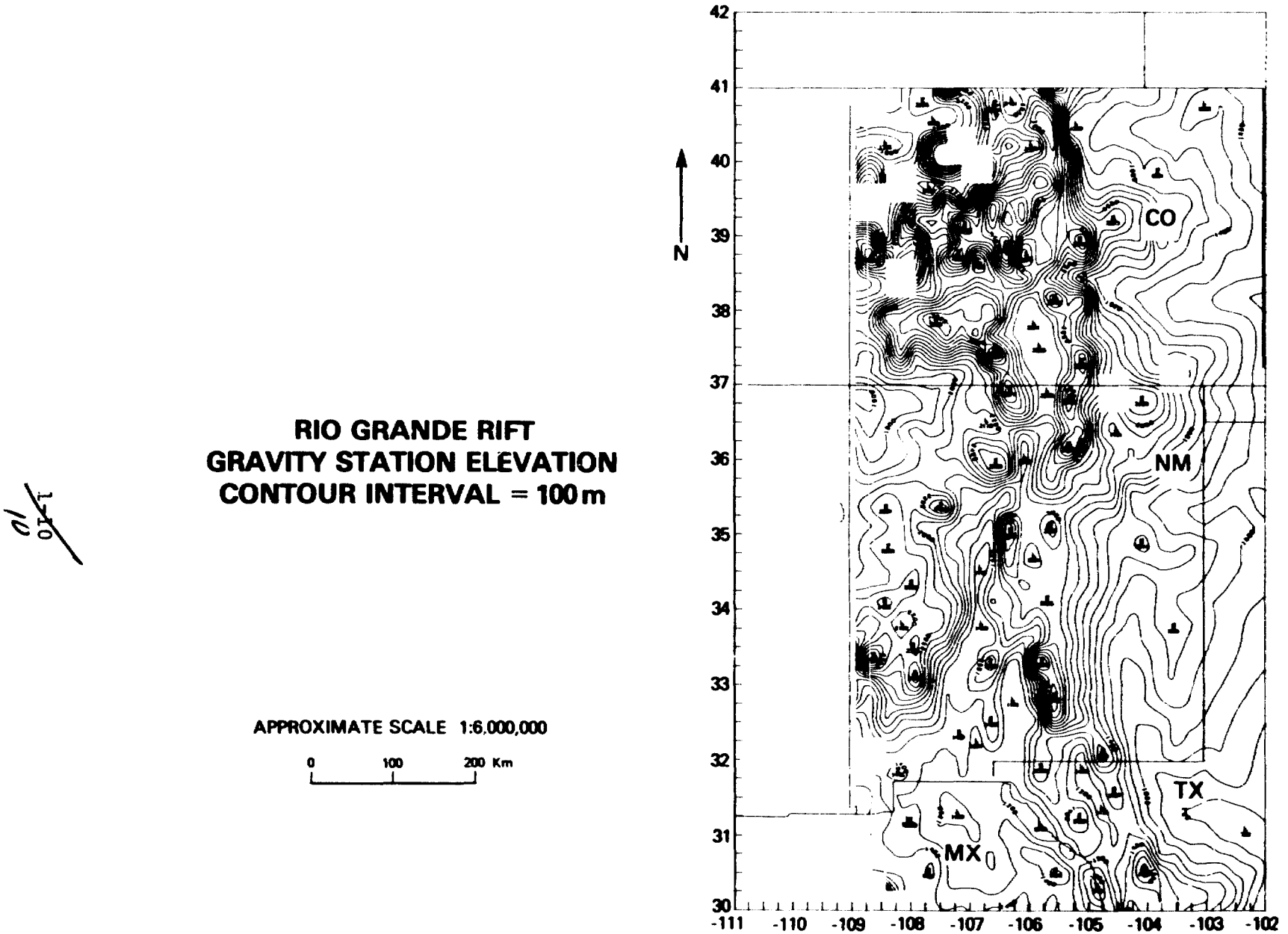

Figure 1B-1: Contour map of gravity station elevation for Colorado, New Mexico, west Texas, and Mexico.

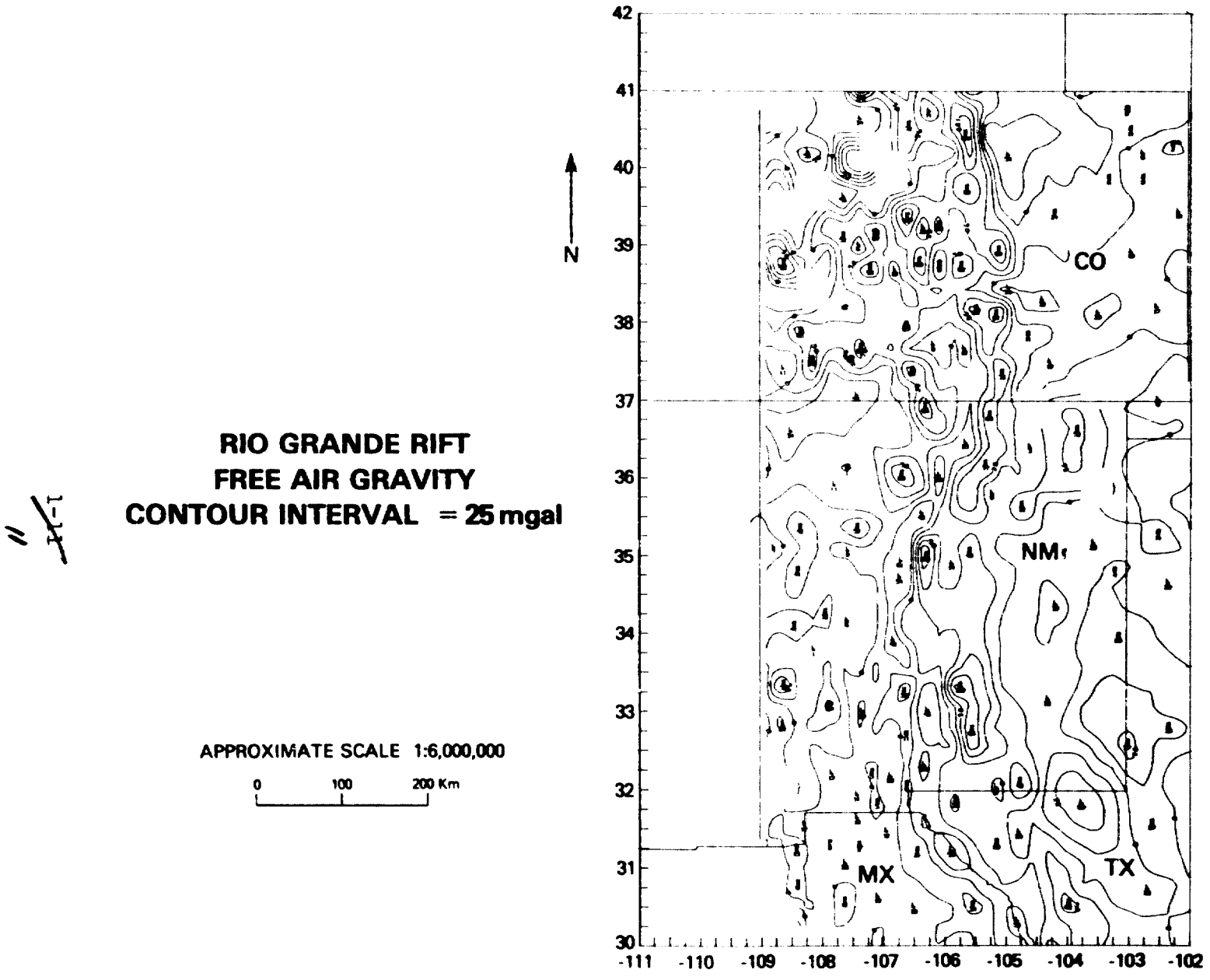

Figure 1B-2: Contour map of Free Air gravity.

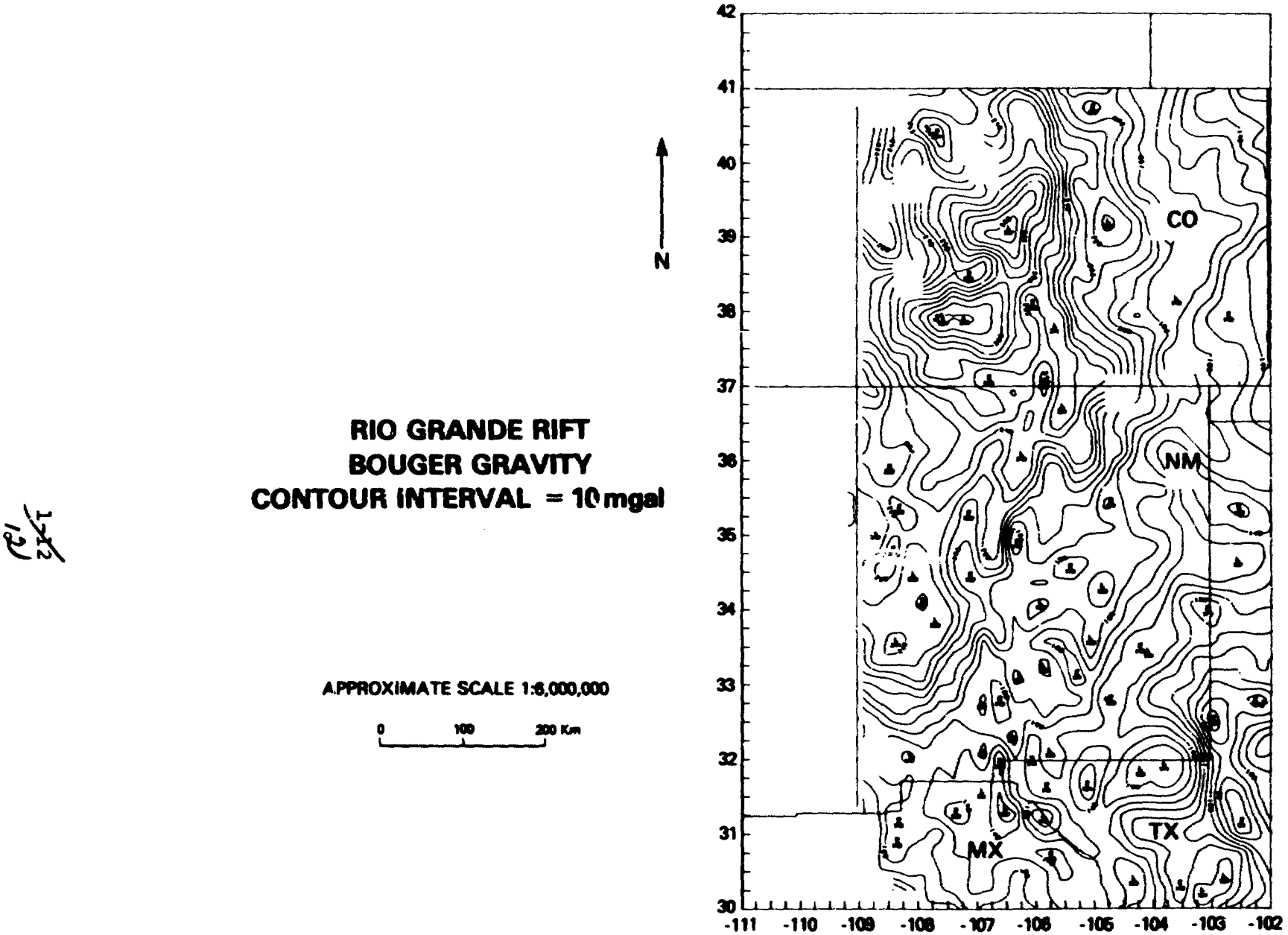

Figure 1B-3: Contour map of Bouger gravity. Though corrected for topography, the effect of elevation is still present as can be seen by comparing areas of steep gradients on this figure and figure 1B-1. The effect of elevation overshadows the rift and causes it to be a minor feature on this map.

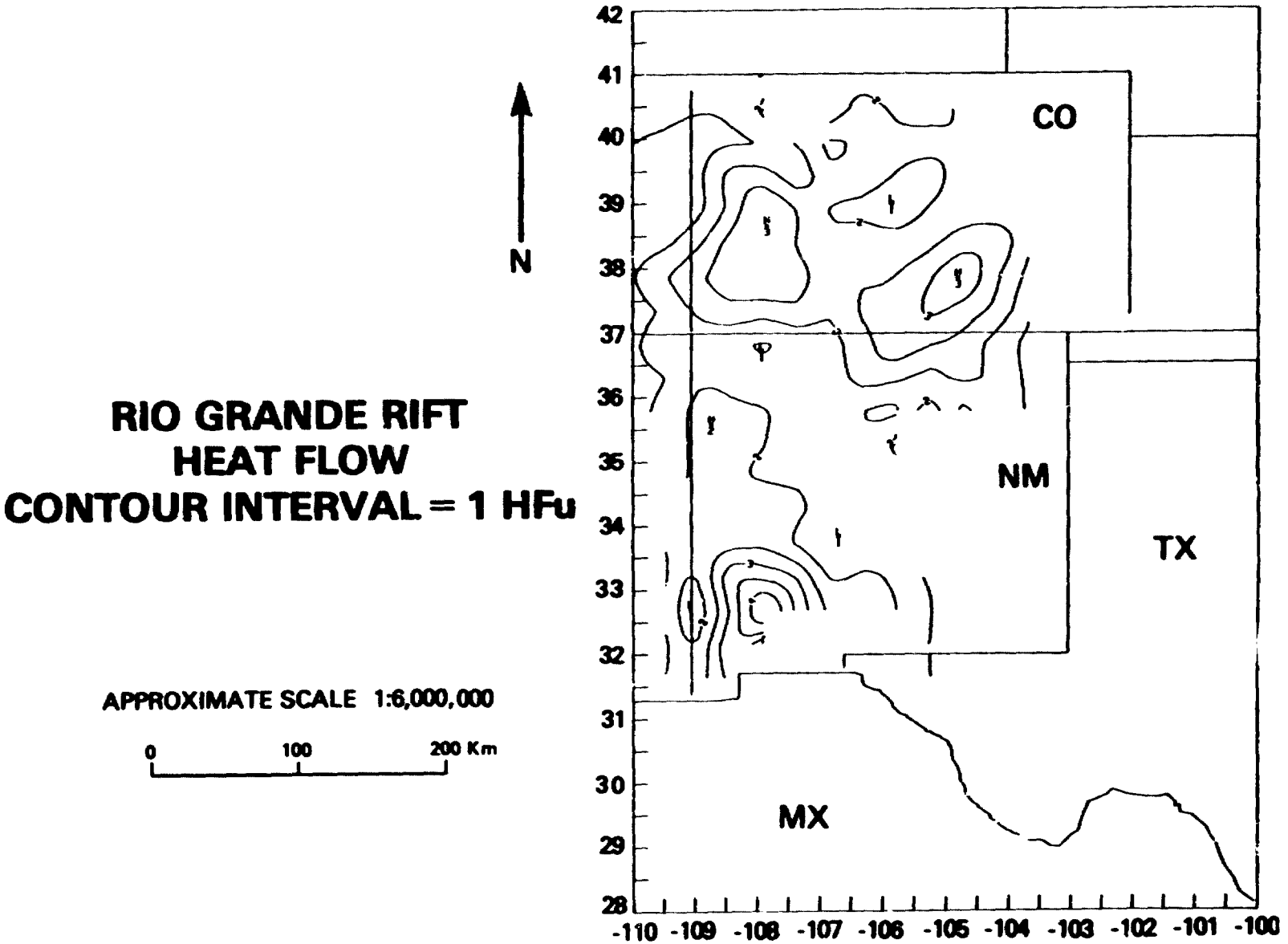

Figure 1B-4: Contour map of heat flow values.

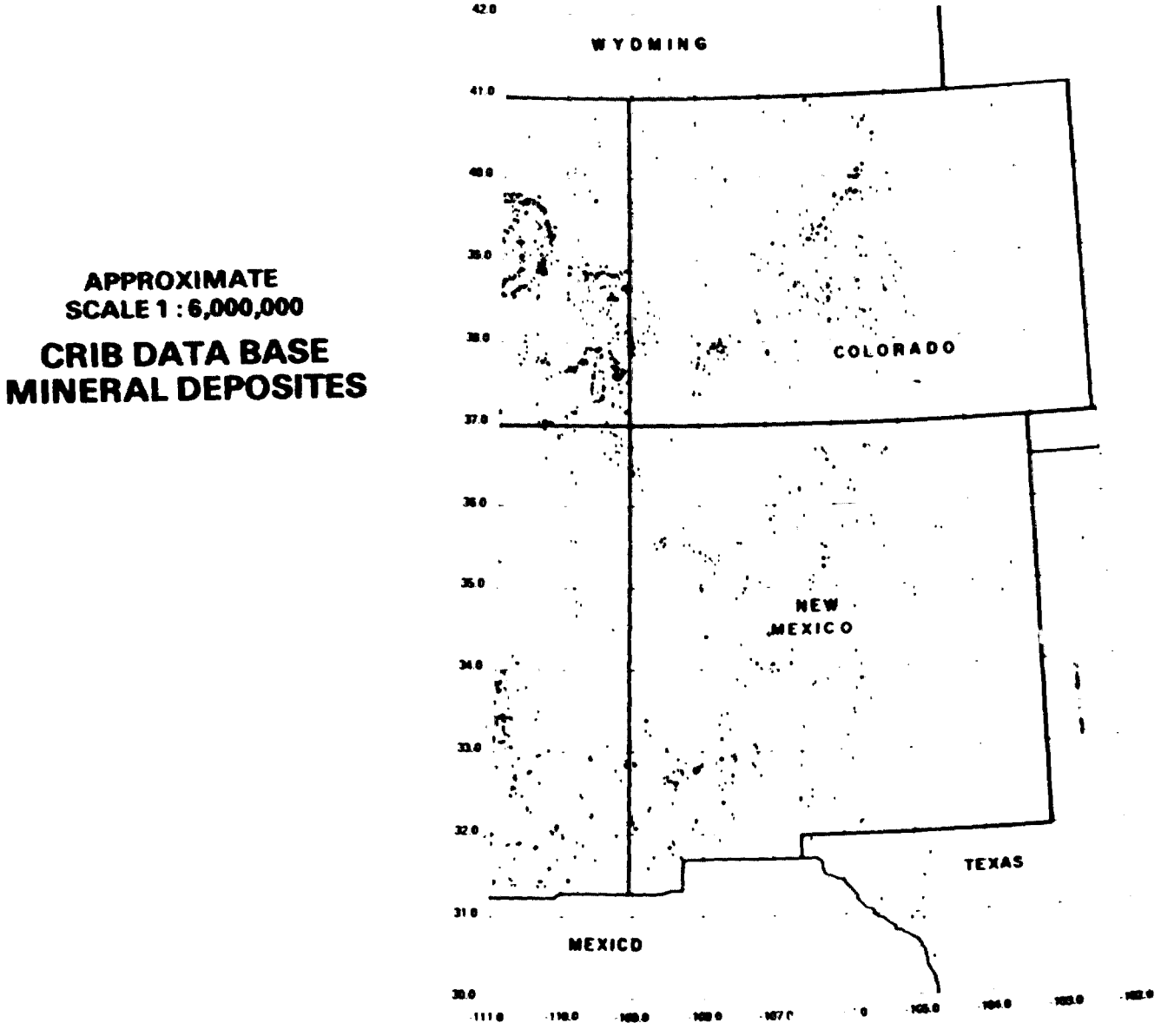

Figure 1B-5: Location map of individual mineral deposits within the Computer Resources Information Bank (CRIB) data set.

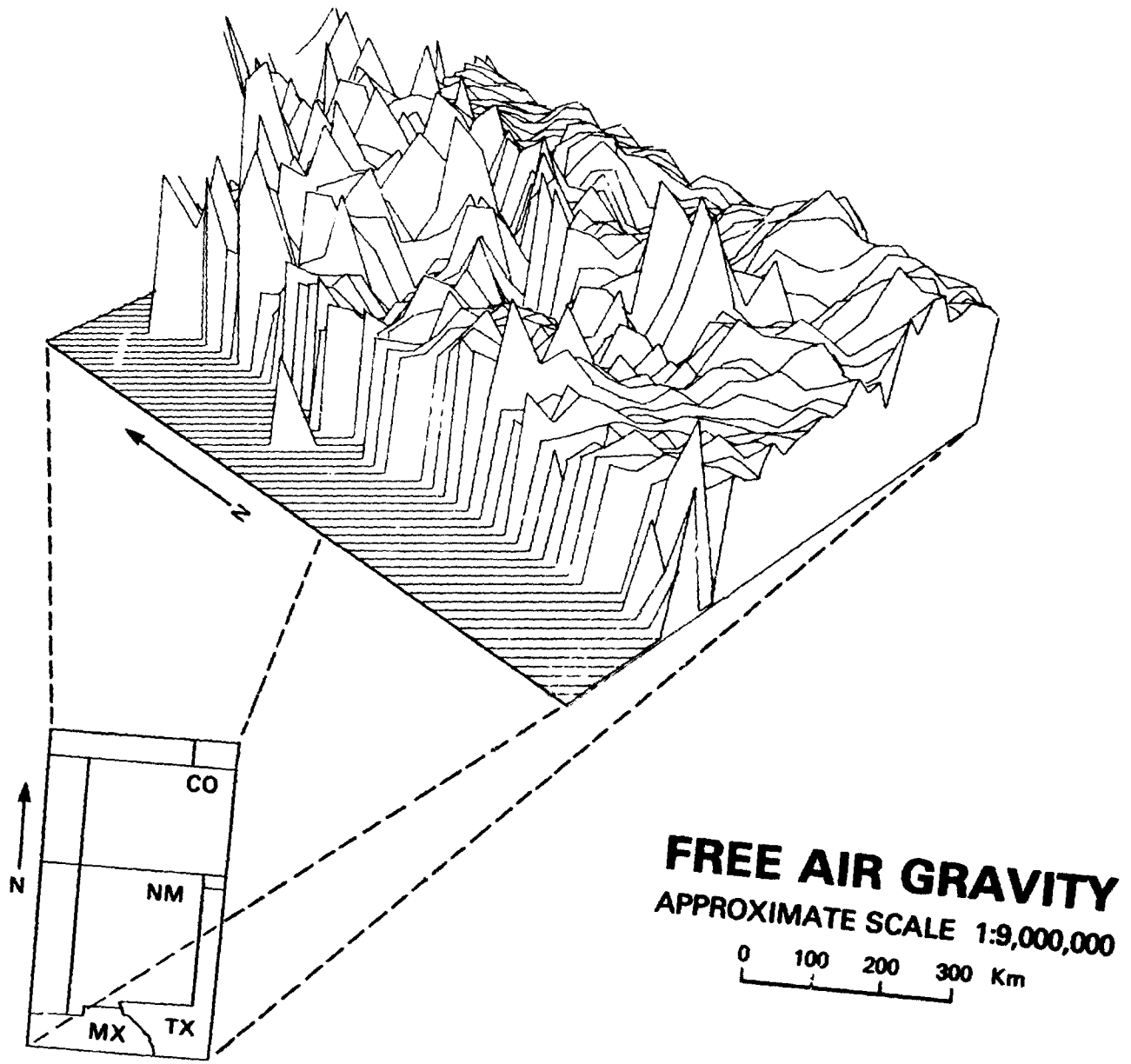

Figure 1B-6: Three dimensional plot of Free Air gravity values shown in Figure 1B-2.

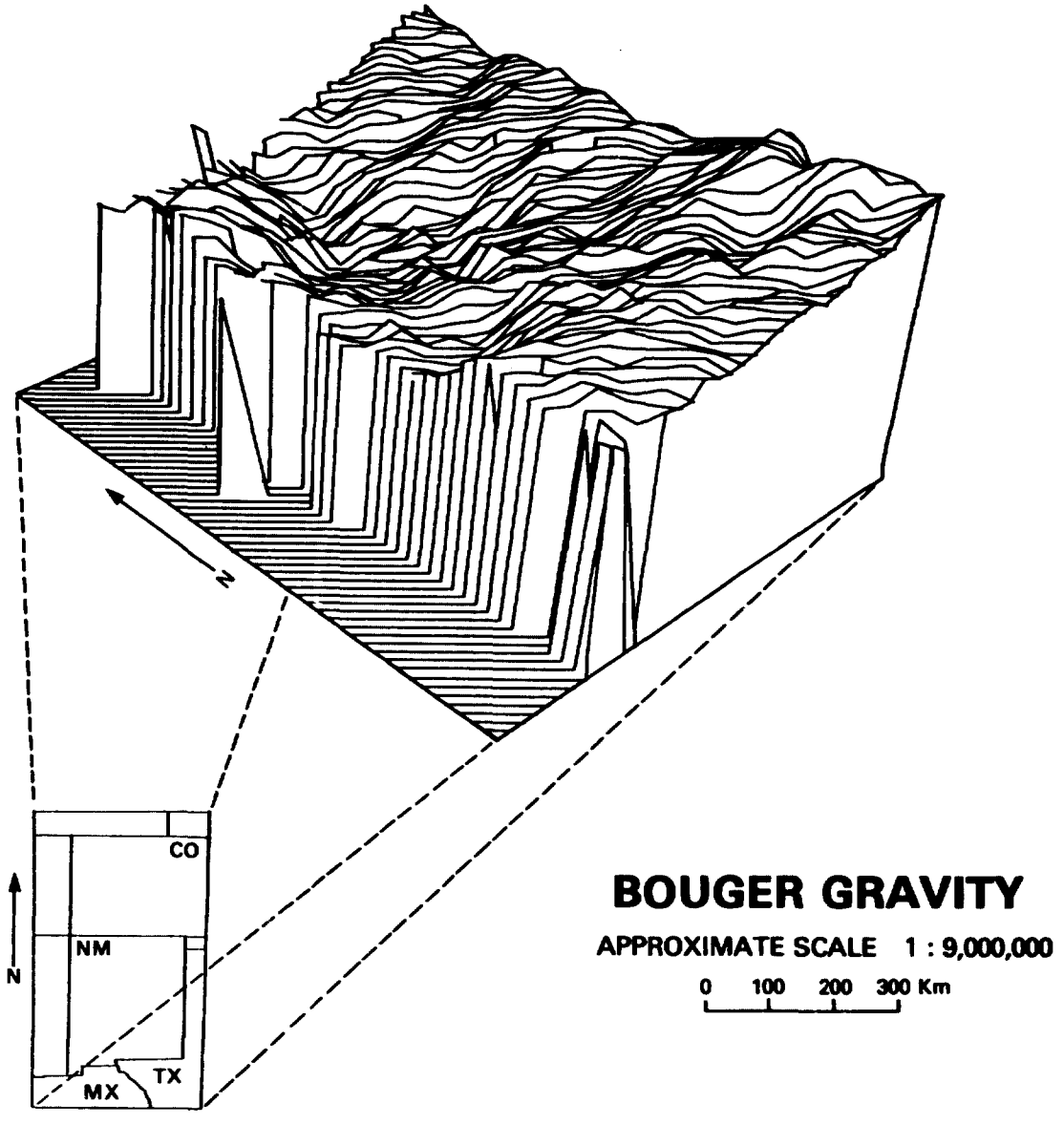

Figure 1B-7: Three dimensional plot of Bouger gravity values shown in Figure 1B-3. Note that the major features on this plot are the large negative area in central Colorado and the east-west trending long-wavelenght undulation along the eastern side of the plot. The Rio Grande rift is a minor, almost indistinct feature.

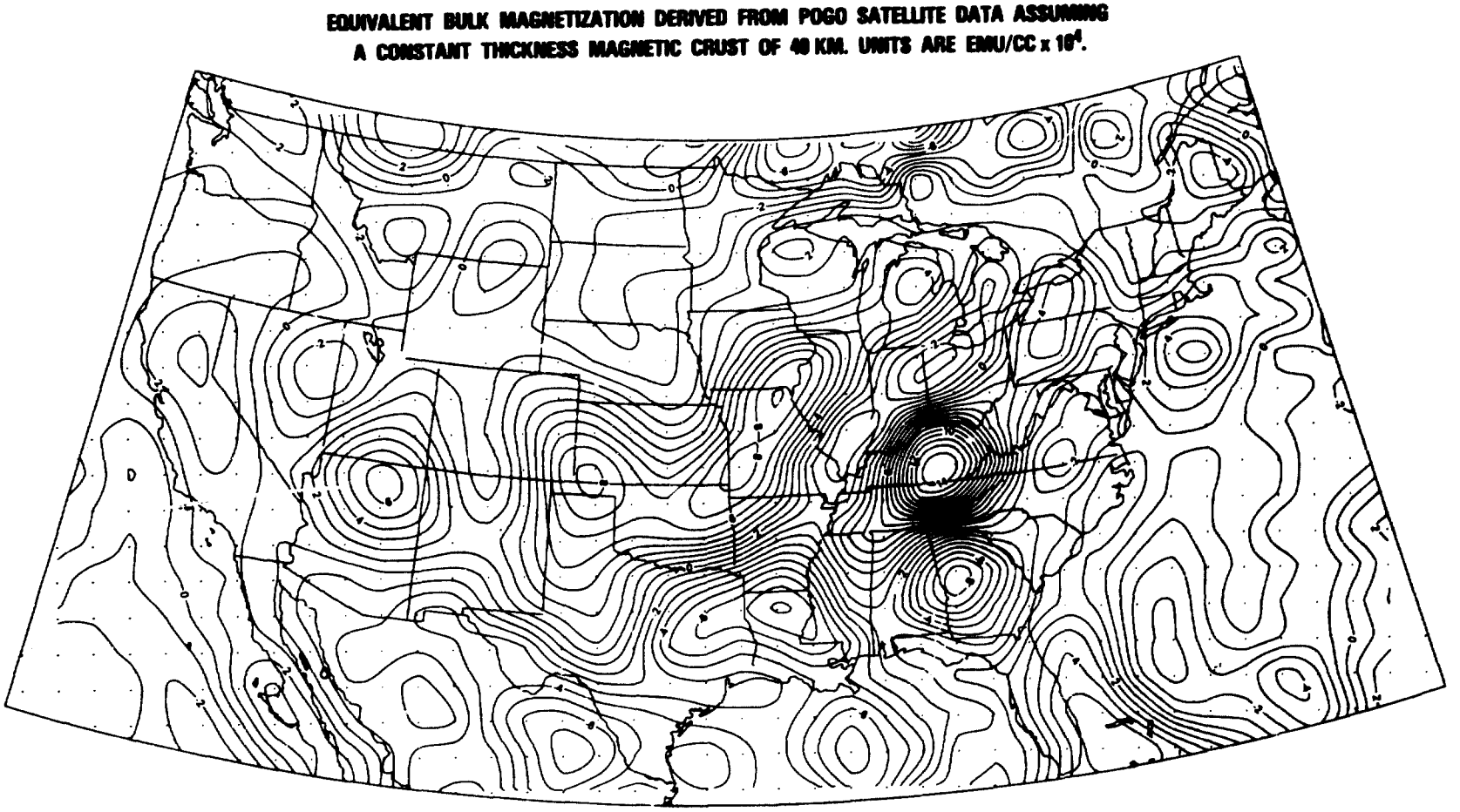

Figure 1B-8: Equivalent source representation of POGO magnetic data for the United States. Note the southward deflection of contour lines across Colorado and New Mexico and the steep gradient trending northwest across west Texas and southwestern New Mexico.

CHAPTER 2

MAGNETIC FIELD MODELING AND CRUSTAL STUDIES

edited by

P.T. Taylor and G.D. Mead

The work described in this chapter falls into two broad areas:

1. Magnetic Field Modeling--using satellite data to develop accurate, up-to-date models of the core field and its secular variation, and to obtain, verify and represent crustal geopotential fields.

2. Crustal Studies--developing models of the structure, composition and evolution of the earth's crust, using the satellite geopotential data, comparative planetology, and appropriate ground-based data.

An overview is provided for both of these areas.

MAGNETIC FIELD MODELING

OVERVIEW

The objective of the magnetic field modeling program is twofold:

o To develop techniques for determining accurate, up-to-date models of the earth's main magnetic field and its secular variation.

o To develop methods for obtaining, verifying and representing crustal geopotential fields so that these data can be used for developing broad-scale models of the composition, structure and evolution of the earth's crust.

A key to research in geomagnetism is the ability to represent magnetic fields from sources internal to the earth in terms of mathematical functions and/or maps which are easily reproducible and in a form useable for modeling studies. Our primary data source is from satellite-borne magnetometers (Pogo in the past and Magsat currently), supplemented by data from geomagnetic observatories, aircraft, ship and land surveys, and repeat stations. The internal geomagnetic field has a natural division into fields from the core of the earth and fields from the earth's crust. The mantle should not be a significant source of magnetic field because its temperatures are mainly above the Curie isotherm, thus eliminating rock magnetism, because the internal circulation of conducting material is believed to be slow compared to that of the core, and because the material circulated is of lower conductivity than that in the core. Thus modeling divides itself naturally into modeling of the core field with spherical harmonic functional representations and modeling of the crustal field with maps and equivalent source functions.

The object of modeling of the core field is, first, to maintain a useful representation of the time-varying field for purposes of navigation, magnetospheric physics and background removal in the study of crustal and magnetospheric fields; and second, to serve as a source of information regarding processes in the earth's core.

While modeling of the core field is an old, established discipline of geomagnetism and is pursued by several groups around the world, in many respects it is still in a rudimentary stage of development. No existing techniques are useful for extrapolation of the field more than one or two years into the future with acceptable accuracy, which means that we do not understand the mechanism for geomagnetic secular variation, nor do we even know how to model it

properly. Recent research seems to indicate that some of the changes formerly attributed to changes of the internal field are in reality due to changing currents in the earth's magnetosphere, a phenomena not yet well modeled in itself. In addition, measurements from magnetic observatories, although accurate in themselves to within about fifty gamma or better, have not been capable of representation by global models any better than an rms of several hundred gamma.

Research is thus directed toward the general problems of accurate modeling of the core field of the earth and its long term or secular variation.

The object of modeling the crustal field is to provide a tool or tools to the solid earth geophysicist and geologist for regional scale crustal modeling. Because crustal fields at satellite altitude are very small (0-20 gamma) in the presence of the core field (20,000-50,000 gamma) and magnetospheric fields (0-2000 gamma), detection and representation of such fields is first of all a problem of extracting the signal from the background "noise" of the other fields and then developing appropriate mathematical representations of the resulting fields, such as equivalent source models. A good beginning has been made in solution of these problems and some useful results will be presented in the following sections.

Many factors enter into the calculation of crustal fields, including the model used to subtract the core field, the manner in which ionospheric and magnetospheric fields are identified and removed, and the orbital parameters of the satellite. For example, a 1-km error in the vertical position of the satellite would produce an apparent anomaly of 10-30 gammas at satellite altitude, compared with the 2-10 gamma anomalies characteristically seen in the POGO data. It is important, therefore, to verify the reality of the anomaly fields seen at satellite altitudes before attempting to use the data for crustal modeling studies. One such attempt at verification is described in Section 2C below.

A. SPHERICAL HARMONIC MODELS OF THE CORE FIELD

by

R.A. Langel, G.D. Mead and R.H. Estes

OBJECTIVES

The objectives of developing spherical harmonic models of the earth's main or core field are to provide a current, accurate representation of that field and its secular variation for all applications; to provide a research tool for study of the earth's deep interior, and to enable background removal of the core field in the determination of crustal fields.

BACKGROUND

Until Magsat was launched in October 1979, our basic data set was from the Pogo satellites. This has been supplemented by data from magnetic observatories, repeat stations, shipborne and aircraft surveys, and land surveys. Magsat was successfully launched on October 30 and will provide global data at the current epoch. During past years GSFC has published a series of models based on the Pogo and surface data which have become the standard for the rest of the scientific community. However, some basic problems in representation accuracy still remain, both for the main field and for its secular variation. These problems include accounting for the large residuals in the land-based data and the seeming inability to accurately predict secular variation for any appreciable time into the future.

RECENT ACCOMPLISHMENTS

Solution for Biases in Observatory Data

One reason for the large discrepancies between observatory data and field predictions from global models based on this data is the possible existence of large crustal anomalies at the locations of some observatories. If this is the major cause, then it should be possible to include a solution for a fixed bias relative to the spherical harmonic solution at each observatory, in the software which computes the spherical harmonic coefficients. We have developed software to do this and determined bias solutions for 167 observatories. These solutions are being compared to known magnetic anomalies to test the starting hypothesis and the method of solution. A paper is in preparation describing the newly-developed procedures and the solution obtained. A summary of these results is given here.

Annual means from a world-wide network of magnetic observatories represent the most useful data set for determining the secular variation of the internal field. The incorporation of annual means data into a main internal core field model for a particular epoch, however, suffers from the fact that the magnetic field measured at the observatory is the vector sum of the main internal field and a contribution due to local crustal magnetization,

$$\bar{B} = \bar{B}_i + \bar{B}_c$$

where $\bar{B}_c$ may change appreciably over the distance of a few kilometers. While $\bar{B}_i$ varies with time, however, $\bar{B}_c$ remains constant. Thus, models of secular variation based on time derivatives of annual means observations, i.e.,

$$\dot{\bar{B}} = \dot{\bar{B}}_i$$

are not influenced by the local anomalous field.

GSFC has developed a field modeling technique which solves for the main internal field and its secular variation simultaneously, using both annual means and other data types (satellite, marine, airborne, survey). The annual means data is accommodated by solving for the local observatory bias, $\bar{B}_c$, at each observatory. This allows the data to properly distribute its influence among the secular variation and constant parameters of the model in a least squares sense. The local biases, $\bar{B}_c$, which are estimated along with the field model, provide some physical measure of the local anomaly field.

A GSFC internal field model based on a spherical harmonic expansion to degree and order thirteen (for both constant and linear time terms) using this procedure has been developed utilizing quiet Pogo 2, 4, 6 data and a selected network of 167 world-wide magnetic observatories for the interval 1960-1976. The selection of observatories was based on spatial distribution, quality of data, and continuous operation.

The overall sigma of the least squares fit to the observatory annual means data was on the order of 15 gamma, while the magnitudes of the recovered observatory biases ranged from a few gamma to a few hundred gamma. Notably large biases were recovered for two Antarctic stations (on the order of 3,000 and 4,000 gamma) and the San Miguel observatory (1,800 gamma), which is located near the North Atlantic rise. The model fit to the Pogo satellite data was on the order of 7 gamma.

We are now attempting to compare the observatory biases determined from the model with estimates of the anomaly field in the neighborhood of the observatories.

Evaluation of Internal Field Models

As new models of the core field and its secular variation are generated from Pogo, Magsat and/or ground-based data, it is important to be able to evaluate these models for their ability to represent the field accurately over a given time span or to predict the field into the future. We have acquired from NOAA a data set consisting of annual means of the vector field measured at magnetic observatories around the globe. These data can then be used to evaluate various models.

In one study (Mead, 1979), four recently published field models (AWC/75, IGS/75, Pogo 8/71 and IGRF 1975) were evaluated by comparing their predictions with the annual means from 140 observatories from 1973 to 1977. Histograms were made of the residuals representing the difference between the observatory annual means and the predictions of each model. The histograms for ΔB and ΔI are shown in Figure 2A-1 and 2A-2. The following conclusions were drawn:

1. Three of the four models, namely, AWC/75, IGS/75, and POGO 8/71, were nearly equal in their ability to predict the magnitude and direction of the recent field. This is particularly surprising in the case of POGO 8/71, since only scalar data, taken over a restricted time period of 1966-1970, were used to construct the model.

2. A fourth model, IGRF 1975, was significantly poorer in its ability to predict the current field.

3. All models seem to be able to extrapolate predictions quite well several years outside the data range used to construct the models.

In another study (Mead et al., 1979), time derivatives of the vector field were determined at each observatory location and compared with the secular variation predictions of several models. The standard deviation of the residuals are shown in Table 2A-1. The IGS/75 and AWC/75 are slightly better than the Pogo model in their ability to predict the secular variation over the time spans indicated.

Software Modification

Several modifications to existing model generation software have been completed. Some of these are generally needed to handle the various data types, while others are specifically needed for the Magsat mission. In the first category are modifications to allow input of time derivative data (needed for repeat data) as well as measured component data, ability to utilize a covariance matrix from a previous model to derive a model with new data rather than restarting utilizing all data, and ability to utilize the output of the field model program as input to the SOLVE program, which can efficiently combine two models in a least squares sense using the covariance matrices. The output of the field model program may also be used as input to the ERODYN error analysis program to investigate the influence of truncation modeling errors and to establish the uncertainties of the field model parameters obtained from a least squares fit.

A possible bias in the Magsat data is the angle of the vector sensor relative to the spacecraft. While this is carefully measured prior to launch, it is conceivable that mechanical shifts could occur during the launch environment. We have modified the field modeling software to solve for any bias which exists in spacecraft coordinates. Simulations were conducted to evaluate the accuracy with which such a separation would be possible. With ideal data biases in angle were recovered to within an arc second. This solution deteriorated when simulated noise was added, however, with biases of as much as 40 arc seconds. Application of this software to Magsat data will occur early in 1980.

Data Collection

As a part of the correlative data effort of the Magsat Project, observatory, repeat station, aeromagnetic, and shipborne magnetic data have been collected for use in field modeling. The principle use of these data is to enhance the calculation of secular variation for the period of time between the Pogo and Magsat data. Future collection should include data after Magsat, to allow extension of Magsat models into the future in an optimum way.

Initial Magsat Results

Very little Magsat data is yet available for analysis. Nevertheless, we have obtained three days from the first two weeks which seem to be quieter magnetically than the surrounding days. Based on data from November 5, 6 and 10, we have derived the first model based exclusively on Magsat data. Only scalar data were used, since attitude determination of adequate accuracy was not yet available. Subsequent plots of the data used in the model indicates that conditions were not really magnetically quiet, so the model is not of very high quality. Substantial improvement will be made when more data is available.

This Magsat model was used to calculate the magnitude of the earth's field over a regular grid at 400 km altitude. The values were contoured, and the resulting map of the earth's field intensity at epoch 1980.0 is shown in Figure 2A-3.

FUTURE EMPHASIS

Aside from the Magsat project, this effort was disapproved in FY80. Within the project, funding for correlative data has not yet been received. Our plans thus are limited to creation of models at the Magsat epoch and limited modeling for the time period commencing with the first Pogo launch (October 14, 1964) and ending with the demise of Magsat. Without additional correlative data the latter models will be somewhat limited.

REFERENCES AND PUBLICATIONS

Mead, G.D., "Quantitative Models of the Earth's Internal Field -- Status and Future Trends," in Quantitative Modeling of Magnetospheric Processes, Ed. by W. P. Olson, Geophysical Monograph 21, American Geophysical Union, 1979

Mead, G.D., R.A. Langel, and R.H. Estes,"Evaluation of the AWC 75, IGS 75, POGO 2/72 and POGO 2/79 Field Models and their Secular Variations" (Abstract), EOS 60, 812, 1979.

Figure 2A-1

HISTOGRAMS FOR ΔB
425 OBSERVATORY ANNUAL MEANS: 1973.5 TO 1976.5

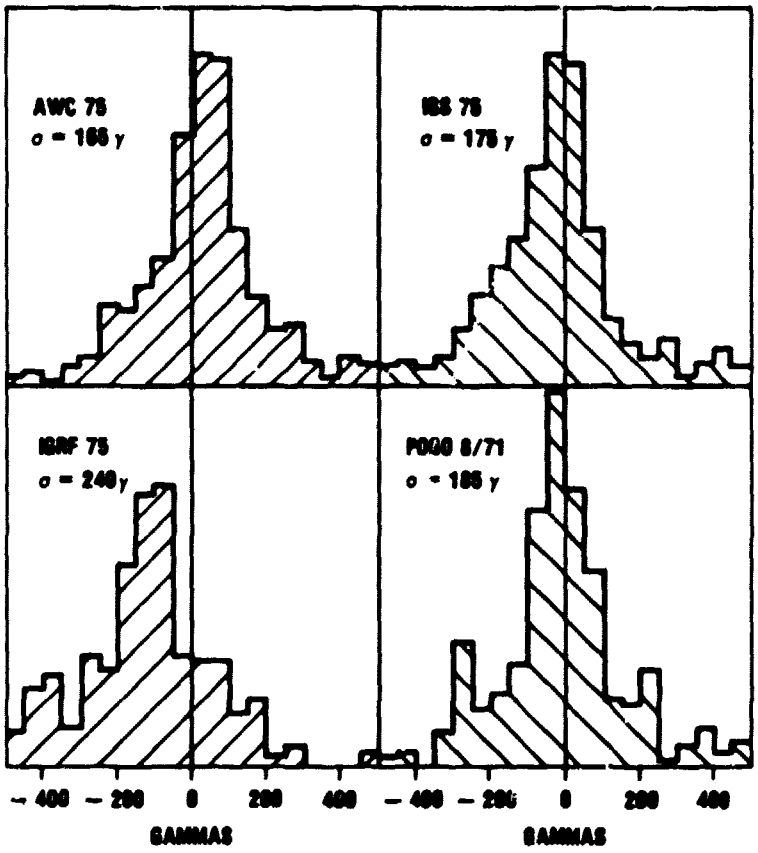

Figure 2A-2

HISTOGRAMS FOR ΔI
425 OBSERVATORY ANNUAL MEANS: 1973.5 TO 1976.5

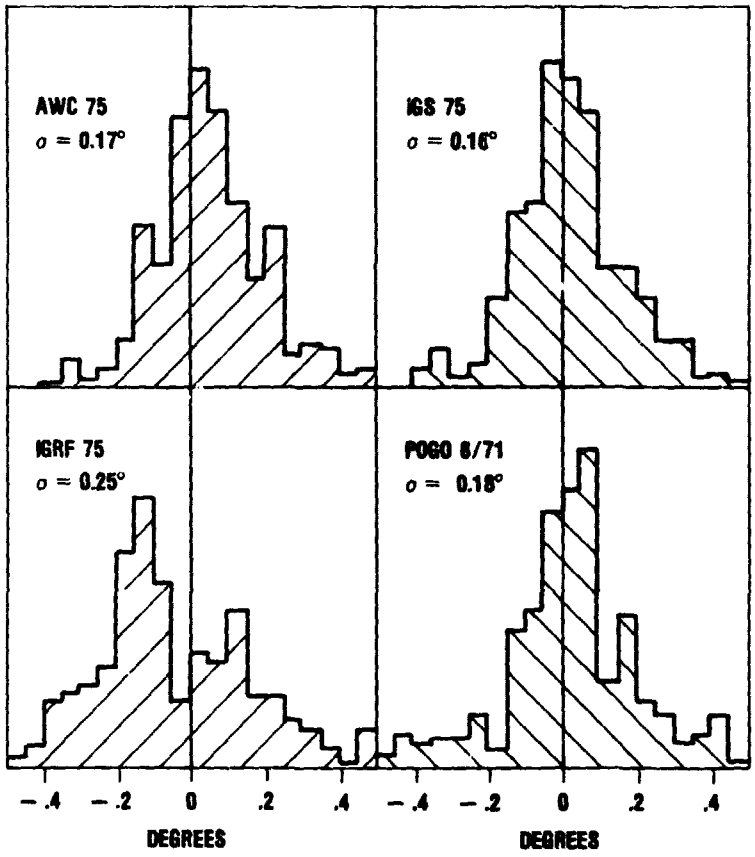

Figure 2A-3. CONTOURS OF FIELD MAGNITUDE - 400 KM ALTITUDE
PRELIMINARY MAGSAT MODEL - EPOCH 1980
Contour Interval - 2500 gammas

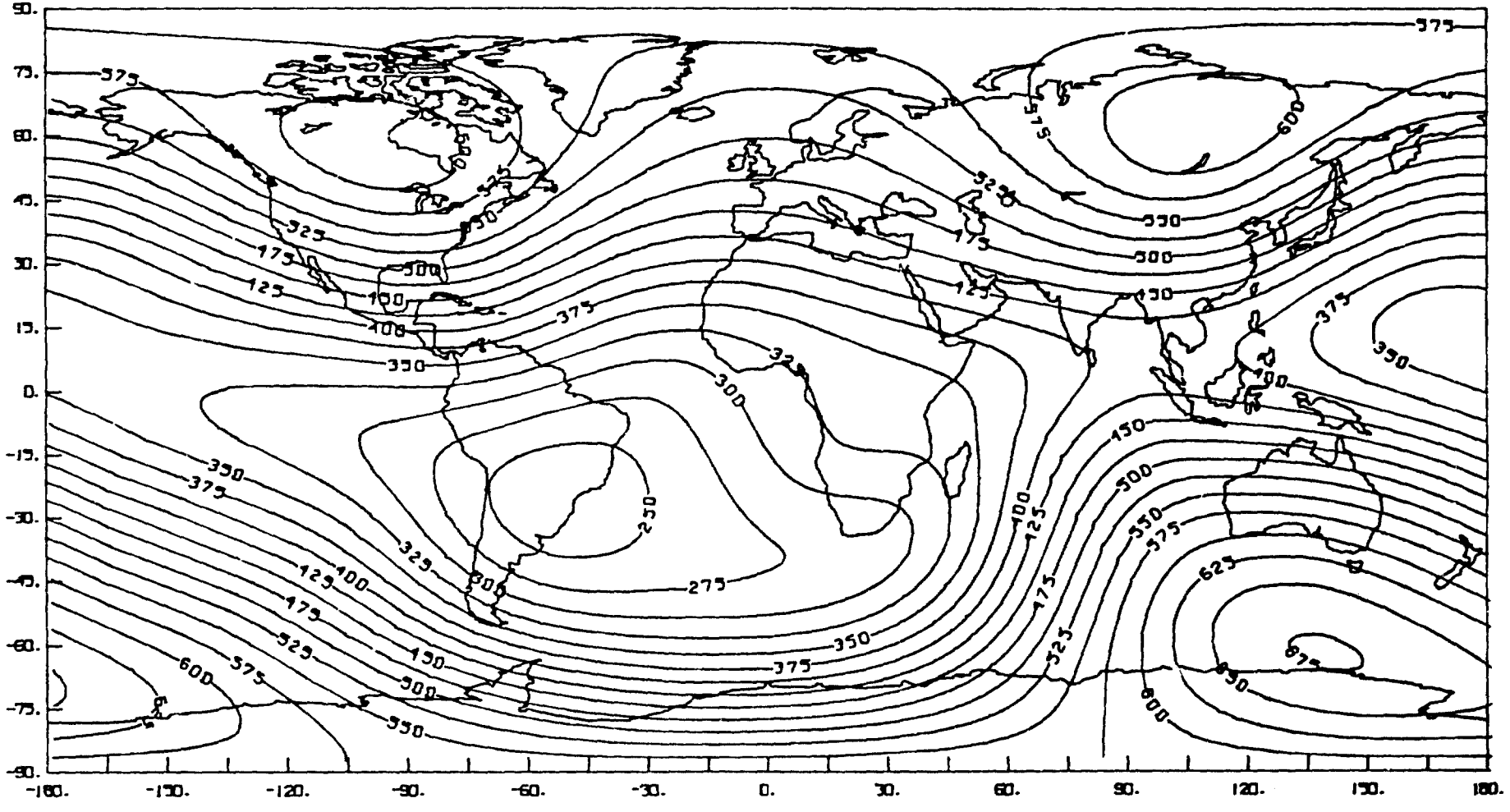

FITS TO OBSERVATORY SECULAR VARIATION
(STANDARD DEVIATION)

	D (DEG/YR)	H (γ/YR)	Z (γ/YR)
1968-1972			
IGS 75	.013	4.5	6.0
AWC 75	.017	4.0	5.5
POGO 2/79	.020	5.0	7.5
1972-1976			
IGS 75	.026	5.0	10.0
AWC 75	.020	4.5	8.5
POGO 2/79	.030	5.0	10.0

Table 2A-1. Standard deviation of the residuals between measured and predicted secular variation at 100 magnetic observations

B. CRUSTAL ANOMALY REPRESENTATION

by

R.A. Langel

OBJECTIVE

Fields from crustal anomalies are of small magnitude relative to the main field of the earth and to many magnetospheric fields. The objective of this effort is to carefully separate the fields from these three sources in order to isolate the crustal fields and to represent them in a manner suitable for analysis by geophysicists modeling the structure, composition and evolution of the crust.

BACKGROUND

Since the initial effort by Regan and coworkers, several refinements have been made to techniques for isolating and representing anomaly fields. In last year's report we showed a comparison of an anomaly map derived from Pogo data with a corresponding map derived from aeromagnetic data for the western portion of Canada. That map, and the accompanying report, has now been accepted for publication in the Canadian Journal of Earth Sciences (Langel et al., 1980). Also presented were new techniques developed by Mayhew (1979), since published, and their application to create a revised averaged anomaly map of the world between $\pm 50^{\circ}$ latitude and to derive a reduced-to-the-pole map of the continental U.S.

RECENT ACCOMPLISHMENTS

Separation of the Measured Field into its Various Sources

This effort is focussed on isolating the crustal anomaly fields from the core and external fields. External fields are particularly a problem at high latitudes because fields from ionospheric currents have the same spatial scale as the anomalies. Using techniques of hand selection of data developed for use at high latitudes, we have now obtained anomaly maps of both the north and south polar regions, reproduced here as Figures 2B-1 and 2B-2. Work in this area is continuing. A particular problem is presented by the vector data from Magsat at high latitudes, as illustrated in Figure 2B-3, which shows field perturbations from field-aligned currents. These currents are present on almost every pass and are much larger in magnitude than anomaly fields. New techniques will be needed to cope with this problem.

Equivalent Source Representation

The equivalent source software described in last year's report has now been applied to all longitudes and latitudes between 50°S and 90°N. The result for ±50° is shown in Figure 2B-4. (Several refinements are necessary before the northern high latitude portion is ready for presentation.) The resulting contour plots show anomaly fields free from the effects of altitude variations from location to location and with much of the noise filtered out. This type of representation now permits easy display of these fields on various projections and scales.

The software for equivalent source representation has now been revised to incorporate vector data from Magsat. As of this writing, these have not yet been utilized. Their addition should resolve present problems in reduction to the pole near the geomagnetic equator and should allow separation of remanent magnetization normal to the ambient direction of the earth's field.

Regional Representations

Utilizing equivalent source techniques, studies have been undertaken both in Australia and in Greenland. Figure 2B-5 (from Mayhew et al., 1980) shows the derived apparent magnetization contrast for Australia, overlying a sketch tectonic map. The main conclusion of the paper has to do with the optimum dipole spacing in a regional equivalent source solution. This was found to be about 2.7° for Pogo data. It is expected that this spacing depends upon the altitude of the data and will thus be smaller for Magsat, providing increased resolution.

The effort to model Greenland is cooperative with Dr. Leif Thorning of the Geological Survey of Greenland. We have derived the equivalent source model for Greenland and provided it to Dr. Thorning, who is proceeding with its interpretation.

Magsat Results

Magsat has now been successfully launched and is providing data which will be invaluable in all areas of geomagnetism. Figure 2B-6 shows a plot of the difference between the scalar magnetometer reading and a 13th degree model fit to selected Magsat data for one completed orbit. Because the accuracy of the model is as yet unknown, it is premature to draw any firm conclusions. Study of the figure shows perturbations at high latitudes which are similar to those seen on Pogo and ascribed to ionospheric and magnetospheric sources. Also seen are perturbations at lower latitudes which could be caused either by ionospheric fields or by crustal anomalies or by errors in the field model. Further analysis is proceeding.

FUTURE EMPHASIS

With the resources approved for FY80, our effort will be concentrated on completing the equivalent source representation for latitudes $50^{\circ}S$ to $90^{\circ}N$ so that it can be easily utilized in modeling of the earth's crust. We expect to publish these results in the coming year. We are still unable to reduce these maps to a common inclination when near the geomagnetic equator, and theoretical effort to solve this problem will continue. Due to the expense of deriving the equivalent source models in terms of computer time, derivation for southern high latitudes is now dependent upon the possible availability of sufficient standby time on the computer. Thus these will not be available in the near future.

REFERENCES AND PUBLICATIONS

Mayhew, M.A., "Inversion of Satellite Magnetic Anomaly Data," Journal of Geophysics, 45, 119-128, 1979.

Langel, R.A., R. Coles and M.A. Mayhew, "Comparison of Magnetic Anomalies of Lithospheric Origin Measured by Satellite and Airborne Magnetometers Over Western Canada," Canadian Journal of Earth Sciences, in press, 1980.

Figure 2B-1

NORTH POLAR ANOMALIES IN SCALAR MAGNETIC FIELD FROM THE POGO SATELLITES

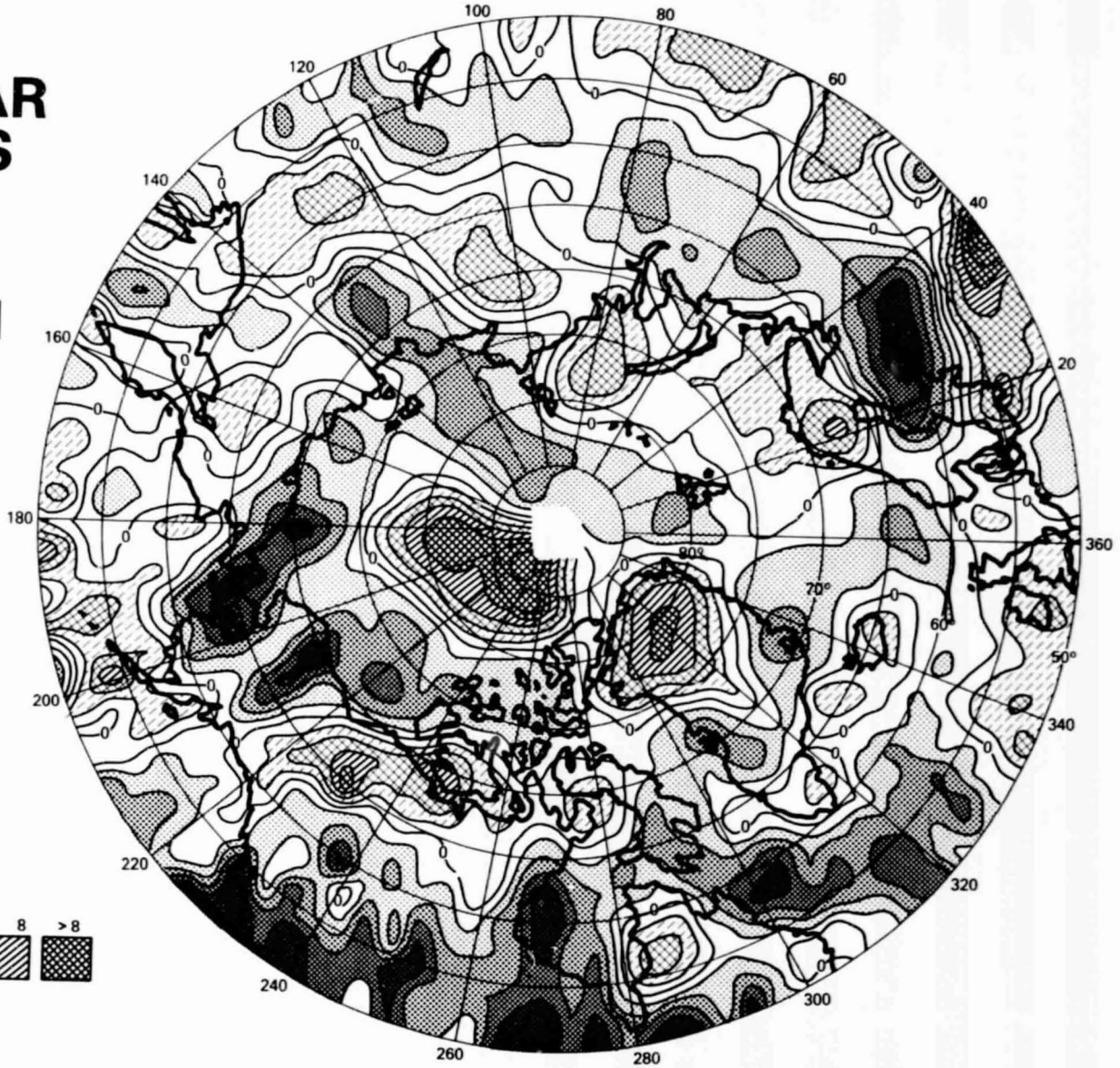

Figure 2B-2

SOUTH POLAR ANOMALIES IN SCALAR MAGNETIC FIELD FROM THE POGO SATELLITES

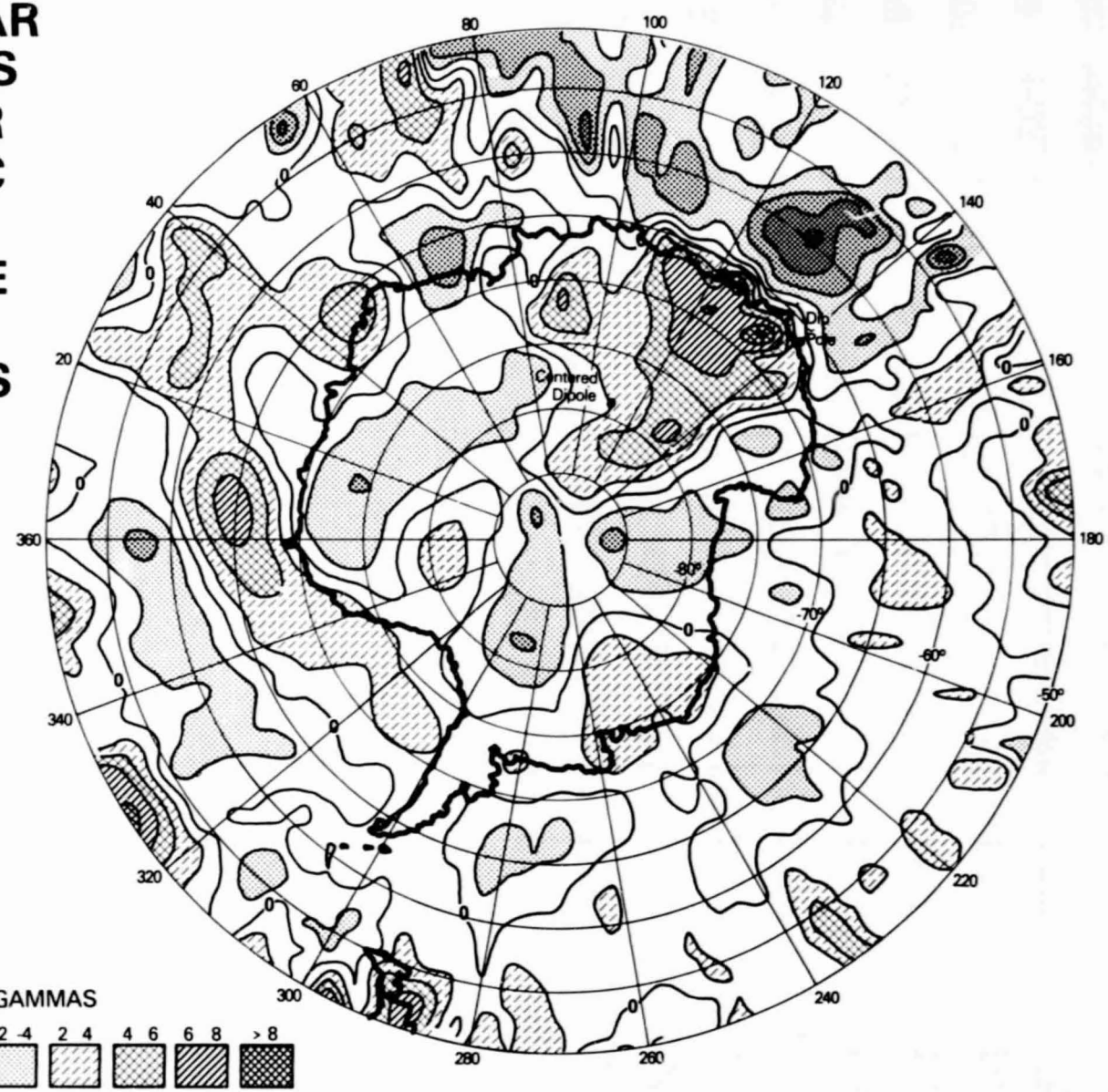

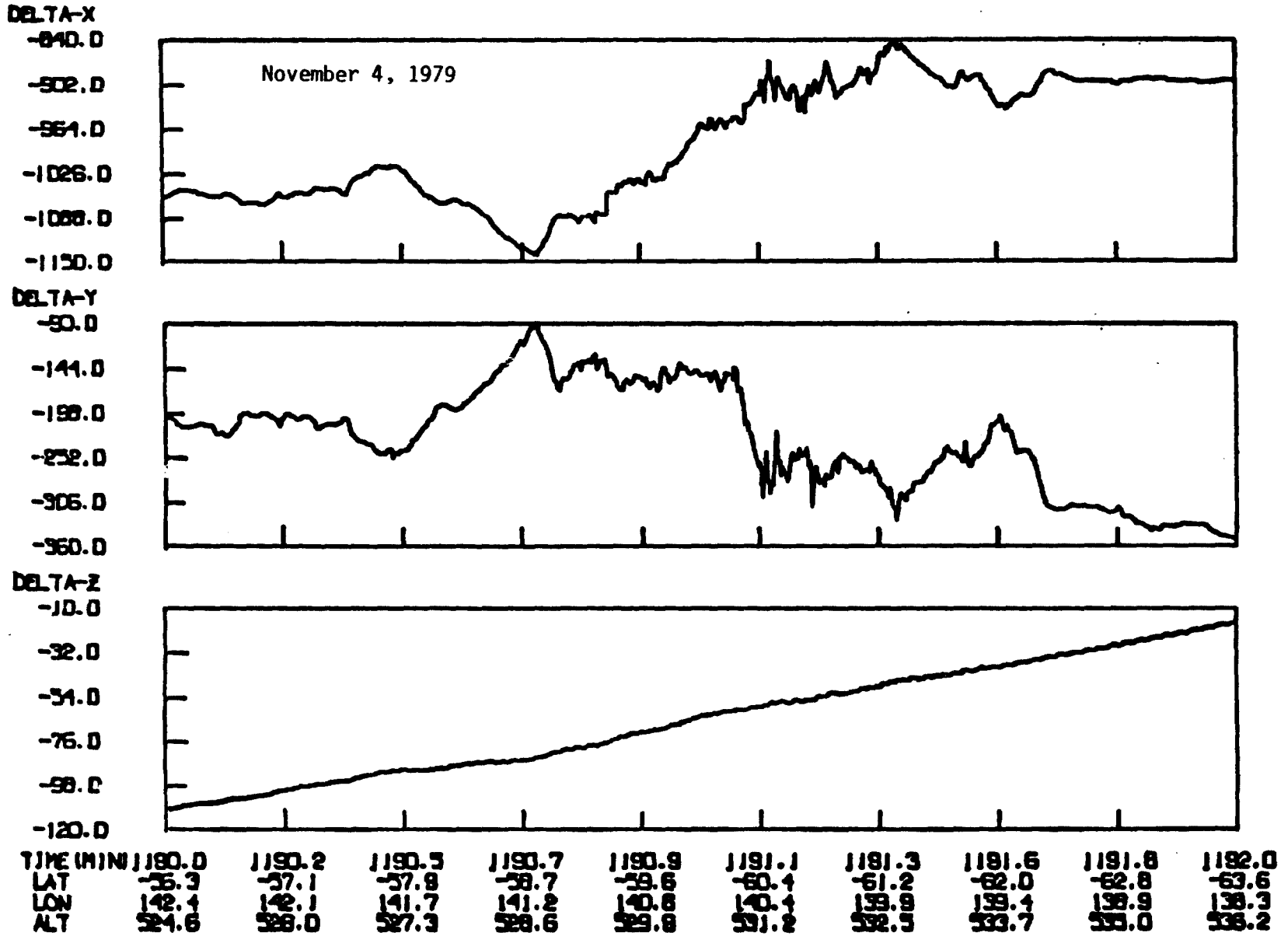

Figure 2B-3. Preliminary results from Magsat, showing a two-minute segment of data taken near the southern auroral zone. Field-aligned currents are clearly seen in the transverse field components.

Figure 2B-4. SCALAR MAGNETIC ANOMALY MAP FROM THE POGO SATELLITES REDUCED TO 500KM ALTITUDE

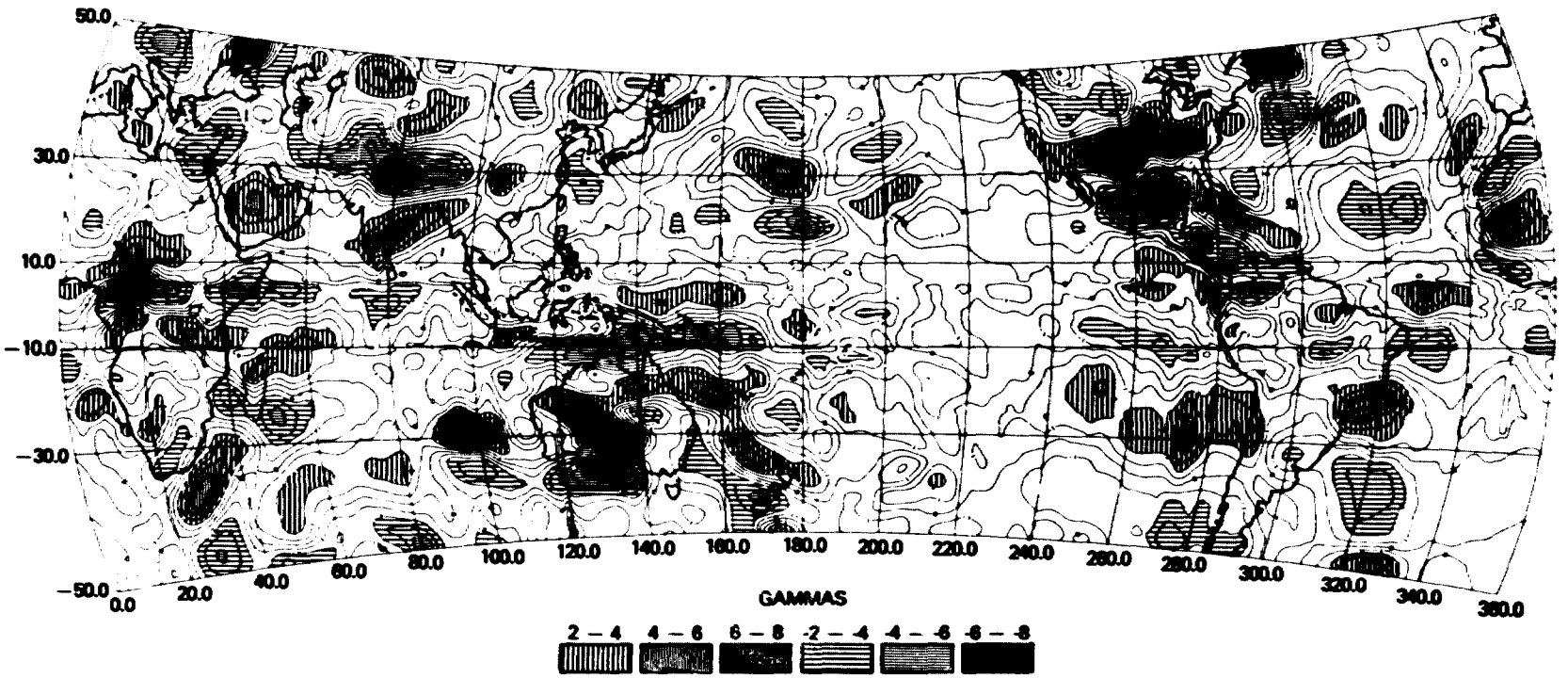

Figure 2B-5

APPARENT MAGNETIZATION CONTRAST (EMU/CC x 10^4) OVERLYING A SKETCH TECTONIC MAP

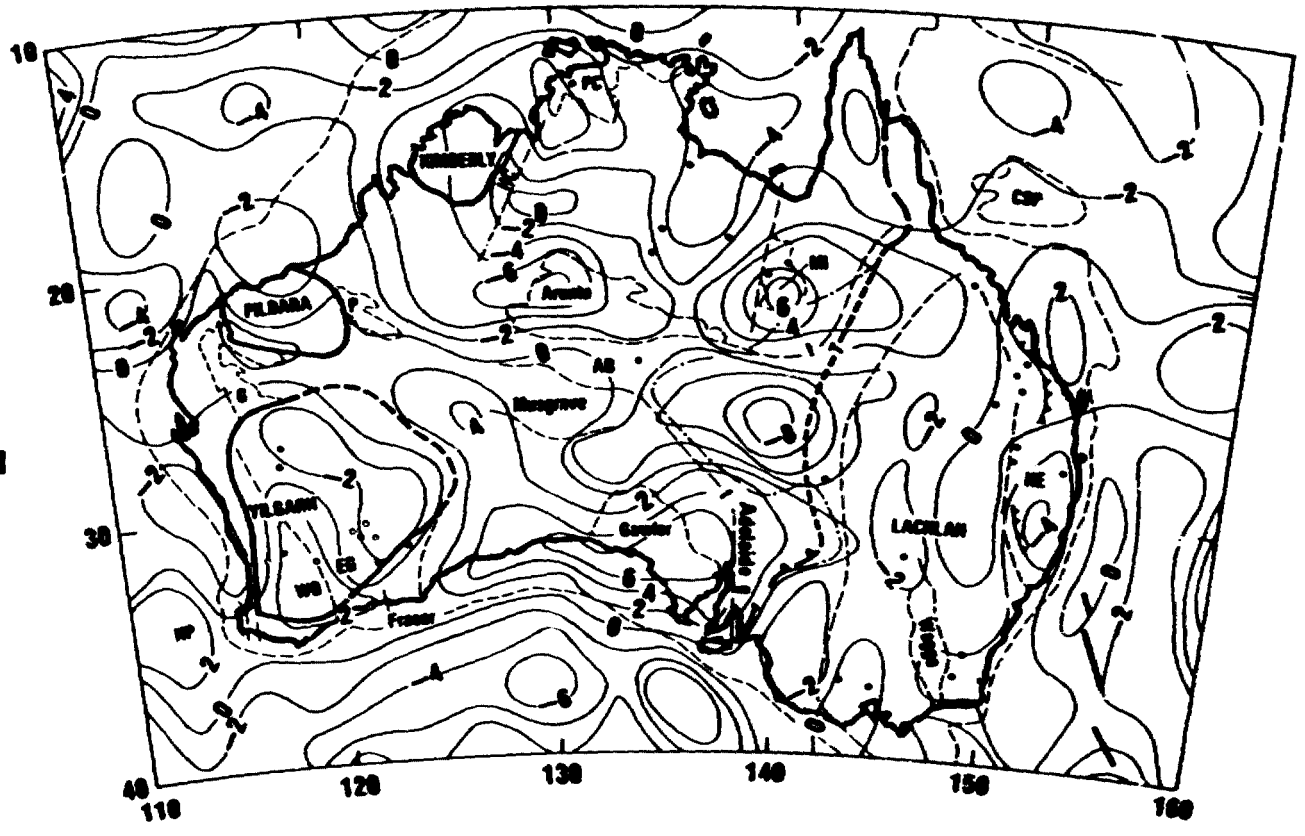

THE YILGARN, PILBARA, AND KIMBERLY PROVINCES ARE EXPOSED SHIELD REGIONS OF ARCHEAN AGE

T IS THE WESTERN BOUNDARY OF THE TASMAN OROGENIC ZONE

● HEAT FLOW > 1.5 HFU
○ HEAT FLOW < 1.5 HFU

2/20
37

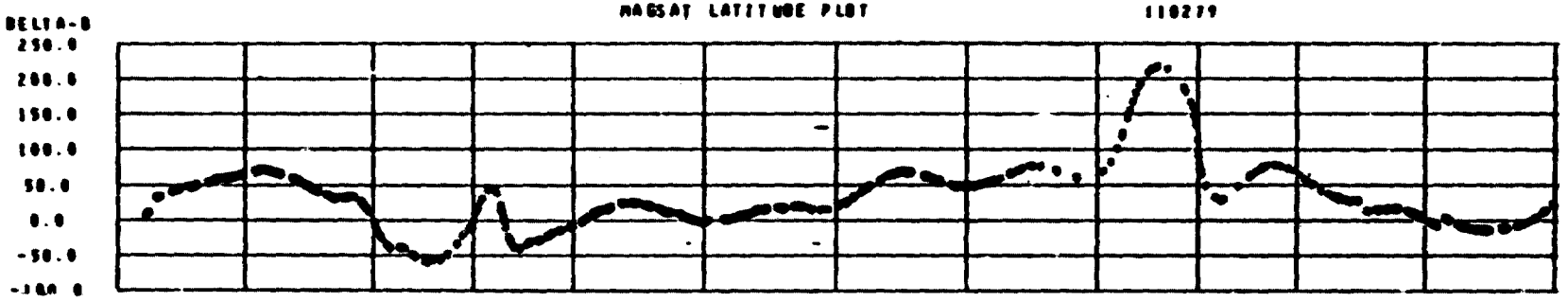

Latitude	30	60	60	30	0	-30	-60	-60	-30	0
Longitude		-124	75		60		44	-116		-132
Altitude (km)		415	356		408		518	578		529
Time (U.T.)		1:24	1:39		1:55		2:11	2:26		2:42

Figure 2B-6. Difference between measured field magnitude and model field for one complete Magsat orbit, November 2, 1979.

C. ANOMALY VERIFICATION: COMPARISON OF POGO MAGNETIC DATA WITH AEROMAGNETIC MEASUREMENTS

by

P.T. Taylor

OBJECTIVES

This study was carried out to correlate, in detail, surface magnetic data with the Pogo satellite-derived orbital magnetic field measurements. In addition, a comparison between Pogo satellite magnetic fields computed by several different methods would be made. These satellite and aeromagnetic fields would also be compared with the surface free-air gravity anomaly continued upward to satellite altitude.

Since a great deal of time, effort and funds will be expended on the interpretation of Pogo magnetic fields, additional verification of the "geologic" reality of these satellite measurements was thought appropriate (cf. Langel et al., 1980).

BACKGROUND

As part of the Code 922 Crustal Modeling effort a study was made of the Pogo satellite-derived magnetic anomaly map of the United States. Certain regions were selected for further geologic investigation. In order to conduct this study as completely as possible, a comparison was made between the Pogo magnetic anomaly map of the U.S. with the surface magnetic map for this same region, being compiled by Dr. Isidore Zietz of the U.S. Geological Survey. In a majority of parts of the United States selected for comparison there was no significant agreement between these two data sets.

In order to further investigate this discrepancy a small area was chosen for detailed and quantitative comparison. The region selected lies off the coast of the northeastern United States. Specifically, this sector lies between latitudes 37^{o} to 41^{o} North and longitudes 65^{o} to 75^{o} West, roughly east of the New England and New Jersey coasts (Figure 2C-1). This area was chosen for several reasons: (1) it contains a magnetic anomaly measured at satellite altitude; (2) digital aeromagnetic measurements obtained from a carefully controlled detailed survey were available (Figure 2C-1); and (3) sufficient gravity measurements were present to establish a significant comparison (Figure 2C-2).

RESULTS

The satellite magnetic fields were computed by several different methods: (1) the equivalent source technique (Mayhew, 1978; Figure 2C-3); and (2) analytically adjusting the different altitude profiles to the same datum (Henderson and Cordell, 1972; Figure 2C-4).

The aeromagnetic field measurements were contained upward in four steps (50 km, Figure 2C-5; 100 km, Figure 2C-6; 200 km, Figure 2C-7; and 400 km, Figure 2C-8). A gridding program was used to generate equally-spaced data prior to the upward continuation, the Purdue upward continuation algorithm was employed (Bowman et al., 1979). All potential fields were computed for an altitude of 400 km. The upward continued free-air gravity data are shown in Figure 2C-9.

These data types were compared: (1) the surface and satellite magnetic fields, Figure 2C-10; (2) The satellite magnetic and upward continued free-air gravity fields, Figure 2C-11; (3) the satellite fields computed from different methods.

SIGNIFICANCE

It is obvious that the surface and satellite magnetic fields do not agree in this region. However, the satellite magnetic and upward continued free-air gravity fields do indicate some correspondence. There are, no doubt, several possible reasons for these correlations. Only one will be discussed.

FUTURE EMPHASIS

A possible explanation for the similarity between the satellite magnetic field with the upward continued free-air gravity data is that the effect of the anomalous gravity field had not been entirely removed from the computation of the Pogo orbits. The Pogo orbital reductions were done in the mid-1960's by APL/JHU. They employed what was then one of the best gravity field models, of degree and order eight by eight, a field which was derived by APL. We want to recompute the orbital data in our study area, using the newer GSFC GEM-10B gravity field model, and use the revised orbital data to recompute the satellite-measured anomaly field.

REFERENCES AND PUBLICATIONS

Bowman, P.L., L.W. Braile, V.W. Chandler, W.J. Hinze, A.J. Luca and R.R.B. van Frese, "Magnetic and Gravity Anomaly Correlations and its Applications to Satellite Data," NASA Technical Memorandum 79702, 155 p., 1979.

Henderson, R. and L. Cordell, "Reduction of Unevenly Spaced Potential Field Data to a Horizontal Plane by Means of a Finite Harmonic Series," Geophysics, 36, 856-866, 1971.

Langel, R.A., R. Coles and M.A. Mayhew, "Comparison of Magnetic Anomalies of Lithospheric Origin Measured by Satellite and Airborne Magnetometers over Western Canada," Canadian Journal of Earth Sciences, in press, 1980.

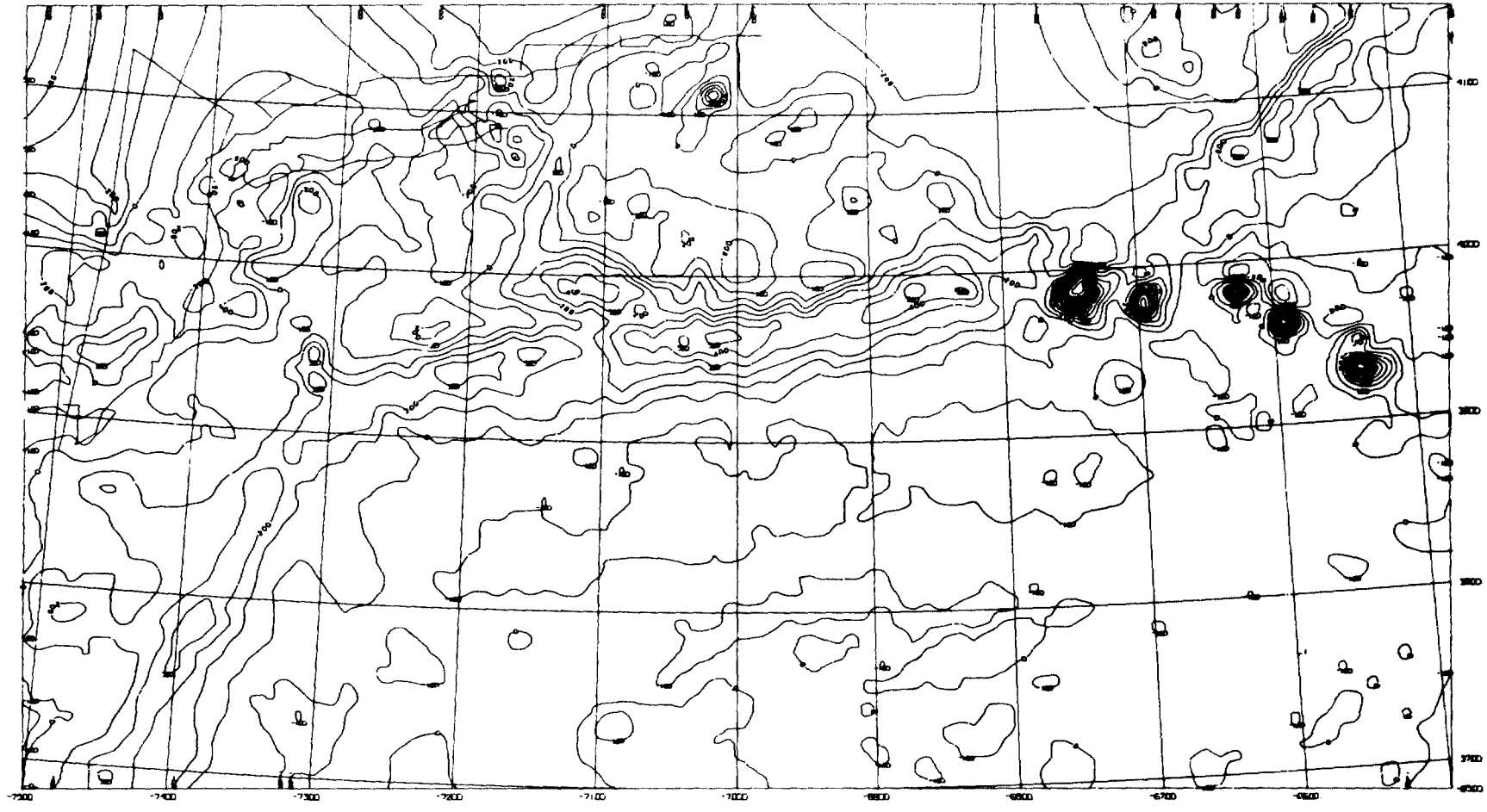

Figure 2C-1

Project Magnet Aeromagnetic Data

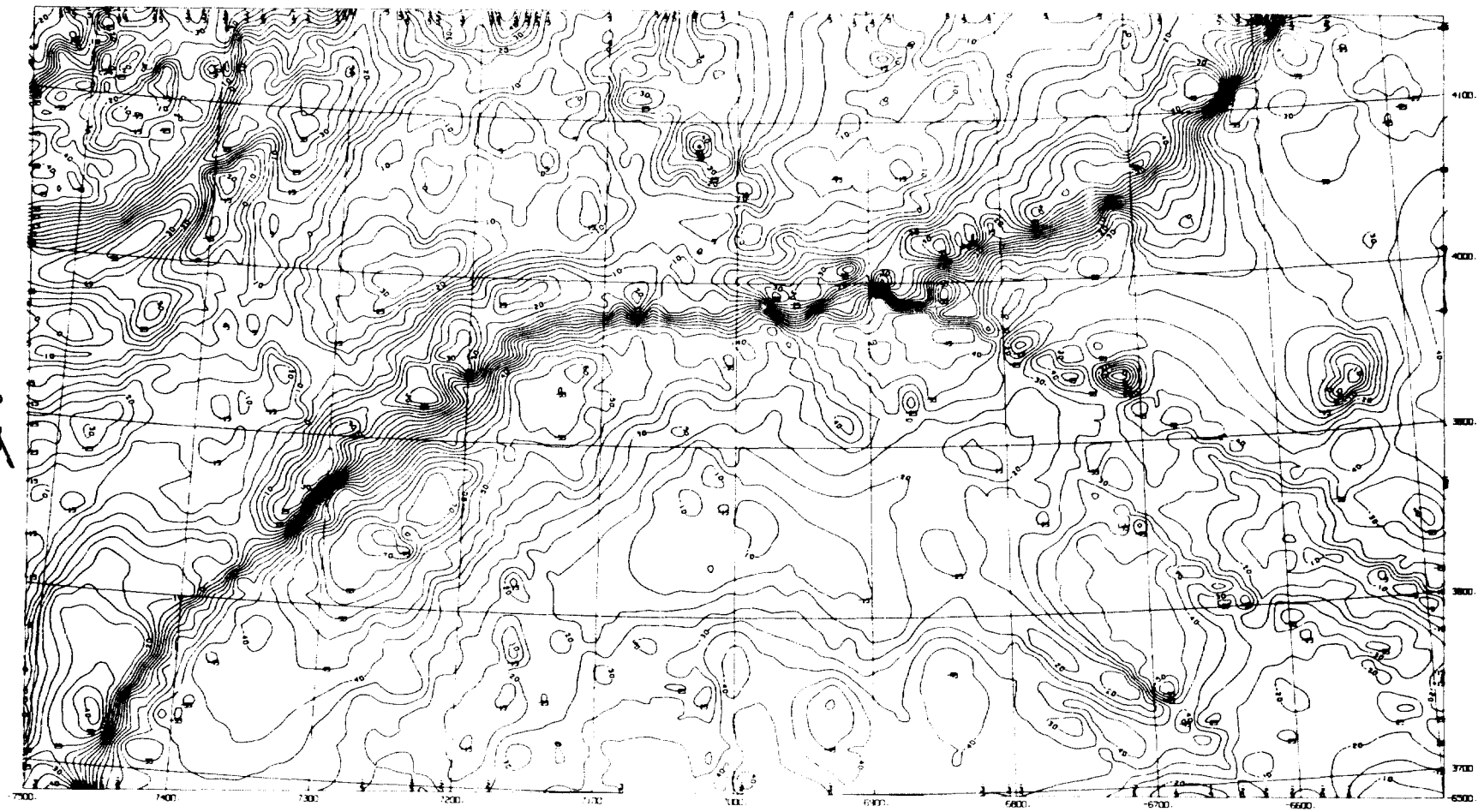

Figure 2C-2

Free air anomaly at Surface

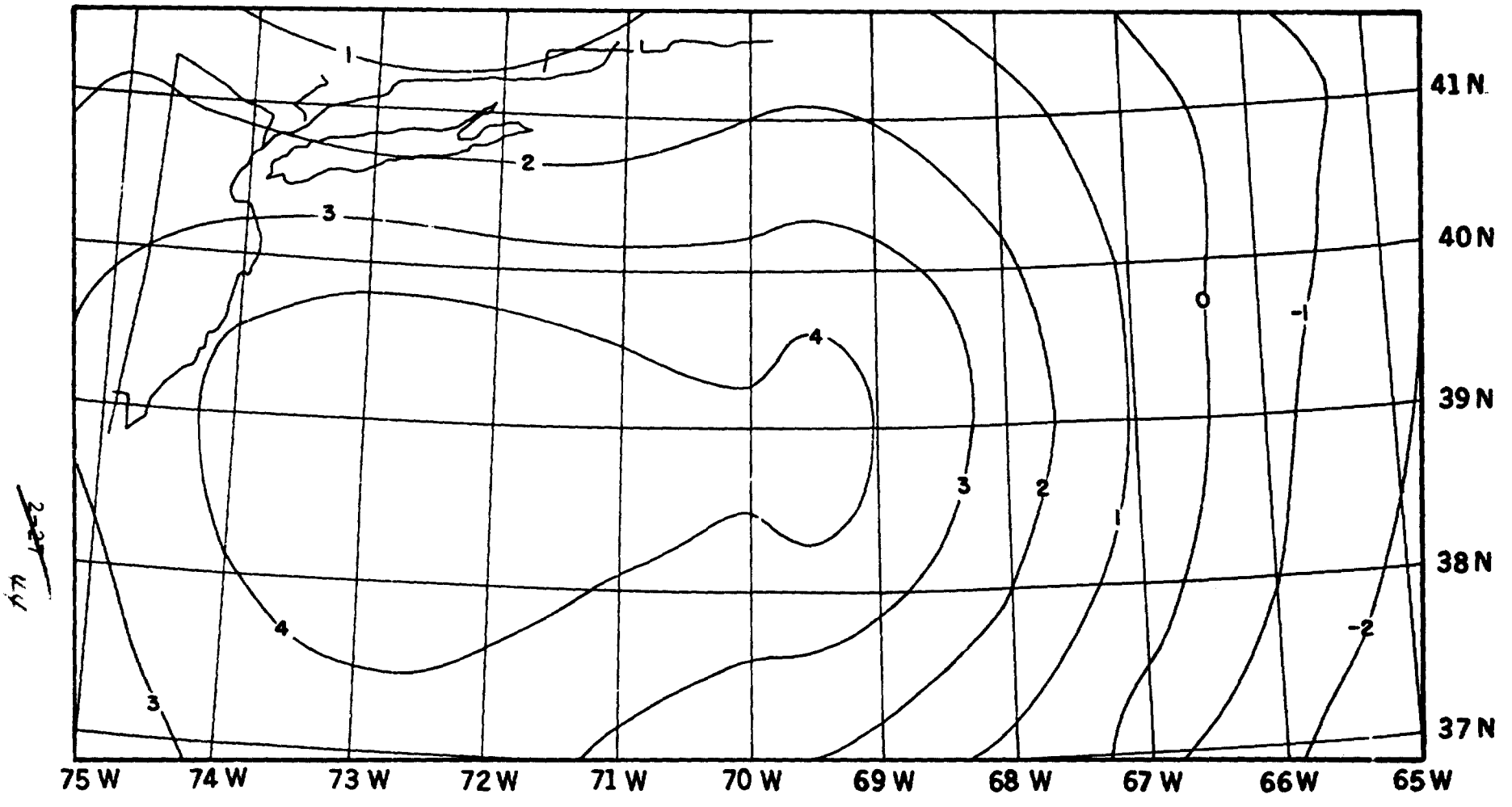

Figure 2C-3

Equivalent Dipole Source from Pogo data
at 400 km. C.I. = 1 Gamma

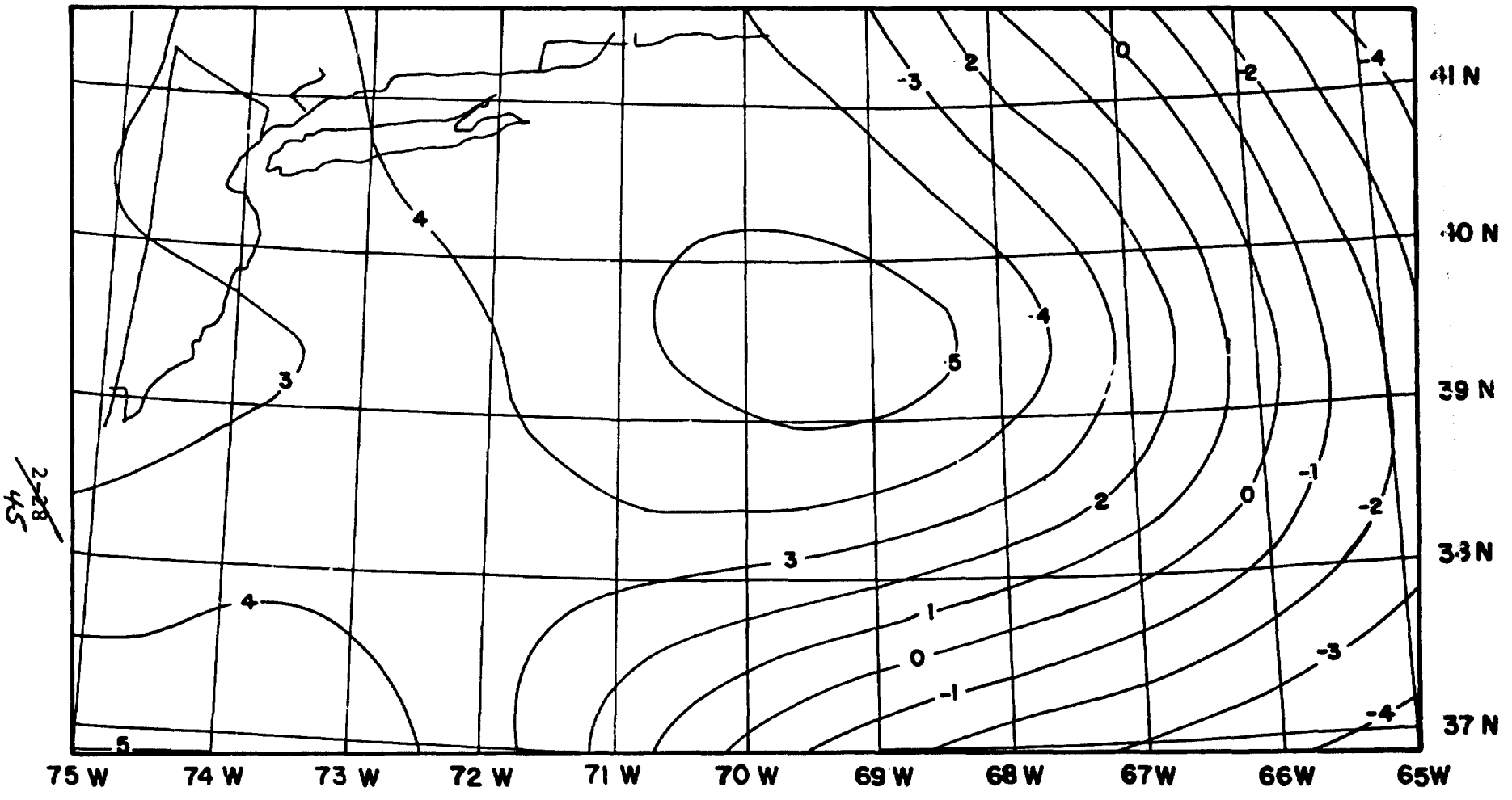

Figure 2C-4

Pogo data adjusted to 400 km. using
Henderson and Cordell method
RING CURRENT REMOVED
C.I. = 1 Gamma

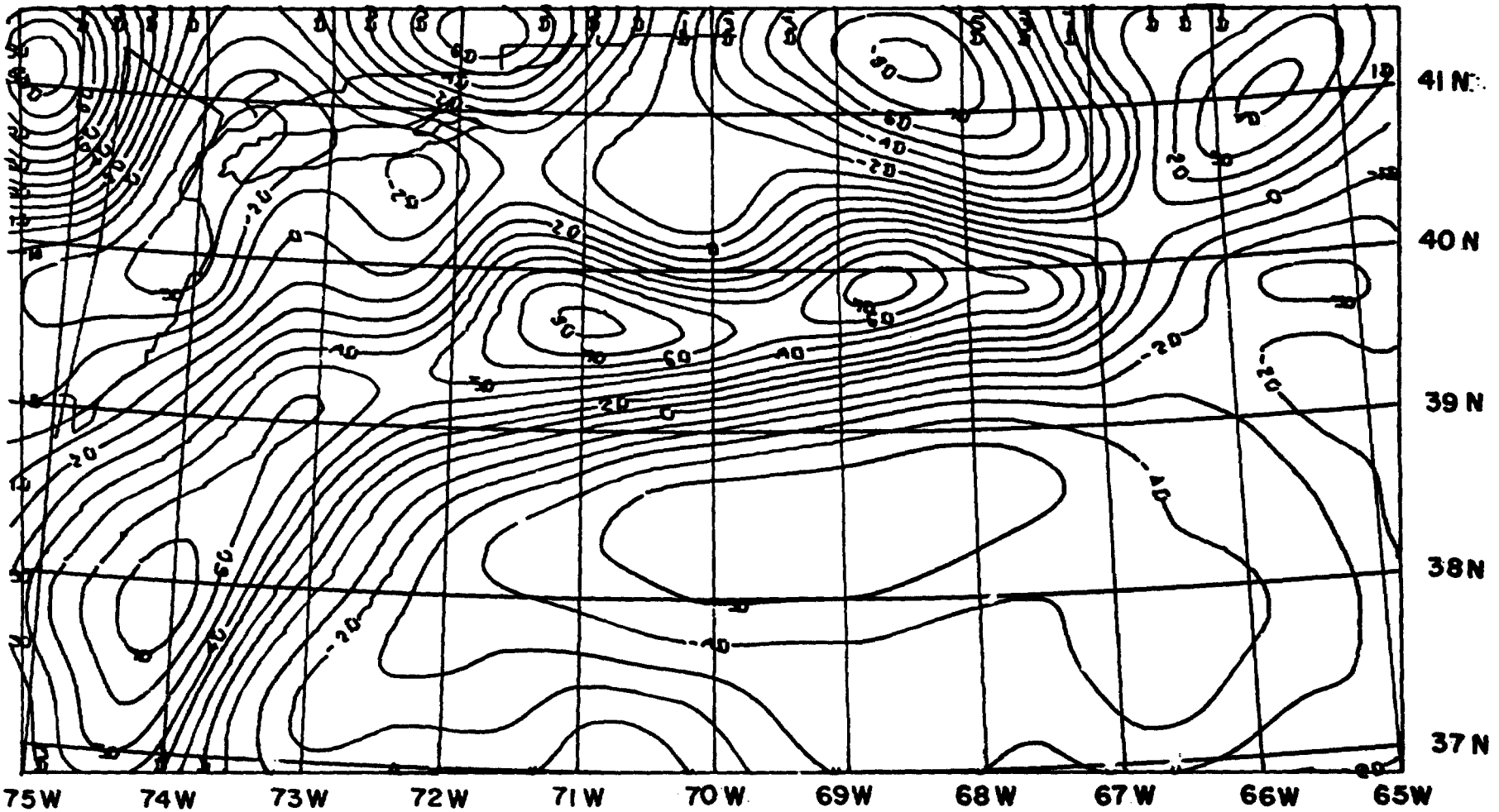

Figure 2C-5

Aeromagnetic data upward continued
to 50 km C.I. = 10 Gammas

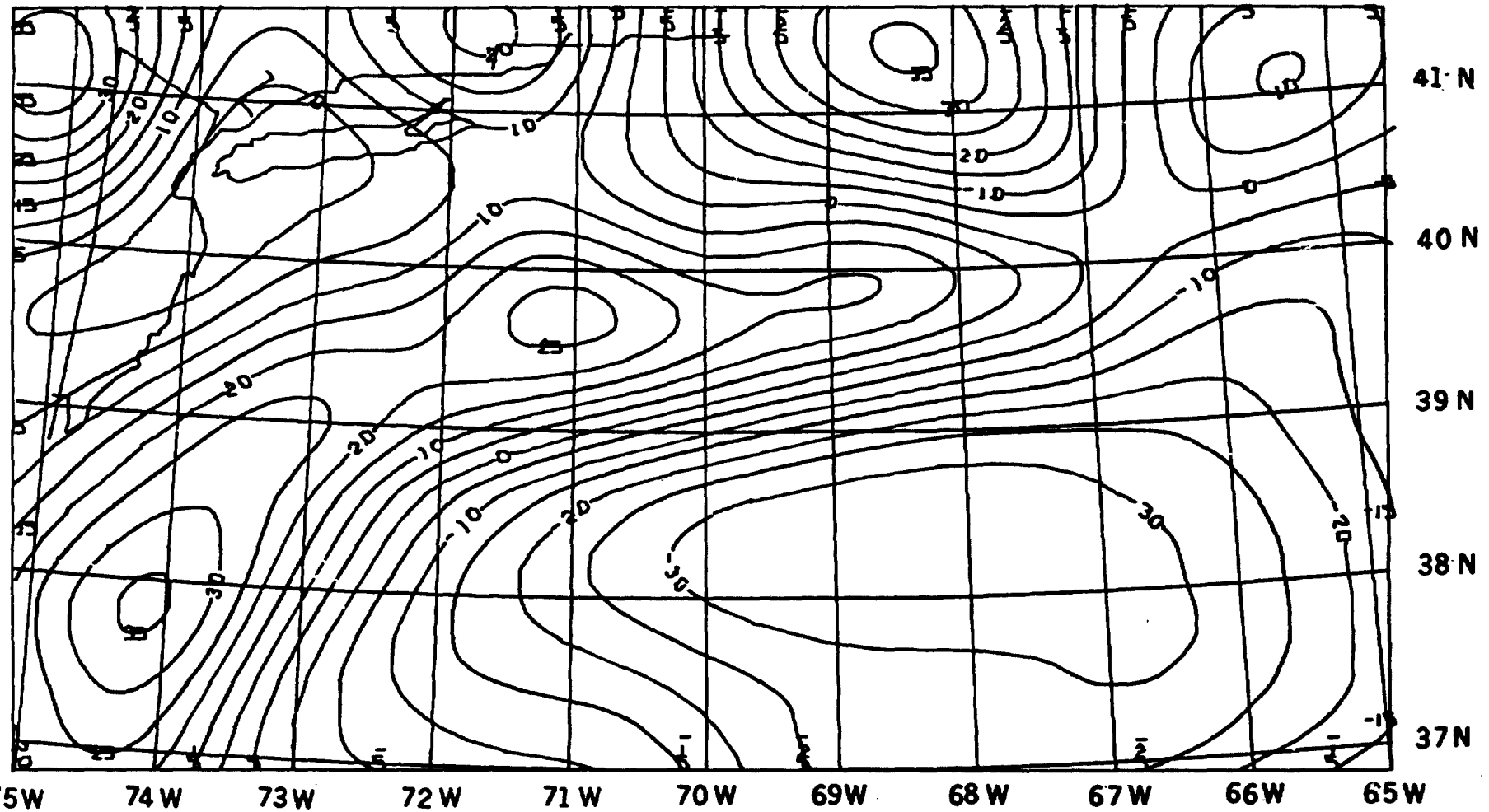

Figure 2C-6

Aeromagnetic data upward continued
to 100 km C.I. = 5 Gammas

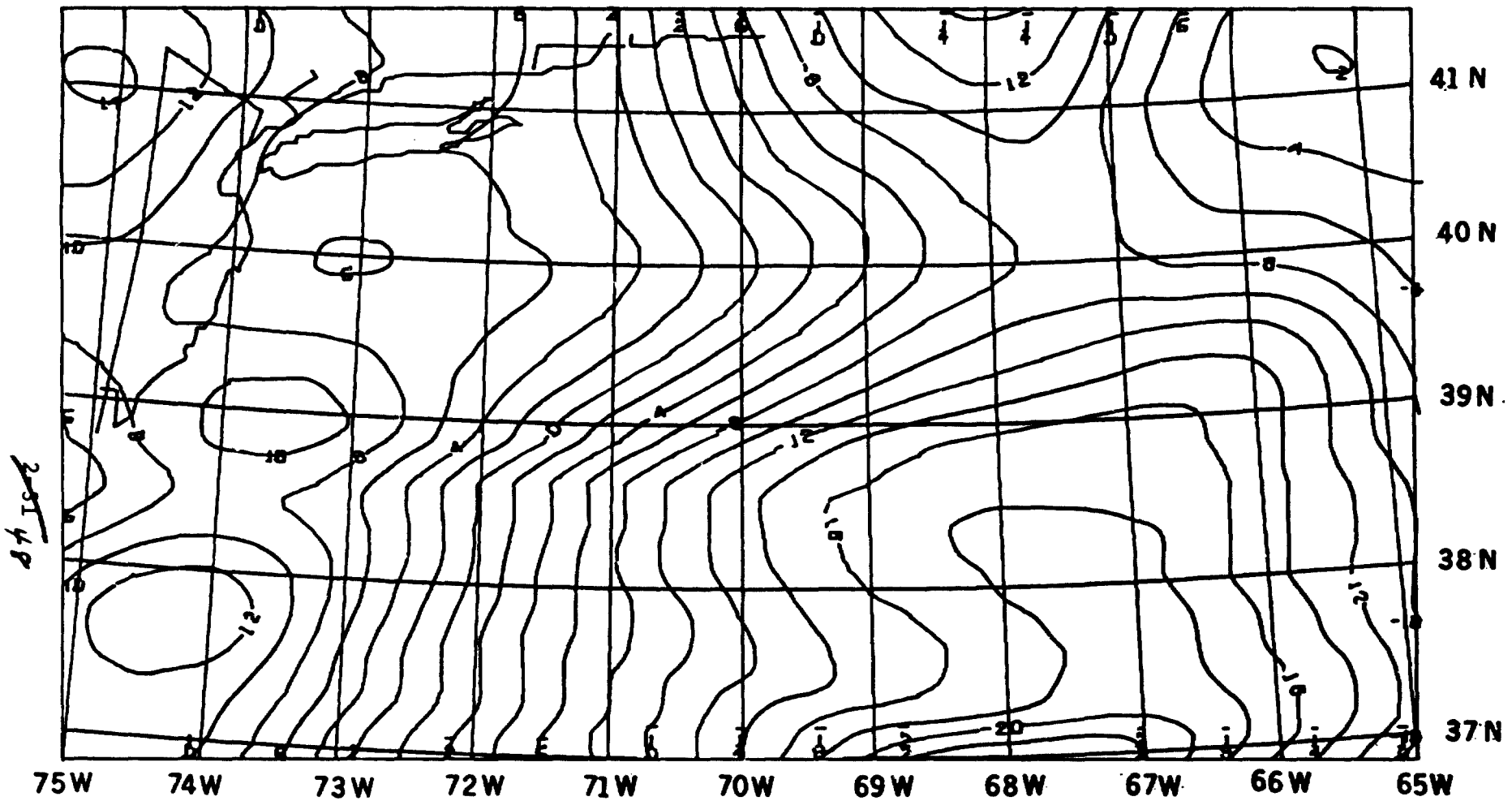

Figure 2C-7

Aeromagnetic data upward continued
to 200 km C.I.= 2 Gammas

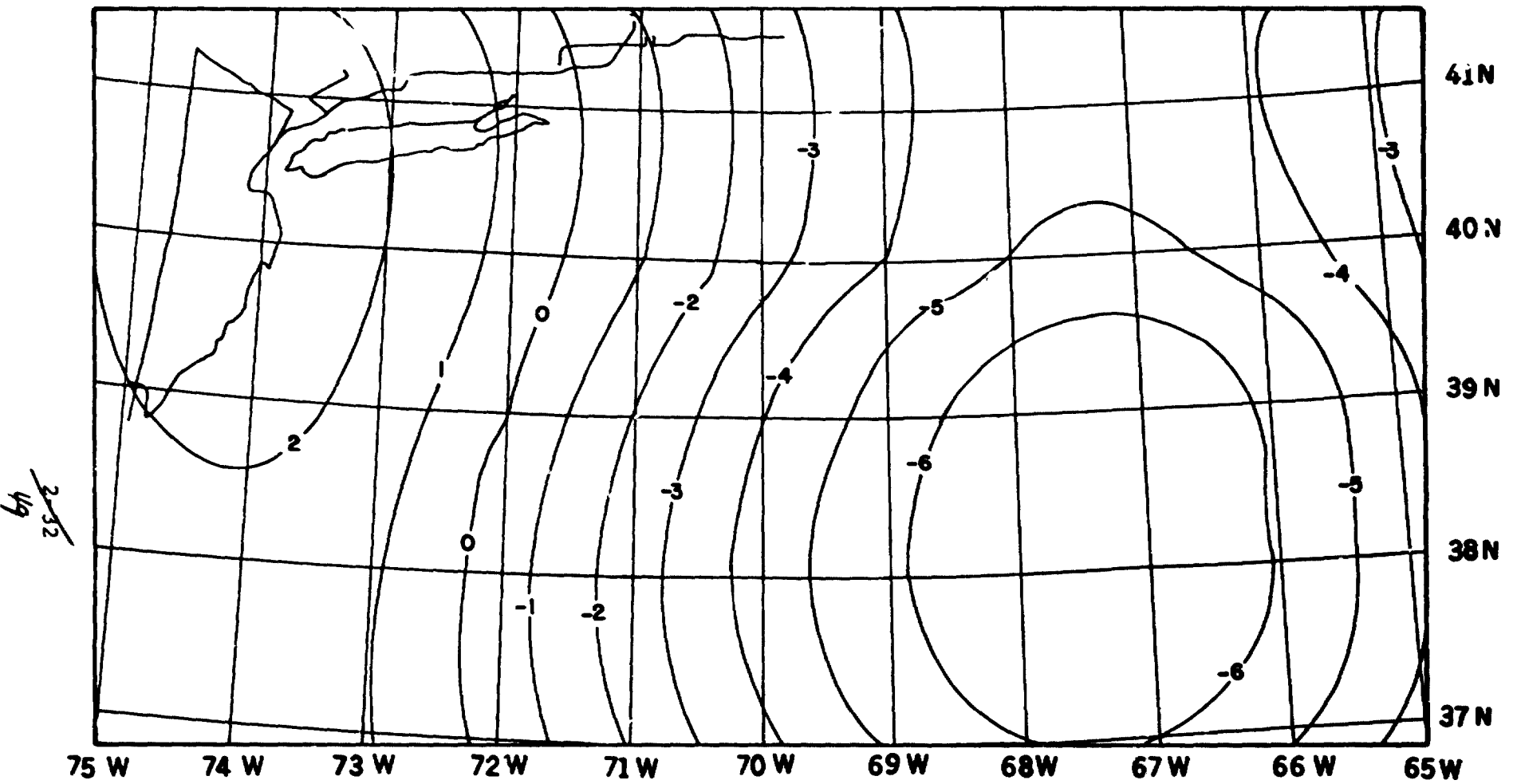

Figure 2C-8

Project Magnet Aeromagnetic data upward continued to 400 km. C.I. = 1 Gamma

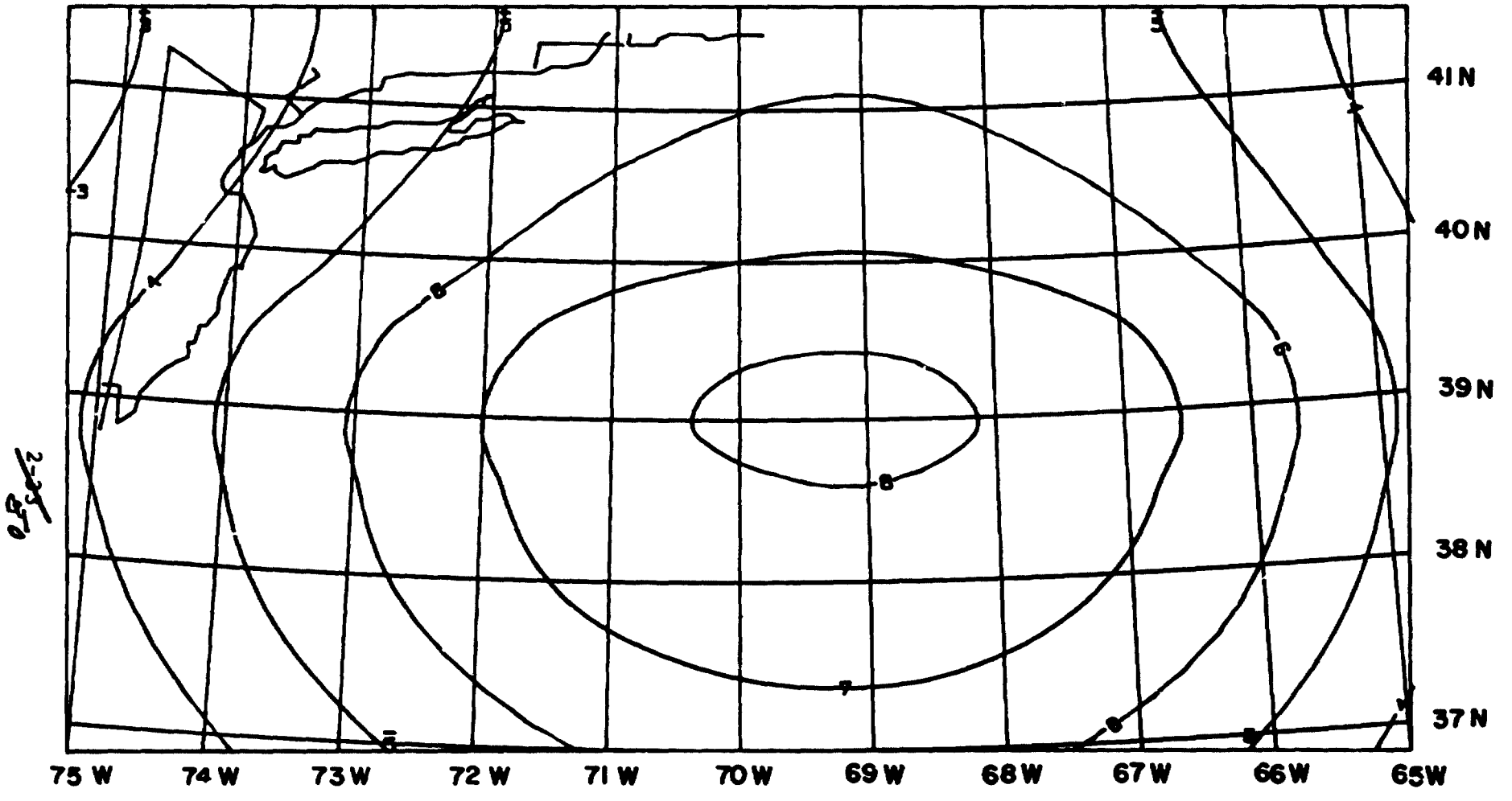

Figure 2C-9

Free Air anomaly upward continued to 400 km. C.I. = 1 Gamma

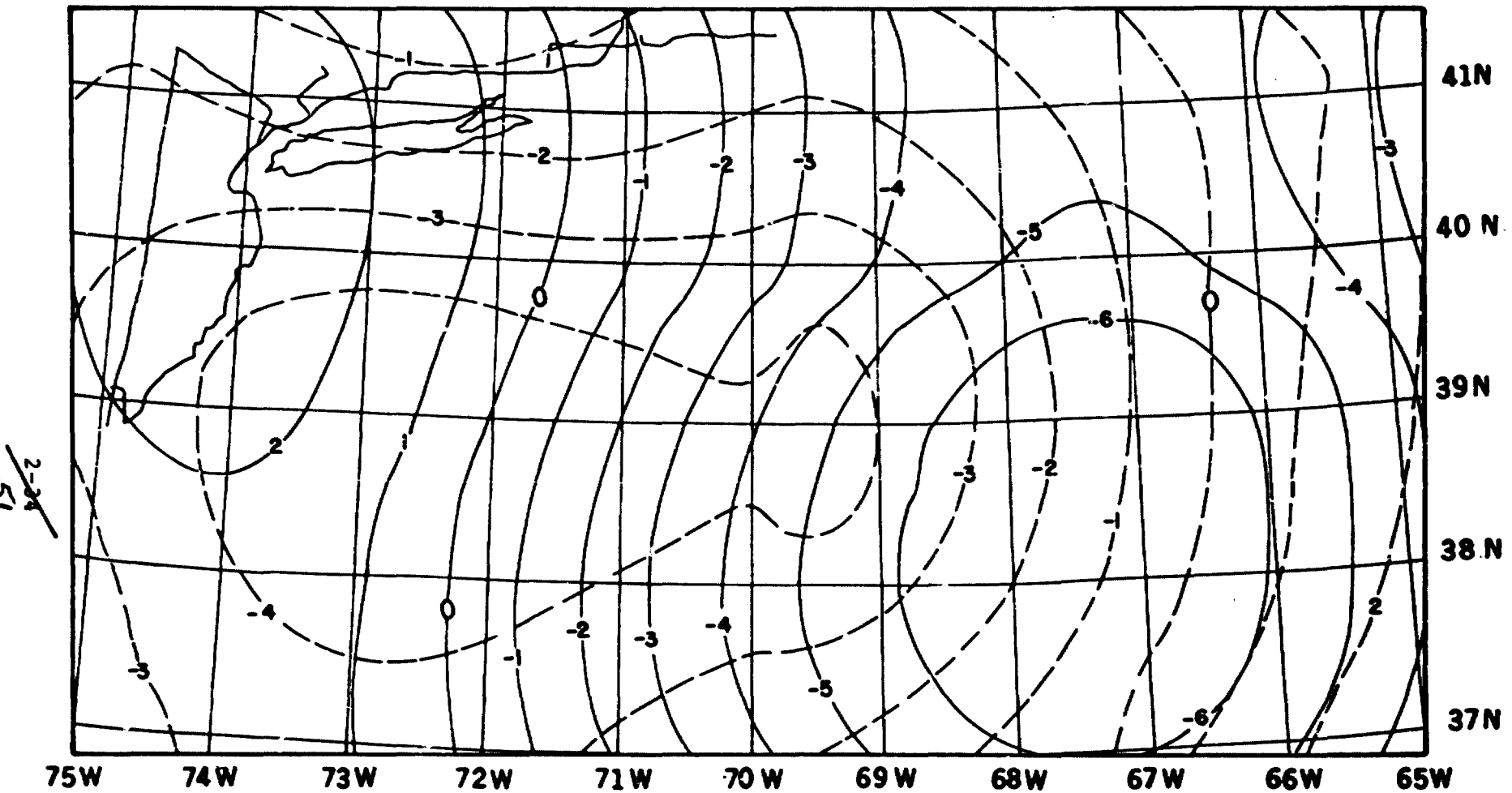

Figure 2C-10

Upward continued aeromagnetic data (solid) and
Equivalent dipole source (dashed)

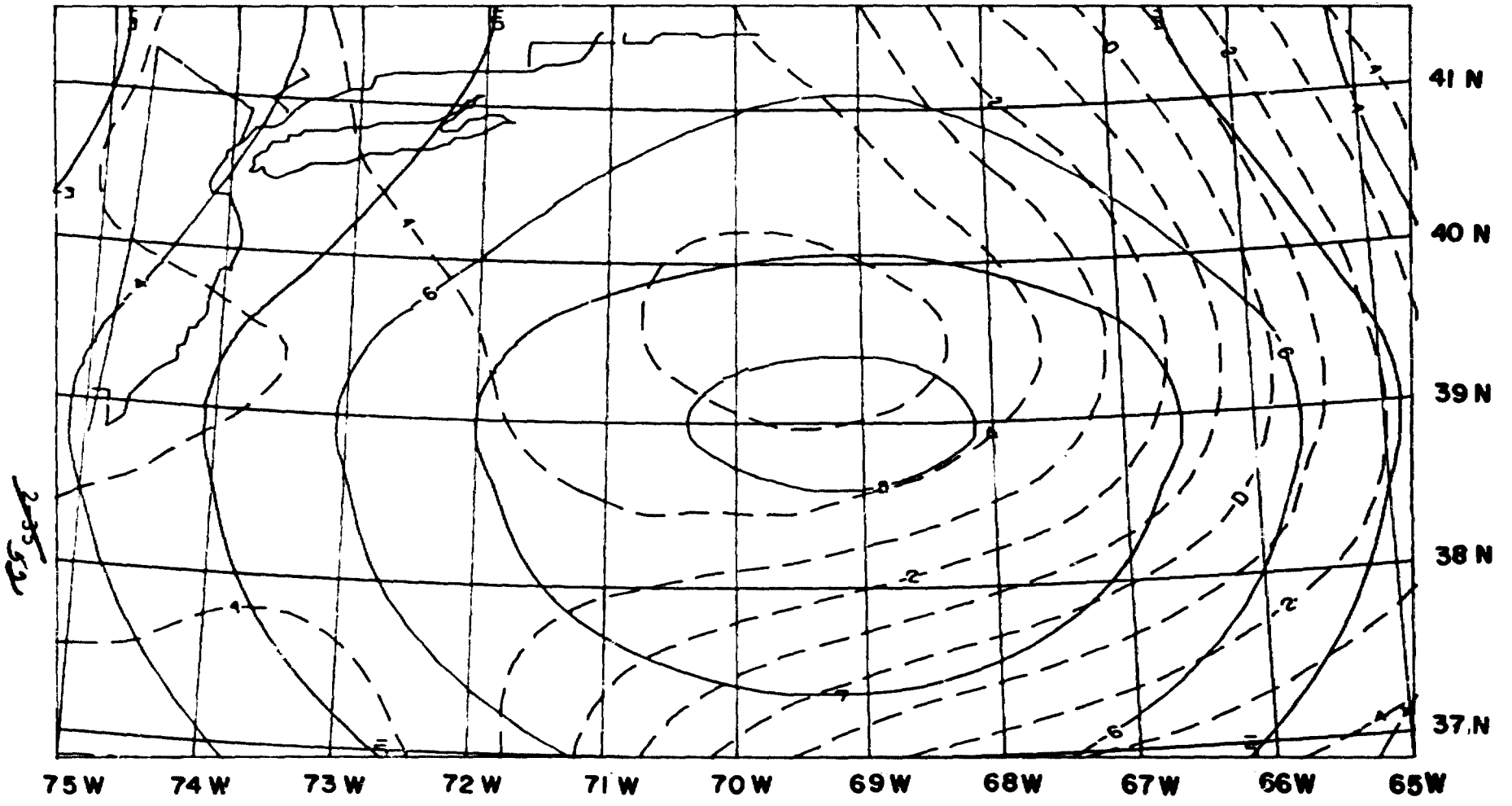

Figure 2C-11

Free Air anomaly (solid) and corrected
Pogo data (dashed) using Henderson and Cordell method

CRUSTAL STUDIES

OVERVIEW

The major objective of the crustal studies program is to use satellite-derived geopotential fields (gravity and magnetic) and techniques of comparative planetology to describe the nature, geometry, structure and evolution of the major elements of the earth's crust and upper mantle. The satellite derived magnetic field modeling efforts were described in the first section of this chapter ("Magnetic Field Modeling"), while the gravity field measurements are outlined in Chapter 4 ("Gravity Field Modeling").

The greatest limitation to this program is that only long-wavelength data are obtained from spacecraft orbiting several hundred kilometers over the earth's surface. In previous magnetic field studies we have used data obtained from three Pogo satellites, which were active between 1965 and 1972. In the near future, however, we will be able to employ the results from Magsat, which was successfully launched on October 30, 1979. Magsat is measuring both the vector and scalar magnetic fields at altitudes from 325 to 550 km; an effort will be made to utilize both data types in our crustal studies program. Analysis of the Pogo magnetic field measurements will still continue, and further refinement of some of the original orbits, using the GEM-10B field, is planned.

Satellite gravity data over land areas is currently limited to resolutions of about 500 to 1000 km. When data from Gravsat are available (planned for the mid-1980's), greater spatial definition of anomalies is expected.

Results from comparative planetology studies will be used to help define and constrain the nature and evolution of the earth's continental crust.

The crustal modeling program represents the core effort in our crustal studies investigation. Work on interpreting an anomaly in Kentucky is almost complete. A refined crustal thickness model for the eastern continental margin of the United States is beginning to be computed; this newer representation will be utilized in geopotential anomaly interpretation.

D7

D. REGIONAL MODELING: THE KENTUCKY ANOMALY

by

M.A. Mayhew, H.H. Thomas and P.J. Wasilewski

OBJECTIVES

The objectives of crustal modeling are to develop methods for using satellite magnetic and gravity data to investigate regions of nonrenewable resource potential by constructing geophysical/geological models of subsurface structure and composition and to gather correlative data and utilize it to refine crustal geological and geophysical models based on Magsat data. Correlative data will include laboratory measurements of rock magnetic properties, aeromagnetic, heat flow and seismology data.

BACKGROUND

Surface geology and drill cores to crystalline basement can, in many cases, give clues to the lithology of inaccessible levels in the Earth's crust. In regions where the sampling of rocks from depth is inadequate, indirect methods may suffice. Gravity anomalies, as an indicator of rock density, will frequently agree in sense and magnitude with magnetic anomalies; in cases where there is a lack of agreement, petrologic and physical conditions must be modelled so as to explain them. Seismology offers another indirect means of estimating rock composition at depth, but is, by itself, unable to accurately delineate rock type due to the many rock types which have similar seismic velocities. Heat flow models are unconstrained as to depth of heat production sources and thermal conductivity of intervening rock types, so unambiguous models are obtained infrequently. The aforemented data sets can often jointly constrain models so as to improve the odds for a unique solution.

Tectonic style, to the degree that associated rocks have nearly the same composition, may serve as a basis for interpreting magnetization models. Rifts, sutures, subduction zones, etc., produce characteristic rock types and thus are expected, with minor modifications for individual cases, to form a foundation for a comprehensive global model. Conversely, the models may aid in locating hidden structures with their contained mineral resources.

RECENT ACCOMPLISHMENTS

Inversions of long wavelength Pogo satellite magnetic anomaly data to an equivalent layer magnetization model reveals a very magnetic source region centered in south central Kentucky (Figure 2D-1). The magnetization maximum coincides with a gravity high elongated north-south and extending into Tennessee. The outline of the source delineated by gravity contours is also discernible in aeromagnetic anomaly patterns (Figure 2D-2). The above data along with the results from two USGS seismic refraction lines (Figure 2D-3) are combined in a two-dimensional model of the source region of the Kentucky anomaly (Figure 2D-4). The model suggests a large mass of rock which is both dense and very magnetic. We presently interpret this body to be a mafic (gabbroic) plutonic complex formed prior to the Grenville event (1.0 b.y.).

The gravity high associated with the magnetic anomaly is thought by Keller et al. (1975) to be one of a chain of highs extending down from the upper midwest formed by late Precambrian rifting. This view is supported by their analysis of a basement drill core (Figure 2D-5) containing riebeckite syenite (a sodium iron-rich rock frequently formed by hydrothermal fluids during the early stages of rifting). An abnormally high content of magnetite and hematite (Lidiak, personal communication, 1979) in a gabbroic core from just northwest of the region (Figure 2D-5) is probably indicative of the magnetization of the anomalous body.

FUTURE EMPHASIS

Measurements of the magnetic properties and mineralogical compositions of drill core samples which are derived from the mafic rocks at depth will be made to allow petrological refinements to our geophysical model.

REFERENCE

Keller, G.R., B.K. Bryan, A.E. Bland and J.K. Greenberg, "Possible Precambrian Rifting in the Southeast United States," Trans. Am. Geophys. Union, 56, 602 (abstract), 1975.

Figure 2D-1

EQUIVALENT BULK MAGNETIZATION DERIVED FROM POGO SATELLITE DATA ASSUMING A CONSTANT THICKNESS MAGNETIC CRUST OF 40 KM. UNITS ARE EMU/CC x 10^4.

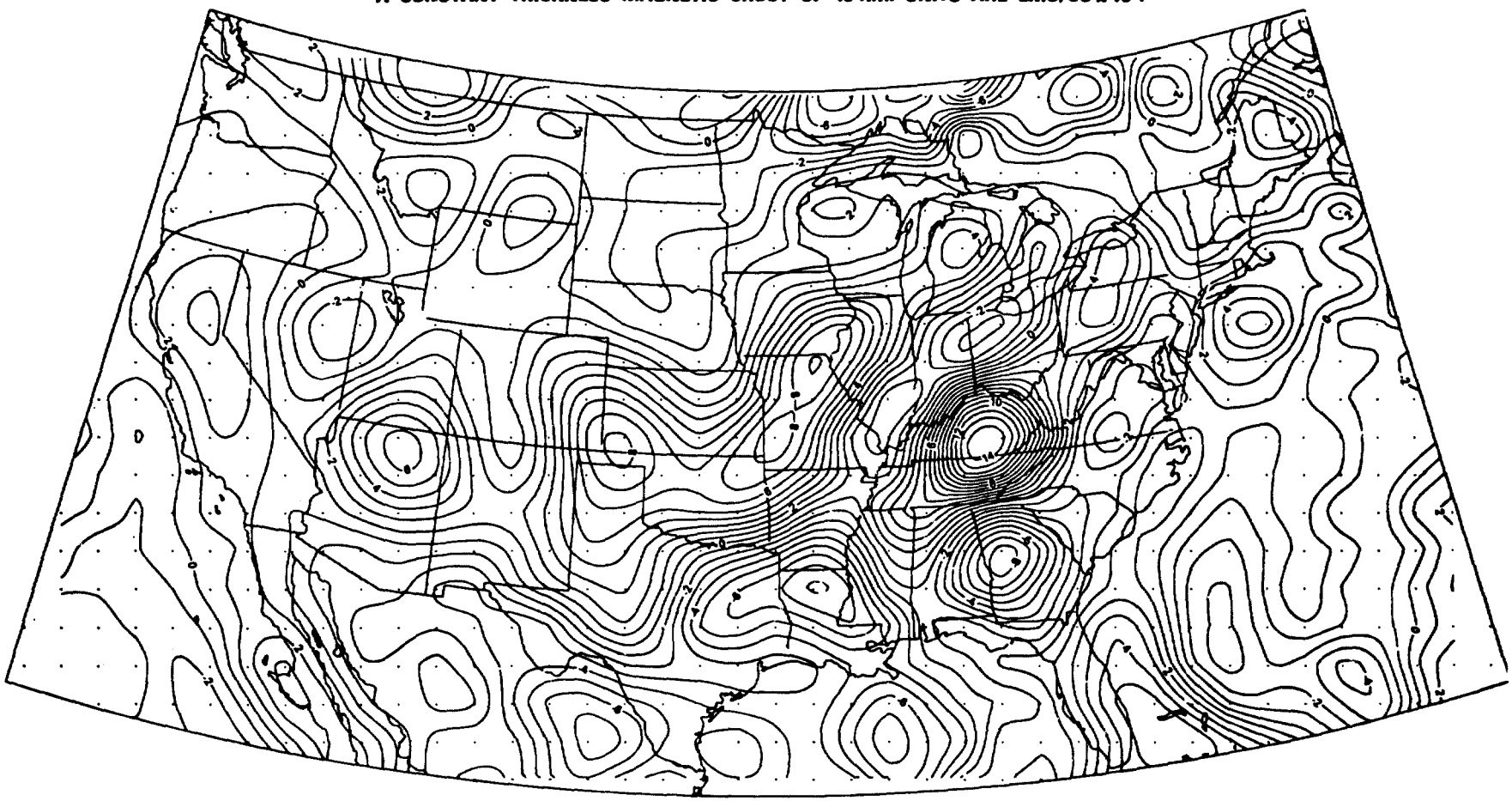

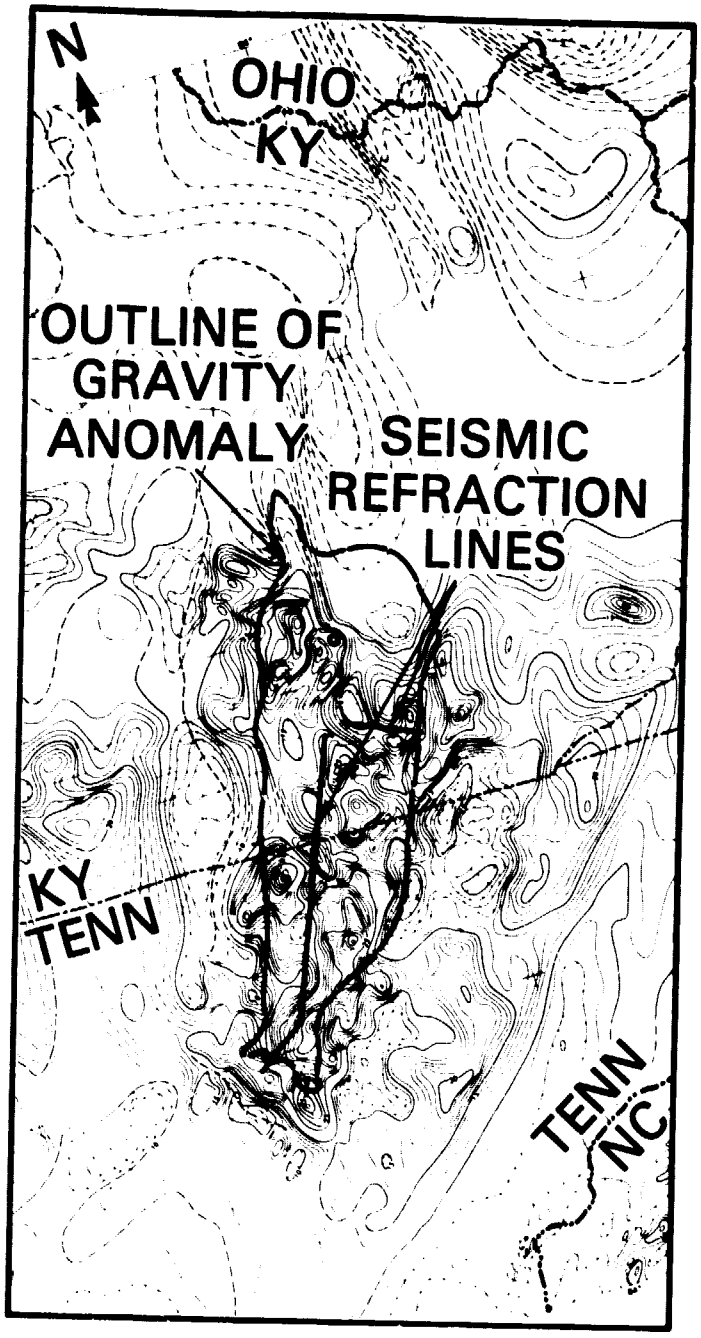

Figure 2D-2. Aeromagnetic Anomaly Map

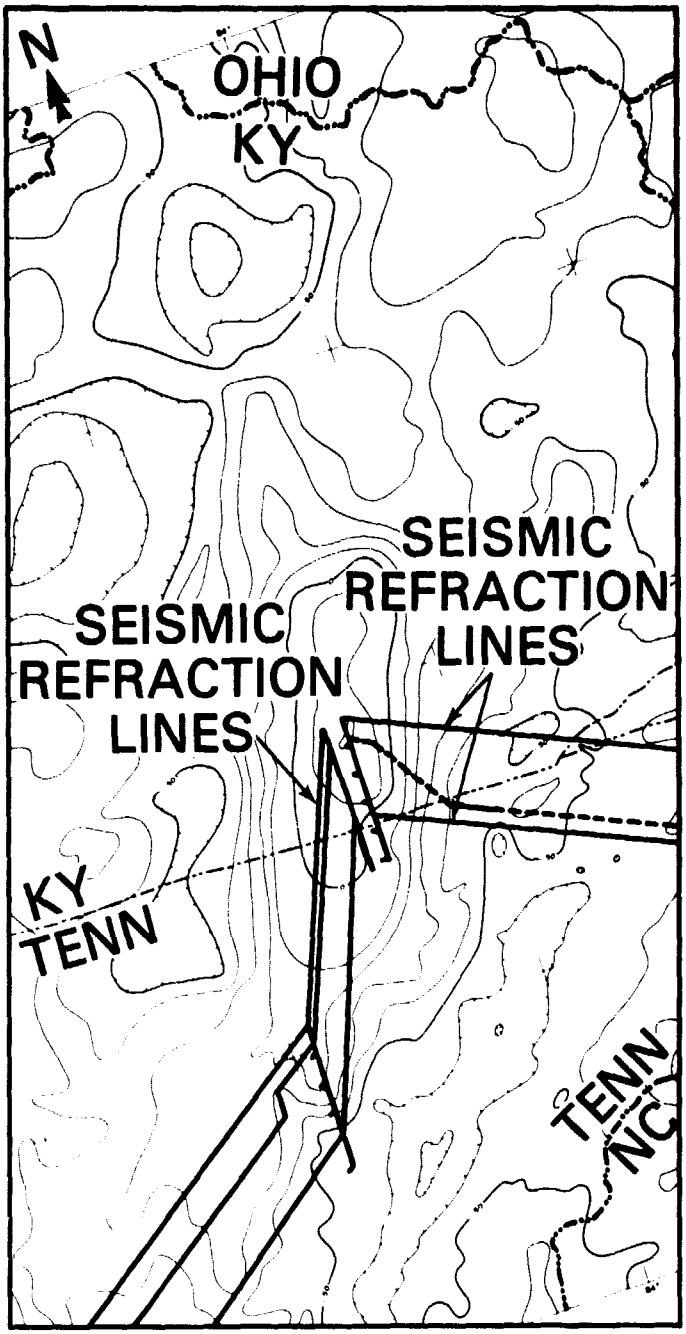

Figure 2D-3. Seismic Refraction Showing Thickening of Intermediate Crustal Layer

Figure 2D-4. **TWO DIMENSIONAL MODEL OF KENTUCKY ANOMALY**

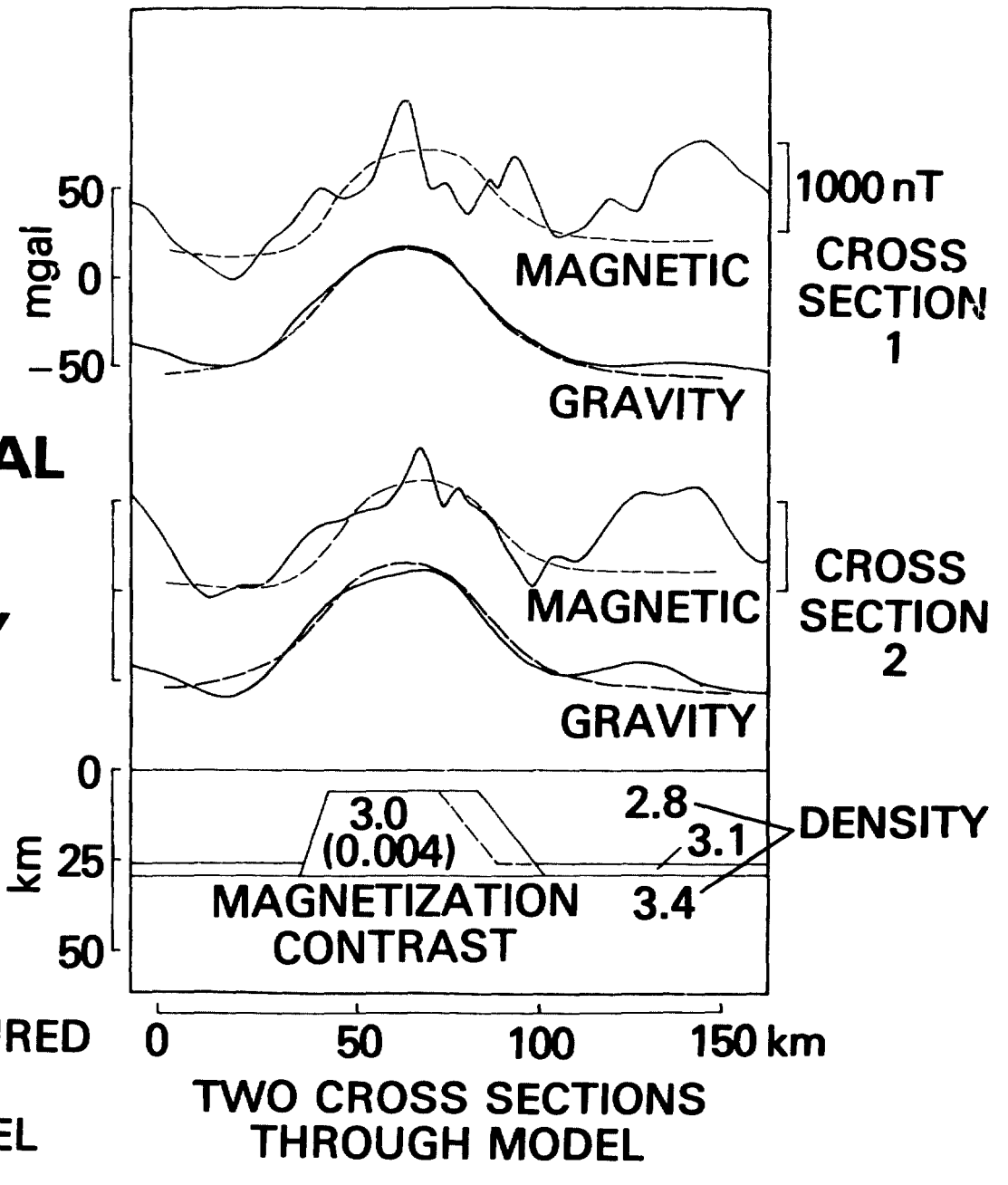

SOLID LINE = MEASURED

DASHED LINE = MODEL

Figure 2D-5

DRILL HOLES IN VICINITY OF "KENTUCKY" ANOMALY

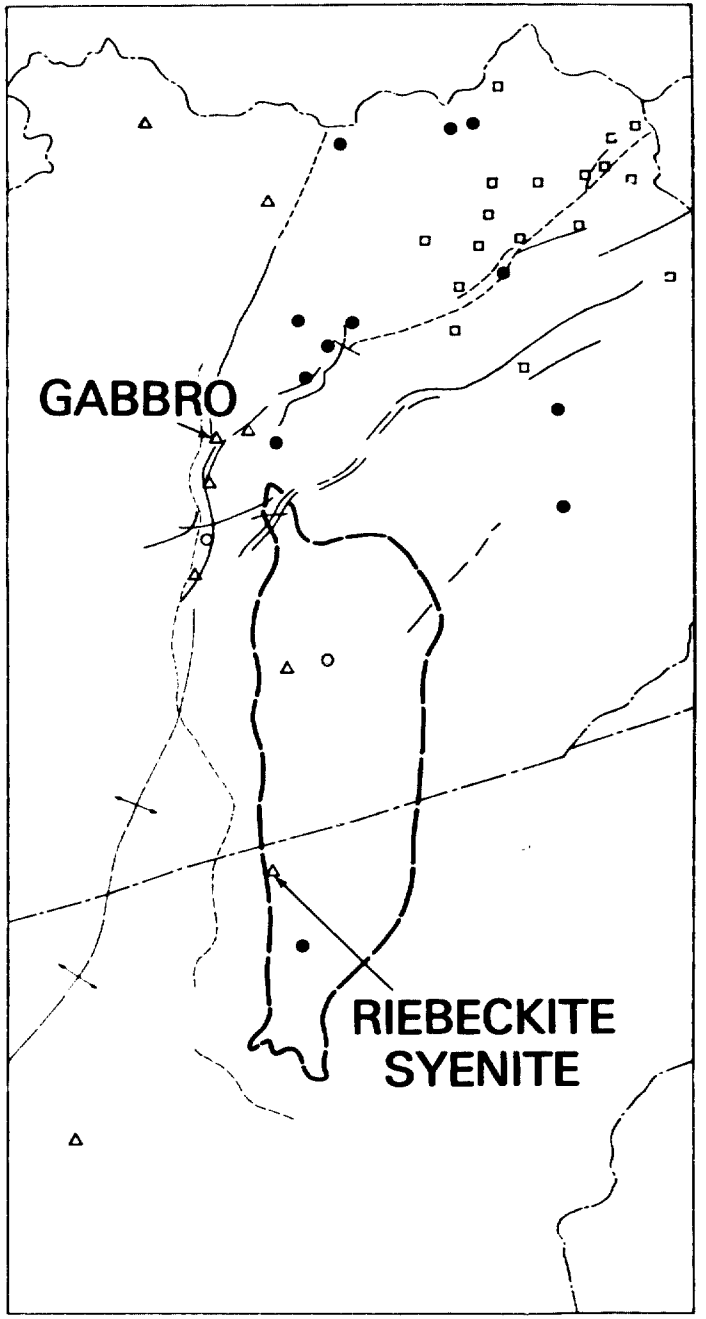

- △ VOLCANICS
- • MED-HIGH GRADE METAMORPHICS
- ○ LOW-GRADE METAMORPHICS
- □ PLUTONICS

E. REGIONAL MODELING: THE IVREA ZONE

by

P.J. Wasilewski, M.A. Mayhew and H.H. Thomas

OBJECTIVES

The objective of this study is to model the Ivrea Zone, thought to be either a continental suture or an ophiolite, as an example of a total metamorphic crustal sequence.

BACKGROUND

The Ivrea-Verbano zone comprises the western petrologic subdivision of the pre-Alpine metamorphic basement of the southern Alps in northern Italy. The Ivrea Zone plus the Strona-Ceneri zone to the east outcrop to the southeast of the Insubric Line, a mylonite zone approximately 800 km long, which extends from Greece westward to the French Alps. To the northwest of the Insubric Line are the Pennine nappes of Alpine age. Berckhemer (1969) has suggested, from observations of regional gravity anomalies and seismic structure that this terrain represents a "Crustal Chip," upturned so as to reveal rocks from the lower continental crust and upper mantle and is thus an area in which to study the petrologic nature of the crust-mantle (the Moho) boundary.

Recently, Fountain (1976) completed a model of the region based on a study of the seismic velocities of rocks from the Ivrea-Verbano and Strona-Ceneri zones (Figure 2E-1). These same rocks have been made available to us for a characterization of their magnetic properties.

RECENT ACCOMPLISHMENTS

Initial magnetic measurements on rocks from the Ivrea-Verbano and Strona-Ceneri zones of northern Italy argue for a 10-15 km thick magnetic layer bounded by the Conrad and Moho seismic discontinuities (Figure 2E-1). The data suggest that a 1-2 km thick transition layer at the Conrad discontinuity is the most magnetic zone in the magnetic layer.

FUTURE EMPHASIS

Aeromagnetic and gravity data will be, along with Fountain's seismic model, incorporated into a geophysical model of the region.

REFERENCES

Berckhemer, H., "Direct Evidence for the Composition of the Lower Crust and the Moho," Tectonophysics, 8, 97-105, 1969.

Foutain, D.M., "The Ivrea-Verbano and Strona-Ceneri Zones, Northern Italy: A Cross-Section of the Continental Crust-New Evidence from Seismic Velocities of Rock Samples," Tectonophysics, 33, 145-165, 1976.

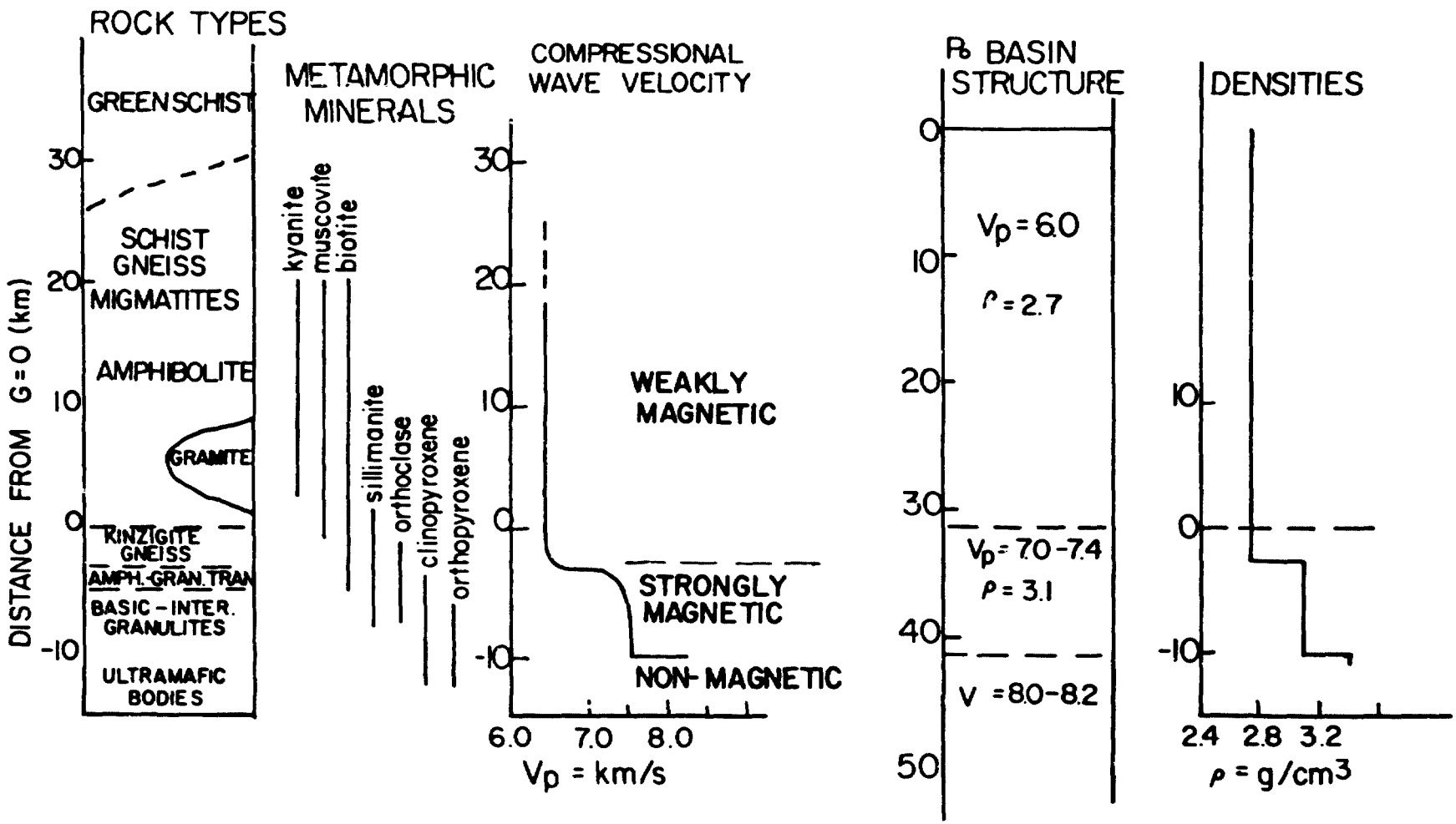

Figure 2E-1. Geophysical model of the Ivrea Zone (Modified from Fountain, 1976)

F. INTERPRETATION OF GEOID ANOMALIES IN THE VICINITY OF SUBDUCTION ZONES

by

D. C. McAdoo

OBJECTIVES

The objective of this study is the determination of density distributions in and around lithospheric slabs which are being consumed by the mantle beneath island arcs. Such determinations are primarily intended to improve the understanding of forces acting on subducting slabs.

BACKGROUND

A number of workers including McKenzie (1969) have observed that an apparent global correlation exists between trench/island arc belts and gravity highs. Expectations are that the subducting slabs possess a relative cold, dense interior which arises due to: (i) sluggish thermal diffusion from the surrounding warm mantle; (ii) elevation of mineralogical phase transitions. Gravity anomaly observations near trenches are dominated by shallow, crustal density effects and are not useful for constraining the density variations associated with slabs. Good intermediate wavelength gravity data (200-1500 km) are needed to constrain these deeper density variations. In particular sea surface altimetry data are well-suited to this task. The altimetry data directly yield an expression of the marine geoid. Further, it can be shown that direct observations of the geoid are superior to gravity anomaly observations for estimating the intermediate wavelength portion of the gravity field.

RECENT ACCOMPLISHMENTS

The approach adopted in this study is that of solving direct problems rather than inverse ones. To date work has concentrated on the southwest Pacific region. Published results detailing the shape and position of the top of the Benioff zone are used to define the position of the subducted slab beneath the Tonga-Kermadec and the New Hebrides island arc. These position results were obtained from an extensive compilation of individual earthquake hypocenter locations. The subducted slab is represented as a thin surface of anomalous mass per unit area. The surface is comprised of planar facets. Maps of predicted geoid anomalies are computed from appropriate composite integration (e.g. Figure 2F-1). In addition to slab effects, the young lithosphere of marginal basins--when contrasted with older, thicker lithosphere seaward of island arcs--gives rise to an increase in geoid height over these basins. Figure 2F-2 shows the total predicted geoid contribution of the North Fiji, South Fiji, Lau-Havre, and New Hebrides basin assuming isostasy and referencing the heights to a zero datum which corresponds to 75 my old lithosphere (see Turcotte and McAdoo, 1979).

The predicted geoid map (Figure 2F-1) was computed using an areal density of 3.2×10^5 gm cm^{-2} for the New Hebrides slabs and 1.0×10^5 gm cm^{-2} for the Tonga-Kermadec slab. A slight slab effect due to the adjacent New Guinea/Solomon island arc complex is included in this map. The general agreement between this model result (Figure 2F-1) and the mean sea surface map* in Figure 2F-3, derived from GEOS-3 altimeter data is apparent. Superposition of the marginal basin model result (Figure 2F-2) onto the slab model results in Figure 2F-1 yields a somewhat improved agreement with the sea surface map (Figure 2F-3). Specifically, this superposition increases computed geoid heights--both mean and peak--to levels approaching the sea surface map heights. Note that the mean and trend in the observed sea surface map are retained. It has not been necessary in this study to model shorter wavelength anomalies resulting from crustal and bathymetric variations.

The preliminary indication is that higher inferred density anomalies of the New Hebrides slab (3.2×10^5 gm cm^{-2}) may be due to the particularly important contribution of phase transition elevation on this young, rapidly sinking slab--a slab in its primary stage of development. This work is described in detail by a manuscript in preparation.

SIGNIFICANCE

This study has demonstrated that sea surface altimetry is particularly well-suited to the task gaining information about density distributions that are associated with subducting slabs. These inferred densities are helpful in understanding forces acting on slabs.

FUTURE EMPHASIS

This study will be extended to as many trench-island arc complexes as possible. Refined interpretations should be facilitated by use of Seasat altimeter data and development of high spatial resolution of sea surface maps.

REFERENCES AND PUBLICATIONS

McKenzie, D.P., "Speculations of the Causes and Consequences of Plate Motions," Geophys. J.R. Astr. Soc., 18, 1-32, 1969.

Turcotte, D.L. and D.C. McAdoo, "Geoid Anomalies and the Thickness of the Lithosphere," J. Geophys. Res., 84, 2381-2387, 1979.

*Part of an unpublished map due to J.G. Marsh

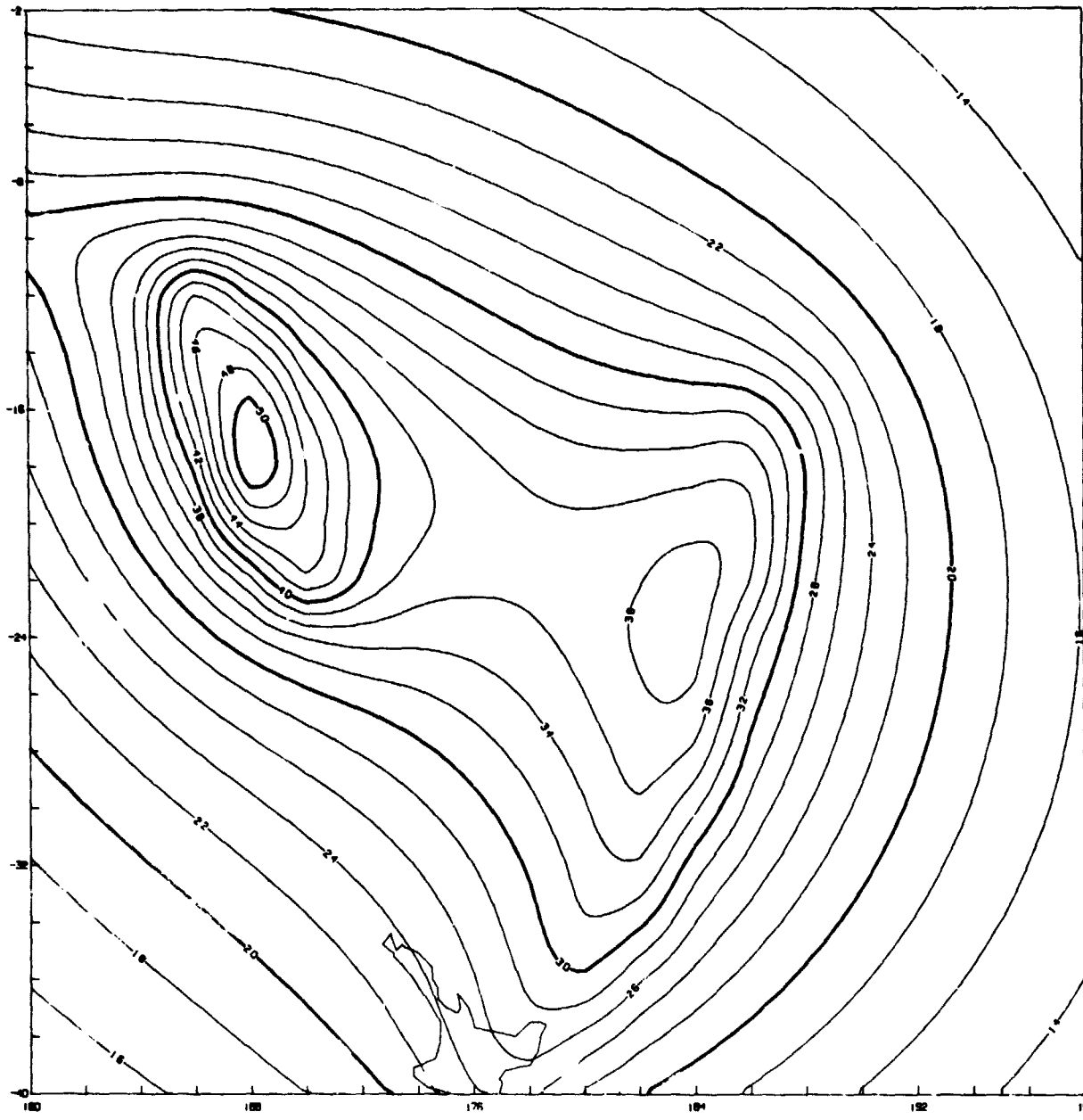

FIGURE 2F-1. Predicted geoid anomalies in meters due to Tonga-Kermadec and New Hebrides slabs.

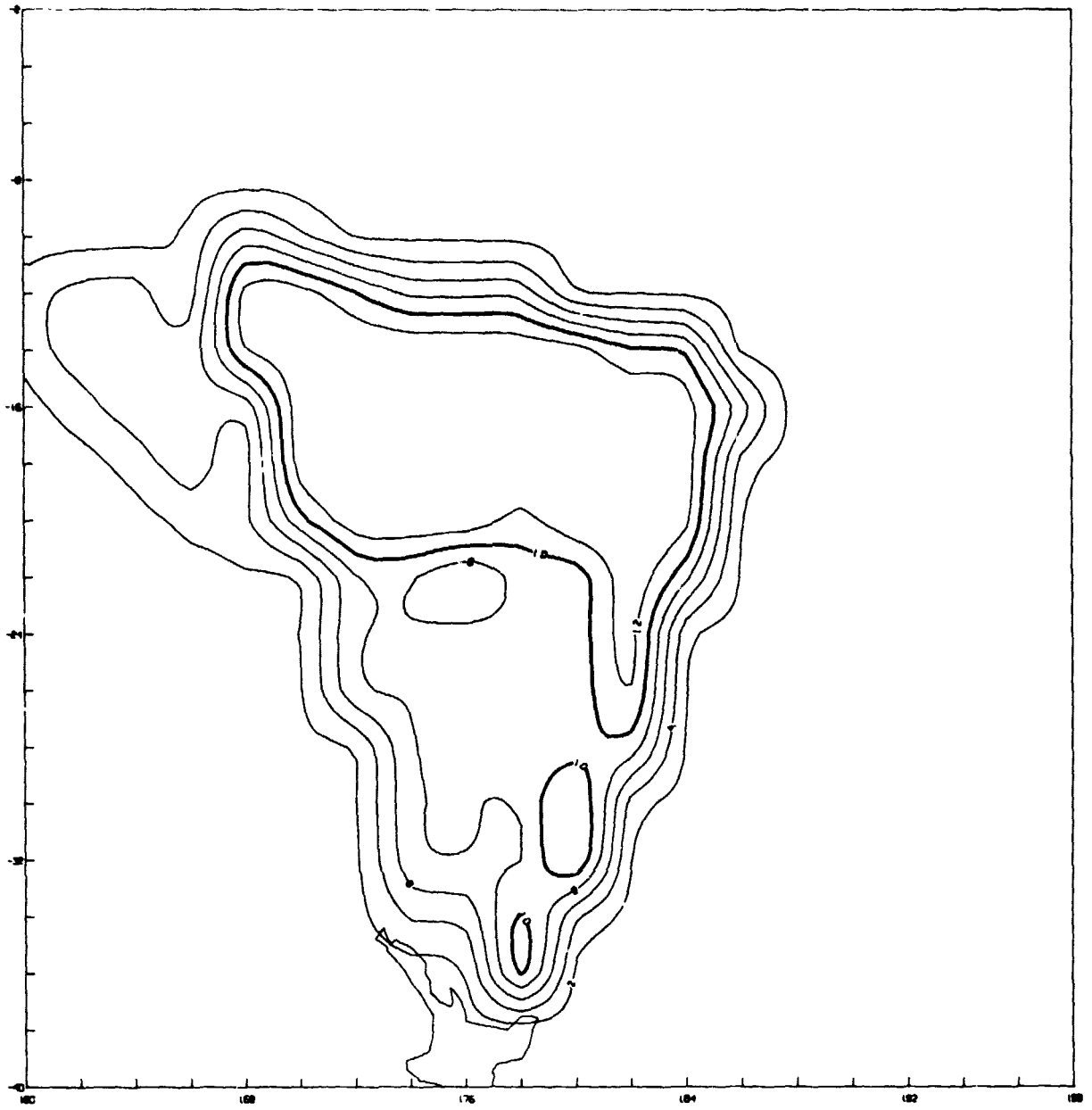

FIGURE 2F-2. Predicted geoid anomaly in meters due to young marginal basins (N. Fiji, S. Fiji, Lau-Havre, New Hebrides). Referenced to 75 m.y. old lithosphere.

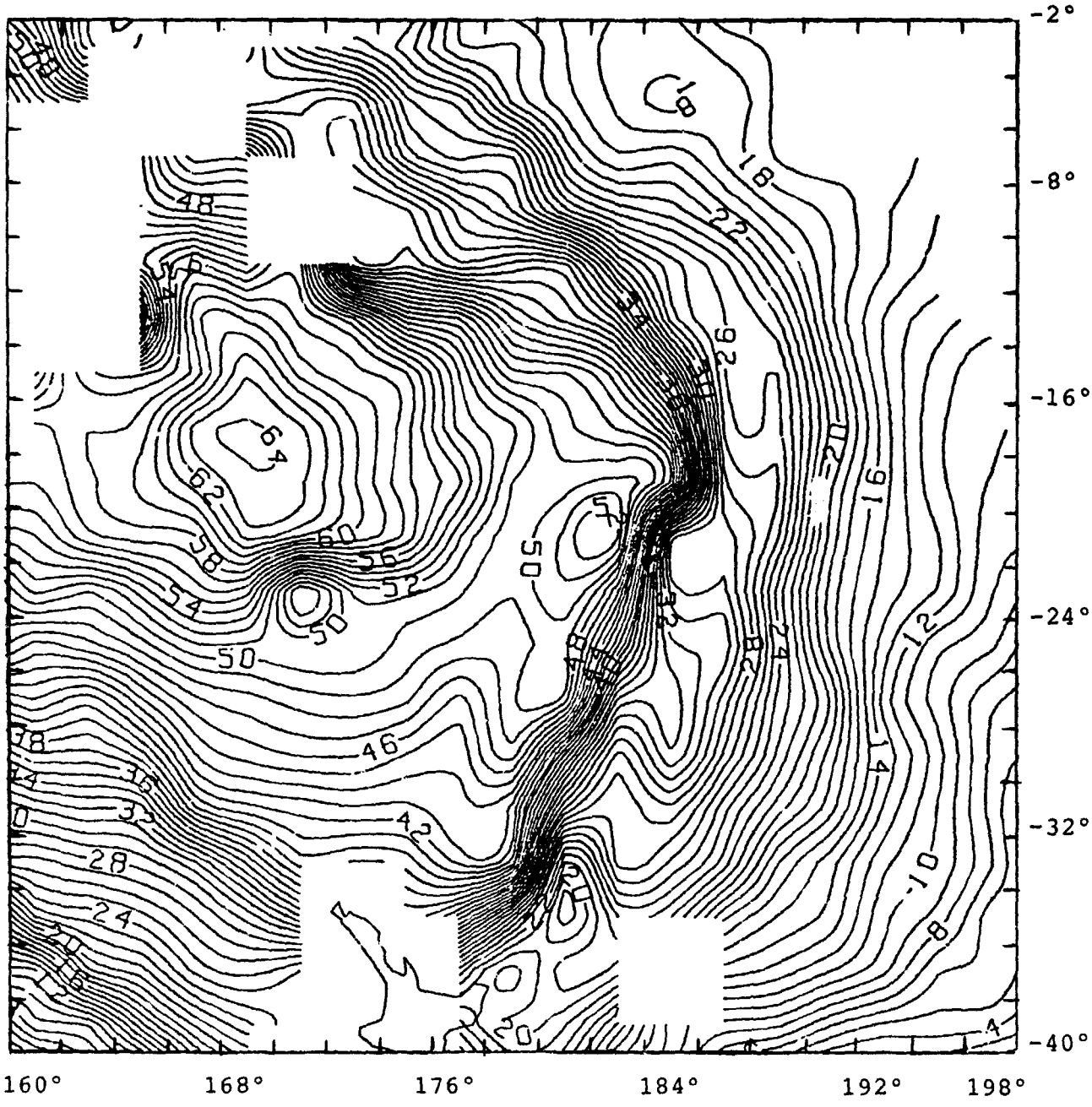

FIGURE 2F-3. Ocean surface (meters) derived from GEOS-3 altimeter data. Unpublished map due to J. G. Marsh.

D/

G. GLOBAL GEOLOGY AND GEOPHYSICS USING SATELLITE-DERIVED DATA

by

Herbert Frey

OBJECTIVES

Through use of satellite-derived geopotential data in combination with other global data sets we hope to (a) develop a generalized characterization of the broad scale properties of the lithosphere and (b) identify interesting and important geopotential anomalies and tectonic structures for detailed study and modeling.

BACKGROUND

Global magnetic anomaly maps derived from Pogo data have been studied previously in conjunction with global free-air gravity data from the GEM-10B, degree and order 13-30 field. That work demonstrated numerous cases where magnetic and gravity anomalies were coincident, and that many of these locations corresponded to known tectonic structures. Further study using additional global data sets was undertaken in order to refine these relations and begin a global characterization of the lithosphere.

RECENT ACCOMPLISHMENTS

Global distribution of rifts and sutures have been folded into the combined magnetic and gravity anomaly study to determine the relation of these anomalies to major tectonic boundaries. Major shield areas often show positive magnetic anomalies and often are the location of a strong gradient in the free-air gravity field. Anomalies in the gravity and magnetic fields are related to regions of present and past tectonic activity. Several major rift systems, both Cenozoic and older, show association with magnetic and gravity anomalies, as do portions of the recent Alpine-Himalayan suturing. Older sutures do in some cases seem to be related to anomalies, but many old tectonic boundaries often bound the anomalies, suggesting in some instances the anomalies are associated with discrete lithospheric blocks. Details are reported elsewhere (Frey, 1979).

Seismic epicenter and recent volcanism data have also been studied in a preliminary way. In general, magnetic anomalies seem to avoid regions of concentrated seismic or volcanic activity, although a few isolated exceptions do exist.

FUTURE EMPHASIS

Additional global data will be added to the above study. Of particular interest is heat flow, crustal thickness and radiometric age information. Once assembled a quantitative analysis of correlations between data sets will be undertaken, dividing the globe into equal area blocks and assigning values representing the data types to each block. Standard statistical tests will be applied.

To date the effort has concentrated on the continental crust. Detailed study of the anomalies in the oceanic lithosphere will be carried out, with topography and age data being combined with the geopotential information.

REFERENCES AND PUBLICATIONS

Frey, H., "Global Geophysics and Geology: Correlations of Satellite-Derived Gravity and Magnetic Anomalies with Rifts and Sutures," EOS, Trans. Am. Geophys. Union, 60, 398 (abstract), 1979.

H. GEOPHYSICAL ATLAS

by

P.D. Lowman, Jr. and H.V. Frey

OBJECTIVES

The objective of the geophysical atlas is to provide a tool for interpretation of satellite-derived geophysical data by presenting a variety of geophysical maps, of both surface and satellite-derived parameters, on a common scale and projection.

BACKGROUND

The geophysical atlas was first planned under RTOP 161-08-01 as part of a synthesis of earth dynamics data, and carried on under other RTOPs concerned with crustal modeling. The first version, in reduced size, was published in 1979 (Lowman and Frey, 1979), as described in the previous ESAD research report (TM 80550). Papers describing the atlas have been presented at national and international meetings, stimulating several hundred requests from industry, universities, and individual scientists and educators. The maps included in the atlas are being used at GSFC for studies of satellite-derived gravity and magnetic data, and for planning the Crustal Dynamics Program.

RECENT ACCOMPLISHMENTS

The 1:80,000,000 scale map, "Global Tectonic and Volcanic Activity of the Last One Million Years," has been thoroughly revised in preparation for submission to the Journal of Geophysical Research, and a manuscript prepared discussing its scientific implications. The revisions include modifications of continental tectonics on the basis of recent publications in the geophysical literature, in particular several papers reporting Landsat-derived mapping of central Asia. A particularly important improvement is addition of numerical plate motion rates to the map (Figure 2H-1), drawn from a recent compilation by Minster and Jordan (1978), a complete revision of the 1974 paper by Minster et al. This is the first time the Minster et al. values have been shown on a detailed global tectonic map.

The tectonic activity map has many applications and implications. It has been used as a base map for planning measurements in the Crustal Dynamics Project both at GSFC and NASA Headquarters, and by the author and others in teaching physical geology. The implications of the map stem primarily from its capability for illustrating visually already-known or suspected relationships and problems.

The most important of these problems is the question of how completely a rigid plate model describes the tectonic behavior of the Earth's crust. The map shows clearly that large areas of continental crust, in Asia, North America, Europe, and parts of South America, are behaving plastically rather than as aggregates of micro-plates. A similar problem is the relation between continental and oceanic crust. Classic plate theory considers the continent-ocean dichotomy to be essentially superficial, the primary dynamic units being the lithospheric plates.

A tectonic relationship brought out, apparently for the first time, by the map is the widespread occurrence of volcanoes on the upper blocks of continent-continent convergence zones, particularly in the Alpine-Himalayas chain. Volcanism within the last million years is shown in little-known areas as the Atlas Mountains, Rumania, Siberia, and the Seward Peninsula. This may require a re-thinking of present ideas on the relation of tectonism to volcanism.

In addition to the tectonic activity map, additional maps for the next major revision of the atlas have been prepared. These include polar maps of Pogo magnetic anomalies, an equivalent source representation of the magnetic field anomalies between $\pm 50^{o}$ latitude and satellite free air gravity maps for degree and order 13-30.

FUTURE EMPHASIS

Plans have been made for future revised and expanded editions. The first of these will be a folio size version of the present edition, with minor additions and corrections, to be published in 1980. Following this, a completely new edition will be undertaken, with improved gravity and magnetic maps and a number of new thematic maps illustrating such geophysical data as heat flow, mantle seismic velocity, and depth-coded seismic activity. Consideration is being given to having the atlas published by a non-NASA scientific organization to insure wider distribution.

REFERENCES AND PUBLICATIONS

Lowman, P.D., Jr., "A Global Tectonic Activity Map," (abstract), Abstracts with Programs, 1979 Annual Meeting, Geological Society of America, V. 11, No. 7, 469, 1979.

Lowman, P.D., Jr. and H.V. Frey, "A Geophysical Atlas for Interpretation of Satellite-Derived Data," NASA TM 79722, Goddard Space Flight Center, Greenbelt, MD 20771, 54 p., 1979.

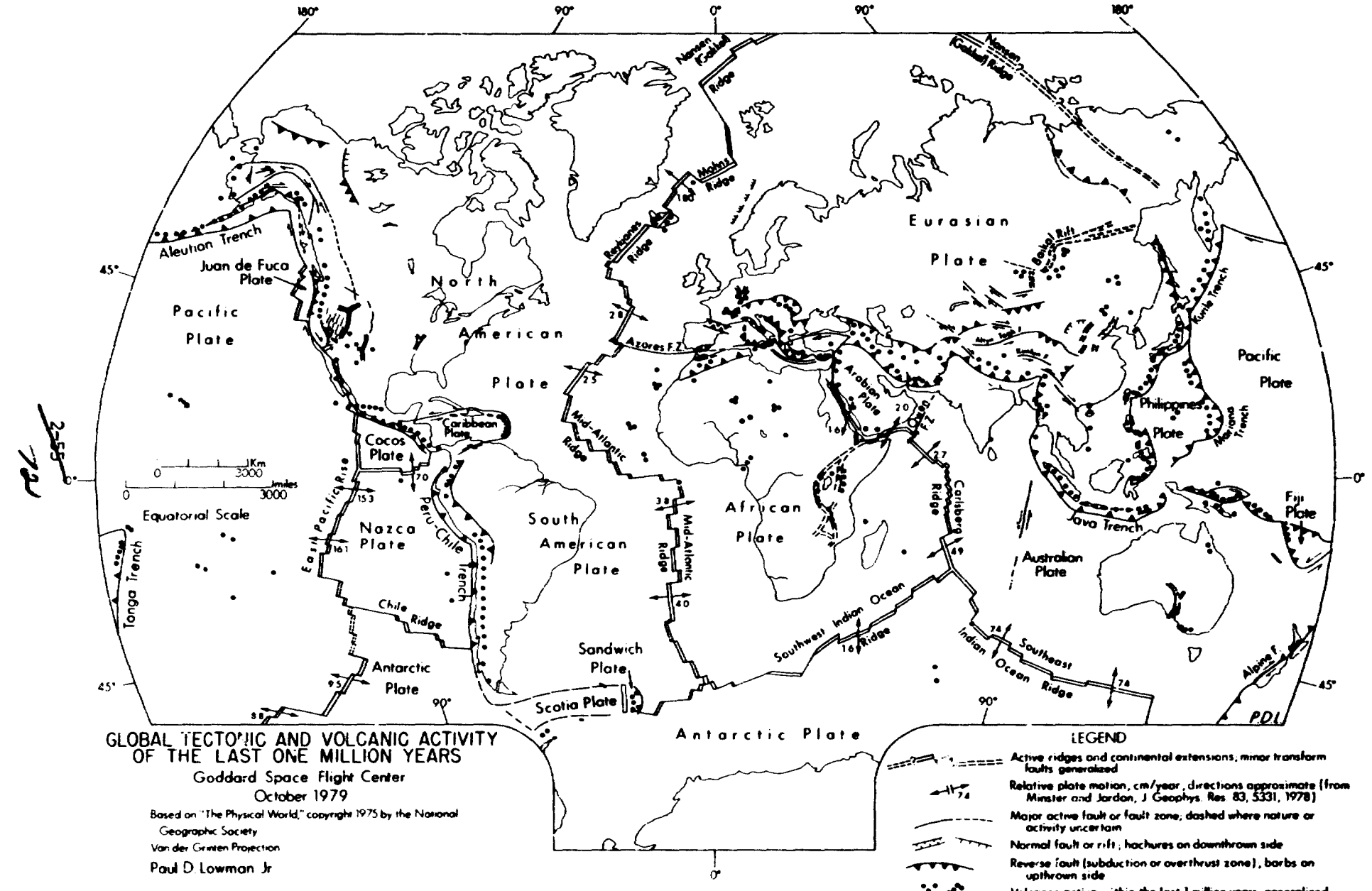
GLOBAL TECTONIC AND VOLCANIC ACTIVITY
OF THE LAST ONE MILLION YEARS
Goddard Space Flight Center
October 1979
Based on "The Physical World," copyright 1975 by the National Geographic Society
Van der Grinten Projection
Paul D. Lowman Jr.
LEGEND
Active ridges and continental extensions; minor transform faults generalized
Relative plate motion, cm/year; directions approximate (from Minster and Jordan, J. Geophys. Res. 83, 5331, 1978)
Major active fault or fault zone; dashed where nature or activity uncertain
Normal fault or rift; hachures on downthrown side
Reverse fault (subduction or overthrust zone), barbs on upthrown side
Volcanos active within the last 1 million years; generalized (some isolated basaltic centers omitted)
Equatorial Scale
Pacific Plate
North American Plate
Eurasian Plate
Nazca Plate
South American Plate
African Plate
Australian Plate
Antarctic Plate
Cocos Plate
Caribbean Plate
Philippines Plate
Juan de Fuca Plate
Scotia Plate
Sandwich Plate
Arabian Plate
Aleutian Trench
Tonga Trench
Peru-Chile Trench
Java Trench
Kuril Trench
Mariana Trench
Mid-Atlantic Ridge
East Pacific Rise
Chile Ridge
Carlsberg Ridge
Southwest Indian Ocean Ridge
Southeast Indian Ocean Ridge
Azores F.Z.
Owen F.Z.
Gakkel Ridge
Baikal Rift
Alpine F.
Fiji Plate
PDL

Figure 2H-1

D12

I. COMPARATIVE PLANETOLOGY/CRUSTAL EVOLUTION

by

Herbert Frey and P.D. Lowman, Jr.

OBJECTIVES

Use comparative planetary data to provide constraints on modeling the early evolution of the Earth's crust in order to better understand the development of the continental crust over time.

BACKGROUND

Because most of the early history of the Earth has been lost due to the great activity of this planet, clues about the early evolution are best found in the smaller, less active and less evolved terrestrial planets. For example, it would have been almost impossible to appreciate the importance of impact cratering on the early Earth without the detailed knowledge of the cratering that occurred throughout the inner solar system before 4 billion years ago. Likewise the study of volcanic and tectonic structures on planets like Mars, where they are more slowly developed and preserved for longer times, provides insight into the role of lithospheric properties and internal processes responsible for these features. We have previously investigated both the early crustal development of the Earth and how it was affected by major basin-forming impacts and the tectonic and volcanic structures of Mars as clues to the early tectonic history of the Earth. Details of these studies are described in "Earth Survey Applications Division Research Report - November 1979."

RECENT ACCOMPLISHMENTS

More realistic models of the response of the Earth's crust to major impacts were included in a revision of a manuscript on early crustal evolution. We have also concluded a detailed comparison of the size distribution of major impact basins on Mercury and the Moon, in order to place constraints on the population of large impacting bodies that struck the terrestrial planets (including the Earth) before 4 billion years ago. Mercury seems to have only 37% as many basins 200 km or larger as does the Moon (Frey and Lowry, 1979).

We have continued our study of martian rift valleys and collected Viking imagery for the study of intracanyon plateaus.

Recognition and description of pseudocraters on Mars, formed when lava flows come into contact with surface or subsurface ice, has been published (Frey et al., 1979). A detailed search for additional locations of these small volcanic domes in the northern plains of Mars is underway. Preliminary results indicate that volcanic landforms are fairly common but pseudocraters are rare outside of the original discovery area.

FUTURE EMPHASIS

Numerical modeling including convective heat transport and heat deposition by impact will be undertaken for major basin-forming events on the Earth 4 billion years ago. The modeling should make possible an assessment of the plate or micro-plate nature of the Earth's lithosphere during the early Archaean.

Comparative analysis of rift-type structures on Mars and the Earth will continue with emphasis on the role of lithospheric properties in determining the development of the structures. Terrestrial precambrian rifts will be studied as well as more recent structures. The association of volcanism with rift structures will be investigated.

The distribution of pseudocraters and small volcanic landforms on Mars will be mapped as a function of terrain type, and thermal calculations for the genesis of pseudocraters will be undertaken to determine the thickness of lava flows and the depth of ice necessary to allow formation of these features.

Comparative analysis of the gravity fields of the Earth and Mars and study of gravity anomalies as clues to lithospheric structure will begin. These studies will be tied to the rift valley investigations on both planets.

REFERENCES AND PUBLICATIONS

Frey, H. and B.L. Lowry, "Large Impact Basins on Mercury and Relative Crater Production Rates," in press, Proceed. Tenth Lunar Planet. Sci. Conf., and NASA/GSFC Technical Memorandum 80317, 1979.

Frey, H., B.L. Lowry and S.A. Chase, "Pseudocraters on Mars," in press, Jour. Geophys. Res., and NASA/GSFC Technical Memorandum 80279, 1979.

Lowman, P.D., Jr., "Impact of Technology on Planetology," Ch. 12 in "Impact of Technology on Geophysics," National Academy of Sciences, Washington, DC, 121 p., 1979.

CHAPTER 3

CRUSTAL DEFORMATION AND EARTHQUAKE MODELS

edited by

S. C. Cohen

OVERVIEW

Improving the understanding of global and regional scale motions of the crust and the occurrence of earthquake are the inter-related goals of research efforts in crustal deformations and earthquakes. Crustal deformations are important as the surface expressions of fundamental geodynamic processes. They can provide information on stresses within the earth, the interior rheology, and subsurface structure. Within the context of tectonic plate theory they play key roles in deducing relative plate motions, studying the driving mechanisms for these motions, and assessing plate rigidity. The understanding of crustal deformations also plays a potentially important role in explaining polar motion and in interpreting gravity and magnetic fields and heat flow. On a regional scale crustal deformations can provide information on the accumulation of strain in earthquake-prone areas. Geodetic measurements of such deformation are potentially useful for long-range earthquake forecasting; in addition, the detection of other anomalous crustal movements could contribute to shorter term earthquake predictions. The monitoring of postseismic crustal motions can also be expected to yield important information on earthquake mechanisms, postseismic stress redistribution, and lithosphere and asthenospheric rheology and structure. Fundamental theoretical and computational studies of both earthquakes and other processes that deform the earth's surface are necessary to provide a framework for interpreting geodetic measurements and for modeling the underlying physical processes.

The research efforts of the Earth Survey Applications Division include that of the Crustal Dynamics Project which is a space geodesy project involving the measurements and interpretations of the values of and changes in baseline distances and directions among numerous sites located both within the United States and worldwide. The Division's activities also include a program of fundamental analytic and computational studies, mission simulations, and supportive geologic field studies. The articles in this section describe many of the research activities pursued in 1979. The first paper "Crustal Deformation-Crustal Dynamics Project" describes some of the Crustal Dynamics Project planning activities particularly in regard to the selection of ground sites for the space geodesy measurements. The next paper, "Investigation of Crustal Dynamics Using VLBI," describes several recent measurements using the very long baseline interferometry technique and discusses ongoing technology and software development. The article, "Crustal Structure and Dynamics of Southeastern U.S." describes the development of structural and tectonic models of this area using seismic gravity, and magnetic data. A combined field investigation and Landsat Imagery study of regional deformation in a portion of the

California boundary betweem the North America and Pacific Plates is described in "Plate Boundary Deformation in California." The next paper summarizes work "On the Selection of Station Sites for Observing Strain Steps and Earthquake Forerunners in California." The following two papers, "GSFC Site Stability," and "Geodetic Stability of the Greenbank, West Virginia VLBI Site," describe geologic and seismic investigations of two sites being used in the Crustal Dynamics Project. A theoretical model of postseismic crustal motion and a data analysis study of spatial and temporal patterns in worldwide and regional seismicity are the subjects of the paper "Earthquake and Crustal Deformation Studies." The occurrence of "Global Intra-Plate Volcanisms" is explained in the following paper within the context of a regional stress model derived from space and ground gravity data. The section concludes with a status report on the "Development of a Seismic Data Collection Platform," a proposed space system for storing and relaying seismic data.

A. CRUSTAL DEFORMATION--CRUSTAL DYNAMICS PROJECT

by

H. Frey, R.J. Allenby and P.D. Lowman, Jr.

OBJECTIVES

The Crustal Dynamics Project proposes to apply space methods and technology to advance the scientific understanding of Earth dynamics, particularly in the fields of:

a. Supporting the U.S. national program in earthquake hazard reduction by studying dynamic processes related to earthquakes.

b. Supporting the ongoing national and international program of research in global geodynamics.

BACKGROUND

This new project, managed by Goddard, utilizes accurate geodetic positioning determined by Very-Long-Baseline-Interferometry (VLBI) and Satellite-Laser Ranging (SLR) and incorporates the following smaller projects:

a. San Andreas Fault Experiment (SAFE)

b. Laser Geodynamics Satellite (Lageos)

c. Laser Earth Dynamics (LED)

d. Lunar Ranging Experiment (LURE)

e. Pacific Plate Motion Experiment (PPME)

f. Astronomical Radio Interferometric Earth Surveying (ARIES).

RECENT ACCOMPLISHMENTS

At the request of the Project Scientist, we have investigated the question of sites and observation rationale for both VLBI and laser ranging observations relevant to Crustal Dynamics studies. We have prepared maps and documentation for some 115 sites around the world (Lowman et al., 1979) with a majority located in the western United States and North America, for global plate motion, intraplate rigidity and regional deformation measurements. To this basic list we have added recommendations from the USGS, NGS,

domestic and foreign scientists for a present total of over 200 sites (Figure 3A-1). Recommendations for selection of a basic subset of all proposed sites for occupation in 1980 and 1981 have been prepared and provided to the Project (Figure 3A-2).

FUTURE EMPHASIS

We expect to continue to provide scientific consultation for the Crustal Dynamics Project on the selection and occupation of VLBI and laser sites through 1986. As the data becomes available, we anticipate involvement in crustal dynamics modeling of global plate motion, intraplate rigidity and regional deformation in the western United States.

REFERENCES AND PUBLICATIONS

Lowman, P.D., Jr., R.J. Allenby and H.V. Frey, "Proposed Satellite Laser Ranging and Very Long Baseline Interferometry Sites for Crustal Dynamics Investigations," NASA/GSFC Technical Memorandum 80563, 1979.

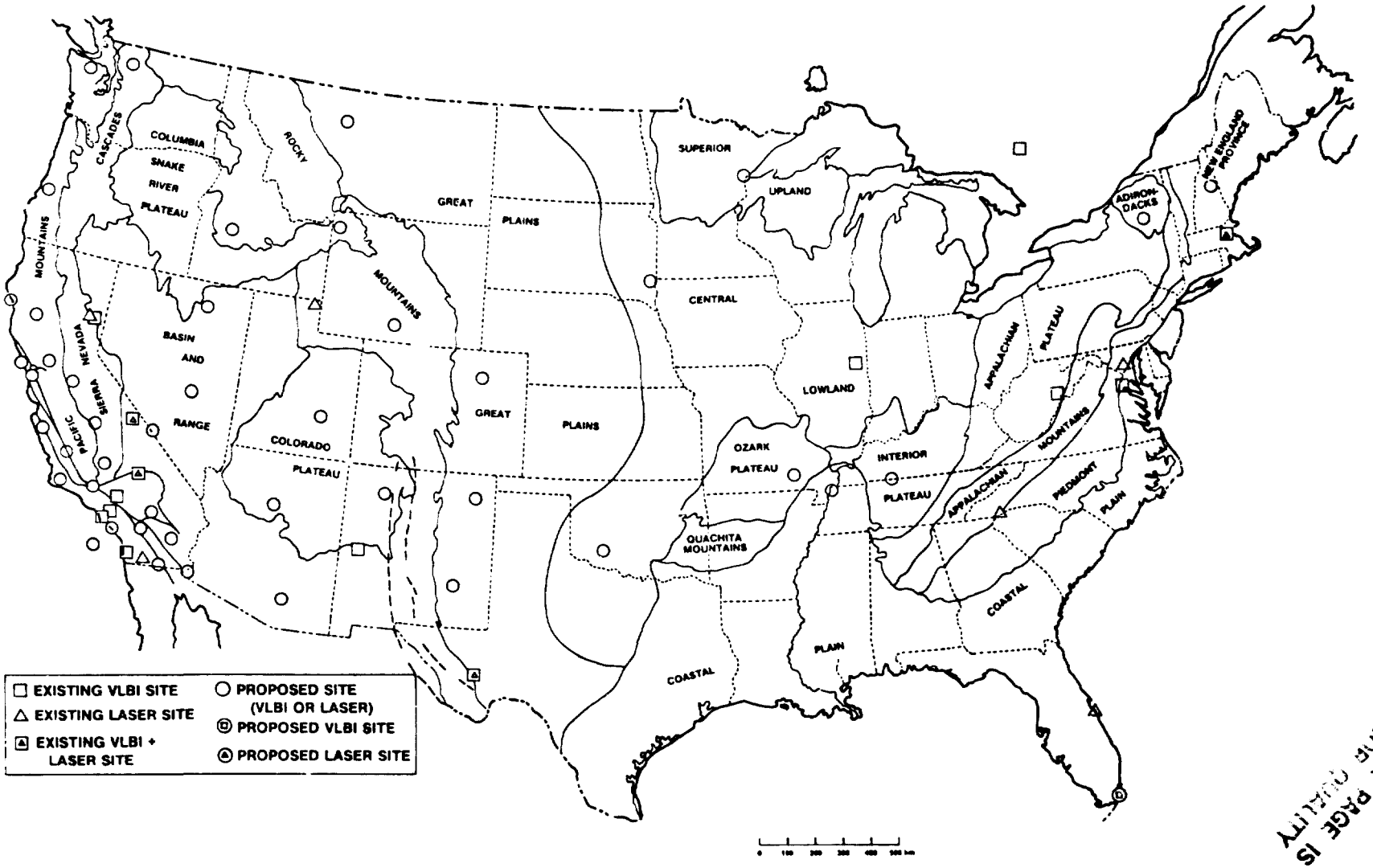

Figure 3A-1: Suggested Areas for Crustal Dynamics Station Locations in the United States

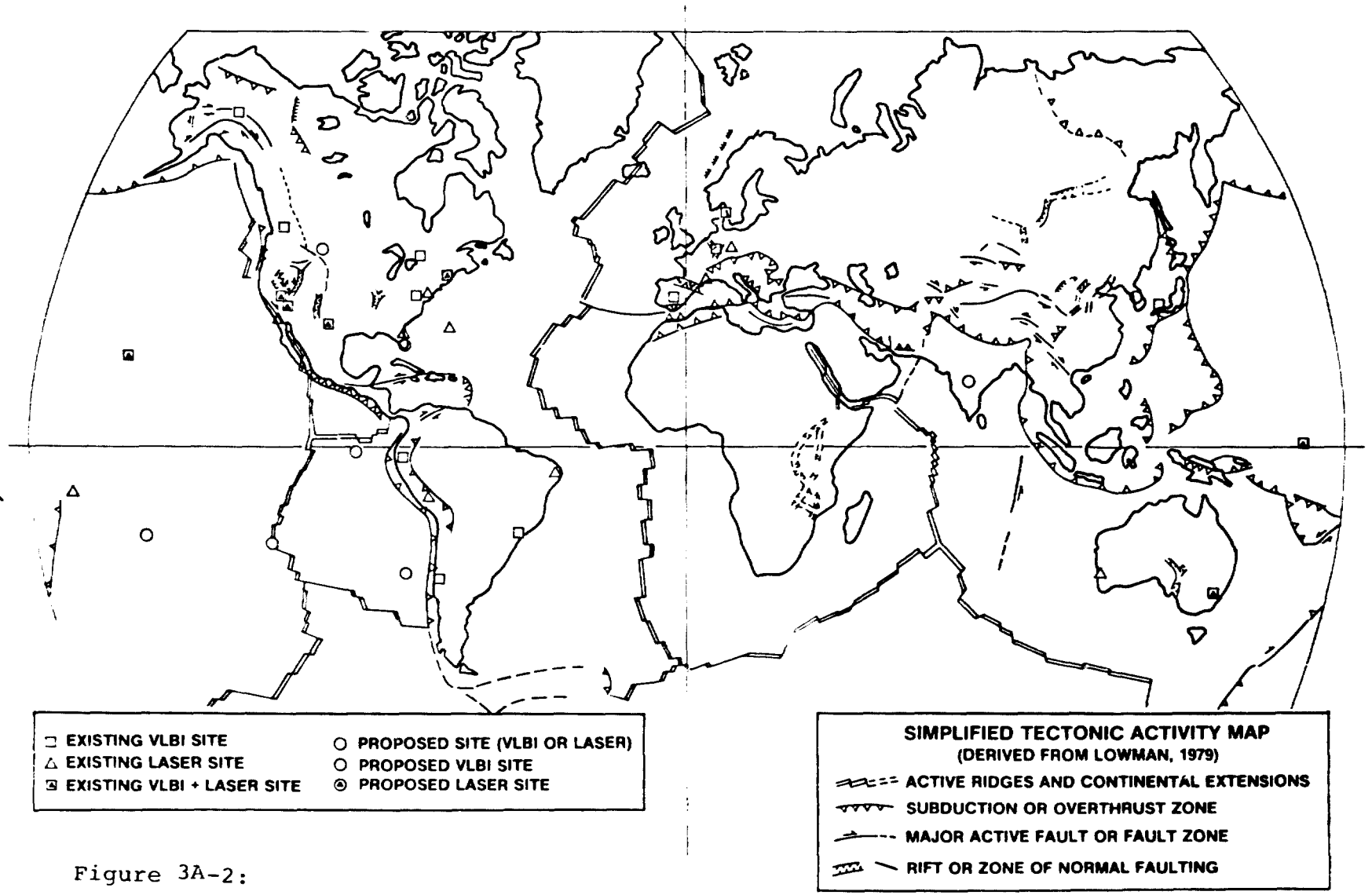

Figure 3A-2:

Basic Network of Global Crustal Dynamics Stations

D,4

B. INVESTIGATION OF CRUSTAL DYNAMICS USING VLBI

by

Chopo Ma and James W. Ryan

OBJECTIVES

The objectives of the recent Very Long Baseline Interferometry (VLBI) activities were threefold: (1) to test the new Mark III data acquisition and correlator equipment and software, (2) to make new observations using the Mark III system, and (3) to analyze VLBI data acquired to date. These objectives are preparatory to the geophysical interpretation of the much more extensive data to be obtained by the Crustal Dynamics Project in the coming years.

BACKGROUND

The VLBI activities are a continuation of efforts begun in 1974 under the proposed Pacific Plate Motion Experiment. Both VLBI and laser activities in high precision geodesy are now gathered in the Crustal Dynamics Project. The goals of the Project are to use the most appropriate space techniques to study the dynamics of the Earth's crust on three scales: global, intraplate, and regional. The VLBI efforts at GSFC have focused on transplate and interplate baselines. In addition, the same observations are used to determine polar motion and variations in rotation rate, which may be related to large scale mass movements within the crust. To meet the geodetic and geophysical objectives, new instrumentation and software have been designed and constructed.

RECENT ACCOMPLISHMENTS

The Mark III data acquisition equipment was deployed successively at the 37-m diameter antenna of Haystack Observatory (HO), Mass., the 43-m antenna of National Radio Astronomy Observatory (NRAO), W. Va., the 40-m antenna of Owens Valley Radio Observatory (OVRO), Ca., the 18-m antenna at Onsala, Sweden, and the 100-m antenna at Bonn, Federal Republic of Germany. In addition to the hardware, the Mark III field operating system, based on the same minicomputer used in the correlator and for data analysis, was designed and deployed to permit automated operation of the tape drive and electronics. Individual station requirements are handled by the software so that the same machine-readable observing schedule can be processed uniformly everywhere.

In 1979 observing sessions occurred during April (HO - NRAO), August (HO - NRAO - OVRO), and November (HO - NRAO - OVRO - Onsala - Bonn). In the last two sessions the DSN 64-m antennas at Goldstone and Madrid participated using Mark II equipment. After initial problems at each new station, especially at OVRO

where a new control room is being constructed, routine operation under the supervision of the VLBI team was achieved. The observing schedules were designed to provide precise first epoch baseline measurements, to examine sources for inclusion in the geodetic source catalog, and to compare different VLBI systems now in use within the Crustal Dynamics Project.

The data from the April and August sessions have been analyzed and look very promising. Simultaneous dual frequency observations at 2280 and 8450 MHz were used to measure the charged particle effect on the data. Cable length calibration instrumentation was used to measure thermal and mechanical effects on the time transfer cable between the station frequency standard and the receiver. The troposphere was modeled using meteorological information recorded at each site. These improvements and the Mark III system reduced the RMS post-fit residual delay below 3 cm.

The data from the last Mark I observing sessions in January, February, and May of 1978 have also been analyzed. While not of the same quality as the Mark III data, the older results complete the history of the North American baselines and give a useful first epoch measurement between North America and Europe. The formal error of the Haystack - Onsala baseline is 2 cm, although a reasonable error estimate is much higher. All data from 1976 to date have been analyzed using local meteorological information. In addition, the Mark III analysis system was applied to data taken by the German Geodetic Institute of Bonn University between Bonn and Maryland Point, Md.

The conference on "Radio Interferometry - Techniques for Geodesy" was held in Cambridge, Mass. from June 19 through 21, 1979. The conference provided an opportunity to discuss the science generated by and to be expected from VLBI geodesy and to demonstrate the Mark III system to the worldwide geodetic community. The Crustal Dynamics group presented a number of papers, which will appear in the NASA Conference Proceedings in early 1980.

FUTURE EMPHASIS

Future work will continue to be in two areas: new observations with refined analysis and interpretation.

The Mark III system will be deployed at Harvard Radio Astronomy Station, Texas in early 1980. The midcontinent site will permit more detailed study of intraplate deformation in North America, particularly across the Basin and Range Province where local deformation has been suggested. The field operating system will be properly documented and tested for complete operation by station personnel. Observations between North America and Europe will be expanded. The interface between the scheduling program and the correlator software will be improved to speed data reduction. Observing sessions will be scheduled every 2-4

months to acquire new data and to test and develop the Mark III system. As new radio sources are checked and found useful, they will be added to the geodetic source catalog.

A considerable effort will be made to support the MERIT (Monitoring of Earth Rotation and Intercomparison of Techniques) program, which is to show the capabilities of modern techniques to measure polar motion and variations in rotation rate. During the MERIT window, August through October, 1980, concentrated observations will be made for comparison with other methods.

In order to take advantage of the improved data, the Mark III analytical software will continue to be upgraded. Within the Crustal Dynamics Project, a coordinated change to the best models for precession, nutation, and sidereal rotation and to epoch 2000.0 source positions will be made. These changes will facilitate comparison of results among the high precision space geodesy techniques. Improved models for source structure and antenna flexure, especially for the Bonn 100-m, will be investigated. The program CALC, which computes theoreticals and partial derivatives on the IBM 360/91, will be moved to the Mark III minicomputer to consolidate operations. SOLV2, an improved version of the parameter adjustment program designed to handle large data sets exploiting arc-parameter elimination, will be ready in early 1980.

C. CRUSTAL STRUCTURE AND DYNAMICS OF SOUTHEASTERN U.S.

by

R.J. Allenby and M.A. Mayhew

OBJECTIVES

The primary objective of this effort is to develop structural and tectonic models of the southeastern United States through a synthesis and re-interpretation of seismic, gravity, and magnetic data.

BACKGROUND

A knowledge of the thickness, composition and dynamic stability of the Earth's crust is critical to locating geodetic sites for NASA's crustal dynamics project, interpreting and modeling gravity and magnetic satellite data. We are initiating such a crustal study in the southeastern U.S. by re-interpreting deep refraction data obtained by the 1965 East Coast Onshore-Offshore Experiment (ECOOE), a cooperative effort that involved 11 participating institutes and obtained over 1100 records from a shot and station array covering portions of Maryland, Virginia, West Virginia, North Carolina, South Carolina, Georgia, Tennessee and Kentucky.

The accuracy of the initial interpretation of these results by James et al., 1968, was reduced by his assumption of a simple, one layer crust above the Moho--an assumption we now know to be erroneous. Since then a substantial body of new refraction data has been collected, improved velocity models based on surface wave dispersion studies have been constructed, and long wavelength satellite gravity and magnetic results have become available. We propose to carry out a synthesis of these data, something that has not hitherto been done.

RECENT ACCOMPLISHMENTS

A complete compilation of station and shot locations and profiles for travel times has been obtained (Hales, 1967). All ECOOE source and receiver locations have been punched and are being plotted. Punching is proceeding on the travel time profiles. It is anticipated that modeling of the ECOOE crustal data will be completed in CY80.

FUTURE EMPHASIS

The initial ECOOE area of study will be expanded utilizing the large amount of neighboring refraction and earthquake data that has become available since the initial ECOOE survey. Pogo, Magsat, satellite gravity and geodetic data will be incorporated into the expanding model.

REFERENCES AND PUBLICATIONS

James, D.E., T.J. Smith and J.S. Steinhart, "Crustal Structure of the Middle Atlantic States," Jour. Geophys. Res., 73, 1983-2007, 1968.

Hales, A.L., "The East Coast Onshore-Offshore Experiment, I. The First Arrival Phases," Air Force Office of Scientific Research, Contract AF49(638)-1542, March 1967.

D/6

N80-20739

D. PLATE BOUNDARY DEFORMATION IN CALIFORNIA

by

P.D. Lowman, Jr.

OBJECTIVES

The objective of the work reported here was to learn more about the distribution of fault movement in the boundary zone between the North American and Pacific Plates in southern California, and in particular about the nature of movement along several faults thought to be related to the San Andreas fault.

BACKGROUND

The Crustal Dynamics Program, including VLBI and satellite laser ranging, will depend heavily in its initial stages on studies of the North American-Pacific Plate boundary zone in southern California. Measurements have already been made of plate motions in this area under the SAFE and ARIES programs, with the general objective of developing a comprehensive and accurate model of crustal deformation. The problem is a complex one for several reasons, a major one being that the plate boundary in this area consists of not one but many active faults in an area of several thousand square kilometers. Experiment planning and data both require knowledge of local tectonics in southern California, and consequently field studies previously carried out as a continuation of a Landsat investigation are now being applied to the Crustal Dynamics Program.

RECENT ACCOMPLISHMENTS

The Elsinore fault of southern California, with a length of about 150 km, is the most prominent member of the San Andreas system south of the Transverse Ranges (Figure 3D-1). It is active though at a low level, and hence is important for understanding SAFE results and for planning future investigations under the Crustal Dynamics Program. A key question is the nature of displacement on the Elsinore and related northwest-trending faults: is it primarily horizontal (strike-slip), as generally believed, or vertical (dip-slip)?

Early investigations using Apollo 9 photographs (Lowman, 1969) revealed that the Elsinore fault is crossed by a number of lineaments that are not offset laterally. This surprising discovery stimulated field reconnaissance that confirmed lack of offset in the Sawtooth Range of San Diego County. Further field investigations were carried out in 1979 to study the nature of the Sawtooth Range-Elsinore fault intersection, and to see if possible strike-slip movement on the northern Elsinore fault could be taken up by movement on two sub-parallel faults, the Earthquake Valley and San Felipe faults, to the east. The technique used was structural reconnaissance of the bedrock geology, which in this area is chiefly Mesozoic, and hence older than any Cenozoic movement on the faults in question. Results were the following.

Elsinore Fault

Structure in batholithic and pre-batholithic rocks has been traced for about 6.5 km (Figures 3D-2, 3D-3) across the Elsinore fault between Vallecito and Mason Valleys. Foliation and flow structure make about a 60° angle with the fault, yet show no significant offset, i.e., not more than a few hundred meters. This conclusion obviously conflicts with contemporary estimates of displacement on the fault, such as that of Crowell and Sylvester (1979) who propose some 30 km on the Elsinore fault. However, the geometry and structural data, which have in this area been independently confirmed by V.R. Todd of the U.S. Geological Survey, seem to point unambiguously to the conclusion that the Elsinore fault is not a strike-slip fault. This implies that it has been formed primarily by crustal extension, not shear.

Earthquake Valley Fault (Figure 3D-5)

The next major fault to the northeast is roughly parallel to the Elsinore fault, and should have similar displacement. A structural reconnaissance around the southeast perimeter of Earthquake Valley, the North Pinyon Mountains, was made to see if there was evidence of substantial strike-slip. The rock covered in this traverse was almost entirely igneous (tonalite), and accordingly, the features mapped (Figure 3D-4) were almost all flow structures (aligned crystals, inclusions, and fractures parallel to these). Such structures were formed of course when the rock was intruded, and hence are Cretaceous in age, far pre-dating the Earthquake Valley fault. It was found that there is no obvious structural dislocation or change (Figure 3D-6) in rock type across the trace of the fault or faults. Furthermore, air photos of mountains bounding the south end of the valley, which should be cut by the fault if it has undergone major strike-slip, show no preferred drainage suggesting a continuation of the fault. It is concluded that the Earthquake Valley fault has not had major (i.e., more than a kilometer or so) horizontal displacement.

San Felipe Fault

The San Felipe fault trends more easterly than do the Elsinore and Earthquake Valley faults, but is clearly a member of the Elsinore fault zone. A key spot for studying displacement on the San Felipe fault is "The Narrows," a gap in Yaqui Ridge. Orbital and aerial photos show that the fault should cut crystalline bedrock there, and if it has undergone major strike-slip, there should be structural or lithologic disruption. A brief reconnaissance of Quartz Vein Wash and adjacent ridges, through which the San Felipe fault is shown on all published maps to pass, was made. It was found that the San Felipe fault either makes a 35-40° turn within a few hundred meters, or stops at Yaqui Ridge. Either possibility rules out major strike-slip, and probably any strike-slip at all.

SIGNIFICANCE

This investigation is of interest as an example of how orbital remote sensing imagery can be used to guide ground investigations of regional structure. The results presented here represent only about three weeks of total field time over a period of several years. However, the area investigated covered several hundred square kilometers, and it was possible by using orbital imagery to narrow this down to the few square kilometers actually mapped in some detail.

More important, the conclusions of this investigation contradict almost all publications on southern California tectonics, in which the series of northwest-trending faults cutting the Peninsular Ranges are considered as strike-slip faults formed by the same forces that produced the San Andreas. The extensional nature of the Elsinore and related faults implies instead that the Peninsular Ranges are probably more closely related to the Basin and Range Province. They were probably formed during a period of crustal extension perhaps 8 to 10 million years ago along with the early Gulf of California, then cut by transform faults of the San Andreas system beginning about 4 million years ago.

The significance of these results for the Crustal Dynamics Program is that present plate motion in this area is probably being accounted for solely by the San Andreas and San Jacinto faults, and that the low level seismic activity along the Elsinore fault is probably not part of the inter-plate movement. If this conclusion is correct, it implies that inter-plate measurements made by space techniques (laser ranging, VLBI, or ground-based retro-reflectors) should have ground sites east of the San Felipe fault.

FUTURE EMPHASIS

Results of this work will be applied to the planning of the Crustal Dynamics Project sites and baselines, and to studies of spaceborne laser ranging techniques. In addition, the conclusions will be useful in interpreting results of the San Andreas Fault Experiment and similar geodetic experiments. The techniques used, namely mapping of flow structures in igneous rocks, may be applied to other faults in southern California if desirable.

REFERENCES AND PUBLICATIONS

Lowman, P.D., Jr., "Geologic Structure in California: Three Studies With Landsat-1 Imagery," California Geology, 29, 75-81, 1976.

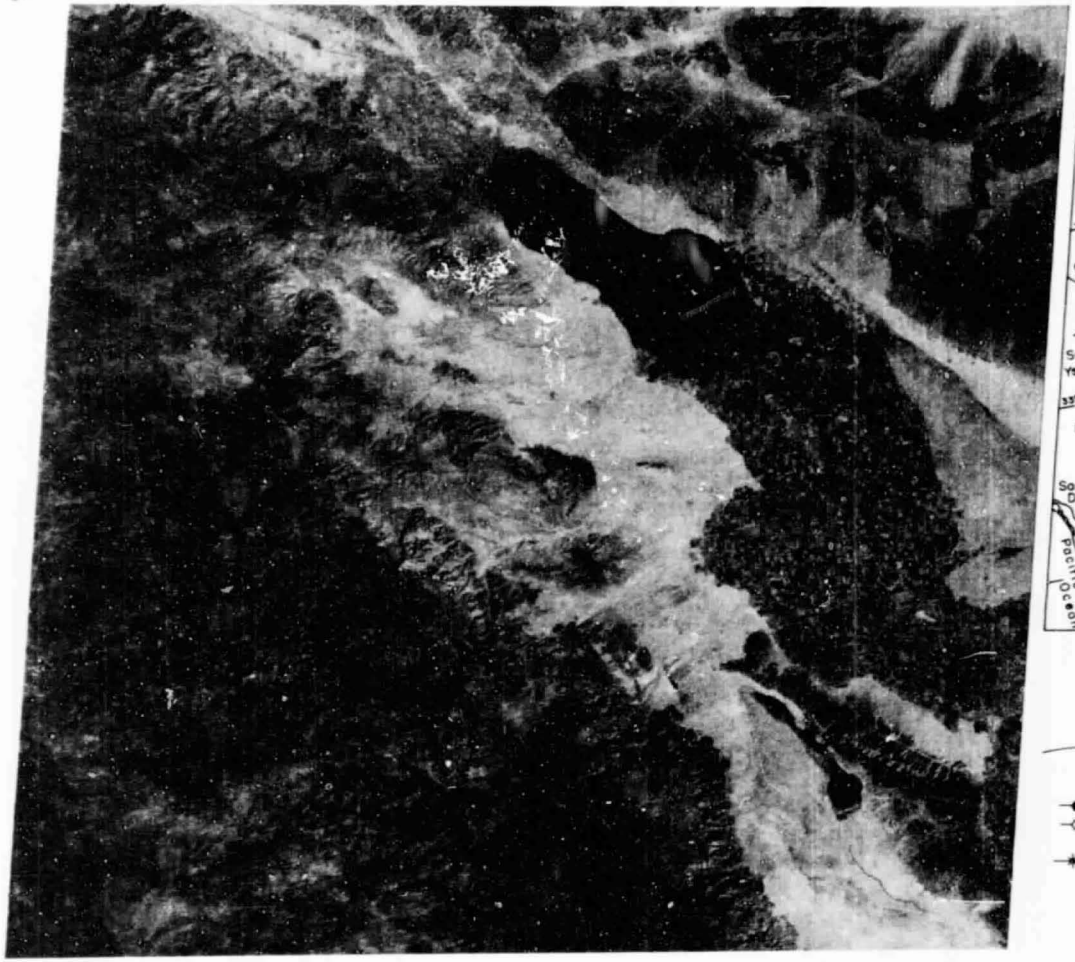

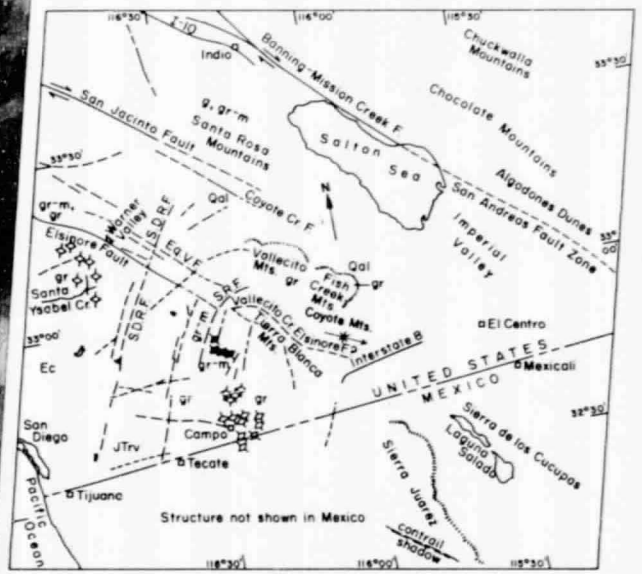

STRUCTURE SKETCH MAP

Peninsular Ranges, San Diego County, California

ERTS-1 Image 1106-17504 (6 Nov. 72)

STRUCTURE

- Fault (solid where confirmed, dashed where inferred or nature not certain).
- Foliation in metamorphic rocks.
- Flow structure in intrusive igneous rocks (inclusions, crystals, etc.).
- Plunging Syncline

LITHOLOGY*

- Qal Quaternary alluvium.
- Ec Eocene nonmarine sediments.
- gr Mesozoic granite rocks.
- gr-m Pre-Cenozoic granite and metamorphic rocks.

* Lithology from Geologic Map of California (1:250,000 sheets)

Paul D. Lowman, Jr.
Goddard Space Flight Center

Figure 3D-1: Landsat image and map of Peninsular Ranges, showing location of Elsinore and related faults.

Figure 3D-2: Photo showing ridge of Sawtooth Range crossing Elsinore fault between Mason (left) and Vallecito Valley (right). Fault intersects ridge at hairpin turn on foad, center (Campbell Grade).

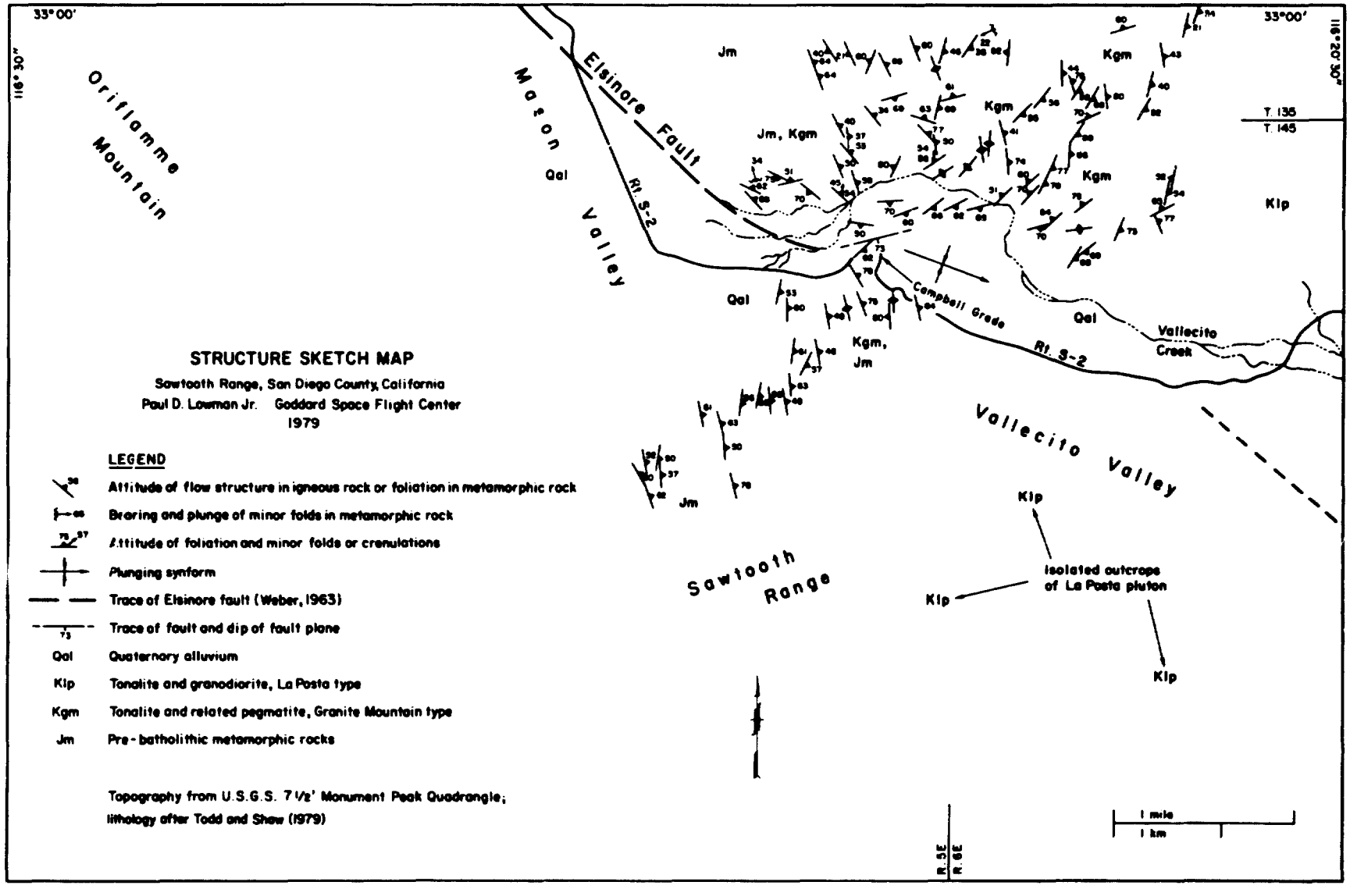

Figure 3D-3: Structure map of Sawtooth Range. Note lack of offset along Elsinore fault.

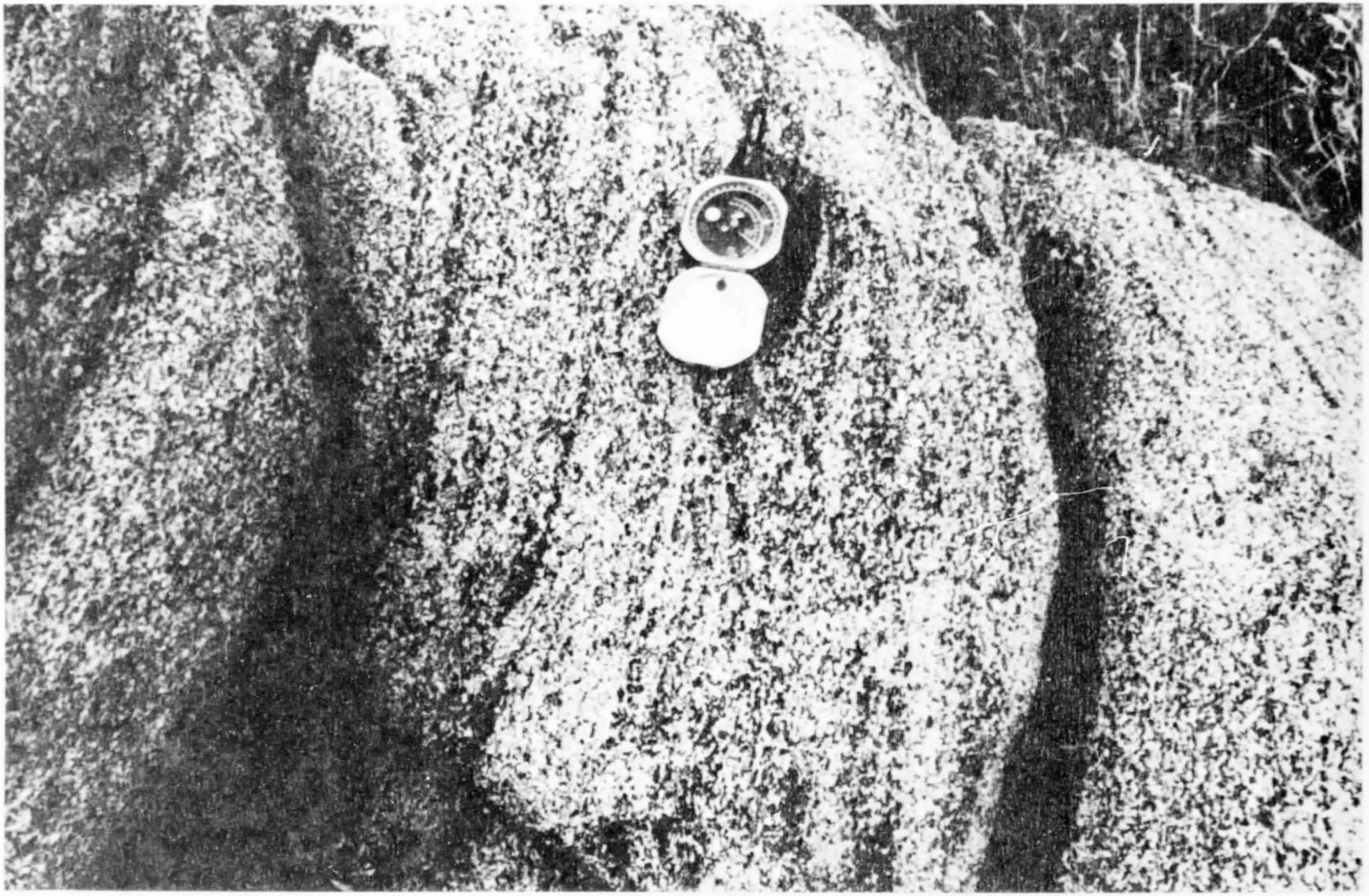

Figure 3D-4: Flow structure, chiefly aligned crystals and inclusions, in Granite mountain tonalite, North Pinyon Mountains.

Figure 3D-5: Air view, altitude about 2500 feet, to northwest showing Earthquake Valley fault (arrows). Grapevine Mountain at lower right; Scissors Crossing at bottom center. See Figure 3D-6 for landmarks.

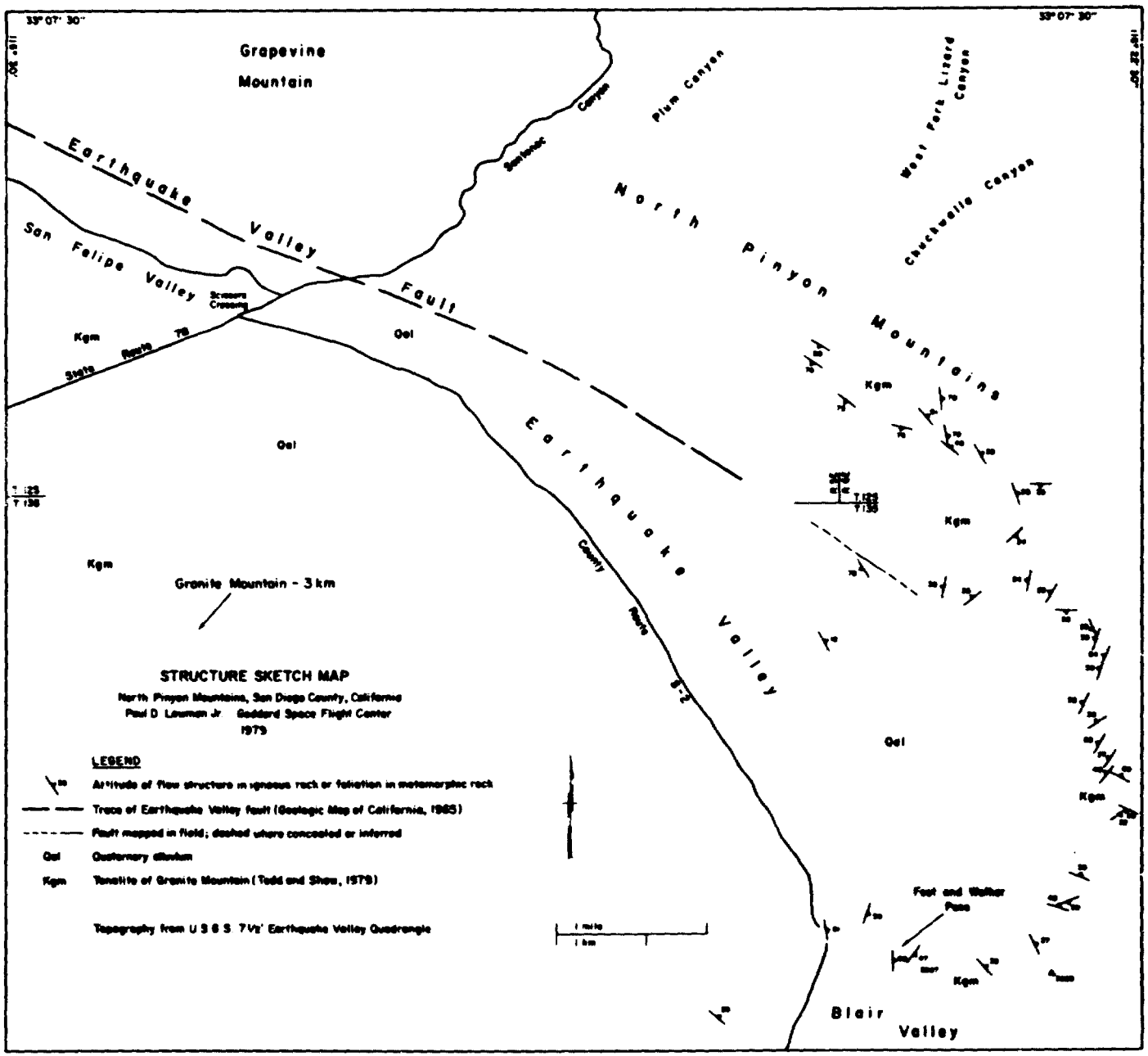

Figure 3D-6: Structure map of Earthquake Valley area. Note lack of structural offset along SE extension of fault (lower right).

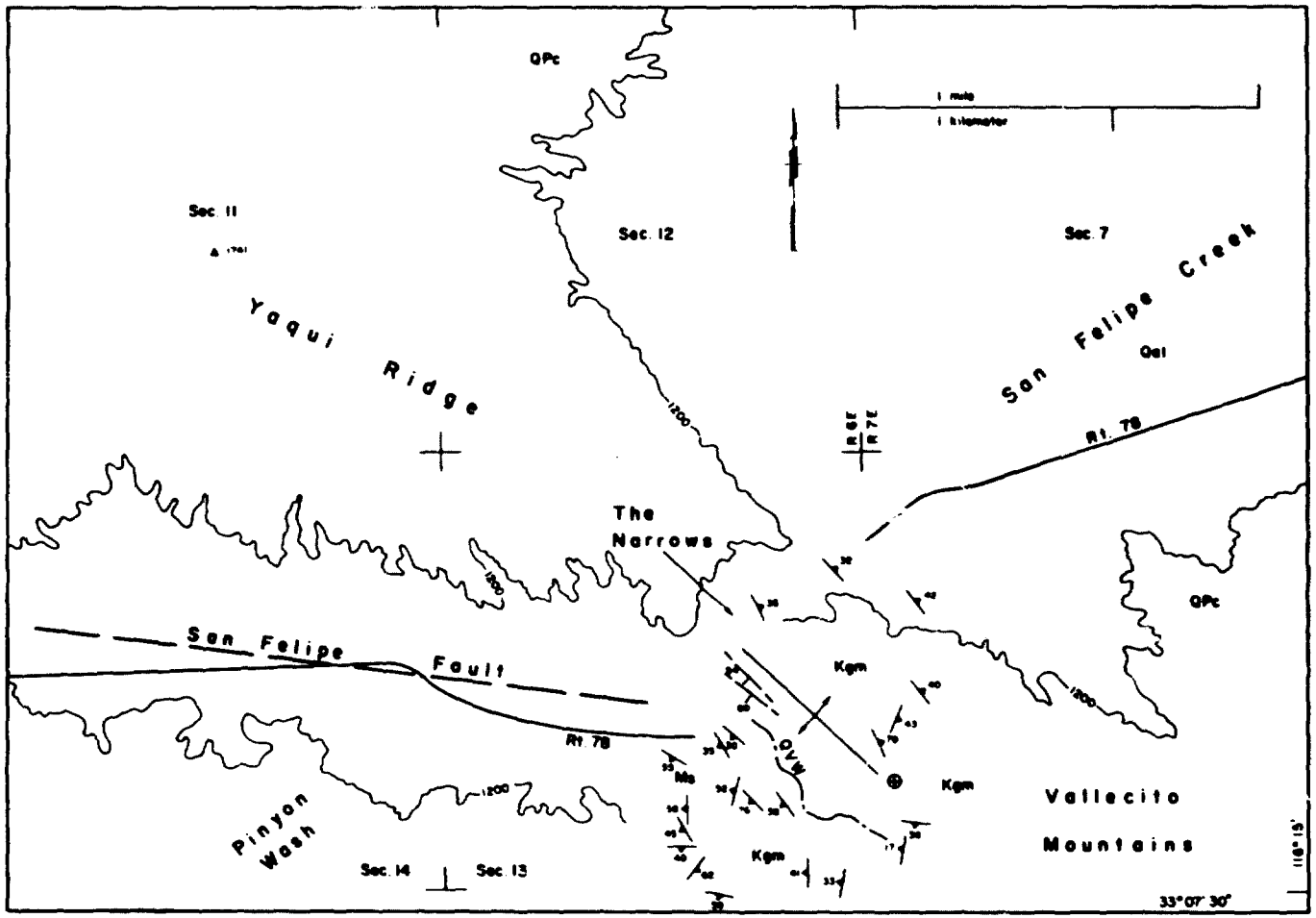

STRUCTURE SKETCH MAP

Quartz Vein Wash, San Diego County, California

Paul D. Lowman Jr. Goddard Space Flight Center

1979

LEGEND

- Attitude of planar structure in igneous or metamorphic rock (⊕ = horizontal)
- Antiform
- Trace of San Felipe fault
- Trace of fault and dip of fault plane
- 1200 — 1200' contour (from U.S.G.S. 7½' Borrego Sink Quadrangle)
- Qal — Quaternary alluvium
- QPc — Pliocene/Pleistocene continental sediments
- Kgm — Tonalite, Granite Mountain type
- Ms — Pre-Cenozoic metamorphic rocks

Figure 3D-7: Structure map of Quartz Vein Wash area. San Felipe fault does not cut SE extension of Yaqui Ridge and it must be deflected 35 to 40° if it controls the trend of Quartz Vein Wash.

D17

N80-20740

E. ON THE SELECTION OF STATION SITES FOR OBSERVING STRAIN STEPS AND EARTHQUAKE FORERUNNERS IN CALIFORNIA

by

H. S. Liu

OBJECTIVES

Allen (1968) has stated that geological features in California might allow us to predict that some segments of the San Andreas fault will be the repeated sites of great earthquakes. The objective of this study is to address the question of where crustal deformation stations should be set up so as to maximize the probability of observing anomalous crustal movements before great earthquakes.

BACKGROUND

Strain steps have been defined in the seismological literature as permanent adjustments in the strain field of the earth following the occurrence of large earthquakes. Press (1965) has shown that strain steps can be observed after large earthquakes. In order to utilize strain steps for earthquake prediction and studies, large networks of strainmeters and tiltimeters, preferably having considerable redundancy, are needed. Such networks are already in operation in Japan and the People's Republic of China.

The methods for calculating strain steps and earthquake forerunners can be found in Liu (1979).

RECENT ACCOMPLISHMENTS

Probabilities for observing strain steps and earthquake forerunners in California and western Nevada were computed. A total of 729 hypothetical observing stations were used in this study. The locations of these stations were chosen to be 0.5° x 0.5° grid intersections covering an area extending from 30°N to 43°N and 114°W to 127°W.

The probability for observing earthquake forerunners or strain steps depends on the sensitivity of the strain measurements. The results of our calculations indicate that if the instrument sensitivity decreases from 10^{-8} to 10^{-7} the maximum value of probability for detecting three or more earthquake forerunners in ten years decreases from 0.95 to 0.49. However, as expected, the locations of the maximum remain unchanged.

A full description of this study has been published in Bulletin of the Seismological Society of America (Liu, 1979).

SIGNIFICANCE

Using the statistical methods of detecting unusual seismic activities, it has been found that the favorable locations for observing crustal deformation in California are in the vicinity of Monterey and in the area surrounding San Bernardino.

FUTURE EMPHASIS

This study proposes the most favorable locations for observing precursory deformation of major earthquakes in California. We have applied the statistical theory of detecting unusual seismic activities to recommend the vicinity of the two ends of the locked sections along the San Andreas fault. There are statistical reasons why a precursory deformation should be expected to occur at locations where the strain steps or earthquake forerunners might have been most frequently observed. In order to understand the geodynamics of these empirical probabilities, it is proposed to develop fracture models of the San Andreas fault for strain propagation. Since an elastic model of stress acccumulation cannot serve as a physical or mechanical basis in discerning the nature of earthquake precursors, we plan to develop fracture models to explain that fracture or opening of the locked fault during the non-elastic period starts from the two ends of the locked section and propagates to the center. The results of the future studies will be verified by the experience of prediction for the Haicheng earthquake. This is important because a single observational station on the spot which is senstiive to precursory strain or deformation had played a major role in the success of earthquake prediction in China.

REFERENCES AND PUBLICATIONS

Allen C. R., "The Tectonic Environments of Seismically Active and Inactive Areas Along the San Andreas Fault System, in Proceedings of the Conference on Geologic Problems of the San Andreas Fault System, Stanford University Publications, Geological Science, XI, 70-82, 1968.

Liu, H.S., "On the Selection of Station Sites for Observing Strain Steps and Earthquake Forerunners in California," Bulletin of the Seismological Society of America, Vol. 69, No. 5, pp (in press), 1979.

Press, F., "Displacements, Strains and Tilts at Teleseismic Distance, J. Geophys. Res., 70: 2395-2412, 1965.

F. GSFC SITE STABILITY

by

W.J. Webster, Jr. and R.J. Allenby

OBJECTIVES

The objective of the GSFC site stability project is to monitor the site's geodetic stability.

BACKGROUND

The STALAS site near GSFC is the main reference station for the laser ranging programs. Accordingly, it is important to know the level of geodetic stability of STALAS. It is also important to detect any regional earthquakes which may influence measurements from STALAS.

RECENT ACCOMPLISHMENTS

A field reconnaissance showed no convincing evidence of surface expressions of faulting and determined that the area is all tertiary and quaternary sediments of a poor grade of consolidation. A telemetered seismic station was established on the nearest bed rock exposure (Ellicott City, MD), and continues to monitor for possible local ground displacements. A low gain seismometer is in operation at the STALAS site for acoustic transfer function measurements.

FUTURE EMPHASIS

A "hammer" refraction survey is planned for late spring 1980 to tie the STALAS site to the Maryland well log network. The well log data has been obtained from Maryland State Geological Survey and has been put into the required form. This will allow an accurate estimation of the elastic properties of the sediments at STALAS.

Since the STALAS pier does not go to bed rock, a complete estimation of the acoustic transfer function is required. The measurement of the seismic velocity in the upper most sediments and the comparison of seismic signals between the STALAS site and Ellicott City will complete the data gathering.

At the conclusion of this effort an intermediate period seismometer will be operated at STALAS in conjunction with the cryogenic gravimeter already in operation to assure that the stability of the site remains constant.

G. GEODETIC STABILITY OF THE GREEN BANK, WEST VIRGINIA VLBI SITE

by

P.D. Lowman, Jr., W.J. Webster, Jr. and R.J. Allenby

OBJECTIVES

A combined geological and geophysical study of the National Radio Astronomy Observatory at Green Bank (Figure -1) was undertaken in support of the VLBI program to assure the stability of the Green Bank site at the 2 to 5 cm level. It is essential to be sure that the sites on the east coast are really stable, locally, since these sites are used as stable references for the interpretation of VLBI results.

BACKGROUND

Because numerous lineaments, including a possible track of the 38th parallel lineament, cross the region around Green Bank (Figure -2), a field survey was undertaken to measure any offset on the lineaments. Such offsets would indicate both the potential for movement and the magnitude over geologic time. Surprisingly, no offsets were found although the lineaments are clearly old, stratigraphically. Initial results of the field survey are in press in Economic Geology.

In addition to the field survey, a short-period high-gain seismometer has been in operation at NRAO for over two years. This system is intended to check for micro-earthquakes in the region around the observatory. Although no activity has been detected within 20 km of Green Bank, the previously known centers of activity near Elkins, W. VA. and West-Central VA. have been responsible for about 20 earthquakes with a maximum magnitude of 3 during the period of operation.

A major water impoundment project is being constructed by VEPCO about 35 km east of the observatory. Because of the possibility of impoundment-induced strain and loading-triggered microseismicity, monitoring at NRAO will be continued to assure that the current stability does not deteriorate as the reservoir is filled to capacity. This is a potential problem because the field survey confirmed the presence of heavily jointed and fractured rock in the area.

FUTURE EMPHASIS

Becuase one of the largest water impoundment projects east of the Mississippi is within 30 km of NRAO, seismic monitoring must continue for the assessment of impoundment-induced seismicity. A measurement of the acoustic noise spectrum in the vicinity of the 140-foot antenna is planned for late spring 1980, together with some measurements of joint intensity to correlate with recently published observations to the east of NRAO.

REFERENCES AND PUBLICATIONS

Webster, W.J., Jr., R.J. Allenby, P.D. Lowman, Jr., H.A. Tiedemann and L.K. Hutton, "Tectonic Motion Site Survey of the National Radio Astronomy Observatory, Green Bank, West Virginia," NASA/GSFC Technical Memorandum 79691, June 1979.

Lowman, P.D., Jr., W.J. Webster, Jr. and R.J. Allenby, "A Search for the 38th Parallel Lineament Near Green Bank, West Virginia," accepted for publication in Economic Geology, 1980.

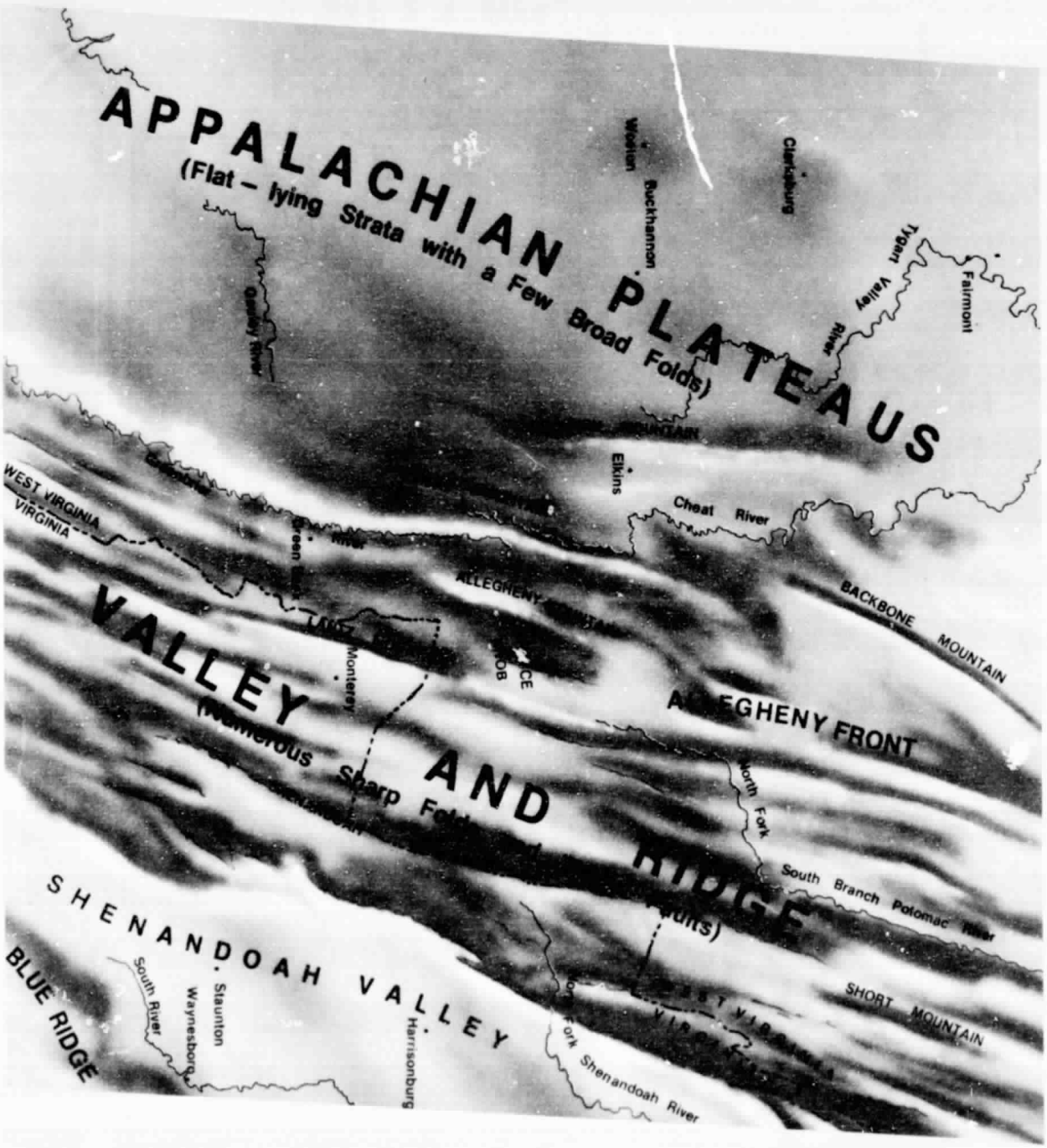

Figure 3G-1: Generalized Geological Map of Green Bank Area.

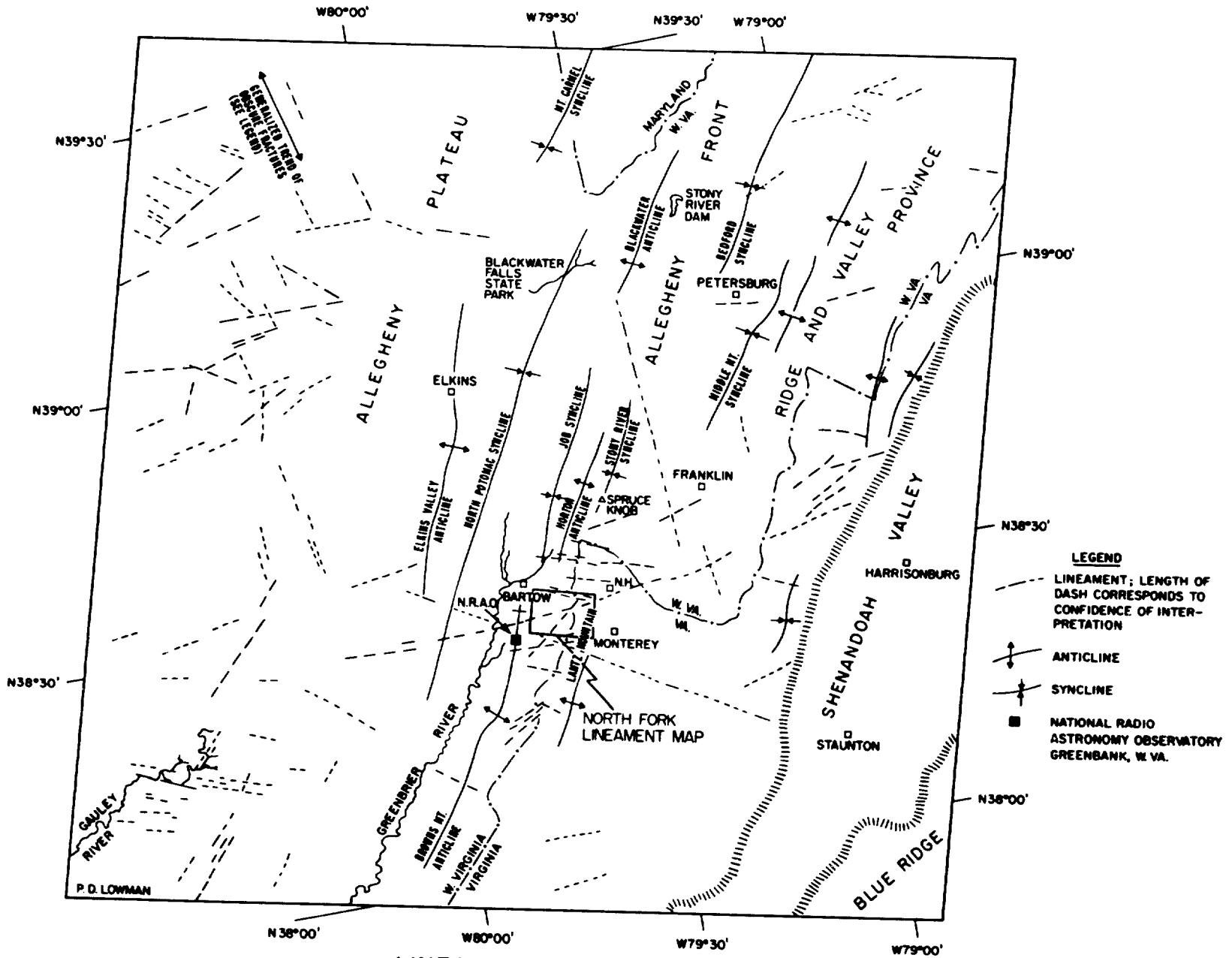

LINEAMENT MAP

BASED ON LANDSAT IMAGE 1172-15310, 11 JAN. 73

PAUL D. LOWMAN

GODDARD SPACE FLIGHT CENTER

Figure 3G-2:

H. EARTHQUAKE AND CRUSTAL DEFORMATION STUDIES

by

S. C. Cohen

OBJECTIVES

This research on earthquake and crustal deformations has as its central objective the elucidation of the physical mechanisms responsible for earthquakes, other fault motions, and regional crustal deformations. Both the development of theoretical models and the analysis of geodetic and seismic data are being utilized to understand the nature of the fundamental geodynamic stresses in the earth and their implications for the occurrence of earthquakes. The work is conducted within the context of NASA's research in solid-earth dynamics and the Crustal Dynamics Project.

BACKGROUND

During 1979 research focused on two earthquake related topics. The first was a study of the time-dependent deformation of the earth occurring coseismic with and following earthquakes. This work is a continuation of efforts begun in 1978. The earth is modeled as a layered viscoelastic medium, and the coseismic displacements, strains, and stresses are governed by its elastic parameters. On the other hand long-time scale postseismic motions, requiring years, decades, or longer, are governed by the anelastic relaxation of shear forces within the asthenosphere. Intermediate time scale postseismic motions, those occurring in hours to months following an earthquake, are assumed to be products of a partial viscoelastic relaxation of the lithosphere.

A second study, concentrating on the temporal and spatial properties of seismic energy release, was initiated in the last few weeks of 1979. In this study earthquake location and magnitude data is used in calculations of the released seismic energy. The temporal characteristics of this energy release are then being examined both on a worldwide basis and a regional basis with the regions being chosen to correspond to known seismic, tectonic, and geologic provinces.

RECENT ACCOMPLISHMENTS

Calculations of coseismic and postseismic strain and stress have been added to the previous calculations of earthquake related displacements. The model that has been developed is quasi-three-dimensional and allows computation of the horizontal components of normal stress and strain as well as the shear stress and strain for earthquakes occurring on strike-slip faults. A summary of some of the salient features of an illustrative calculation is presented in F3H-1. These results show the

dependence of surface displacement (component parallel to fault slip), shear strain and shear stress on distance from the fault. The results are valid for a path along the perpendicular bisector of a 100 km fault. The fault itself is taken to extend from the surface to a depth of 12.5 km. At the time of the earthquake the relative slip across the fault is 1m corresponding roughly to a magnitude 6.5 - 7.0 earthquake. The thickness of the lithosphere is taken to be 50 km. The results reveal that the coseismic displacements on one side of the fault decrease from 50 cm at the fault to 4 cm at 50 km, to a few millimeters at 200 km. Since in this model the fault is locked in position after the earthquake there are no displacements at the fault as either the lithosphere or the asthenosphere relax. However the displacements associated with lithospheric relaxation become comparable to the coseismic displacements of distances of 50 km and more. Similarly the longer time scale displacements associated with asthospheric relaxation also become significant relative to the coseismic ones at distances of several tens-of-kilometers. Note that although the direction of this component of coseismic displacement (taken to be positive) is the same as that of the asthenosphere, the lithospheric relaxation produces a rebound motion in the opposite direction. As for the shear strain, near the fault the coseismic strain dominates at all times. Further away, the strain due to asthenospheric relaxation may come to be a major or dominant contributor to total shear strain as time progresses. The effect of any lithospheric relaxation on strain is small. Note again that the signs associated with the various contributions to the shear strain are different. Although the lithospheric relaxation contributes little to the postseismic strain, it can appreciably effect the stress on the fault. The model predicts a partial recovery of the stress on the fault. This restressing of the fault provides a mechanism for the occurrence of aftershocks.

A comparison has been made between the predictions of the model and geodetic observations associated with the 1906 San Francisco earthquake. Figure 3H-2 shows measured and predicted values of the ratios of postseismic to coseismic changes in some angles associated with a geodetic network observed north of San Franciso (Thatcher, Science, 184, 1282-1285, 1979). The level of agreement between theory and observation is particularly good in view of the fact that no corrections have been made for the straining of the network due to non-earthquake mechanisms (e.g., plate motion). However alternative models involving buried fault slip subsequent to the earthquake can also explain the data and the precision and timeliness of the data are not adequate for resolving any small angle changes that might be associated with lithospheric relaxation.

The analysis of the worldwide seismic data indicated that the year-to-year variations in energy release are modest being only about one order of magnitude, at least for the years 1900-1977.

The results for individual regions of the world show much greater variation. Using a seismic regionalization scheme due to Flinn and Engdahl (Rev. Geophys. 3, 123-149, 1965) the world is divided into 50 seismic-tectonic provinces. In many cases the regional energy release is characterized by sudden jumps due to a major earthquake sequence which interrupts a multiple year quiescent period. The difference in energy between an active and quiescent year may be several orders of magnitude. In addition there are some cases of regional energy release progressing through a series of modest earthquakes. For example the energy release in the California-Nevada region between 1907 and 1971 is roughly equal to the energy release due to just two larger events in 1952.

Another finding of the seismic data study is an apparent positive correlation between the average or background energy release in a region and the maximum energy released in that same region. Such an observation is consistent with the view that regions containing large faults have a large number of earthquakes, hence high average energy, and occasional very large events. Conversely regions having only very small faults have few events and the events that do occur involve sliding over a limited rupture length and are, therefore, of modest size. However the data used in this study is valid for only about 50 years for the average energy and about 81 years for peak energy. It will be necessary to investigate whether the time span of the observations is too short to have reliable data about large events in areas that are generally quiet and whether the correlation is due to an incomplete sampling period.

FUTURE EMPHASIS

Several elaborations and modifications of the postseismic deformation model are under consideration. The present model assumes a linear Maxwell creep law for the asthenosphere. Some experimental evidence indicates that a better approximation to the earth can be achieved using a law in which strain rate is proportional to the cubic power of stress. Additionally there are reasons to believe that a vertical stratification of the lithospheric rheology is important with the upper portion of the lithosphere being more elastic and brittle than the lower. There may also be important horizontal variations in rigidity and rheology with rock in the fault zone being less rigid and more anelastic than its distant counterparts. Since the introduction of each of these modifications is a complex undertaking, the degree with which they will be adopted will be subject to careful consideration. Finally continued comparisons between the predictions of this and alternative models and observations are envisioned.

The seismic energy release studies will continue to explore the spatial and temporal patterns both within individual regions and on a worldwide basis. The data base will be expanded and a study of the correlation among earthquakes occurring in different places and at different times will be undertaken.

REFERENCES AND PUBLICATIONS

Cohen, S.C., "Postseismic Surface Deformation Due to Lithospheric and Asthenospheric Viscoelasticity," Geophysical Research Letters, 6, 129-131, 1979.

Cohen, S.C., "Viscoelasticity and Postseismic Crustal Deformations," EOS, Trans. Am. Geophys. U, 18, 316, 1979.

Cohen, S.C., "Postseismic Viscoelastic Surface Deformation and Stress, Part 1: Theoretical Considerations, Displacement and Strain Calculations, NASA TM 80292, May 1979.

Cohen, S.C. and Cook, G.R., "Postseismic Viscoelastic Surface Deformation and Stress, Part 2: Stress Theory and Computation, Dependence of Displacement, Strain, and Stress on Fault Parameters," NASA TM 80334, August 1979.

Cohen, S.C. and Cook, G.R., "Determining Crustal Strain Rates with Spaceborne Geodynamics Ranging System Data," Manuscripta Geodaetica, 4, 245-260, 1979.

EARTHQUAKE RELATED DISPLACEMENTS, STRAINS, AND STRESSES

MODEL PARAMETERS: FAULT DISPLACEMENT = 1M M ~ 6.5-7.0
FAULT DEPTH = 0-12.5 KM
LITHOSPHERIC THICKNESS: 50 KM
FAULT LENGTH: 100 KM

$\frac{\mu_a}{\mu_l} = 1.5$; $\frac{\mu_a}{\mu} = 1.0$

DISTANCE FROM FAULT	CONTRIBUTOR	DISPLACEMENT	SHEAR STRAIN	SHEAR STRESS
0 km	Coseismic	+ 50 cm	-1×10^{-5}	-7 pascal
	Lithospheric Relax.	0	-4×10^{-7}	+4 pascal
	Asthenospheric Relax.	0	$+1 \times 10^{-7}$	< +.1 pascal
50 km	Coseismic	+ 4 cm	-3×10^{-7}	
	Lithospheric Relax.	- 1 cm	$+2 \times 10^{-8}$	
	Asthenospheric Relax	+ 1 cm	$+1 \times 10^{-7}$	
200 km	Coseismic	+0.3 cm	$+1 \times 10^{-8}$	
	Lithospheric Relax.	-0.2 cm	$< -1 \times 10^{-9}$	
	Asthenospheric Relax.	+0.3 cm	$+5 \times 10^{-8}$	

FIGURE 3H-1

POSTSEISMIC ANGLE CHANGE (1930-1906)
COSEISMIC ANGLE CHANGE (1875-1906)

	ANGLE	OBSERVATION	THEORY
TRIANGLE 2-3-4	2	-.19	-.2
	3	-.17	-.2
	4	-.22	-.2
TRIANGLE 3-4-5	3	-.54	-.2
	4	-.75	-.2
	5	NOT SURVEYED	

FIGURE 3H-2: Ratio of Postseismic to Coseismic Angle Changes Associated with 1906 San Francisco Earthquake and Observed at Fort Ross, California (Data due to Thatcher, Science, 184, 1283-1285, 1975).

I. GLOBAL INTRA-PLATE VOLCANISM

by

Han-Shou Liu

OBJECTIVES

Volcanoes on the surface of the Earth could be expressions of crustal deformation caused by stress concentration in tension. Volcanic activities have occurred within tectonic plates which cannot be associated with plate margin processes due to plate motion. The objective of this study is to investigate the global distribution of the intra-plate Cenozoic volcanism and how it is related to the satellite-determined tensional stress field in the Earth.

BACKGROUND

A large fraction of the Earth's volcanism is due to pressure-release melting of mantle rocks in the ascending limbs of mantle convection cells. The theory of volcanism is that magmas from the asthenosphere penetrate the lithosphere where tensional fracture occur. Therefore, the crucial problem of magma transport from the asthenosphere to the near surface is the maintenance of tensional stress condition in the lithosphere by the ascending limbs of mantle convection.

But this raises a series of critical and fundamental questions. Where are the tensional stress regimes in the lithosphere? Where are the ascending limbs of mantle convection cells? How can convection currents in the upper mantle generate lithospheric stresses? Can we develop upwelling mantle convection systems and associated tensional stress fields to match the distribution of the intra-plate volcanism? We have attempted to clarify the answers to these questions by applying the satellite and surface gravity data to the theory for the convection-generated stresses. In this way, we can study the consequences of accepting this stress theory to see whether it can provide an explanation for intra-plate volcanism.

RECENT ACCOMPLISHMENTS

Space volcanology seeks to ascertain the causes of volcanism and its fundamental connections with dynamics processes. This study has developed a genetic model which accounts for the widespread development and uneven distribution of the Cenozoic intra-plate volcanism in relation to the convection-generated, tensional stress regimes. A clear-cut correlation between Cenozoic volcanism and tensional stress regimes in Africa, Asia, Australia, North and South America and further details of these accomplishments will be found in Liu (1980).

SIGNIFICANCE

The following significant conclusions will be published (Liu, 1980) as a result of this study:

1. It explains the global occurrence of intra-plate volcanism.

2. It establishes the relationship between tensional tectonics and intra-plate volcanism.

3. It provides tensional stress condition for the migration of magmas through the lithosphere by hydrofracturing or corrosion cracking.

4. Crustal doming is explainable in terms of the mechanical consequences of the upwelling mantle convection currents.

5. The linear upwelling convection limbs are consistent with the general trends of some volcanic chains.

6. Ascending convection in the asthenosphere under volcanic areas explains the production of magma by pressure-release melting.

7. The stress system is developed on geophysical theories and geodynamics data. It does not require anomalous asthenosphere beneath volcanic areas. The results are capable of accounting for the absence of intra-plate volcanism in the compressional stress regimes.

FUTURE EMPHASIS

Recent development of polygonal cell systems from hotspot population and laboratory models have focussed attention on the flow patterns in the Earth's mantle. The results of this paper will be applied to investigate crustal tension, doming and rifting. They will also be compared with the polygonal vertices and boundaries in the experimental models of mantle convection.

REFERENCES AND PUBLICATIONS

Liu, Han-Shou. "Convection Generated Stress Field and Intra-Plate Volcanism." Tectonophysics, in press, 1980.

J. DEVELOPMENT OF A SEISMIC DATA COLLECTION PLATFORM

by

W.J. Webster, Jr. and R.J. Allenby

OBJECTIVES

Geophysical data is now being collected all over the globe from a variety of remote and inhospitable locations. In order to develop any kind of a predictive system for natural crustal hazards, such as earthquakes or volcanic eruptions, near real-time collection of data is required. Off-the-shelf DCP's are now available for satellite relaying of low data rate information. A relatively inexpensive, field hardened system is not available that can handle the high data rate seismic information. In cooperation with GSFC Code 700, we have developed a prototype signal processor for a seismic DCP.

RECENT ACCOMPLISHMENTS

A DCP simulator has been constructed that utilizes an event detection algorithm developed by the USGS and compresses a short period seismic signal into a 100 bit per second GOES satellite channel. The simulator performs all the functions required of a field processor and includes additional features such as control from a printing terminal, variable buffer length, and variable microprocessor speed. An evaluation program to determine precise power budgets, optimum microprocessor speed, and buffer lengths has been completed.

In essence, an identified event is recorded in a solid state memory for 180 seconds at a sampling rate of 50 times per second using a 12 bit word for signal resolution. During the 18 minutes that memory one is dumping to the satellite at 100 bps, a second memory is on line to record the next identified event. Figure 3J-1 illustrates the signal processing function.

A Goddard Technical Memorandum describing and evaluating the breadboard system will be completed in early 1980. A condensed version will be submmited to IEEE Transaction, Geoscience Electronics for publication.

FUTURE EMPHASIS

Completion of the evaluation program and preparation of the Technical Memorandum describing the system is the termination of this program.

REFERENCES AND PUBLICATIONS

Allenby, R.J., W.J. Webster, Jr. and J.E. Painter, "Satellite Relaying Geophysical Data," NASA/GSFC X-922-77-273, November 1977.

Figure 3J-1: Examples of Seismic Data Collection Platform Operating on Vertical Axis, Short Period Seismic Signal

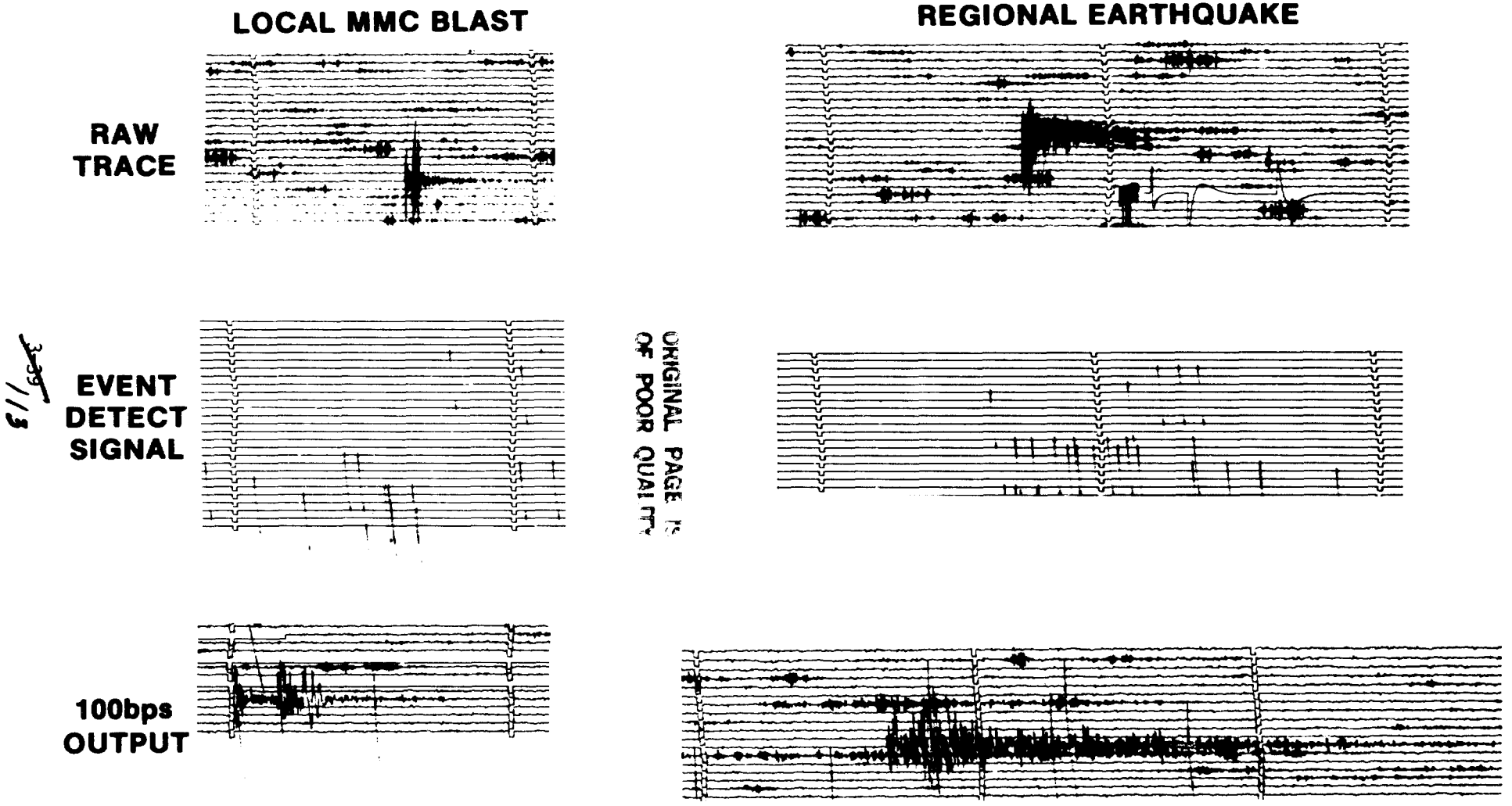

K. CRUSTAL MOTION MEASUREMENTS IN CALIFORNIA (SAFE)

by

D. E. Smith

OBJECTIVES

The objective of this research is to determine the present-day motion of Pacific and North American tectonic plates in California.

BACKGROUND

An experiment was initiated in 1972 to measure the total rate of motion across the San Andreas fault in California. This experiment, known as the San Andreas Fault Experiment (SAFE), is repeated by measuring the distance between two points on opposite sides of the fault, San Diego, California on the Pacific Plate and Quincy, California on the North American plate. According to the plate tectonic theory the distance between these sites will change from year to year as a result of the relative motion of the two plates. In 1972, 1974 and 1976, the San Diego and Quincy sites were occupied by satellite laser tracking systems that simultaneously tracked the Beacon Explorer 3 satellite on several occasions. From these laser tracking data the relative positions of the two sites were derived. The results of these three measurements indicated a steady shortening of the baseline between San Diego and Quincy at a rate of about 9 ± 3 cm/yr. This work was described in detail in last year's annual report and in Smith, et al. (1979).

RECENT ACCOMPLISHMENTS

In the spring of 1979 the San Diego and Quincy sites were re-occupied for the fourth time. The laser systems tracked the Beacon Explorer 3 satellite and from these data a fourth value of the baseline length has been derived. This measurement together with the three previous results are shown in Figure 4K-1. The 1979 result is preliminary but at present confirms the shortening of the baseline observed in previous years and provides an approximate rate of 9 ± 2 cm/yr.

SIGNIFICANCE

With the preliminary analysis of the fourth measurement of this line completed, it appears that the observed rate of motion of 9 cm/yr. is more likely to be correct within the standard deviation. This rate appears to be larger than the geological average and, if confirmed, suggests that we might need to re-evaluate our ideas of large scale crustal motion in California. The larger rate of motion is more consistent with the expected motion across the opening of the Gulf of California and therefore the need to suggest distortion taking place in the Colorado delta and up into Nevada so as to account for a lower rate of motion along the San Andreas, is no longer necessary (in the present time scale).

Clearly the uncertainty in the rate of motion derived here is still too large to force us to re-think our position on the tectonics of this area but it does suggest that some modifications may be neces-

sary in future years. More measurements of this line are necessary and present plans indicate a fifth measurement in the spring of 1981.

REFERENCE AND PUBLICATIONS

NASA Technical Memorandum 80550, Earth Survey Applications Division Research Report, pp. 3-2, 3-5, November 1979.

Smith, D. E., R. Kolenkiewicz, P.J. Dunn, and M.H. Torrence, "The Measurement of Fault Motion by Satellite Laser Ranging," presented at the International Symposium on Recent Crustal Movements, Stanford University, Palo Alto, California, July 25-30, 1977, and published in Tectonophysics, 52, 59-67, 1979.

Figure 4K-1

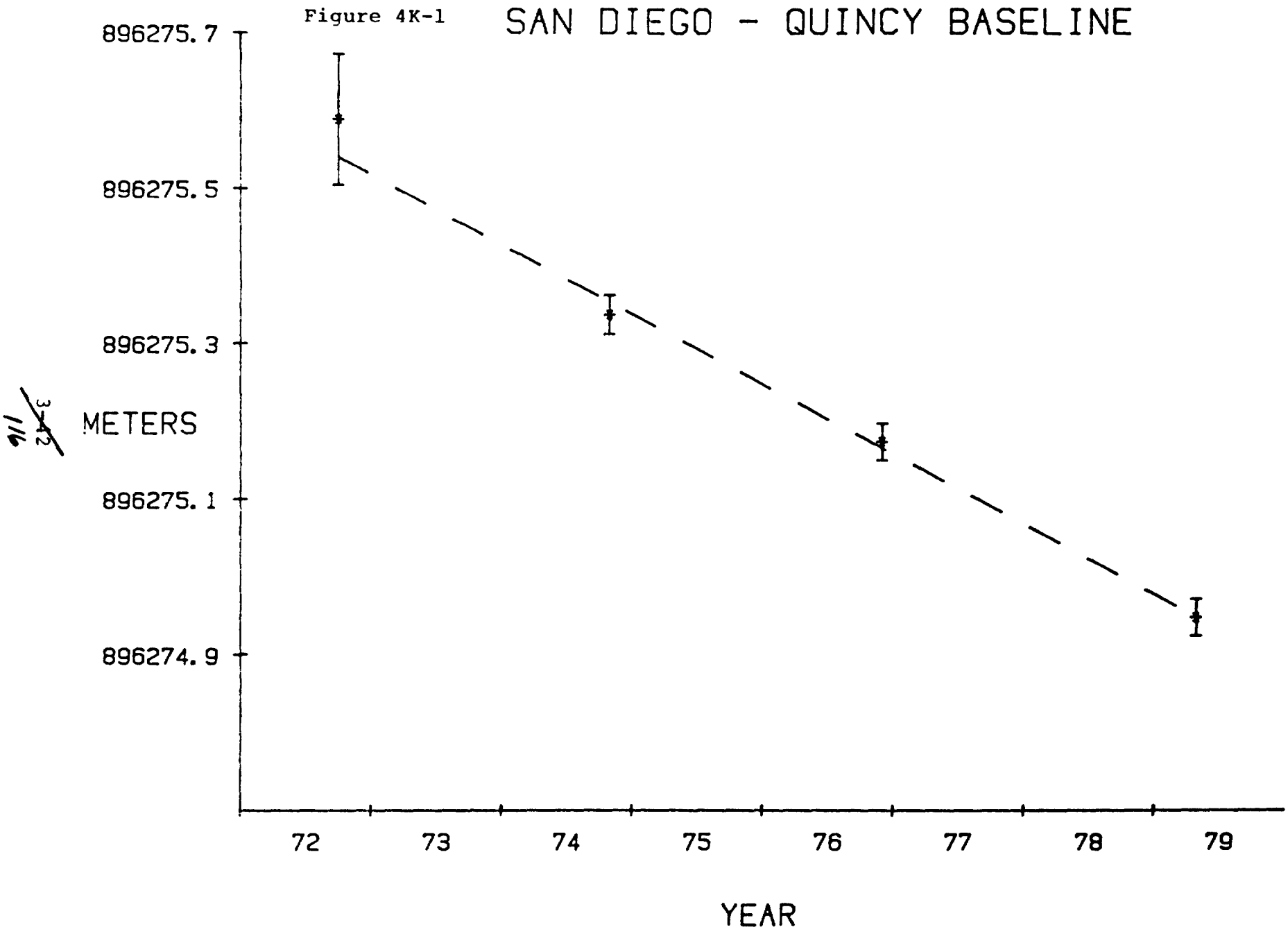
SAN DIEGO - QUINCY BASELINE
896275.7
896275.5
896275.3
METERS
896275.1
896274.9
72
73
74
75
76
77
78
79
YEAR

CHAPTER 4

GRAVITY FIELD MODEL DEVELOPMENT

edited by

W. D. Kahn

OVERVIEW

Knowledge of the earth's gravity field is fundamental to understanding the dynamics of the earth. For solid earth geophysics, knowledge of time variations in the gravity field provides information on the earth's physical properties and geodynamic processes and places constraints on the internal structure of the earth. In oceanography, knowledge of departure of the actual sea surface from a unique equipotential surface of the earth's gravity field (the geoid) can reveal information on oceanic circulation. In addition, other areas which benefit from knowledge of the earth's gravity field are satellite orbit determination and classical geodesy.

This chapter described the development of models for geopotential from satellite tracking data, surface gravity field data, and satellite altimetry. Special investigations are also described, e.g., use of satellite-to-satellite tracking data to derive gravity anomalies and investigate the gravity anomaly patterns for mantle convection implications.

A. GEODYN PROGRAM SYSTEMS DEVELOPMENT

by

B. H. Putney

OBJECTIVES

The purpose of the Geodyn Orbit Determination and Parameter Estimation Program is to recover geodetic and geophysical parameters from satellite data in a state-of-the-art manner.

BACKGROUND

In 1971 the Noname and Geostar programs were combined to form the Geodyn program. The philosophy of the development has been to mold the program very carefully to maintain computer efficiency and good program structure, appropriate orbit and Earth modeling, precise satellite measurement modeling, efficient numerical procedures and careful bench-marking. This care has paid off in the production of several GEM's, precise station locations, improved tidal, GM and polar motion values, consistent baseline determinations. Careful usage and modeling using laser, altimeter and other satellite data from the GEOS satellites, BE-C, Starlette, Lageos, and Seasat satellites as well as many others has allowed these accomplishments.

RECENT ACCOMPLISHMENTS AND SIGNIFICANCE

In support of Seasat the precession and nutation algorithms have been improved. The nutation constants are now being taken from the JPL ephemeris tape and the interpolation schemes have been made more accurate. When dealing with precise orbits it has become apparent that the set of pre-processing corrections, flux values and polar motion values, the ocean tidal model being used on altimeter data, the geographic latitude and longitude (latitude and longitude corrected for polar motion) position of the satellite, need to be known to the user. Consequently the program was modified to print these quantities on option. It turned out that this was a great way to monitor the program and also, probably as important, to find the errors in the observational data handling. The time dependent drag coefficients and the variable area and reflectivity satellite model for the atmospheric drag computation have proved to be important in the Seasat orbit determination. The separate software package using the Bent model for the ionosphere has been expanded to compute ionospheric refraction for instantaneous range-rate, destruct Doppler, azimuth-elevation, X-Y angles, SST data, hour-angle declination and right ascension declination data.

In support of Lageos the additional parameters, speed of light, earth's rotation, along track and other accelerations and the semimajor axis of the earth can now be adjusted. To help with the relativity problem the independent variable in the integration can now be ephemeris time instead of the traditional atomic time.

In the general area of modeling, the albedo perturbation and the earth J2-moon gravitational effect are being implemented. The Jacchia 77 atmospheric density model has been studied for future implementation. The input flux, timing corrections and polar motion tables have been restructured to be external to the Geodyn program. The integration equations can now be partitioned, allowing for smaller core requirements with a large number of parameter solutions. It is now possible to do complete data simulation in Geodyn. Program documentation has been modified in an effort to reflect the current status of the software.

In the software development, we have tried to be responsive to the current needs. Geodyn is a very complex program, consequently, all modifications are difficult. As we handle so many observation data types and complex earth models any modification in one area causes problems to the other areas. At times, the modifications seem to come slowly and when manpower and money are tight progress is even more difficult. Despite these problems, the program has performed well.

FUTURE EMPHASIS

Upgrading the atmospheric drag density model to the Jacchia 77 model is now desirable.

In support of Gravsat, the gravity anomaly formulation and implementation need to be studied, improved and made more computer efficient. In addition Gravsat is a much lower satellite than we have generally dealt with. Efficiently integrating this type of orbit needs to be studied.

An ocean tidal model for satellite perturbations and additional polar motion parameters for high frequency effects appear to be desirable. Investigations will be performed in these areas.

In general, there will be a continued search for improved earth and orbit modeling. As new satellite observation data types appear that are useful in this work, they will be added to the program. In addition, there will be a continued search for techniques and numerical procedures that will cut down computer time and core size without sacrificing the required precision.

A background task is very slowly continuing to convert Geodyn to the CDC STAR computer. With the predicted change-over of computer systems it is important to find a new machine to continue this work. The logistics of accounting, data set management and remote terminals that proved to be ineffective on the STAR, as well as the competition of required software modification for today's projects, have prevented any real progress with this conversion.

B. GRAVITY MODEL DEVELOPMENT

by

F. J. Lerch

OBJECTIVES

The primary objective of this work is the determination of improved values for the spherical harmonic coefficients of the geopotential out to degree and order 36. The general solution will be based upon a combination of satellite tracking, surface gravity, and altimeter data including new data form Seasat. An objective is also to improve the fundamental geodetic constants, the gravitational mass of the earth (GM), the mean equatorial radius of the earth (a_e), the mean equatorial gravity of the earth (g_e) and the flattening of the earth's mean ellipsoid (f). Gravity model improvement is needed to obtain more accurate orbits for analysis of Seasat altimetry, polar motion and tidal parameter determination, and for determination of baselines in crustal motion studies. An objective is also to improve the low degree and order geopotential terms (5 x 5) to correspond to an accuracy of 5 cm on the geoid. This will provide for the separation of the dynamic and stationary sea surface topography from the geoid for the analysis of broad features of ocean circulation. In addition to the 36 x 36 base field, it is planned to refine the harmonic representation to degree 180 so that it can yeild details of the gravity field to a 1° resolution with geoidal accuracy to better than 1m.

BACKGROUND

The following table summarizes the development of recent Goddard Earth Models:

TABLE 4B-1. GEM MODELS AND DATA

Model	Harmonics	Data	References Lerch, et al.
GEM 9	20 x 20	satellite	(1977)
GEM 10	22 x 22	satellite + surface	(1977)
GEM 10A	30 x 30	satellite + surface + altimetry	(1978a)
GEM 10B	36 x 36	satellite + surface + altimetry	(1978a)
GEM 10C	180 x 180	satellite + surface + altimetry	(1978b)

Satellite data:	240,000	laser observations on 10 satellites
	170,000	optical observations on 21 satellites
	500,000	electronic observations on 8 satellites
Surface data:	38,000	1° x 1° free-air gravity anomalies (GEM 10C)
	global	set of 5° mean anomalies (Rapp 1977)
Altimeter data:	700,000	GEOS-3 altimetry measurements

The satellite data resolves principally the long wavelength structure of the geoptential while the gravimetry and ocean altimetry determine the short wavelength features. The most complete current model containing the three types of data is GEM 10B (36 x 36). GEM 10C consists of GEM 10B plus higher degree terms (37 to 180) which were formed from the harmonic analysis of a global set of 1° x 1° blocks of geoid heights obtained from altimetry and gravimetry. Residuals of the geoid heights from GEM 10B were used to compute the extended harmonics in GEM 10C. All three types of data (satellite, surface gravity and altimetry) will be augmented with improved modeling in the new solutions to satisfy the current objectives, including in particular increased accuracy for the geoid.

Table 4B-2 shows the geoidal resolution and accuracy of the current GEM models:

TABLE 4B-2. GEOIDAL ACCURACY OF MODELS

MODEL	HARMONICS COMPLETE	GEOIDAL RESOLUTION	COMMISSION ERROR	TRUNCATION ERROR	TOTAL ERROR
GEM 9	20	1000 km	1.6 m	2.1 m	2.7 m
GEM 10	22	900	1.4	1.9	2.5
GEM 10A	30	650	1.4	1.6	2.4
GEM 10B	36	550	1.3	1.3	2.2
GEM 10C	180	100	1.4	0.3	1.4

Note that the total errors are too large for the geoid when compared to an ultimate goal of 10 cm or the precision of current altimetry (±25 cm for GEOS-3 using 1 second averages). Because of the truncation error the only model that can approach this precision is GEM 10C. However, the commission error in 10C is still quite large due to the inaccuracy of its base field, GEM 10B. Pertinent aspects of the data that contributed to these errors are now discussed with plans for resolving these problems.

RECENT ACCOMPLISHMENTS

The GEOS-3 altimeter data used in GEM 10A and 10B lacked coverage in a broad area across the Atlantic and Pacific oceans. The data to complete this coverage has been made available and should improve the geoid error in our new solutions which are currently being computed. Although sea surface topography (±70 cm) is present in the altimeter data, its usage is justified since the uncertainty of the geoid is considerably larger (±250 cm) for GEM 10, which is the solution based upon satellite and surface gravity data and excludes altimetry. However, part of this error in GEM 10 arises because the ocean gravimetry appears to have some large biases. Figure 4B-1 shows a comparison of satellite, altimetric,

and gravimetric derived anomalies. Note the good agreement of satellite and altimetric anomalies and the poor comparisons with gravimetric data. Rapp has recently provided us with a new set of 5° anomaly data and a set of 1° anomalies derived from altimetry in the ocean area which should help to correct this problem in the new solutions. In addition to improving the ocean gravity anomalies some consideration will be made to improve use of the altimeter data by removing long wavelength quasi-stationary topography as derived from ocean survey as shown in Figure 4B-2.

In the analysis of the global set of 1° x 1° geoid heights employed in GEM 10C which were formed from land gravimetry and GEOS-3 ocean altimetry data, a significant mismatch was found in the heights between the two data types where they merged together at coastal boundaries. A worldwide plot of this misfit is given in Figure 4B-3. These discrepancies, which reach as large as 18 meters, were found to be due to long wavelength systematic errors in the gravity data which can be determined by the satellite model as in Figure 4B-1. These errors have been identified and found to be due to geophysically predicted anomalies in remote land areas or interploated values in the ocean areas; and as a result these anomalies are being removed from the models. In pursuit of this analysis a corrected version of GEM 10C has been made which has provided a much improved power spectrum for crustal analysis and a global set of 1° x 1° gravity anomalies.

It was shown above that improvements are needed in modeling all three types of data, namely satellite, surface gravity and altimeter data in order to improve the accuracy of the geoid to better than 1 m. Hence new models are being developed analogous to those in Table 4B-1, except that the satellite harmonic contributions (over 500,000 new laser measurements) are being augmented to 36 x 36. The new or additional data being processed to improve the geoid (gravity field) are summarized as follows:

(1) Satellite-to-Satellite Tracking Data from GEOS-3/ATS-6 and Apollo/ATS-6.

(2) A global set of 1° x 1° block mean sea surface heights obtained from GEOS-3 and Seasat-A satellite altimeter data using laser reference orbits.

(3) Unified S-Band and laser data from Seasat

(4) Navy doppler data from at least one polar satellite.

(5) A new set of 5° mean gravity anomalies and an improved set of 1° x 1° mean anomaly data, and a 1° x 1° set of altimeter derived anomalies.

(6) BE-C (Beacon Explorer-C) laser observations from the SAFE and the Polar Motion Experiment.

(7) 12 and 24 hour satellite accelerations.

(8) Lageos laser data.

(9) GEOS-3 S-Band and laser data.

(10) Laser data on GEOS-1, GEOS-2, and Starlette.

SIGNIFICANCE

The corrected model of GEM 10C (180 x 180 field) was employed to generate a global set of 1° x 1° anomalies. These anomalies are being used to represent a realistic earth in Gravsat mission analysis. They are estimated to be accurate to about 10 mgals.

FUTURE EMPHASIS

Several solutions of the gravity field will be derived and are described as follows:

	Solution	Harmonics Complete	Data
(1)	Satellite Model	30 x 30	32 satellites
(2)	Combined model	36 x 36	satellite + surface gravity
(3)	Combined model	36 x 36	satellite + surface + altimeter
(4)	Detailed gravity field	180 x 180	global set of 1° x 1° altimetric-gravimetric geoid heights + data in solution (3)
(5)	Isostatic field	180 x 180	1° x 1° topographic heights (bathymetric depths)

It is expected that the geoid error, due to the error of commission of the coefficients in the harmonic fields, will be reduced to less than one meter for each of the new models.

REFERENCES

Lerch, F.J., S.M. Klosko, R.E. Laubscher, C.A. Wagner, "Gravity Field Model Improvement Using GEOS-3 (GEM 9 and 10)," GSFC X-921-77-246, September 1977; and JGR, in publication 1979.

Lerch, F.J., S.M. Klosko, R.E. Laubscher, C.A. Wagner, "Gravity Model Improvement Using GEOS-3 Altimetry (GEM 10A and 10B)," EOS, Vol. 59, #4, p. 260, April 1978a.

Lerch, F.J., S.M. Klosko, C.A. Wagner, R.P. Belott, "Goddard Earth Model Development for Oceanographic Applications," presented at Marine Geodesy Symposium Univ. of Miami RSMAS, October 1978b.

Rapp, R., "Potential Coefficient Determinations from 5° Terrestrial Gravity Data," OSU No. 251, January 1977.

FIGURE 4B-1

COMPARISON OF 5° OCEANIC GRAVITY ANOMALIES (958 BLOCKS)

ALTIMETER-GRAVITY

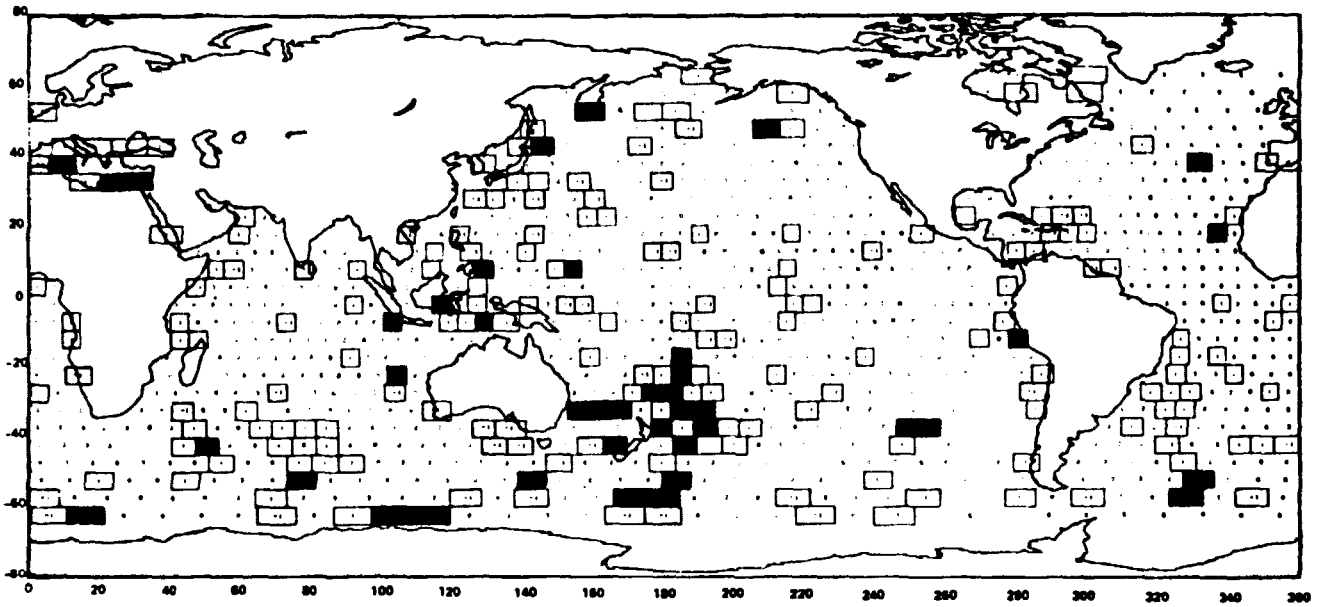

ALTIMETER-GEM 9

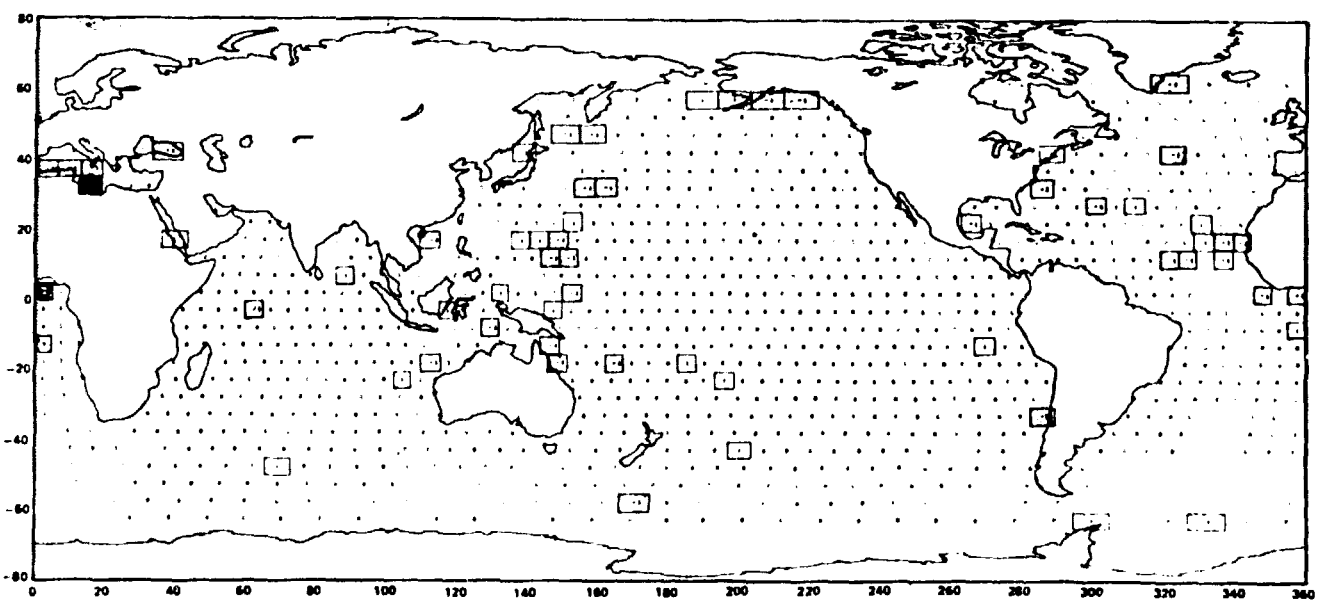

MAGNITUDE OF DIFFERENCE

- 0 LESS THAN 10 MGAL
- □ 10 TO 19 MGAL
- ■ GREATER THAN 20 MGAL

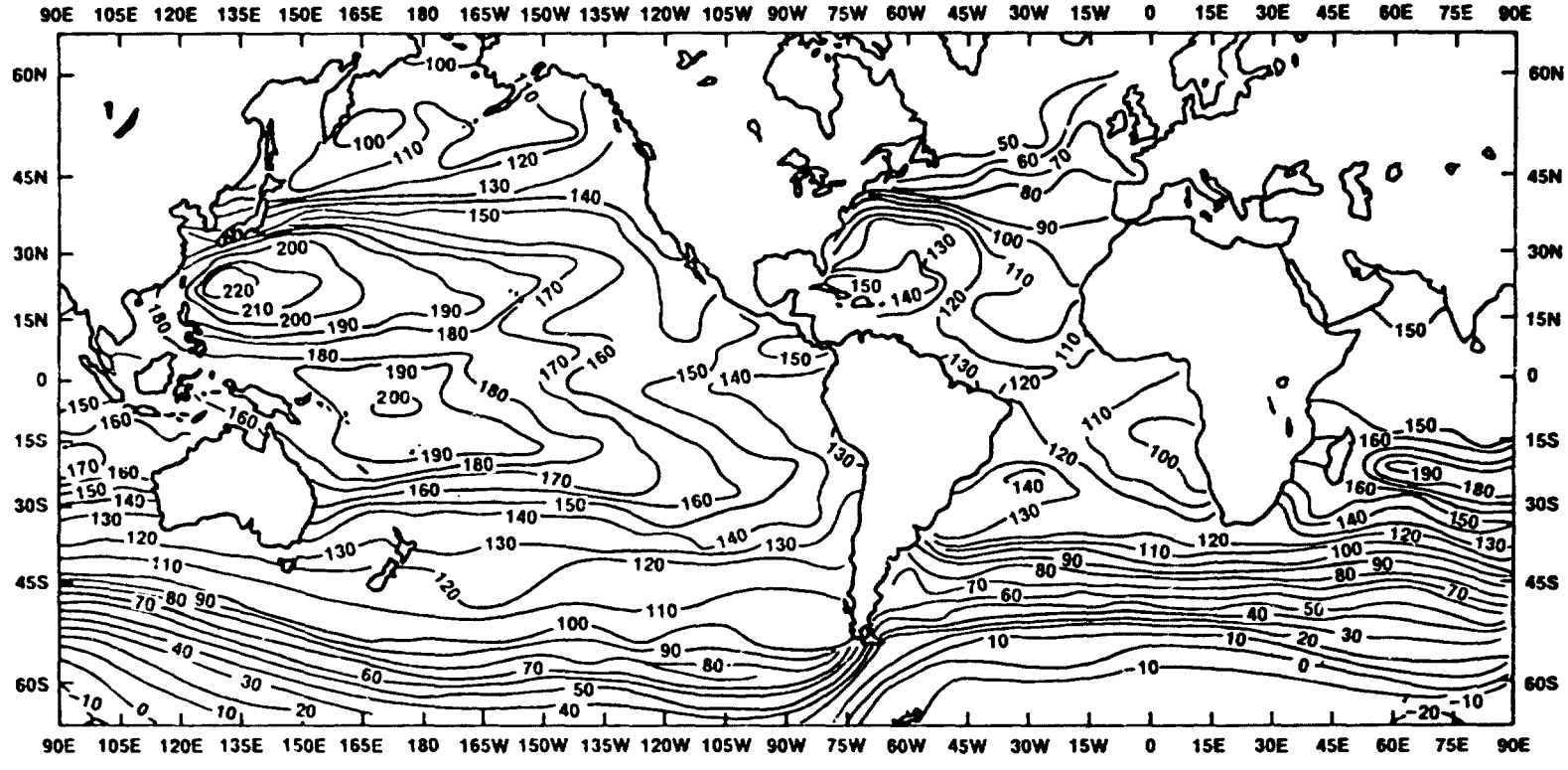

FIGURE 4B-2. Quasi-stationary Dynamic Sea Surface Topography Relative to 1000 db Surface
Wavelengths > 10^3 km
Contour Interval - 10 cm

FIGURE 4B-3. ALTIMETRIC – GRAVIMETRIC GEOID HEIGHT DISCREPANCIES ALONG COAST LINES

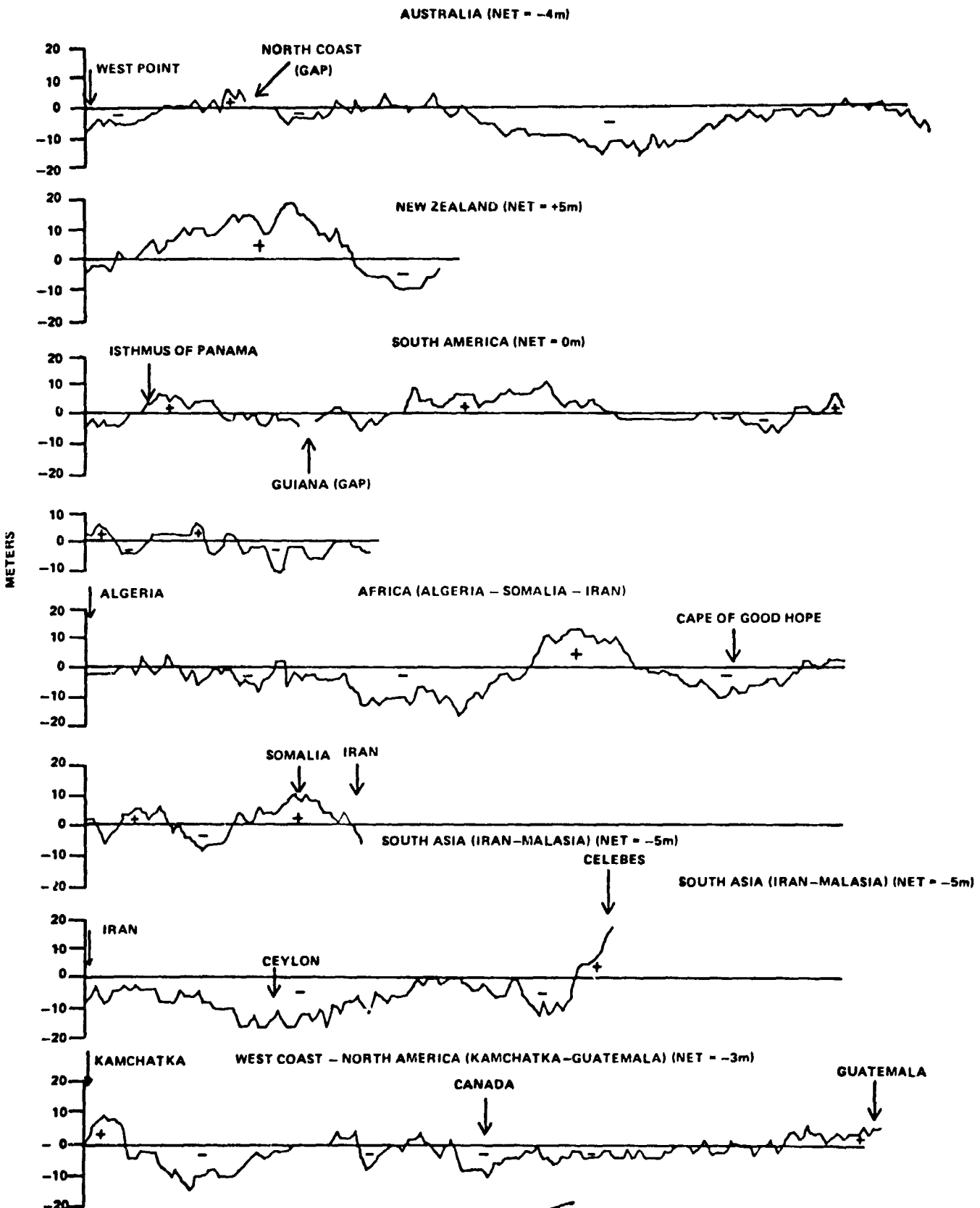

N80-20749

C. GRAVITY MODEL IMPROVEMENT FOR SEASAT

by

F. J. Lerch

OBJECTIVE

The objective is to improve the gravity field model of the earth to reduce orbit error on Seasat for more effective use of the spacecraft altimetry. Seasat altimetry (±10 cm) requires precise knowledge of the radial position of the satellite for oceanographic applications (e.g., tides and ocean circulation).

BACKGROUND

Previously, the gravity field (Lerch, et al., 1977) was improved for GEOS-3 orbits for more effective use of the spacecraft altimetry. Radial errors were reduced from 5m to 1m on GEOS-3 orbits by adjusting the gravity model (GEM 9) with use of the GEOS-3 laser data. It was also shown that combined use of the GEOS-3 altimeter and laser data produced a gravity model, GEM 10-B (Lerch, et al., 1978), that gave significantly further improvement in the radial accuracy of the orbits. These same techniques were recently applied to the Seasat orbits.

RECENT ACCOMPLISHMENTS

Three gravity models, PGS-S1, S2, and S3 (Lerch, et al., 1979), were derived to improve Seasat orbits using the data as shown in Table 4C-1. Laser and S-band data from Seasat was spread over a 3-month lifetime on the spacecraft altimetry. Harmonic analysis (Kaula, 1966) was performed to select the gravitational terms in the models which are important for Seasat orbits. Orbital position perturbations were computed using Kaula's rule for the size of the coefficients and results are presented in Figure 4C-1 for harmonics through degree and order 36. Perturbations above the solid black line, practically all greater than 10 cm, were included in the adjustment of the gravity field. Although the recovery of the coefficients is based upon the total position perturbations of Figure 4C-1, which are mostly due to the along-track component, it is the radial component which is needed for accurate reduction of the satellite altimetry. Radial perturbations (Lerch, et al., 1979), being significantly smaller than the total perturbation, are modeled down to a few centimeters in the adjusted set of harmonic coefficients.

In PGS-S1 and S2 the solution is based upon satellite data only and the harmonics, solid through 30 x 30, are not completely separable (ill-conditioned) in a normal least squares adjustment, where only noise is minimized in the residuals. To achieve separability (that is a solution for all the harmonics) least

squares collocation (Moritz, 1978) was employed where both noise and signal are minimized collectively. The analysis for this method of solution is given in the above referenced report for Seasat. However, in the case of PGS-S3 where GEOS-3 altimetry and surface gravity data are combined with PGS-S2, the normal least squares method gives a well-conditioned solution (GEM 10B plus Seasat data). As with GEOS-3 orbits this latter type of solution (PGS-S3) gave better radial positions for the Seasat orbits.

Seasat altimetry data was employed to estimate the accuracy of the radial position of Seasat orbits with use of the different gravity models. This technique is based upon the condition that at the crossover point of two altimeter tracks the difference in the altimeter measurements is equal to the difference in the radial position of the orbits. The difference in these two quantities is called the crossover residual which should be zero except for errors in the orbits and small effects from atlimeter noise or sea state changes. Here it will be assumed that the residuals are due to errors in each of the two crossing orbits. A global set of 8000 altimeter crossover points were taken over a 12-day period of Seasat altimetry. The rms of the crossover residuals were computed and are given in Table 4C-2, where it is seen that the PGS-S3 model gives the best results with orbit errors of about one meter.

SIGNIFICANCE

Orbit errors on Seasat have been reduced from 3m with GEM 9 to 1.8m with PGS-S2 and 1.3m with PGS-S3. With use of PGS-S3 a time tag correction of 66 ms has been determined for the altimeter data which compares closely with a value of 68.5 ms estimated from altimeter hardware. The new models are being used to generate preliminary orbits for reduction of Seasat altimetry.

FUTURE EMPHASIS

New solutions will be computed which will increase the coverage of the tracking data, improve the orbital modeling of atmospheric drag and solar radiation pressure, improve the preprocessing corrections for the S-band data (antenna offsets and ionospheric refraction), and then increase the weight of the S-band data in the solution because of its high density in orbital coverage. Since the gravity field is modeled to within 10 cm for Seasat radial perturbations, it is felt that the above improvements are necessary in order to realize the benefit from this refined modeling of the gravity field.

REFERENCES AND PUBLICATIONS

Kaula, W., Theory of Satellite Geodesy, Blaisdell Publishing Company, Waltham, Massachusetts, 1966.

Lerch, F.J., S.M. Klosko, R.E. Laubscher, and C.A. Wagner, "Gravity Model Improvement Using GEOS-3 (GEM 9 and 10)," Journal of Geophysical Research, July 31, 1979; and GSFC X-921-77-246, 1977.

Lerch, F.J., C.A. Wagner, S.M. Klosko, R.P. Belott, R.E. Laubscher, and W.A. Taylor, "Gravity Model Improvement Using GEOS-3 Altimetry (GEM 10A and 10B)," presented at the Spring Meeting of the American Geophysical Union, Miami, Florida, April 1978.

Lerch, F.J., J.G. Marsh, "Gravity Model Improvement for Seasat," presented at the Spring American Geophysical Meeting, Washington, D.C., May 1979.

Moritz, H., "Least Squares Collocation," Review of Geophysics and Space Physics, Vol. 10, No. 3, August 1978.

TABLE 4C-1. DATA EMPLOYED IN MODELS FOR SEASAT

PGS-S1 DATA = GEM 9 + SEASAT LASER

PGS-S2 DATA = GEM 9 + SEASAT (LASER + S-BAND)

PGS-S3 DATA = PGS-S2 + GLOBAL GRAVIMETRY AND ALTIMETRY

GEM 9 DATA

Type	No. of Obs.	No. of Satellites	No. of Arcs	Harmonics Complete
optical	150,000	24	287	16 x 16
electronic	477,000	11	97	16 x 16
laser	213,000	9	127	22 x 22
		SEASAT DATA		
laser	16,500	1	8	30 x 30
S-band	5,100	1	8	30 x 30

TABLE 4C-2. ORBIT ANALYSIS EMPLOYING A GLOBAL COVERAGE OF ALTIMETER CROSSOVERS ON SEASAT

MODEL	CROSSOVER RESIDUALS	ORBIT ERROR
PGS-S1	3.0 m	2.1 m
PGS-S2	2.5	1.8
PGS-S3	1.9	1.3

FIGURE 4C-1. **PERTURBATIONS FROM SEASAT FOR HARMONICS THROUGH 36 X 36**

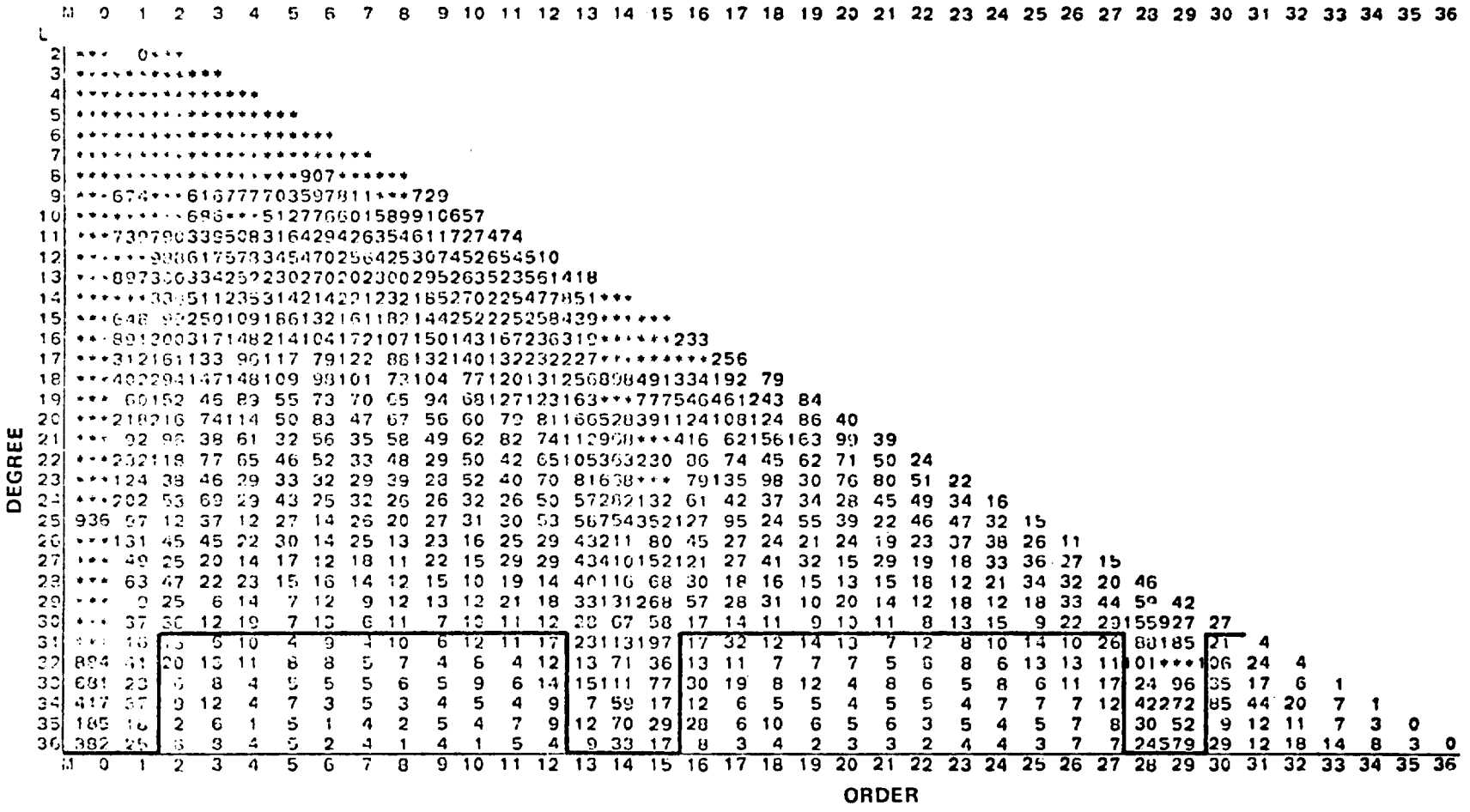

(UNITS ARE CM)

*** > 999 CM

HARMONICS ABOVE SOLID LINE INCLUDED IN SOLUTION

4-36
132

D. THE GRAVITY FIELD IN THE CENTRAL PACIFIC FROM SATELLITE-TO-SATELLITE TRACKING AND IMPLICATIONS FOR MANTLE CONVECTION

By

J. G. Marsh

OBJECTIVE

The objective of this work has been to derive gravity anomalies in the Central Pacific Ocean using GEOS-3/ATS-6 satellite-to-satellite doppler tracking data and to investigate the gravity anomaly patterns for mantle convection implications.

BACKGROUND

The Earth's gravity field has been greatly explored using artificial satellites for some time now. Their behavior is related to the spherical harmonic coefficients of the gravity field which, through accurate tracking of satellites at many altitudes, are found along with the tracking station coordinates. This general method has proven very useful and is presently the chief means of studying the global gravity field. What we report on herein are the recent results of a different method, an independent technique of directly measuring the Earth's gravity field whereby a low orbiting ($\sim$840 km) satellite (GEOS-3) is tracked via Doppler by a much higher ($\sim$40,000 km) satellite (ATS-6) in a synchronous orbit with the Earth. Doppler tracking furnishes the low satellite's velocity (range-rates) as a function of time which can easily be converted to (line-of-sight) (between ATS-6 and GEOS-3) accelerations or gravity anomalies. The gravity values are plotted along the track of the satellite, and using many crossing tracks these values can be contoured into a map of the gravity field at this altitude (i.e., 840 km).

As discussed in an earlier paper (Marsh and Marsh, 1976), the spectrum of the gravity field becomes much flatter beyond about the 12th degree and order. There is general agreement on the nature of the gravity field below about the 12th degree and order, but beyond this point the uncertainties in the derived harmonic coefficients and the resulting gravity anomalies increase substantially. Near the 30th degree and order a single coefficient may be say, 80% in error, although as a group the coefficients may model the gravity field with considerably less error. The actual amount of mismodeling in the gravity field models above (12,12) is difficult to accurately establish, especially over oceans where there is a scarcity of surface data: only formal uncertainties exist. The satellite-to satellite tracking (SST) method provides a direct mapping of the line-of-sight accelerations, thus providing a comprehensive areal test of the accuracy of existing satellite-based gravity models.

RECENT ACCOMPLISHMENTS

We have used the SST method to derive a line-of-sight gravity map relative to a 12th degree and order field model for the central and east equatorial regions of the Pacific Ocean. This work has been an extension of a previous analysis of "destruct" mode SST data over the East Pacific Rise (Marsh and Marsh, 1977). In the present analyses a total of 40 passses of the non-destruct SST data were analyzed covering the mid-Pacific Ocean area. The sub-satellite point of the ATS-6 spacecraft was located at 220°E. longitude when these data were recorded. Orbit solutions were computed for each pass of SST data using a combination of the SST data, direct tracking of ATS-6 and Navy Doppler, laser, C-Band and S-Band tracking of GEOS-3.

The Geodyn orbit computation computer program was used for this analysis with the following forces being modeled: luni-solar gravity, solar radiation pressure, atmospheric drag, and the gravity field of the earth using the GEM-10 gravity model coefficients through the 12th degree and order. The gravity field below (12,12) is well known and any errors in the lower degree coefficients appear as long wavelength features distinct from the wavelengths of interest for the present experiment. The results of the orbit comptuation process gave a set of range-rate residuals (observed minus computed range-range) for each pass of data. In order to minimize the effects of ionospheric refraction, the first and last five minutes of data were deleted from each pass.

Accelerations corresponding to the 40 passes of SST data, derived in the above described manner are presented in Figure 4D-1. Although along each track the measurements are about 65 km apart, the tracks themselves form a rough grid of about 5° resolution. Visual inspection of the accelerations reveals a high degree of consistency along closely spaced tracks and indicates the existence of significant anomaly patterns in several regions. The repeatability of the SST data is displayed in Figure 4D-2 which contains a plot of the range-rate residuals for revolutions 8797 and 8086 which are separated spatially by only a couple of degrees, but temporally by more than a week. Maximum residuals of about 1 mm/s are noted along these passes. The agreement between the two independent passes is quite good with differences in the smoothed residuals generally on the order of 0.1 mm/s or less. Comparisons along the other two pairs of closely spaced tracks (8829, 8900 and 8698, 9025) indicate similar close agreement.

In order to facilitate the analyses of the accelerations, the data were contoured and the map of accelerations measured at the GEOS-3 altitude is presented as Figure 4D-3. The accelerations are line-of-sight values between ATS-6 and GEOS-3, however within 30°-40° of the sub-satellite point they can be considered to be radial accelerations. The precision of the gravity anomalies is about 0.2 mgal at the GEOS-3 altitude of 840 km.

SIGNIFICANCE

The amplitudes of the SST anomalies are everywhere about a factor of ten smaller than the corresponding GEM anomalies at the surface. That is, with an increase in height of 840 km, the altitude of GEOS-3, these gravity anomalies diminish in amplitude by a factor of ten. If a typical source is represented as a point mass, given the gravity anomaly at two elevations allows the depth of the source to be uniquely determined. This simple, but unrealistic, source gives a depth of about 400 km. This is a maximum depth and any distributed source will be shallower. A cyclindrical or line source implies a depth of about 140 km (Marsh and Marsh, 1976). Using direct modeling, Watts (1976) estimated the source for the Hawaiian anomaly to be at a depth of about 120 km.

The Hawaiian and Cook-Austral anomalies, however, correlate closely with residual depth anomalies (Watts, 1976; Crough, 1978) and their sources may lie within the lithosphere itself. The gravity anomaly arises in this case from the bump in the sea floor and also from its compensation, a negative effect, at depth. The great dimensions of these anomalies shows that they are much too large to be supported by the strength of the lithosphere.

A number of the gravity anomalies delineated by the SST method show no correlation with volcanic features on the sea floor. These relations are particularly clear on Figure 4D-3. The northeast lobe of the Hawaii anomaly, the center part of the Christmas Island anomaly and the Pitcarin anomaly are all associated with relatively smooth sea floor. Significant residual depth anomalies are apparently absent near the Pitcarin anomaly and the northeast lobe of the Hawaiian anomaly. If more detailed residual depth studies reveal no anomalies, then the source of the gravity anomalies must be placed significantly deeper in the earth.

FUTURE EMPHASIS

The above described work has been conducted in close cooperation with Professor Bruce Marsh, of the Johns Hopkins University. A complete description of the analyses is contained in a report by Marsh, Marsh, Williamson and Wells, 1979.

An additional 50 passes of SST data have recently been acquired over the Central Pacific. These new data when combined with the 40 passes used in the present analysis promise to provide a coniderably more detailed gravity map in this region. In addition, the global set of Seasat altimeter data with a precision of 10 cm will be used to complement the SST data. This total data set is expected for form an important basis for more definitive mantle convection analyses in the Pacific which have previously been seriously hampered by the lack of real observational data.

REFERENCES AND PUBLICATIONS

Crough, S.T., "Thermal Origin of Mid-Plate Hot-Spot Swells," Geophys. J.R. astr. Soc., 55, 451-469, 1978.

Marsh, B.D., Marsh, J.G., "On Global Anomalies and Two Scale Mantle Convection," Journal of Geophys. Res., Vol. 81, No. 29, pp 5267-5280, 1976.

Marsh, J.G., Marsh, B.D., Conrad, T.D., Wells, W.T., Williamson, R.G., "Gravity Anomalies Near the East Pacific Rise with Wavelengths Shorter than 3300 km Recovered from GEOS-3/ATS-6 Satellite-to-Satellite Doppler Tracking Data," NASA TM 78553, 1977.

Marsh, J.G., Marsh, B.D., Williamson, R.G., Wells, W.T., "The Gravity Field in the Central Pacific from Satellite-to-Satellite Tracking and Implications for Mantle Convection," paper in publication, 1979.

Watts, A.B., "Gravity and Bathymetry in the Central Pacific Ocean," J. Geophys. Res., 81, 1533-1553, 1976.

Figure 4D-1

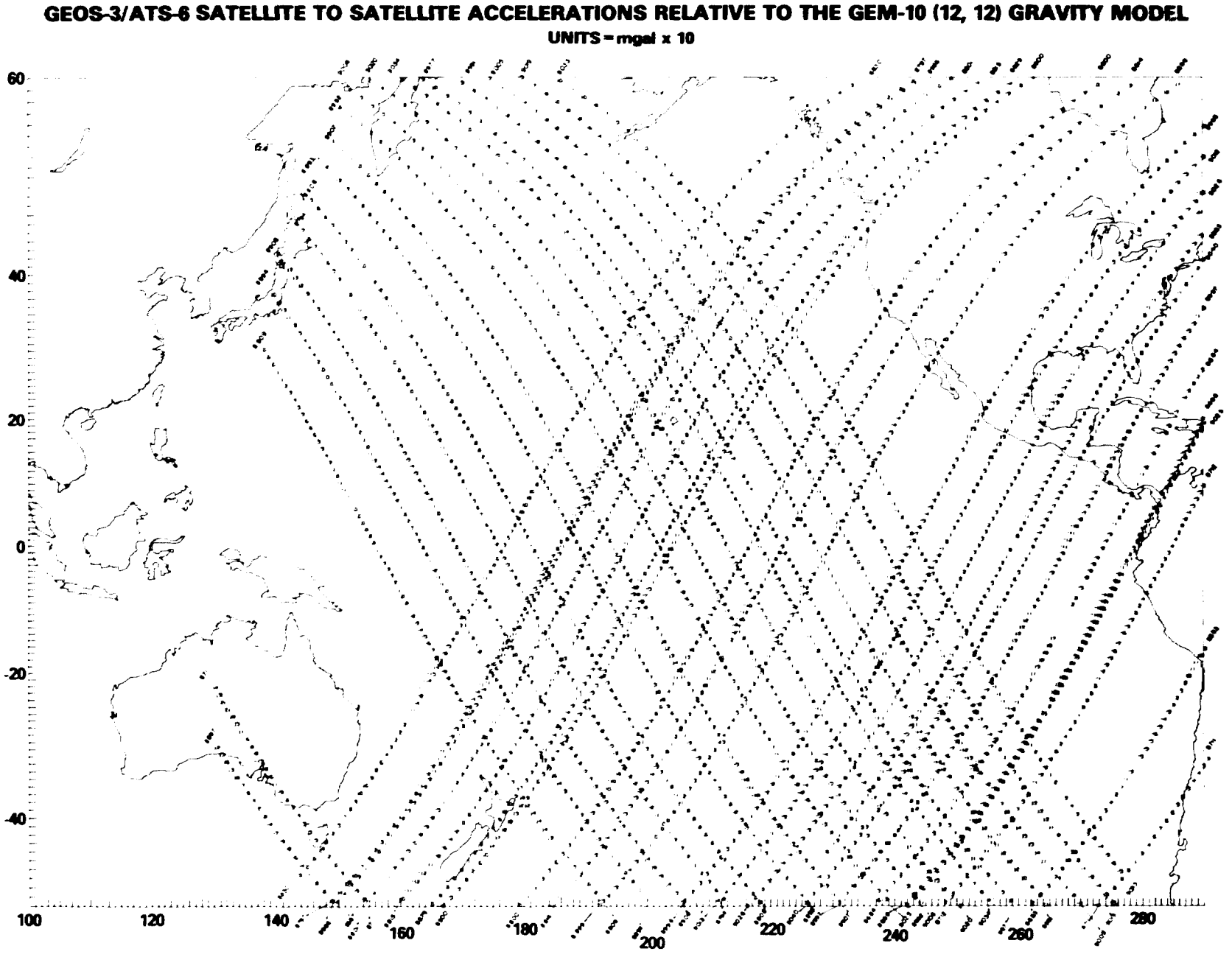
GEOS-3/ATS-6 SATELLITE TO SATELLITE ACCELERATIONS RELATIVE TO THE GEM-10 (12, 12) GRAVITY MODEL
UNITS = mgal x 10
60
40
20
0
-20
-40
100
120
140
160
180
200
220
240
260
280

Figure 4D-2. **GEOS—3/ATS—6 SATELLITE TO SATELLITE RANGE RATE RESIDUALS WITH RESPECT TO THE GEM—10 (12, 12) GRAVITY MODEL ALONG OVERLAPPING GROUND TRACKS**

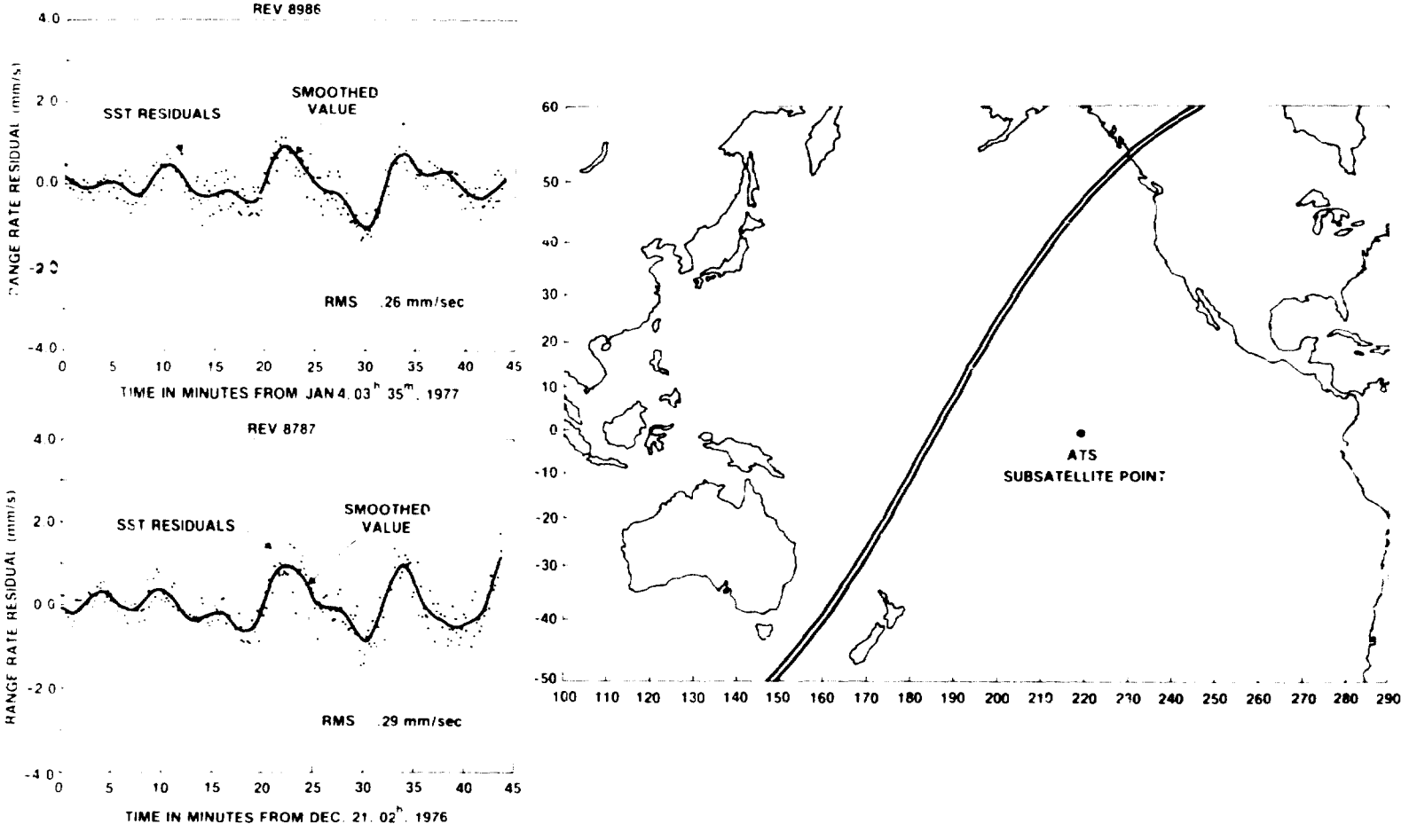

N80-20751

E. UNEXPLAINED LAGEOS PERTURBATION

by

D. P. Rubincam

OBJECTIVE

The purpose of this work is to discover what unknown perturbation is operating on Lageos and model it in the Geodyn orbit determination computer program.

BACKGROUND

An unmodeled perturbation is causing the semimajor axis of Lageos' orbit to decrease secularly at the rate of 1.1 mm day^{-1} (see Fig. 4E-1). It is important to understand and model this perturbation so that Lageos can be used to study geophysical phenomena which require high precision, such as plate motion.

Last year the following perturbations were ruled out as being the unknown perturbation: general relativity, resonance with the gravitational field, interaction with the magnetic field, the Poynting-Robertson effect, and planetary perturbations. These mechanisms fail to give a secular effect or do not explain the observed magnitude of the secular decay. In the latter case they fail by two orders of magnitude or more.

RECENT ACCOMPLISHMENTS

The following mechanisms have recently been investigated: gravitational radiation, drag from near-earth dust, the Yarkovsky effect, the Schach effect, terrestrial radiation pressure, charged particle drag, and neutral particle drag.

Gravitational radiation and drag from dust cause a secular decrease in the semimajor axis. However, it was found that gravitational radiation fails by 26 orders of magnitude to explain the observed decay. Drag from dust fails by at least two orders of magnitude when assuming a generous upper limit on the concentration of interplanetary dust near the earth. These two mechanisms have been ruled out.

The Schach effect was discovered in the course of this investigation by Milton Schach. Its operation is illustrated in Fig. 4E-2. Here a slowly or nonrotating satellite is heated up on its sunward side. The photons of thermal radiation carry away more momentum from the hot sunward side than the cold shadowed side, giving the satellite a net acceleration $\dot{\vec{v}}$ in the direction away from the sun.

If the satellite cools off and warms up instantly when moving through the shadow, then the acceleration is zero in the shadow and the acceleration over arc FED tends to cancel with that over arc FAB by symmetry when the satellite is in sunlight. However, if the satellite has some thermal inertia, then it takes some time to cool off and heat up when moving through the shadow. Qualitatively we can think of a thermally inertialess satellite passing through a rotated shadow inside of which $\dot{\vec{v}}$ is zero. In this case the acceleration over arc FE cancels that over arc FA, but no cancellation occurs for arc ABC. This leads to a net acceleration when averaging over one revolution which tends to increase the semimajor axis.

The Schach effect operates only when the orbit is shadowed. As pointed out before, the unknown perturbation operates whether the orbit is shadowed or not. The Schach effect is ruled out.

Terrestrial radiation pressure on Lageos can cause the semimajor axis to increase over short periods of time (about 60 days). Its signature on the orbit is absent from Fig. 4E-1, which shows a steady decrease over 3 years. This mechanism is ruled out.

Charged particle drag may be the unknown perturbation. The observed rate of orbital decay falls within the limits predicted by various theories of charged particle drag (Chopra, 1961). However, theories of charged particle drag are in a too uncertain state to permit a definite conclusion.

The observed secular decay can be explained by atmospheric drag from neutral helium, provided the exospheric temperature is 2200 K. Neutral hydrogen cannot explain more than 12 percent of the observed decay regardless of exospheric temperature.

In summary, it appears that atmospheric drag, whether from charged or neutral particles, is the cause for the secular decerease in the semimajor axis of Lageos' orbit. The results will be reported in detail in a Technical Memorandum in preparation.

SIGNIFICANCE

The helium drag interpretation requires a high exospheric temperature. However, a high abundance of helium at Lageos' altitude helps solve the "helium problem" of discovering an escape flux to balance its influx from the earth's crust (Kockarts, 1973). The new Schach effect may be important for studies of the lifetimes of the particles in the rings of the outer planets. The explanation of the unknown perturbation as atmospheric drag permits its adequate modeling in the Geodyn orbit determination program, permitting accurate geophysical investigations to be done.

FUTURE EMPHASIS

Future work will focus on the continued monitoring of the secular decrease in the semimajor axis, its modeling in Geodyn, and investigation of other proposed mechanisms as they arise.

REFERENCES AND PUBLICATIONS

Chopra, K. P., "Interactions of Rapidly Moving Bodies in Terrestrial Atmosphere," Reviews of Modern Physics, 33, 153-189, April 1961.

Kockarts, G., "Helium in the Terrestrial Atmosphere," Space Science Reviews, 14, 723-757, 1973.

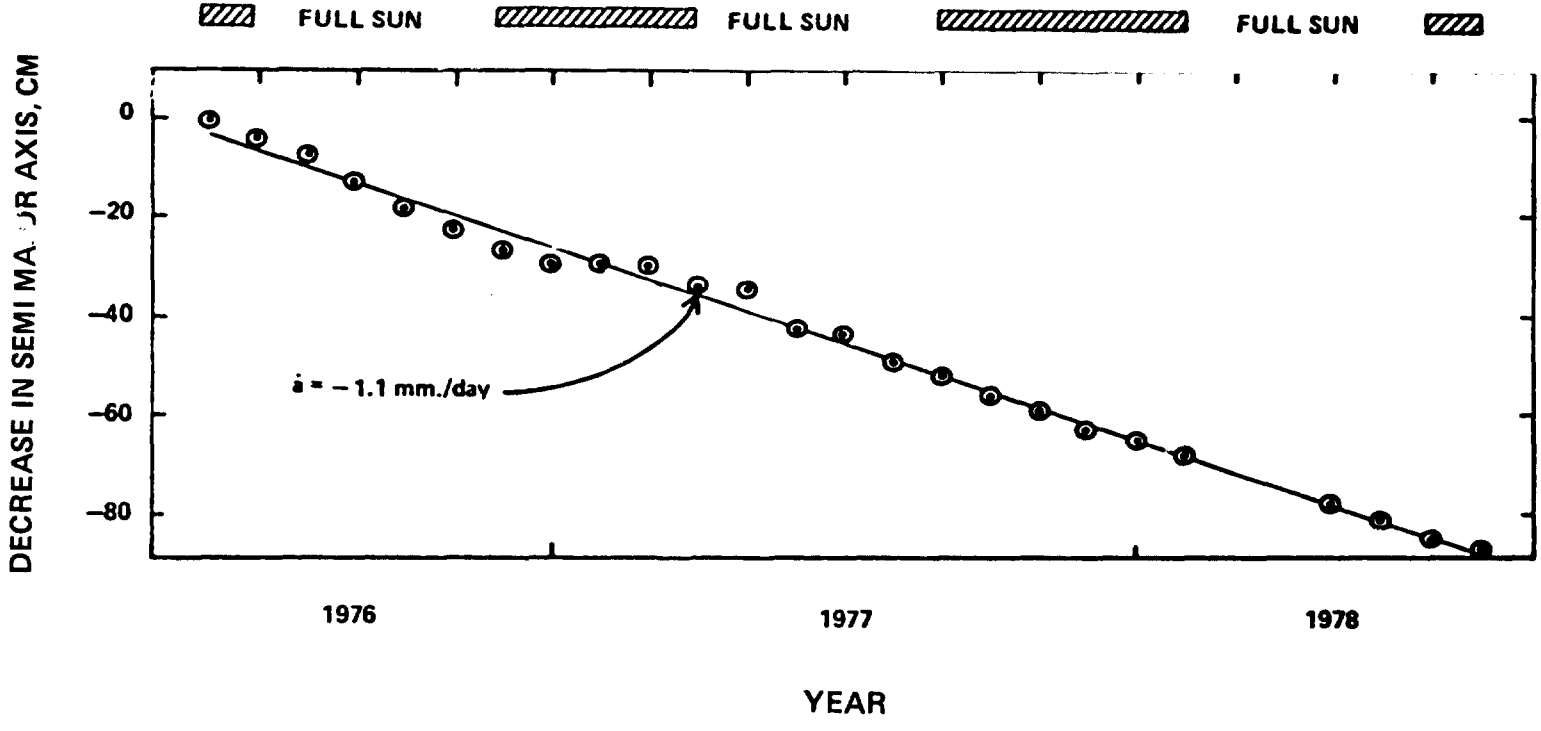
DECREASE IN LAGEOS SEMI MAJOR AXIS
27 MONTHS BEGINNING MAY 1976
FULL SUN
FULL SUN
FULL SUN
DECREASE IN SEMI MAJOR AXIS, CM
0
-20
-40
-60
-80
ȧ = – 1.1 mm./day
1976
1977
1978
YEAR

Fig. 4E-1.

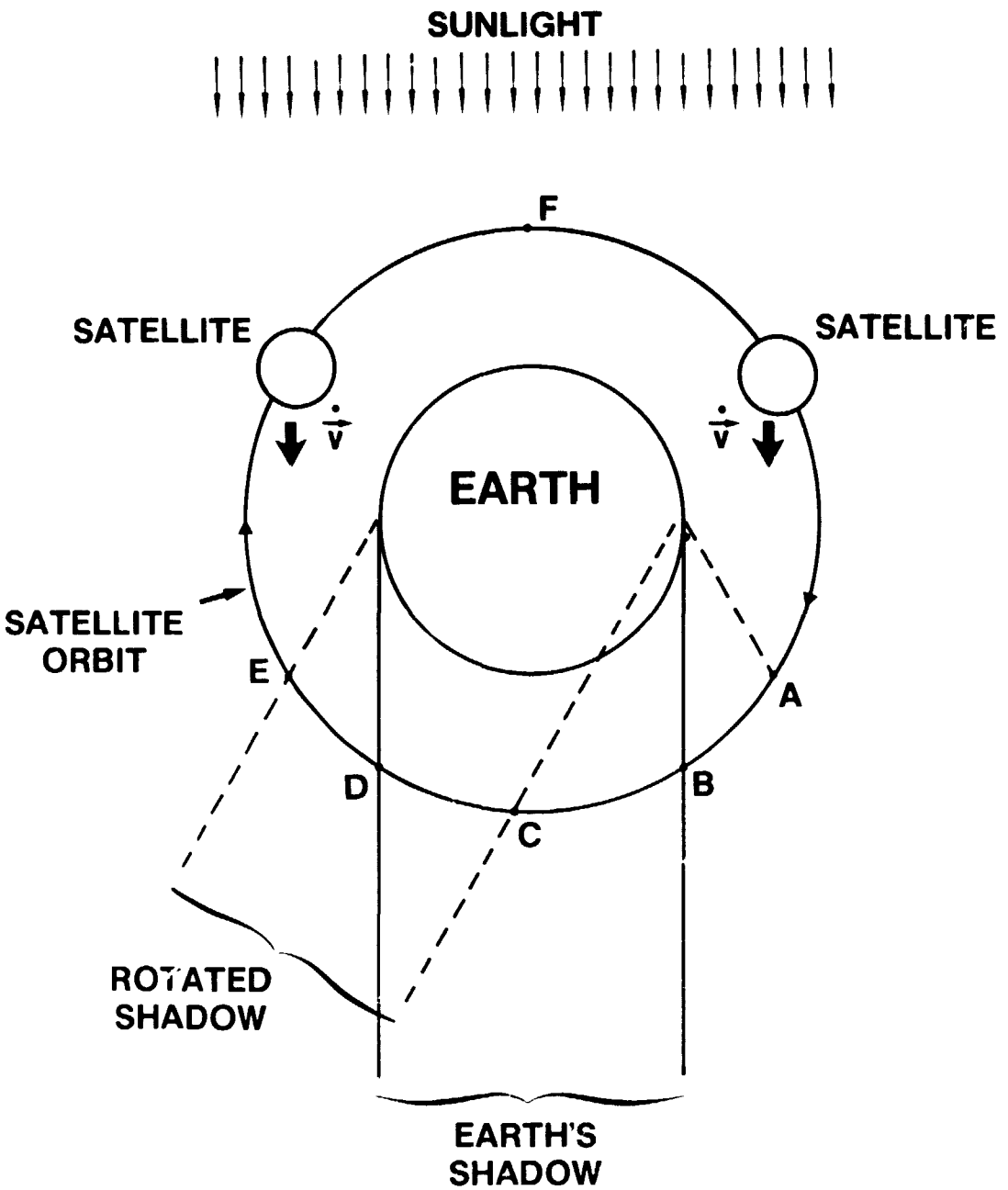

Figure 4E-2. Schematic illustration of the Schach effect.

CHAPTER 5

GLOBAL EARTH DYNAMICS

edited by

M. A. Graber

OVERVIEW

Compared with studies of the earth's crust and surface geology, the study of the earth's interior structure and dynamics is challenged by the problems of probing through thousands of kilometers of rock. Direct evidence can be obtained from phenomena in which the earth's entire structure participates dynamically. These include normal modes excited by seismic events and irregularities in the motion of the rotation axis. Quasi-static features such as the earth's gravity field are directly determined by the internal structure. Localized seismic waves can be traced through the earth to give a profile of the physical parameters along the ray's path.

The association of the Earth Survey Applications Division with satellite orbit determination has tended to direct the global earth structure studies toward satellite orbital parameters. In this chapter, the results of studies of satellite-derived gravity fields and polar motion are presented. The studies range from straightforward time series analysis to the inversion of detailed gravity fields giving information on mantle convection and lateral density variations deep within the earth.

A. MANTLE CONVECTION AND SUBCRUSTAL STRESS

by

Han-Shou Liu

OBJECTIVES

As geoscientists strive to study mantle convection problems, they face a choice: develop mantle convection models based on speculative ground or compute mantle convection patterns and subcrustal stress fields from geodynamics data. With the advent of satellite gravity data, the second alternative seems increasingly promising. The objective of this study is to investigate what information about mantle convection patterns and subcrustal stress fields under the United States may be obtained from this type of calculation.

BACKGROUND

By applying the laminar viscous flow model of the Earth's mantle, Liu (1977, 1978, 1979a, and 1979b, 1980) has endeavored to find a band pass of harmonics from the satellite data which would provide stress conditions for the development of geodynamical features in Africa, Asia and Australia. The stress conditions are due to mantle convection. It is well known that the peculiarities of the geological and geophysical features in the western United States are very prominent. Therefore, it may be worthwhile to apply these ideas and methods to investigate the tectonic, metallogenic and seismological provinces in the United States and show how many of their features are in accordance with crustal deformation associated with stresses due to mantle convection.

RECENT ACCOMPLISHMENTS

Gravity data of the Earth have been applied to calculate the stress field under the United States caused by mantle convection. It has been found that the stress vectors in the crust of the United States are comprised of several consistent stress patterns. The remarkable radial divergent field in the western United States is one of the patterns. The northeast-southwest compression in California is another pattern. This pattern seems to be caused by the upwelling mantle convection cell which is approximately centered at (42°N, 248°E), close to the location of the Yellowstone volcanic field (44.5°N, 248.5°E). Improved gravity data and more complicated laws than that of Newtonian viscosity, could be assumed and the improvement or otherwise of this fit would be valuable tests.

SIGNIFICANCE

The stress field under the United States has been developed and seems to be consistent with the tectonic, metallogenic, and seismologic features in the North American continent.

REFERENCES AND PUBLICATIONS

Liu, H.S. "Convection Pattern and Stress Systems under the African Plate," Physics of the Earth and Planet. Inter., 15, 60-68, 1977.

Liu, H.S. "Mantle Convection Pattern and Subcrustal Stress Field Under Asia," Physics of the Earth and Planet. Inter., 16, 247-256, 1978.

Liu, H.S. "Mantle Convection and Subcrustal Stress Under Australia," Modern Geology, Vol. 7, 29-36, 1979a.

Liu, H.S. "Convection Generated Stress Concentration and Seismogenic Models of the Tangshan Earthquake," Physics of the Earth and Planet. Inter., 19, 307-318, 1979b.

Liu, H.S., "Convection Generated Stress Field and Intra-Plate Volcanism," Tectonophysics (in press) 1980.

Liu, H.S. "Mantle Convection and Subcrustal Stress Under the United States," acceptable for journal publication.

D30

N80-20753

B. INFORMATION THEORY DENSITY DISTRIBUTION

by

D. P. Rubincam

OBJECTIVES

The objectives of this project are to make a rational inference as to what the density distribution of the Earth is and investigate its geophysical significance, particularly with regard to convection in the mantle.

BACKGROUND

The inverse technique used in this project is Information Theory Inference (ITI). An explanation of its philosophy and general approach may be found in Rubincam (1979).

The first problem to be solved using ITI was to infer a spherically symmetric density distribution using the known mass M_E and moment of inertia C_E of the earth as constraints. Here the earth was divided into infinitesimal cubes of equal volume. Indistinguishable particles of identical mass were distributed among the cubes. The density at any point was then the number of particles in the cube in question times the mass of the particles, divided by the volume of the cube. Each possible distribution of particles amongst the cubes was given a probability of P_i and Shannon's information measure was maximized subject to constraints $\Sigma P_i M_i = \bar{M}_E$ and $\Sigma P_i C_i = \bar{C}_E$, where M_i and C_i are the mass and moment of inertia, respectively of the ith model and $\bar{M}_E$ and $\bar{C}_E$ are experimentally measured values for mass and moment of inertia.

The problem was then shown to be completely analogous to the grand canonical ensemble in statistical mechanics, where particles are distributed among energy levels. The canonical ensemble methods were then used to obtain the average number of particles in each cube. The resulting average density distribution is a half Gaussian:

$$\bar{\rho}(r) = 12.30e^{-1.46r^2/a_E^2} \text{ gm/cm}^3$$

This work was published in Rubincam (1978).

Subsequent work focused on the lateral variations in the density distribution. The problem here was to find the most likely three-dimensional density distribution $\bar{\rho}(r)$ using the spherical harmonic coefficients $\bar{C}_{lm}$ and $\bar{S}_{lm}$ of the geopotential as constraints. The coefficients are almost the only source of information on lateral density variation. Only recently has seismic data given some crude information on this. The emphasis

in this work is to relate the density variations to possible convection in the mantle.

The problem in lateral variation was solved using the statistical mechanical techniques described above, plus these important assumptions: the density distribution can be written as a sum of spherical harmonics of the form

$$\rho(\vec{r}) = \rho(r,\phi,\lambda) = \sum_{\ell=0}^{\infty} \sum_{m=0}^{\ell} \sum_{i=1}^{2} \bar{\rho}_{\ell mi}(r)\, \bar{Y}_{\ell mi}(\phi,\lambda)$$

and the lateral variations are taken to be small perturbations on top of the well-known spherically symmetric density distribution. In Dziewonski, et al., (1975), a parameterized model was taken to be in the gross radial distribution.

The resulting information theory coefficients in the above equation have the form $\bar{\rho}_{\ell mi} \sim r^{\ell}$ where ℓ is the degree of the harmonic.

A computer program was written to compute and plot relative density variations in the mantle for shells of varying radii on a cylindrical projection and slices through the center of the earth along various great circles. The plots revealed that the total relative density variations in the mantle are about 0.002 g/cm^3 after stripping off 30 km of compensated crust, and about 0.02 g/cm^3 for the same thickness of uncompensated crust. The hydrostatic bulge was removed from the $\ell = 2,4$; $m = 0$ terms in the spherical harmonic expansion in all cases, using the equilibrium flattening of 1/299.76 (Khan and O'Keefe, 1974).

RECENT ACCOMPLISHMENTS

The slices through the center of the earth are now produced using color-coded computer-generated pictures. Figures 5B-1 and 5B-2 are examples of a slice based on the color photographs. The track of the slice is shown in Fig. 5B-3. This slice was chosen to pass through the Hawaiian Island chain from Midway Island to the Big Island of Hawaii. In Fig. 5B-1 30 km of compensated crust is removed and the density interval between contour lines is 0.0002 g/cm^3. In Fig. 5B-2 30 km of uncompensated crust is removed, and the interval between contour lines is 0.002 g/cm^3. Both are based on the GEM 10B gravity field.

The relative density variations have also been plotted on a tectonic activity map (Lowman and Frey, 1979, p. 40); Fig. 5B-4 is based on the color map. Here no topography or crust is removed, and the density variations are assumed to be distributed inside of a sphere. The figure shows what the density distribution looks like at the very surface of the sphere. By ignoring the crust and topography the meaning of this map becomes a bit abstract, but it should be indicative of where mass excesses and deficiencies occur. Its closest relative is a gravity anomaly map. The total relative density variation in Fig. 5B-4 is about 0.005 g/cm^3. It is also based on the GEM 10B gravity field, and the equilibrium

flattening has been removed from the $\ell = 2,4$; $m = 0$ terms according to the new equilibrium flattening of 1/299.83 (Nakiboglu, 1979). The density difference between contour lines is 0.0014 g/cm^3.

To produce Fig. 5B-4 it was necessary to invert map coordinates to obtain latitude and longitude from the Van der Grinten projection. The reason for doing so is that the computer plots out a regular array of points at which the density is computed on the Lowman map, which uses the Van der Grinten projection. The latitude and longitude at each array point are required in the spherical harmonic expansion of the density distribution. The forward problem of computing Van der Grinten map coordinates from latitude and longitude was also solved using an algebraic approach, in contrast to the trigonometric approach of O'Keefe and Greenberg (1977). The inverse and forward problems will be published in "Inverting Map Coordinates to Obtain Latitude and Longitude in the Van der Grinten Projection," a Technical Memorandum now in preparation.

Density variations have been plotted on orthographic maps to compare with tectonic activity in the polar regions. Also, section density maps (slices through the earth parallel to the equator) have been obtained to display the density distribution in three dimensions.

The question of how to introduce elasticity into the earth models at the theoretical level has been solved. The problem here is: how does one fold completely determined seismic velocity curves into the probablistic approach of information theory? The answer here is to use the moments of the curves as constraints upon the earth models. An infinite number of such moments will reproduce a given curve exactly (aside from pathological cases of no physical interest). The practical application of this method has yet to be achieved; there appears to be no analog from statistical mechanics which can take over, as there was in the case of the density distribution based on the mass and moment of inertia of the Earth.

The foundations of ITI have been further investigated and elaborated in Rubincam (1979). The problem of how to generalize Shannon's information measure to the case of continuous probability distributions was decisively answered in favor of Shannon's original proposal, rather than going to the Kullback measure.

SIGNIFICANCE

The most obvious conslusion one can draw from Figs. 5B-1 and 5B-2 is that one must have a good idea of what the crust is doing (i.e., compensated or uncompensated) before a model of the crust is removed; the two give remarkably different answers. We know that a compensated crust is more nearly correct. However, the entire crust is not in isostatic equilibrium. For example, the density variation under Hawaii has almost completely disappeared in Fig. 5B-2, indicating the Hawaiian Islands are uncompensated features of the crust. We conclude that better models of the crust are called for.

Figs. 5B-1 and 5B-2 also appear to give little evidence of motion in the mantle, although the high density feature near the East Pacific Rise in Fig. 5B-1 is offset from top to bottom. This may be indicative of motion; and the spreading rate here is a very high 15 cm/yr. However, can one really get a good idea of convection in the mantle from just a density map? Could not a low density region be a rising plume and a high density region a descending one, even though a picture does not give obvious indications of motion? It seems that modeling of convection is also called for.

The surface density map shown in Fig. 5B-4 gives a general idea of where mass excesses and deficiencies occur. Clearly mass excesses occur where subduction takes place in trench-mountain range and trench-island arc areas. Examples are the Himalayas, the Andes, and the Tonga Trench. Mass excesses occur at the slower-moving ocean ridges, such as the Mid-Atlantic Ridge. This is in keeping with current thinking about ridges: they are areas of low density, but there is a lot of mass in the form of a mound; the mound more than compensates for the low density and gives a mass excess. At the faster-moving ridges there is little correlation with mass excesses; the East Pacific Rise is an example. (The difference between the fast and slow ridges was first noted by David E. Smith). The reason why this occurs is not clear. Other areas of mass excess occur at proposed hot spots; examples are Yellowstone, the eastern tip of South America, the Hawaiian Islands, and the tip of Antarctica at South America. They give positive signals probably because they are examples of recent and not yet compensated volcanism, and partly dynamically supported by a rising plume.

Examples of areas of mass deficiency are Canada and Fennoscandia; these are due to depression of the surface by glaciers in the last Ice Age. Other areas with deficient mass seem to be related to the abyssal plains, such as Somalia and possibly India, the deepest feature in the geoid. Many areas of mass excess and deficiency have no correlation with surface features, and presumably refer to processes deep inside the earth.

FUTURE EMPHASIS

Future studies will focus on further investigation and interpretation of the lateral density distribution based on the gravity field. This will include better three-dimensional maps; the density structure of local regions, such as the Hawaiian Islands or the Himalayas; and the exclusion of density differences in the core, which are believed to be small (but nonetheless present for otherwise convection in the core could not take place).

Much of the future work will involve the practical inclusion of elasticity into the earth models. At present the density variations are smooth: models based only on gravity data cannot contain discontinuities, such as intrusions or plate boundaries. This can only come from elasticity data, such as seismic velocities. Hence the inclusion of elasticity data will make the models more realistic.

REFERENCES AND PUBLICATIONS

Dziewonski, A.M., A.L. Hales, and E.R. Lapwood, "Parametrically Simple Earth Models Consistent with Geophysical Data," Physics of Earth and Planetary Interiors, 10, 12-48, 1975.

Khan, M.A., and J.A. O'Keefe, "Relation of the Antarctic Gravity Low to the Earth's Equilibrium Figure," Journ of Geophys. Research, 79, 3027-3030, 1974.

Lowman, P.D., and H.V. Frey, "A Geophysical Atlas for Interpretation of Satellite-Derived Data," NASA Technical Memorandum 79722, February 1979.

Nakiboglu, S.M., "Hydrostatic Figure and Related Properties of the Earth," Geophysical Journal of the Royal Astronomical Society, 57, 639-648, 1979.

O'Keefe, J.A., and A. Greenberg, "A Note on the Van der Grinten Projection of the Whole Earth onto a Circular Disk," The American Cartographer, 4, 127-132, 1977.

Rubincam, D.P., "Information Theory and the Earth's Density Distribution," NASA Technical Memorandum 78088, February 1978.

Rubincam, D.P., "Information Theory and the Earth's Density Distribution: Revised Edition," NASA Technical Memorandum 80586, August 1979.

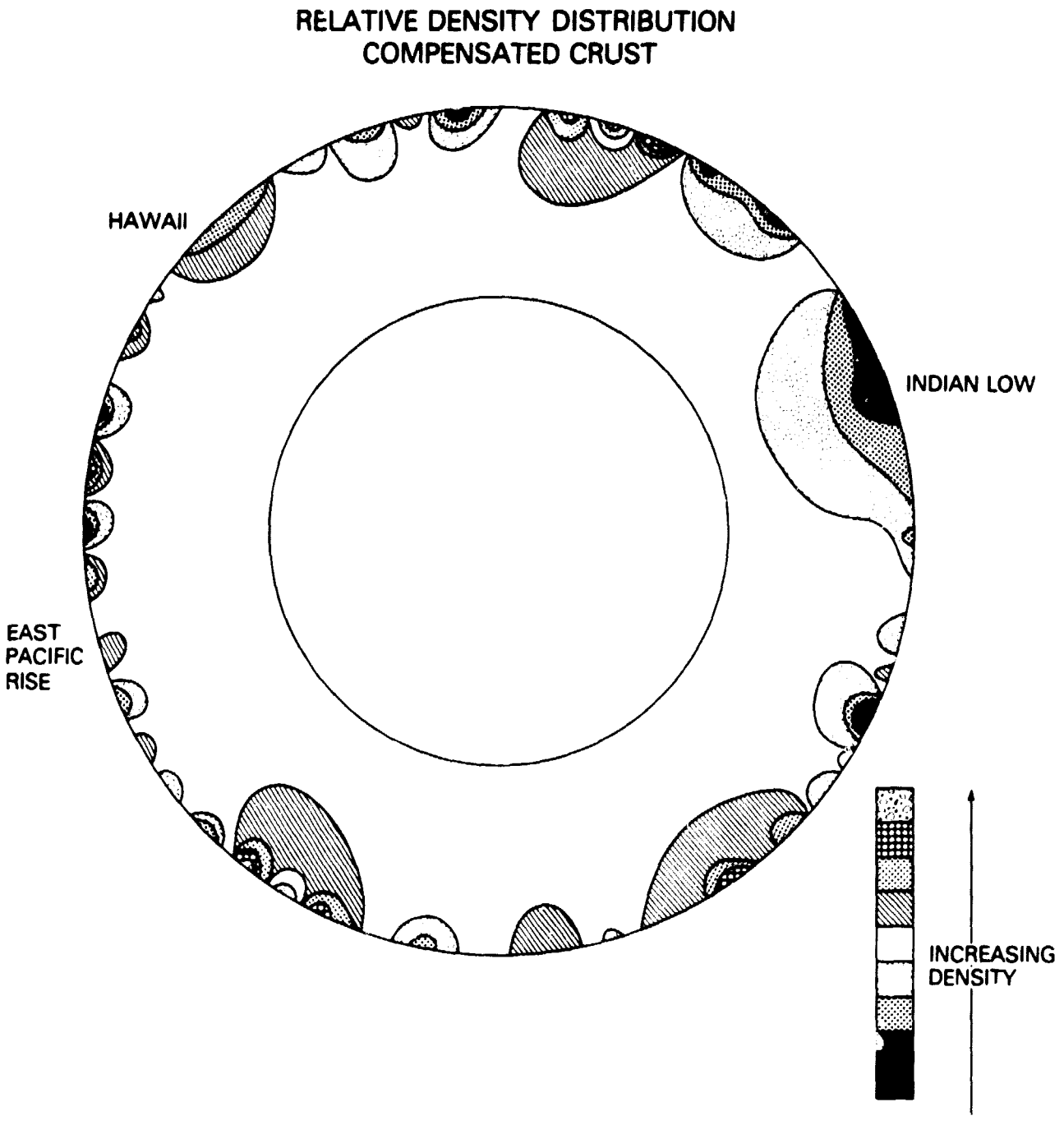

Fig. 5B-1. Slice through the center of the earth; compensated crust.

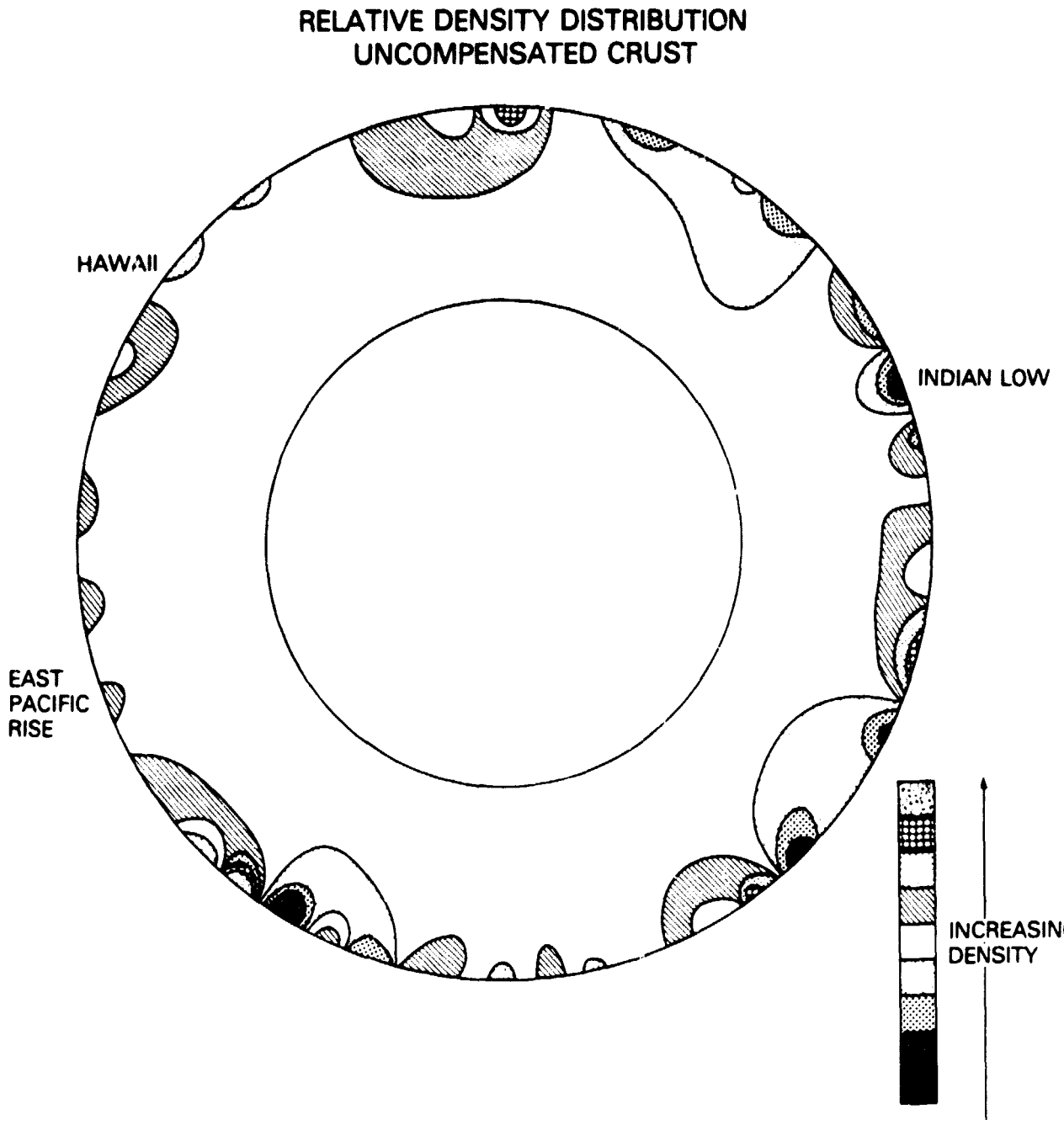

Fig. 5B-2. Slice through the center of the earth, uncompensated crust.

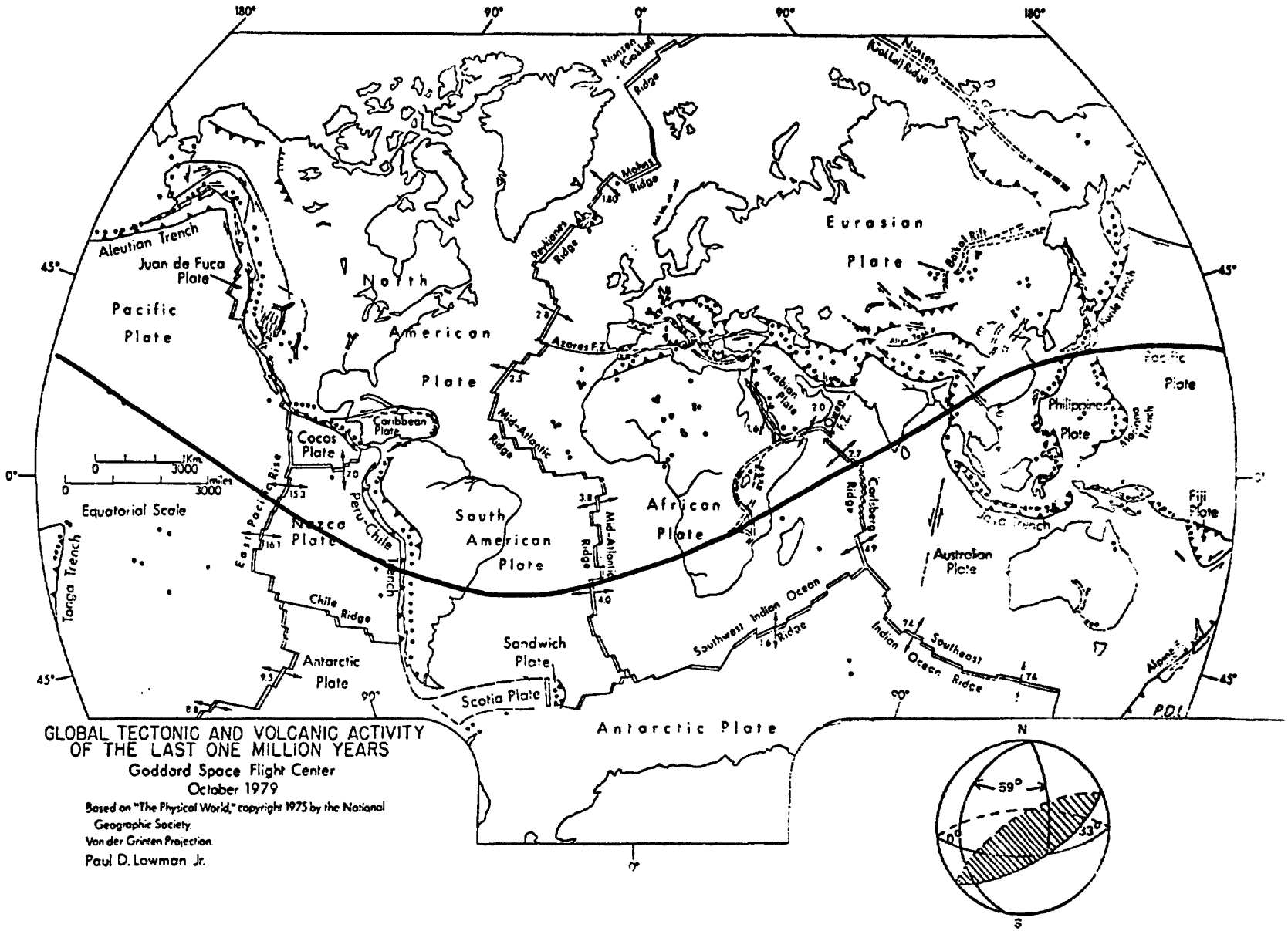

Fig. 5B-3. Track of the slice shown in Figs. 5B-1 and -2

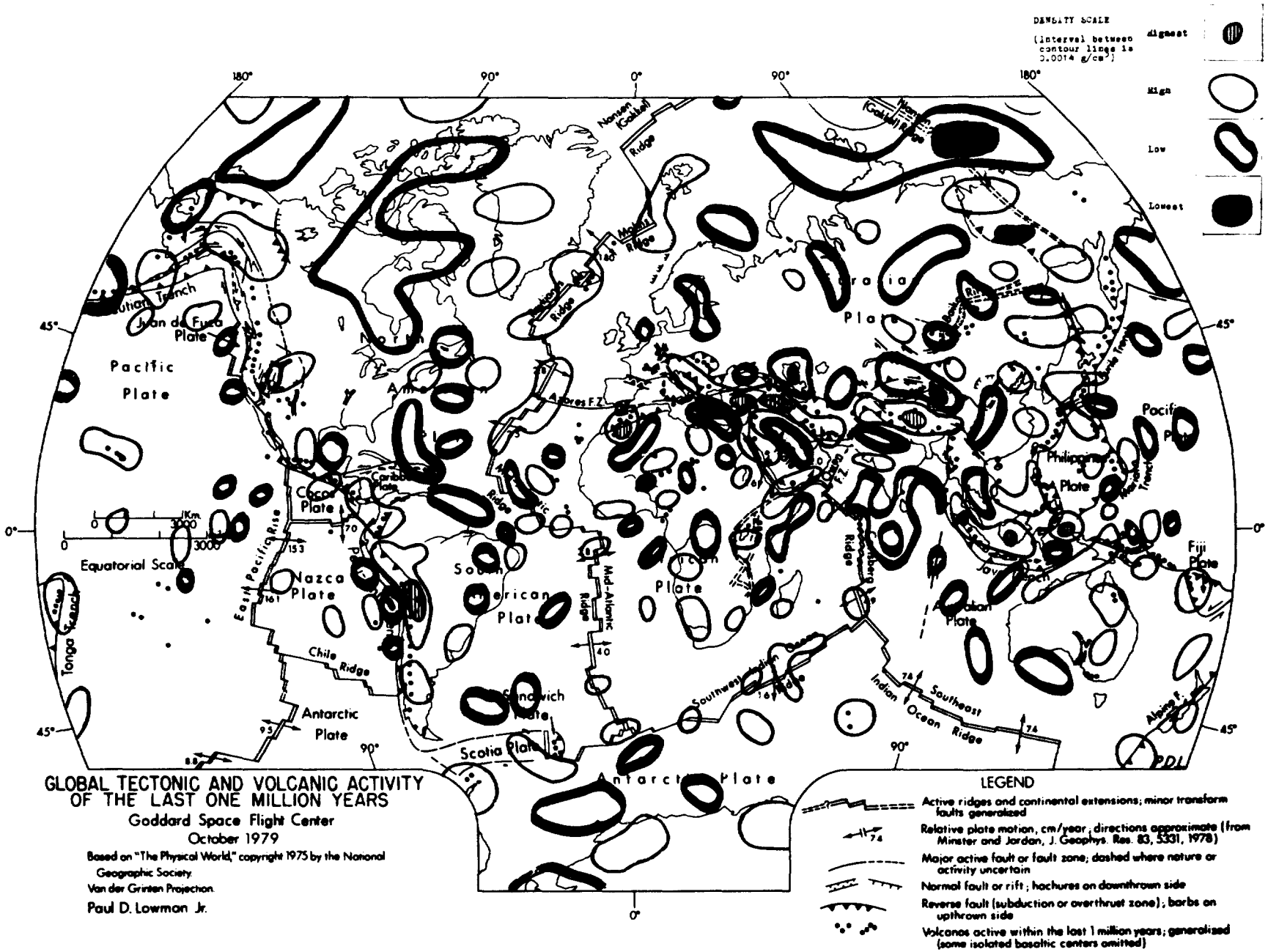

GLOBAL TECTONIC AND VOLCANIC ACTIVITY OF THE LAST ONE MILLION YEARS

Goddard Space Flight Center

October 1979

Based on "The Physical World," copyright 1975 by the National Geographic Society.

Van der Grinten Projection.

Paul D. Lowman Jr.

LEGEND

- Active ridges and continental extensions; minor transform faults generalized
- Relative plate motion, cm/year; directions approximate (from Minster and Jordan, J. Geophys. Res. 83, 5331, 1978)
- Major active fault or fault zone; dashed where nature or activity uncertain
- Normal fault or rift; hachures on downthrown side
- Reverse fault (subduction or overthrust zone); barbs on upthrown side
- Volcanos active within the last 1 million years; generalized (some isolated basaltic centers omitted)

Fig. 5B-4. Surface density variation and tectonic activity map.

C. THE ENCHANCED NODAL EQUILIBRIUM OCEAN TIDE AND POLAR MOTION

by

B. V. Sanchez

OBJECTIVES

The objective of this investigation was to ascertain the possibility of ocean tidal excitation to account for a 18.6 year polar motion component detected by data analysis.

BACKGROUND

Recent data analysis by Markowitz (1979) indicates the existence of a polar motion component with periodicity and phase corresponding to the motion of the lunar ascending node.

The "pole tide" or ocean response to the Chandler wobble has been analyzed by various investigators, the analysis of ocean tidal data seems to indicate that the ocean response to the wobble is modified in amplitude and phase as compared to the theoretical equilibrium response and that the enhancement in amplitude shows a latitude dependency.

RECENT ACCOMPLISHMENTS

The concept of an enhancement function which modifies the equilibrium tide can be applied also to the ocean response to the graviational disturbing forces. Such an enhancement function can be expressed in terms of spherical harmonics with adjustable coefficients. It is then possible to express the tidal contributions to the products of inertia in terms of the enhancement function coefficients, which can then be estimated so as to obtain the polar motion components indicated by the analysis of the data. The estimated coefficients can be used to predict the modified behavior of the equilibrium tide.

Markowitz (1979) analyzed 79 years of ILS (International Latitude Service) data and 17 years of IPMS data (International Polar Motion Service), his results are given in Table 1 below. In order to estimate the values of the coefficients that will fit the polar motion data a general purpose adaptive iterator for nonlinear problems (Campbell, et al.) has been used. The results are given in Table 2, below, in both cases the coefficients were estimated so as to obtain polar motion components within 1 cm of the mean values given by Markowitz' analysis. No constraints were imposed on the values obtained for the phase angles.

The formulation of the expression for the equilibrium ocean tide took into consideration the effects of ocean loading and the self attraction of the water as well as conservation of mass. The distribution of oceans and continents was introduced by means of the ocean function with coefficients given by Balmino, Lambeck and Kaula (1973).

DATA	X(CM)	Y(CM)	PHASE, X	PHASE, Y
ILS	28 ± 13	22 ± 13	1903.7 ± 1.2Y	1904.4 ± 1.5Y
IPMS	22 ± 13	25 ± 13	1905.7 ± 1.5Y	1906.7 ± 1.4Y

TABLE C-1. AMPLITUDE AND PHASE OF NODAL WOBBLE FROM MARKOWITZ DATA ANALYSIS

DATA	X(CM)	Y(CM)	PHASE, X	PHASE, Y
ILS	27.48	22.84	1905.37	1904.97
IPMS	21.27	25.85	1905.44	1905.5

TABLE C-2. AMPLITUDE AND PHASE OF NODAL WOBBLE FROM NUMERICAL MODEL.

The corresponding enhancement functions and tidal heights are shown in Figures 5C-1 to 5C-5 below (also shown is the unmodified equilibrium tide).

SIGNIFICANCE

The results indicate that a modified equilibrium tide could provide the excitation required to generate the polar motion component detected in the data. The magnitude of enhancement obtained in this study does not appear altogether exorbitant, especially in the case of the IPMS data. However since no ocean dynamics have been incorporated into the formulation of the enhancement function the results should be considered as indicative of a possibility rather than as a quantitative determination of ocean behavior.

REFERENCES AND PUBLICATIONS

Balmino, G., K. Lambeck, and W.M. Kaula, 1973, "A Spherical Harmonic Analysis of the Earth's Topography," Journal of Geophysical Research, 78, pp. 478-481.

Campbell, J., W.E. Moore, and H. Wolf, 1964, "Minmax: A General Purpose Adaptive Iterator for Nonlinear Problems," Analytical Mechanics Associates, Inc.

Markowitz, W., 1979, "Independent Polar Motions, Optical and Coppler; Chandler Uncertainties," Report to IAU Commission 19 and 31, Montreal, August 1979.

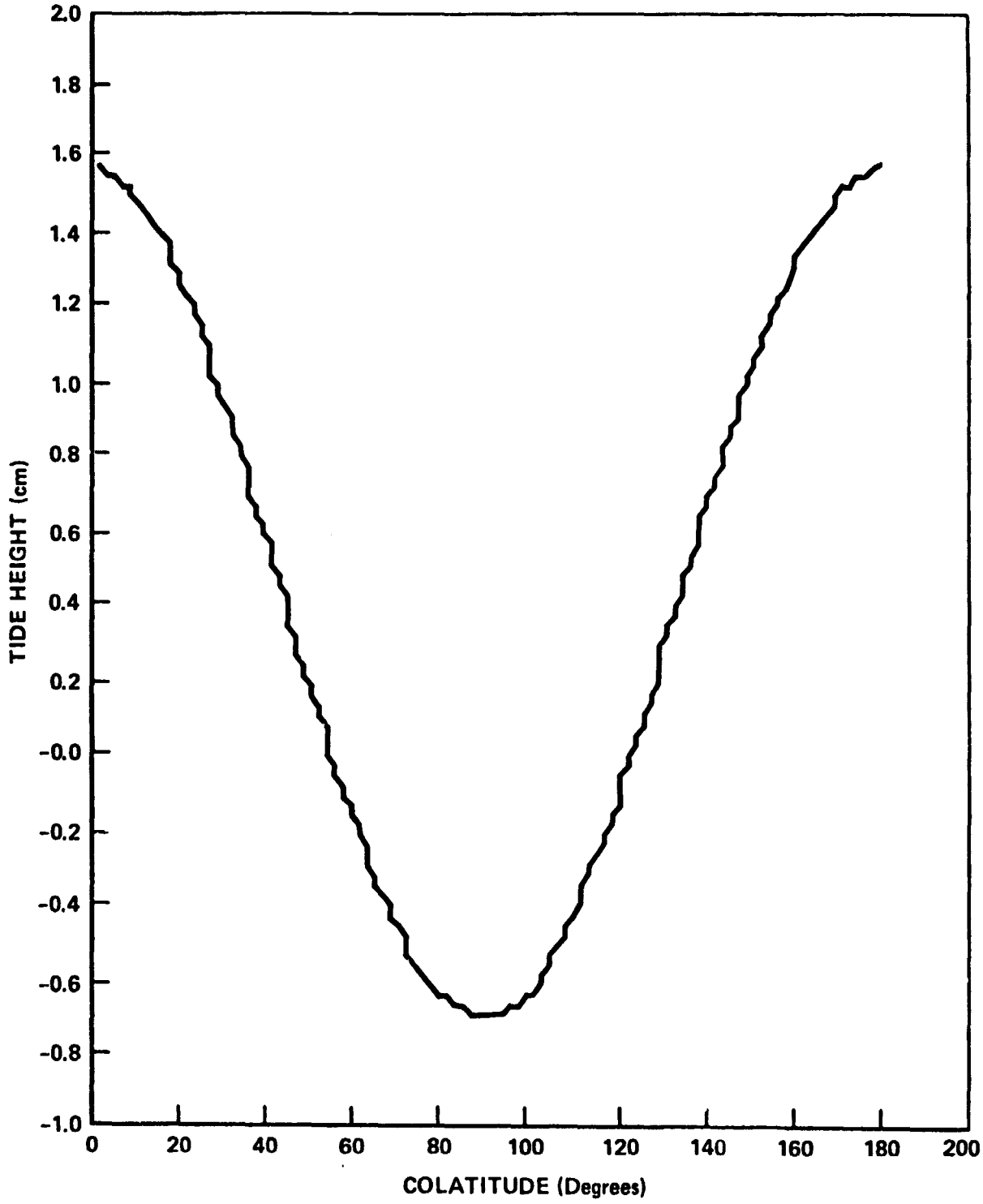

FIG. 5C-1. UNMODIFIED TIDE HEIGHT

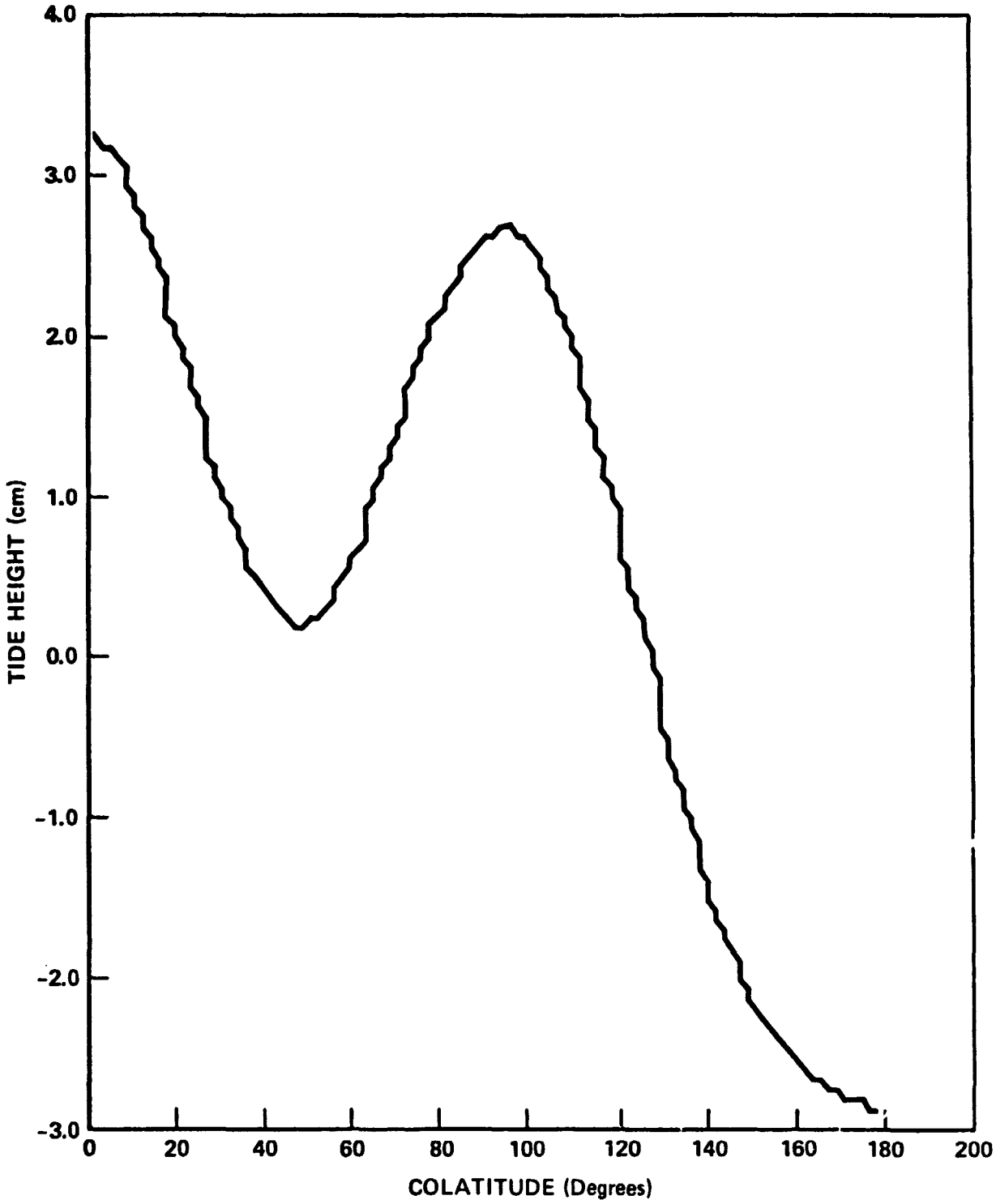

FIG. 5C-2. MODIFIED TIDE HEIGHT (IPMS)

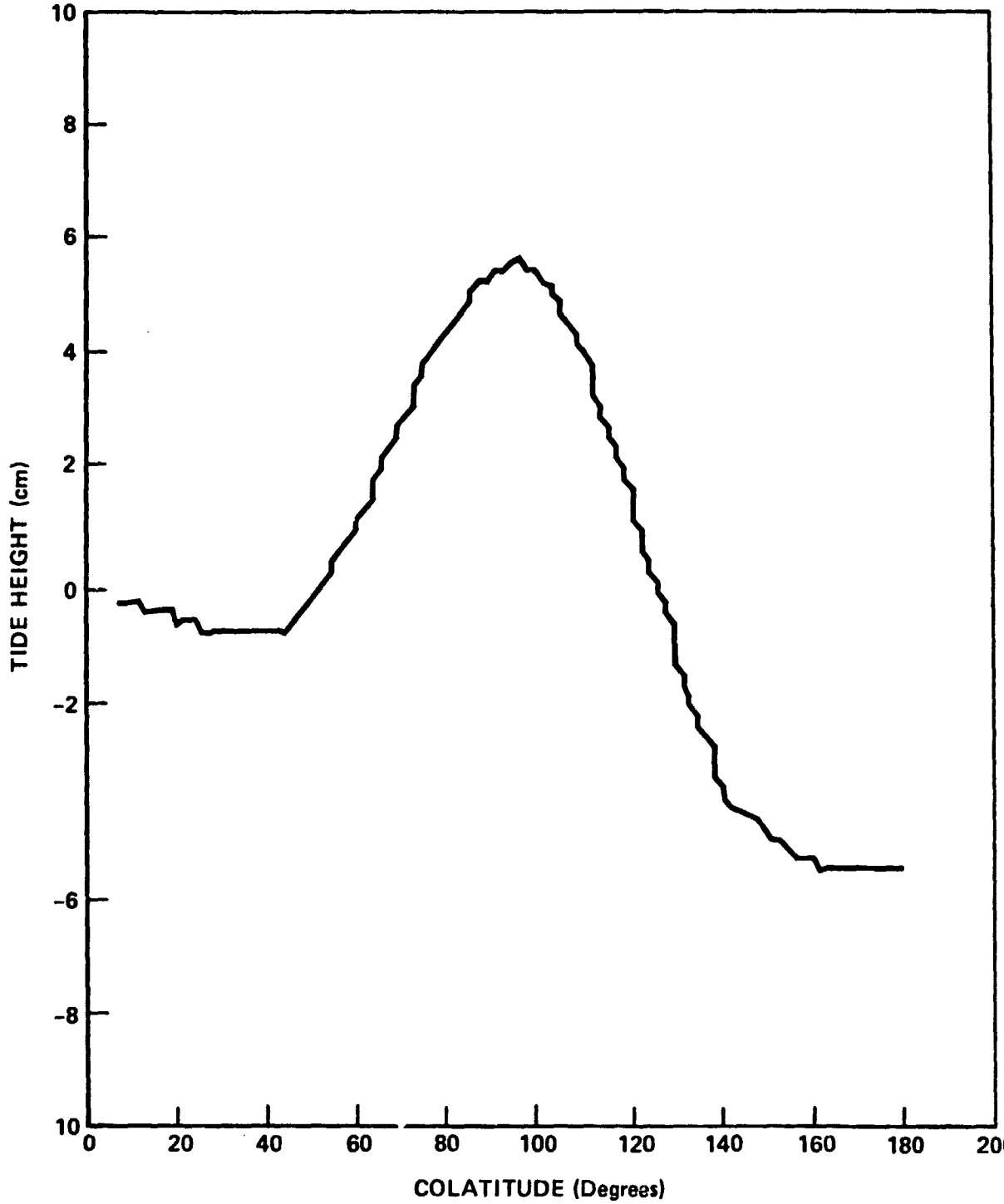

FIG. 5C-3. MODIFIED TIDE HEIGHT (ILS)

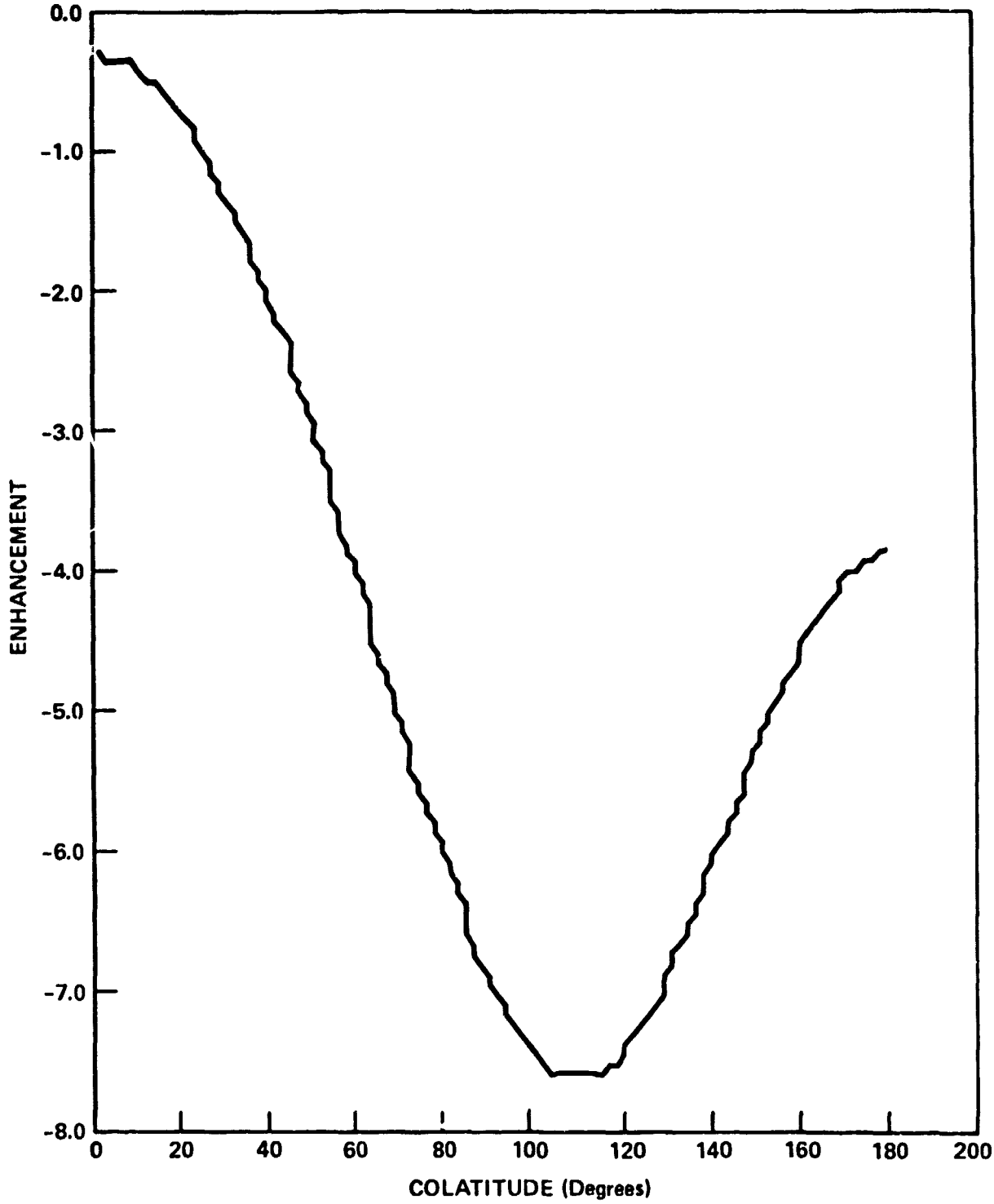

FIG. 5C-4. ENHANCEMENT FUNCTION (ILS)

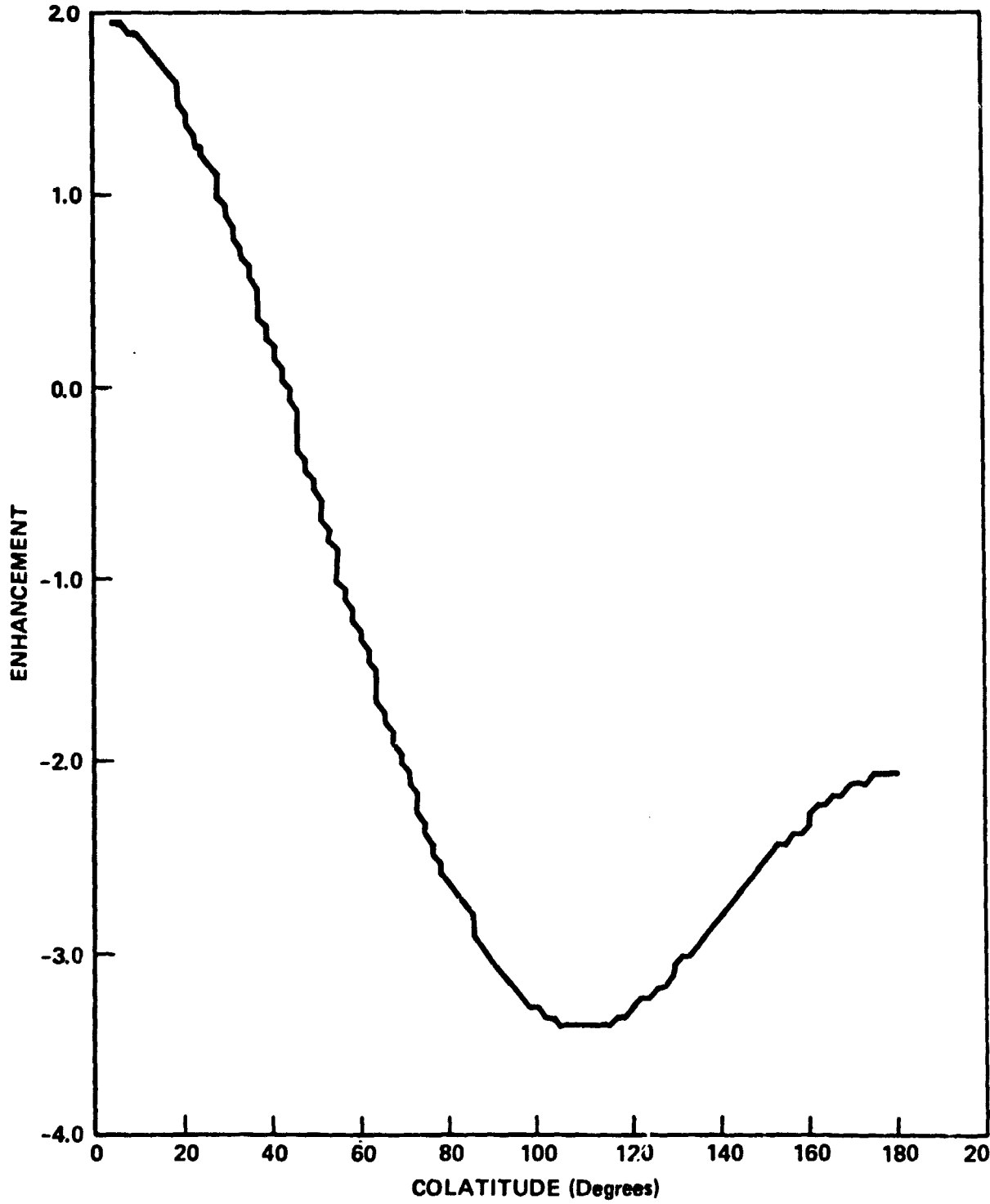

FIG. 5C-5. ENHANCEMENT FUNCTION (IPMS)

D. POLAR MOTION RESEARCH

by

M. A. Graber

OBJECTIVES

The purpose of polar motion research is to study the motion of the rotation axis of the Earth in a coordinate system fixed within the Earth and to correlate this motion with other geophysical processes.

BACKGROUND

The motion of the pole was first measured 85 years ago. The introduction of modern high-speed computers has reopened the field, where the great masses of numbers made analysis difficult.

RECENT ACCOMPLISHMENTS

The ability to model 50-day Lageos arcs to relatively small residuals opens up a new area of polar motion analysis at GSFC. Using standard Fourier analysis orders of magnitude, data over 50 days will provide a frequency resolution to the inverse of the data length, or 0.02 cycles per day. This provides sufficient discrimination to allow searching the high-frequency region for the presence of tidally-induced polar motion and to look for possible excitations near one or two cycles per day.

The typical manner for performing this type of analysis is to first solve for a series of pole positions and then to perform a Fourier analysis of this time series. However, with the satellite range data, the optimal method is to include the high-frequency component in the condition equation for the polar motion which is within the Geodyn computer program. This technique will solve for just two additional parameters, a phase and an amplitude.

After numerous computer set-up problems, Geodyn was modified to study the frequency structure in the polar motion of multi-arc Lageos and Starlette data. Amplitudes were determined for the following frequencies:

Cycles per Day	0".01
+2.00	0.69
+1.00	0.60
-0.93	1.71
-1.00	31.70
-2.00	0.78

The amplitudes in the range 0.6 - 0.8 x 0".01 are considered to be noise. The O_1 tide is not modeled in Geodyn's precession-nutation subroutines, so the 1.71 x 0".01 amplitude at -0.93 cpd is believed to be a tidal phenomenon.

The large amplitude at -1.00 cpd was totally unexpected. Current thoughts tend toward a Geodyn oversight as the cause. However, modeling this effect reduces the Lageos residuals on a 60-day arc by 15 cm. This reduction in itself is valuable.

SIGNIFICANCE

This area of research is important because the pole position time series is sensitive to the internal structural properties of the Earth. Differences in geophysical models show small differences in the polar motion. Determining the driving mechanism for the central 431-day process in the Earth's wobble will require detailed knowledge of the motion for its solution.

FUTURE EMPHASIS

During the next year, the large diurnal term will be studied in an attempt to determine the origin of the phenomenon.

REFERENCES AND PUBLICATIONS

Graber, M. A., "Analysis of Daily Latitude Variations," Journal of Geophy. Research, 84, 5437-5442, 1979.

Graber, M. A., "Analysis of Star Pair Latitudes," Journal of Geophy. Research, 84, 5443-5445, 1979.

E. A DETERMINATION OF GM

by

D. E. Smith

OBJECTIVES

To make an informed estimate of the numerical value of the product of the earth's mass (M) and the gravitational constant (G) from the analysis of the orbit of the Lageos spacecraft.

BACKGROUND

The parameter, GM, is a scale parameter in geodesy and geophysics that determines the absolute size of the earth, the acceleration of gravity and the scale of the dynamical motions of earth satellites. GM is particularly important in dynamical satellite geodesy because it scales all inferred coordinates and distances, both center of mass and relative. Thus, if an accurate position or distance is required from dynamic satellite geodesy, in contrast to a precise one, then an accurate value of GM is necessary. If we assume that an accuracy of 6cm is required in center of mass coordinates then the required proportional GM accuracy is 6cm/6378 km (the earth's radius), or 1×10^{-8}, which is the ultimate accuracy goal of this and subsequent studies.

Previous determinations have been largely based on interplanetary missions such as Mariner, also, lunar laser, and recently, satellite laser tracking of Lageos and other low altitude satellites. Of these earlier determinations, those by laser ranging to the moon and to Lageos are the most accurate and indicate a value of approximately $398600.45 \pm .02$ km^3 sec^{-2}. The planetary mission results suggest a larger value around 398600.8 km^3 sec^{-2} but with a standard deviation not inconsistent with the laser results. The studies described here are based exclusively on laser tracking of the Lageos spacecraft during 1977 and 1978 by systems in North and South America, Europe, and Australia.

RECENT ACCOMPLISHMENTS

During 1977 and 1978, the Lageos spacecraft was tracked from (twelve) sites around the world, some regularly and some only occasionally or for a short period. These systems belonged to the NASA/GSFC and NASA/SAO tracking networks and also to organizations in Germany and the Netherlands. The tracking data ranged in quality from about $\pm$ 10 cm for the NASA/GSFC systems to nearly 1 meter for some of the others. A total of 400,000 range measurements to Lageos obtained by these stations were used in this analysis. Orbital arcs were fitted through the data for each calendar month and combined into a single solution to provide estimates for the station coordinates, GM, polar position every 5 days, a solar radiation constant, and a tidal amplitude and phase. The value of GM obtained from this solution was 398600.41 km^3 sec^{-2}. The

station coordinates obtained in this full solution were then used in an analysis of the monthly orbital arcs in which GM, the pole, a solar radiation constant and a tidal amplitude and phase were adjusted in each arc (the station coordinates held fixed). Twenty-four values of GM were obtained, one each month for the years 1977 and 1978. These twenty-four values are shown in Figure 5E-1 together with the values obtained from interplanetary missions and lunar laser ranging. The arithmetic average of the 24 Lageos values is 398600.408 km^3 sec^{-2} with a formal uncertainty of the average of 0.004 km^3 sec^{-2}. This uncertainty is very unrealistic because the values appear to be non-random and a better value is probably 0.01 km^3 sec^{-2}. We then arrive at a final value of

$$GM = 398600.41 + 0.01 \text{ km}^3 \text{ sec}^{-2}$$

from the 1977 - 1978 Lageos tracking data. (As far as is known this is the total data set available for this period.)

It is obvious from Figure 5E-1 that these latest Lageos values are significantly lower than any of the earlier sets of values by at least 0.04 km^3 sec^{-2}. The internal precision of the Lageos values appears to be very high and there seems little doubt that the difference between these Lageos results and, say the lunar laser, are due to some systematic effect in one or the other of the results unless the standard deviations are grossly underestimated. The major limitations on the Lageos solution are related to general relativity, the along track acceleration, tides, and the geopotential model, although it seems unlikely that any of these could substantially alter the result.

General relativity has not been included in this analysis because these effects are not presently available in the Geodyn program with which this analysis was conducted. The special relativistic effect of the range correction has been included.

Lageos is accelerating in the along track direction at about 2.86×10^{12} meters sec^{-2}. The cause of this acceleration is not known but it is consistent with a small air drag perturbation. This acceleration has been modeled in each of the monthly arcs at the constant value given above. The acceleration is known not to be constant from month-to-month from studies of the decay in semi-major axis; the variations amounting to about 50%. This acceleration, although of unknown origin, or its variation is not thought to contribute any significant error to the estimate of GM. Tests of individual monthly arcs using different accelerations in which GM is estimated show very little variation. This is probably because this along-track acceleration is very small, approximately 10^{-13} g.

Earth and ocean tides perturb the motion of Lageos by a measurable amount. The solid earth contributes about 80% of the perturbation and this can be computed reasonably accurately from knowledge of the second degree Love numbers. The ocean tides are less well known

and the models complex and more difficult to compute their effect on the satellite. However, the tidal periods for the ocean are the same as for the solid earth and to a first approximation the ocean tides can be accounted for by modifying the solid earth Love number. This was the procedure used here; the Love numbers k_2 and ϵ_2 were allowed to adjust in each monthly orbital arc to account for the ocean tides. The remaining error (from the ocean tides) is probably about 5% of the total tidal effect and appears unimportant with respect to its effect on GM. This has been confirmed by estimating GM in several of the months with the ocean tides completely ignored. In comparison with the situation just described, the change in the recovered value of GM was insignificant.

The geopotential model used in these calculations was the GEM 10 model truncated to degree and order 20 and we believe the truncated model includes all terms that contribute 1 centimeter or more perturbation. We know our ability to determine the orbit of Lageos is no worse than one meter and since uncertainties (and probably a lot better) in the geopotential are presently the limiting factor we believe an upper bound can be placed on the geopotential error. Changing from GEM 10 to GEM 9 produces no significant change in the average value of GM obtained from the 24 monthly orbits and only marginally changes the individual monthly values. We have concluded the effect of geopotential error on the recovered value of GM is minimal.

SIGNIFICANCE

The value for GM of 398600.41 $\pm$ .01 km^3 sec^{-2} obtained from Lageos appears to be strong, well determined, uncorrupted by other perturbing forces and probably of higher accuracy than any previous solutions. Twenty-four solutions attest to its repeatability on a monthly basis to $\pm$ 0.02 km^3 sec^{-2}. The accuracy of the present value is only 2.5 parts in 10^8 and is not yet adequate for absolute positioning on the earth's surface that is desirable for crustal dynamics studies with Lageos.

The present study shows that Lageos is an extremely powerful tool for estimating GM and that routine estimation of GM during the next few years should steadily improve our knowledge of the numerical value of this parameter.

FUTURE EMPHASIS

Monthly solutions for GM will be obtained in the manner already described thus expanding the data set and ultimately achieving an accuracy of at least 1 part in 10^8.

Figure 5E-1

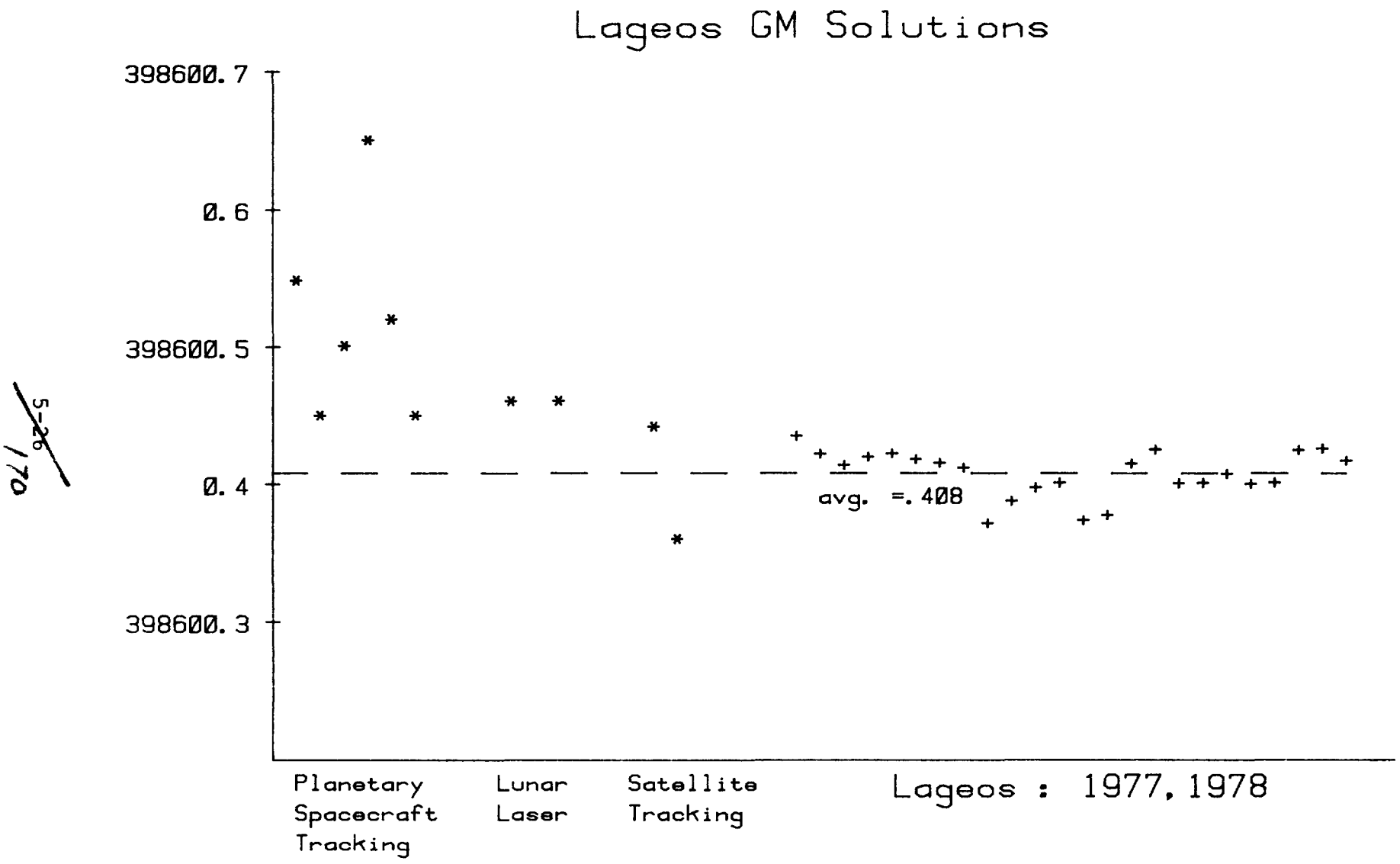

5-26

F. POLAR MOTION AND EARTH ROTATION RESULTS FROM LAGEOS

by

David E. Smith

OBJECTIVES

The objective of this study is the determination of precise positions of the earth's pole of rotation, and variations in the length of day for contributing to our understanding of the excitation of polar motion and the relationship of climatic and meteorological effects to changes in the earth's angular momentum.

BACKGROUND

Last year's report described the basic method for deriving polar motion from laser tracking of the Lageos spacecraft. Since then, improvements have been made to our modeling of the gravity field and in our knowledge of the coordinates of the tracking stations enabling polar motion to be computed more precisely, and for the simultaneous measurement of the length of day. A further year of tracking data (1978) has been analyzed providing a total of 32 months of Lageos polar motion and earth rotation measurements. The present status of the Lageos polar motion and length of day measurements for the period May 1976 through December 1978 are presented here.

RECENT ACCOMPLISHMENTS

Monthly orbital arcs of Lageos were determined for the thirty-two month period. From these arcs a set of station coordinates, second degree Love number and phase, solar radiation coefficient and along-track accelerations were derived simultaneously with estimating the x,y position of the pole and the difference between atomic and universal time every 5 days. The pole and time solutions were obtained whenever the data set would permit. The observations of universal time were used to estimate the excess length of day (LOD) and are shown in Figure 5F-1 together with the x,y pole. Annual and semi-annual terms were fitted to the polar motion in the manner described in last year's report and the resulting standard deviation of the observed values is about 0.015 arcseconds (compared to about 0.020 arcseconds last year). Similar analysis of the excess LOD gives about 0.4 milliseconds accuracy after the annual and semi-annual terms are removed.

SIGNIFICANCE

These new results are a significant improvement over last year's results and now include length of day observations for the first time at an accuracy level slightly better than the classical methods. This is encouraging at this very early stage of analysis since improvements in data quality, number of tracking stations and orbit modeling can be expected over the next year or two.

FUTURE EMPHASIS

Continue the development of the techniques and models so as to approach the few thousandths of a second of arc accuracy in polar motion and about 0.1 msec in length of day.

REFERENCE

NASA Technical Memorandum 80550, "Earth Survey Applications Division Research Report, pp. 5-28, 5-32, November 1979.

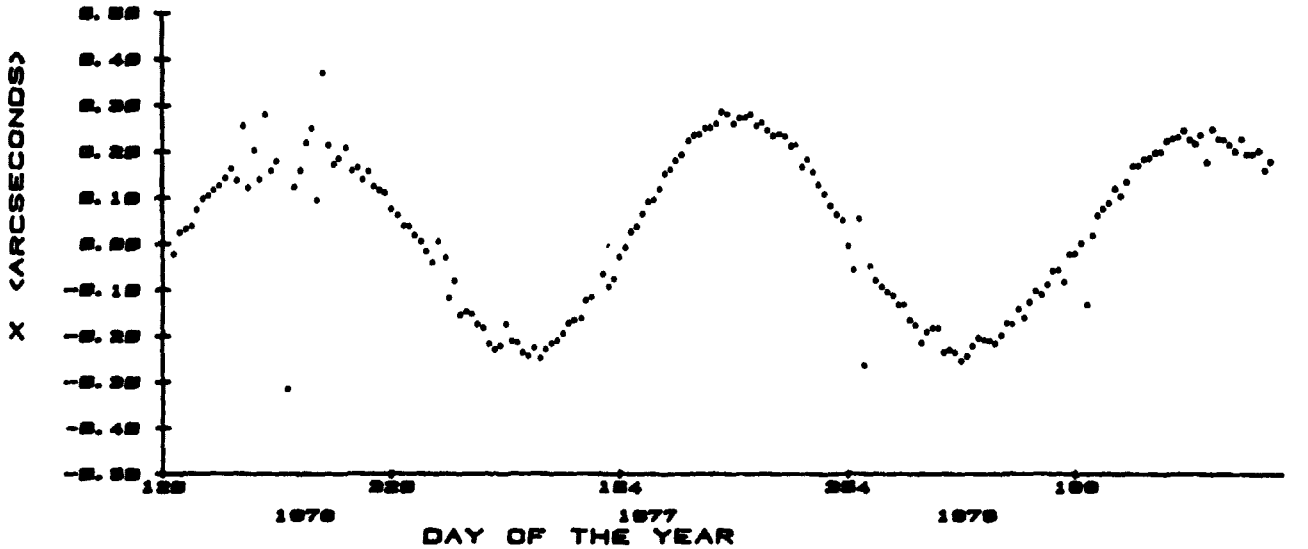

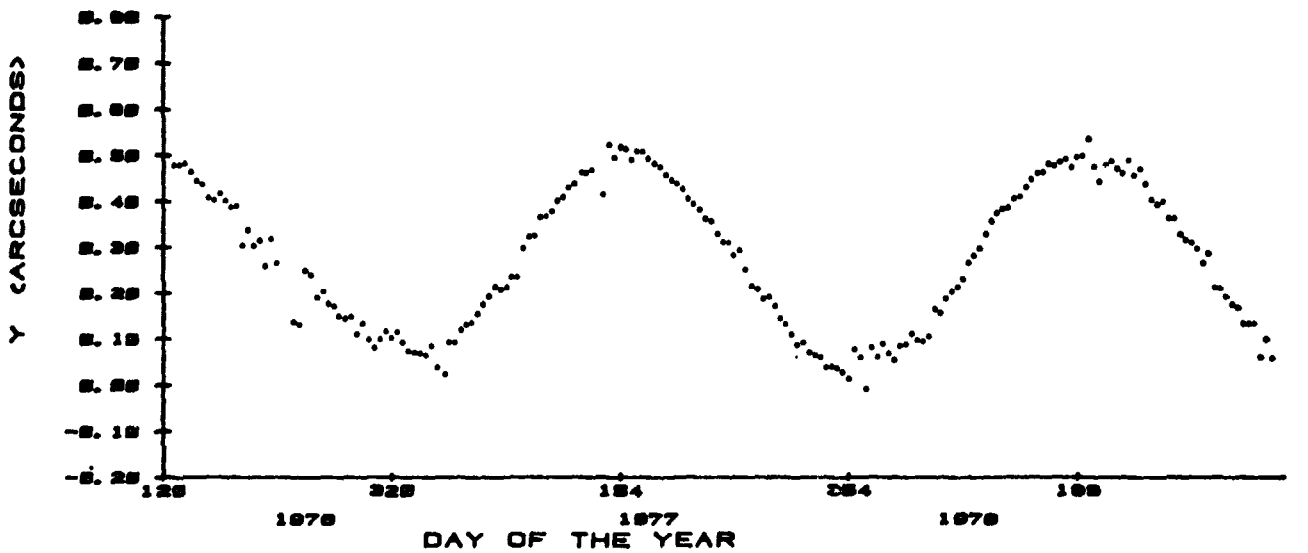

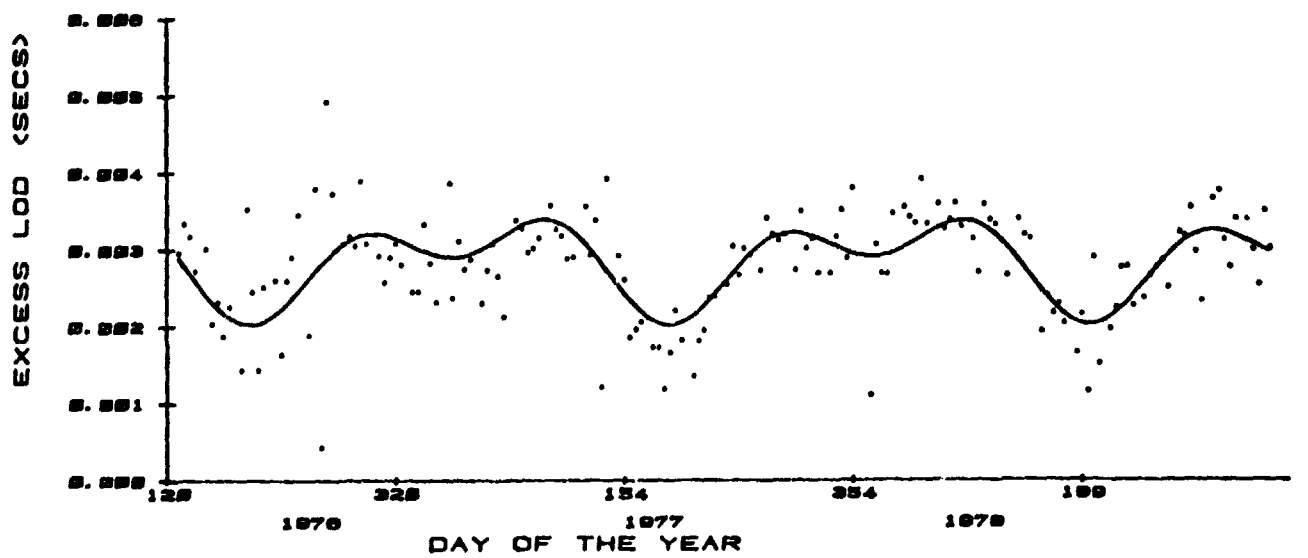

Figure 5F-1. Polar Motion and Length of Day

CHAPTER 6
SEA SURFACE TOPOGRAPHY, OCEAN DYNAMICS AND GEOPHYSICAL INTERPRETATION

edited by
J.G. Marsh

OVERVIEW

The overall goal of this program is to apply remote sensing data to studies of dynamic ocean and Earth processes. The primary data types are satellite altimetry data, orbit perturbation data and gravity data. These data are analyzed in conjunction with surface observations, for example, ocean temperature and density measurements.

Global sets of satellite altimeter data have been collected during two satellite missions: The GEOS 3 mission (1975 to 1978) and the Seasat mission (1978).

Research programs are underway in the following areas to analyze and interpret the altimeter data:

- The development and implementation of techniques for the calibration and performance evaluation of the altimeter systems.
- The analysis of sea state effects on the altimeter height measurements.
- The computation of regional as well as global mean sea surfaces which can be used as basic reference surfaces for analyzing dynamic ocean topography associated with ocean circulation.
- Detailed analyses of the Gulf Stream and the associated eddy systems to improve our understanding of near surface as well as abyssal circulation.
- The analyses of orbit evolution data for the computation of ocean tidal parameters which are important for studies of dynamic ocean circulation modeling and for precision orbit determination.
- The determination of density distributions in and around lithospheric slabs which are being consumed beneath island arcs to improve the understanding of forces acting on subducting slabs.

A description of these research programs is presented in the following sections.

Contributors to this chapter include Robert Cheney, Theodore Felsentreger, Ronald Kolenkiewicz and James Marsh.

A. THE SEASAT ALTIMETER HEIGHT BIAS USING FOUR BERMUDA OVERFLIGHTS

by

R. Kolenkiewicz

OBJECTIVE

The objective of the Seasat-Altimeter height calibration effort is to obtain an accurate value of the precision of the altimeter measurement, the bias in the altimeter measurement after it has been subjected to the process of correcting for the instrument and geophysical effects during the computation of the altimeter data tape and the bias in the time tag assigned to the measurement. Applications of this information include, e.g., determination of the semi-major axis of the ellipsoid best approximating the geoid.

BACKGROUND

The Seasat A spacecraft was launched from Vandenberg Air Force Base on June 26, 1978. Until spacecraft failure on October 10, 1978, the Seasat altimeter has taken data on several thousand passes. In order to obtain full usage of these data a calibration (or height bias determination) of the altimeter is necessary.

The validation of the altimeter measurement from the spacecraft to the mean sea surface requires situations in which this distance can be accurately inferred, independent of the altimeter data itself. Effectively, this can be done using satellite passes which are nearly overhead at island laser tracking sites. This technique has the advantage that an accurate a priori knowledge of geoid heights is not required.

The Seasat altimeter calibration period began on September 10, 1978, and continued until the spacecraft's failure on October 10, 1978. During this period, there were ten Bermuda overflights, four of which were supported by the Bermuda laser and are usable for the altimeter height calibration. The ground tracks for these four passes across Bermuda are shown in Figure 6A-1. The tracking and altimeter data from these four revolutions have been reduced and the combined data set is used to estimate the bias in the altimeter altitude measurements.

The basic calibration geometry is shown in Figure 6A-2. Assuming a pass directly over a laser tracking station with continuous laser and altimeter tracking, the measurements directly over the tracking station can be used for bias estimated by equating the altimeter measurement, corrected to the ellipsoid, with the laser measurement also corrected to the ellipsoid. Equating the two measurements, as shown in Figure 6A-2 leads to the following relation:

$$h_a - b + h_t + h + h_{ga} = h_{gs} + h_m + R \qquad (1)$$

where

h_a = measured altimeter height above the sea surface after the instrument and atmospheric refraction corrections have been applied,

b = bias in the altimeter measurement,

$h_t + \delta h$ = tide measurement as determined by the tide gauge at the time of the altimeter pass. This measurement includes non-tidal temporal sea surface variations,

h_{ga} = geoid height at the altimeter subsatellite point,

R = measured distance from the laser tracking station to the laser corner cube reflector corrected for atmospheric delay and spacecraft center of mass offset,

h_m = height of the tracking station above the mean sea level (or the geoid) at the tracking station,

h_{gs} = geoid height at the tracking station.

The altimeter measurement bias can be determined then to the accuracy with which each of the above terms is known, e.g.:

$$b = h_a + h_t + h + h_{ga} - [R + h_{gs} + h_m] \qquad (2)$$

The terms in brackets on the right-hand side of Equation (2) constitute the ellipsoidal height normally calculated in orbit determination programs, while the terms outside the brackets give the ellipsoidal height (based on the altimeter measurement), a measured tide and a geoid model. With this interpretation, the calculation can be performed whether the satellite is directly over the laser site or not. However, only at the direct overhead point will the two geoid heights in Equation (1) cancel.

In practice, the altimeter cannot accurately track directly over the laser site because of land in the altimeter footprint, and the laser does not track directly overhead because its Az-El mount cannot follow the high azimuth rates in the vicinity of the point of closest approach (PCA). However, this is no real problem because an accurate overhead orbit can be estimated with a gap in the data around the PCA. For Day 256 and Day 265, the orbits were estimated using available laser data on the overflight pass plus the following pass. Laser data available for these passes, plus the other two calibration dates, is shown in Table 6A-1. For Day 259 and Day 274, laser data were supplemented by S-Band data from Merritt Island and Rosman on the calibration pass and adjacent revolutions. In all cases, the laser data from Bermuda were weighted with standard deviation of 10 cm, while all other laser data were weighted with a standard deviation of 1 m. The orbit height over Bermuda is thus determined predominantly by the Bermuda laser, and the height accuracy over the island is estimated to be better than 5 cm. This accuracy estimate is based on a true laser noise level of 5-8 cm, with any bias well below the noise level.

After deleting measurement points which have been significantly influenced by the presence of land in the footprint, the altimeter data can be smoothed across Bermuda to obtain extrapolated altimeter residuals at the groundtrack points of closest approach to the laser site. These extrapolated residuals can then be used along with the laser orbit and various corrections to obtain the altimeter height bias.

RECENT ACCOMPLISHMENTS

As the altimeter cannot produce sea surface measurements across the island, the "residuals" were computed, using Equation (2), for the period when the altimeter was not significantly influenced by land and extrapolated across the island. Waveforms for data points in the vicinity of Bermuda were analyzed for all four calibration passes to determine any evidence of land effects. AGC records for this data were also analyzed as an aid in detecting the influence of land in the altimeter footprint, although AGC effects on height are only second order. All points with any evidence of land in the waveforms were deleted. Any additional points which showed evidence of anomalous height behavior near Bermuda were also deleted. The resulting data set, shown in Figure 6A-3, with edited points indicated by O's and accepted measurements indicated by X's can be used to estimate geoid heights along the ground truth across Bermuda for each of the four calibration passes.

There are some simplifications that were made in Equation (2), primarily in the h_a term. In practice, this quantity must be obtained from the measured altitude data, corrected for propagation effects, instrumentation errors, and sea state effects. Most of these corrections are at the centimeter or decimeter level. In addition, there are a few other corrections to be made due to idiosyncrasies of some of the data and/or reductions.

The raw and smoothed altimeter residuals for a typical Bermuda overflight are shown in Figure 6A-4. The smoothed residuals were obtained by using the ALTKAL smoother (Fang and Amann, 1977). The points of closest approach to the laser site are indicated, and the residuals at these times are listed in Table 6A-2 as the starting point for the bias estimations. If these passes were all over the laser site, we would have four different calibration values. However, none of them cross directly over the laser. Figure 6A-5 shows the different corrected residuals, plotted as a function of distance from the laser site (measured in the northwest direction). Assuming the geoid to be linear along this direction, as has been confirmed by GEOS-3 altimeter data (Martin and Butler, 1978), a straight line fit has been made to the four points in order to estimate the corrected residual at the laser site. The best estimate of the intercept with the zero distance point is

$$b = 0.11 \pm .15 \text{ m} \qquad (3)$$

Several points should be noted about the estimation and utilization of this bias number. First, it has used the derived timing correction of 68.6 ms and, should this correction require subsequent revision, the height bias will require a corresponding revision. Secondly, it is assumed that altimeter data users will:

1. Apply the 68.6 timing correction to their data and

2. Apply a sea state bias correction which amounts to approximately 5% of the significant wave height.

Based on these assumptions that these corrections will be applied to the data on the altimeter data tape, the estimate of the bias in the height is 0.11 $\pm$ .15 m. This bias is to be subtracted from the measured altimeter height.

SIGNIFICANCE

The absolute bias calibration for the Seasat-A altimeter has been measured. This correction can be applied to these data to enable investigators to determine important geophysical parameters.

FUTURE EMPHASIS

The south-north Seasat passes, one north of the laser site and one south of the laser site will be used to tie together all north-south Bermuda orbits (four with laser support, six without) in an effort to confirm the results obtained thus far.

REFERENCES AND PUBLICATIONS

Fang, B. R. and D. W. Amann, "ALTKAL - An Optimum Linear Filter for GEOS-3 Altimeter Data," NASA CR-141429, August 1977.

Martin, C. F, and M. L. Butler, "Calibration Results for the GEOS-3 Altimeter," NASA CR-14143, September 1977.

Tapley, B. D., G. H. Born, H. H. Hagar, J. Lorell, M. E. Parke, J. M. Diamante, B. C. Douglas, C. C. Goad, R. Kolenkiewicz, J. G. Marsh, C. F. Martin, S. L. Smith, III, W. F. Townsend, J. A. Whithead, H. M. Burne, L. S. Fedor, D. C. Hammond, N. M. Mognard, "Seasat Altimeter Calibration, Initial Results," Science, Vol. 204, pp 1410-1412.

Kolenkiewicz, R., and C. F. Martin, "Preliminary Determination of the Seasat Altimeter Height Bias," presented at the 1979 Spring Meeting of the American Geophysical Union, Washington, D.C.; EOS Transactions, American Geophysical Union, Vol. 60, No. 18, May 1979.

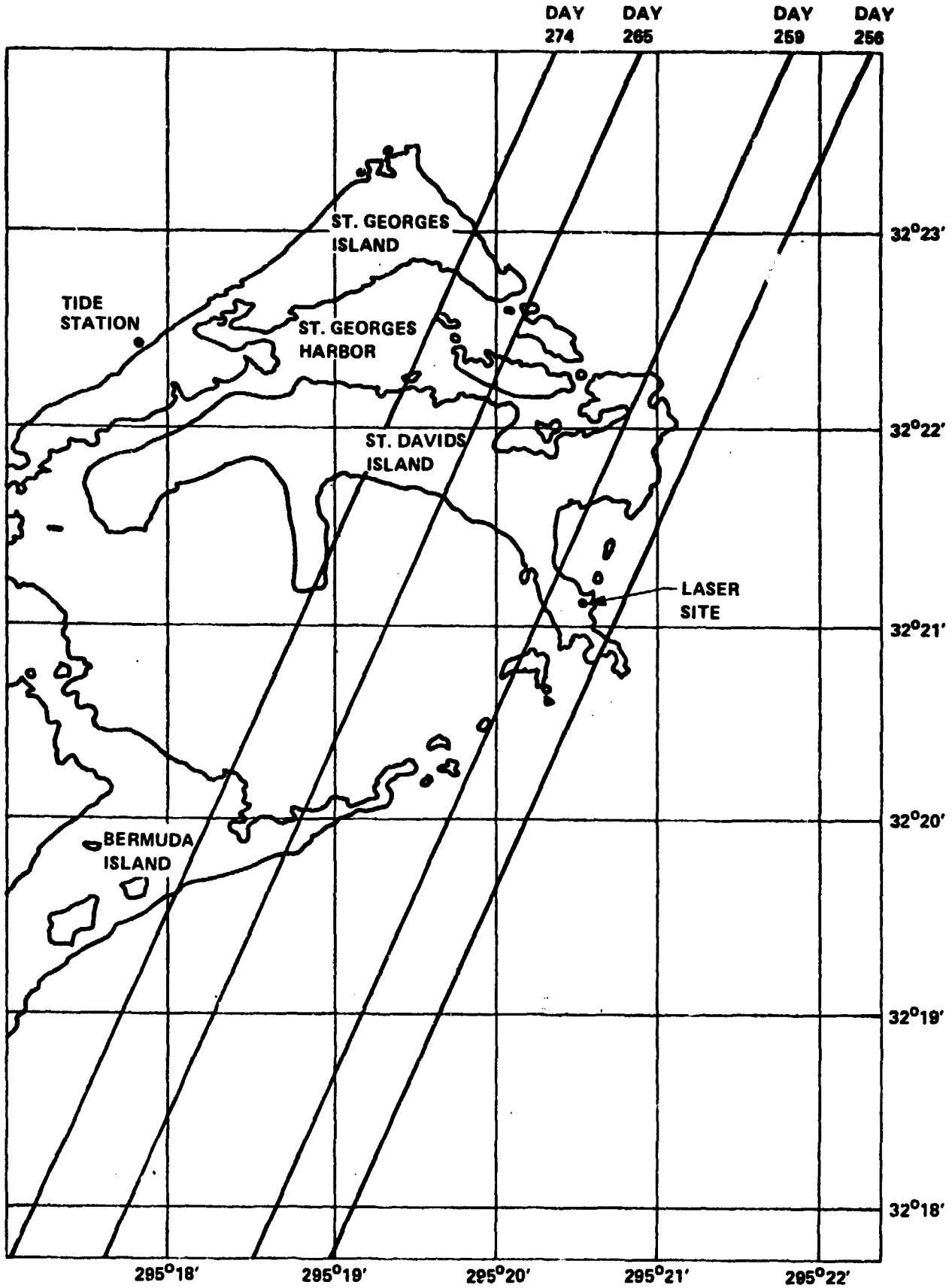

FIGURE 6A-1. **GROUND TRACK OF BERMUDA OVERFLIGHTS**

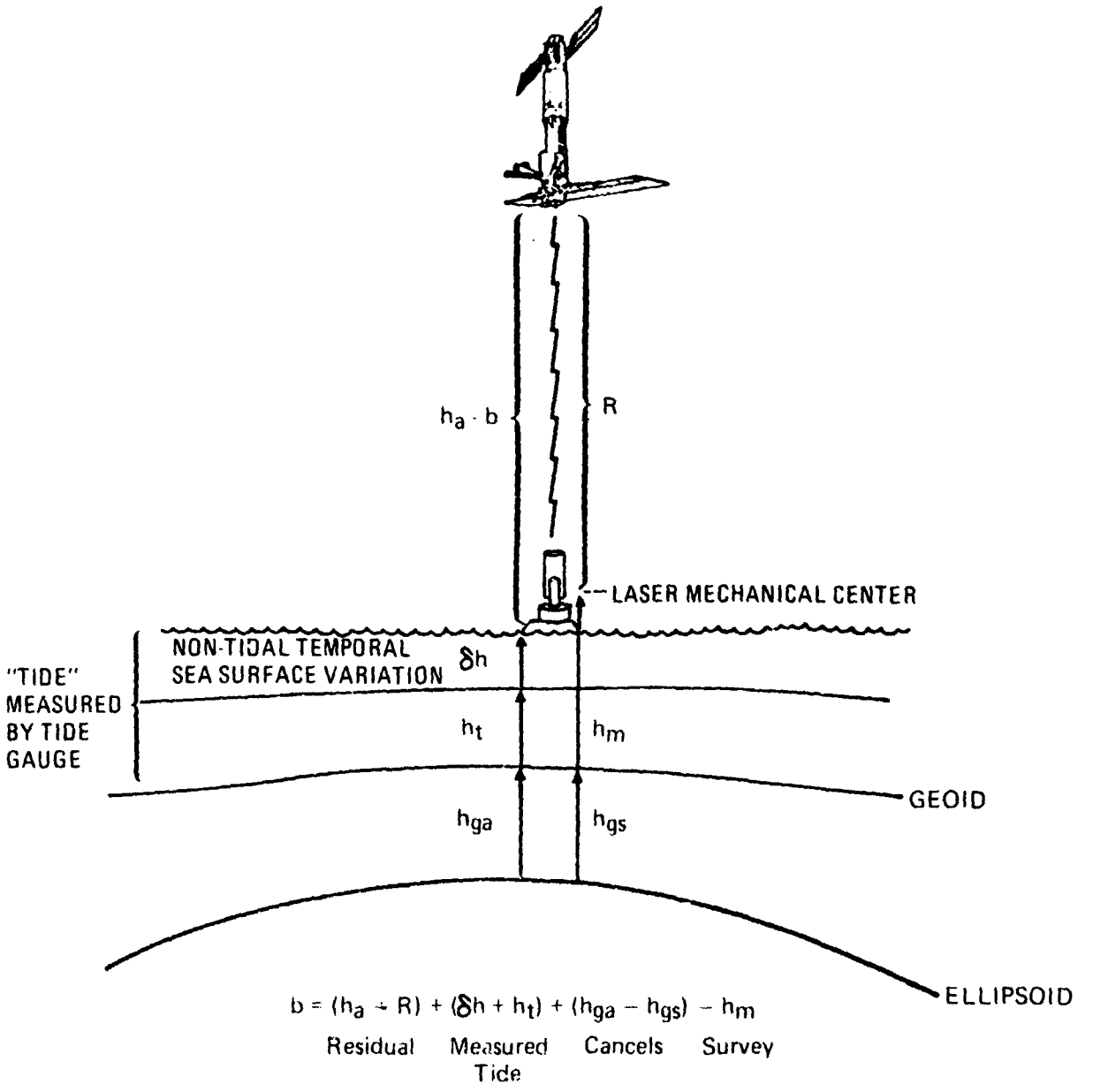

Figure 6A-2. Calibration Geometry

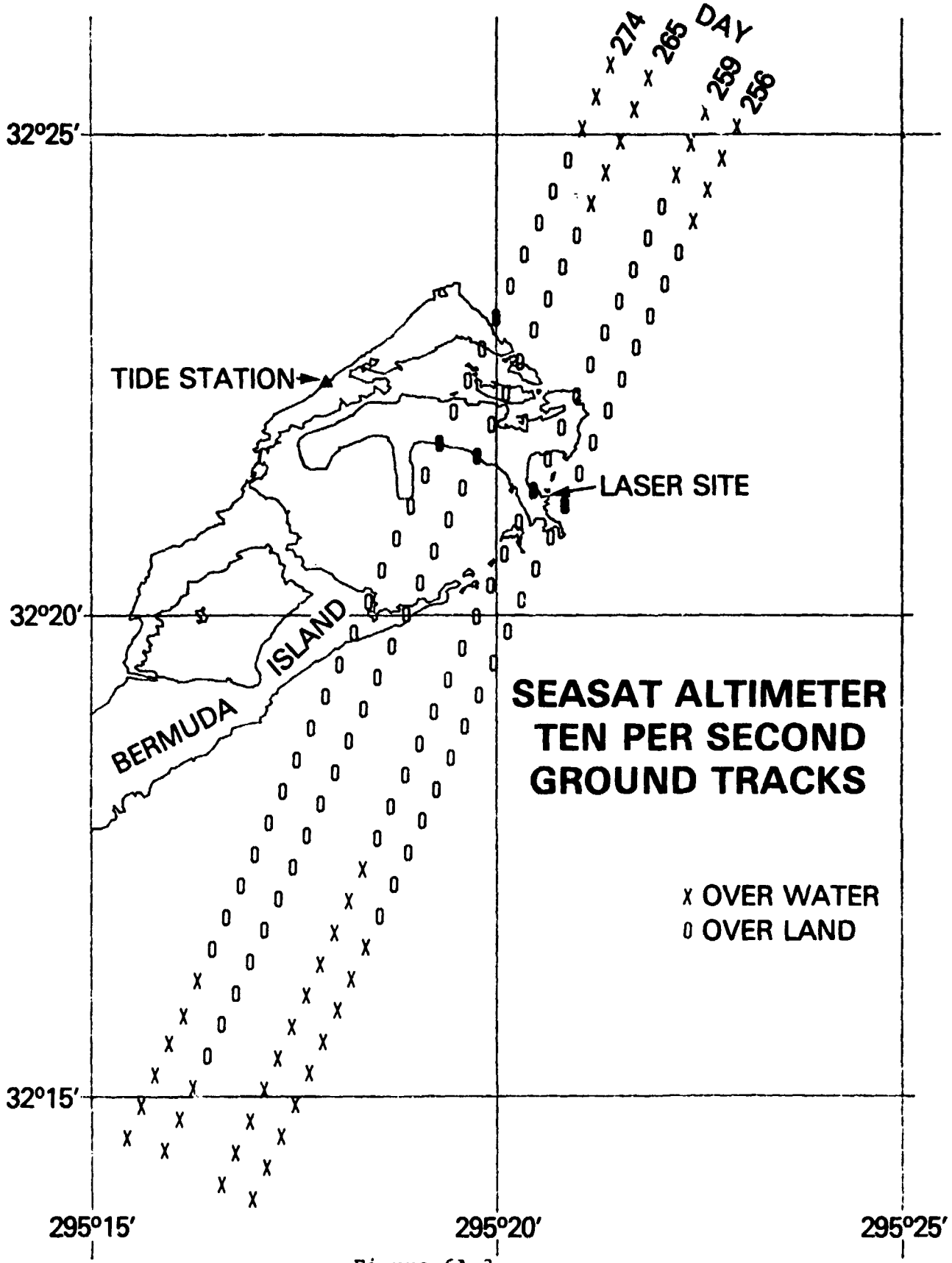
DAY
274
265
259
256
32°25′
32°20′
32°15′
TIDE STATION
LASER SITE
BERMUDA
ISLAND
SEASAT ALTIMETER
TEN PER SECOND
GROUND TRACKS
X OVER WATER
0 OVER LAND
295°15′
295°20′
295°25′

Figure 6A-3

Figure 6A-4. Seasat Altimeter Residuals

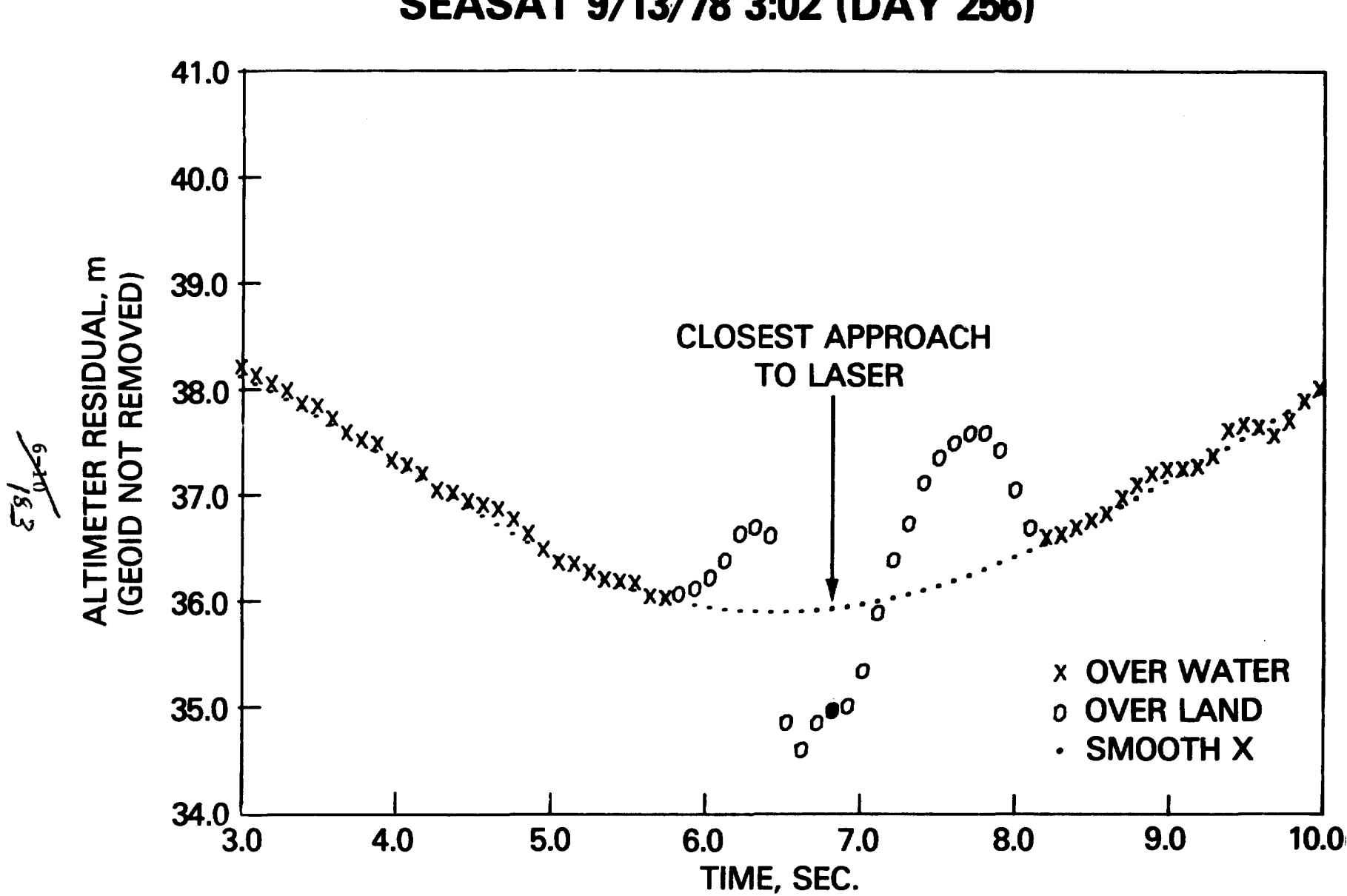

SEASAT BIAS

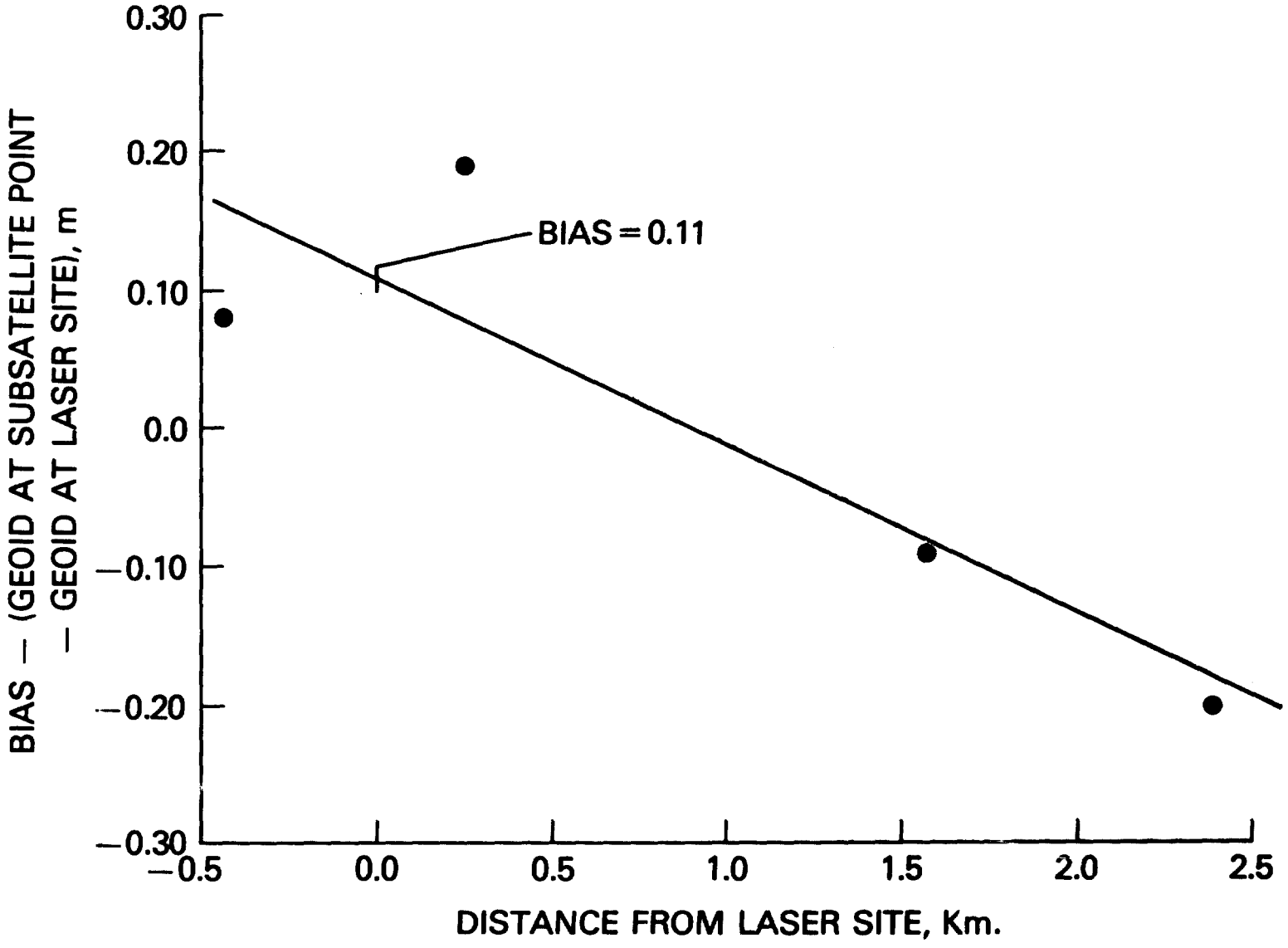

Figure 6A-5

Table 6A-1. Laser Overflight Tracking Support

	Overflight Revolutions			Pass After Overflight	
Day	Bermuda	Grand Turk	Goddard	Patrick	Goddard
256	X	X		X	
259	X	X			
265	X		X	X	X
274	X	X			

TABLE 6A-2. **SEASAT CALIBRATION PASSES**

DAY NO.	256	259	265	274
RESIDUAL, m	35.85	35.90	35.61	35.44
GEOID AT LASER, m	−39.97	−39.97	−39.97	−39.97
TIDE, CORRECTION, m	0.02	0.05	0.04	0.24
DRY TROPOSPHERE, m	−2.33	−2.31	−2.34	−2.32
WET TROPOSPHERE, m	−0.25	−0.19	−0.26	−0.33
IONOSPHERE, m	−0.02	−0.02	−0.02	−0.02
CENTER OF GRAVITY, m	6.04	6.04	6.04	6.04
ACCELERATION/6.5, m	0.08	0.07	0.08	0.07
TIMING (68.6 m sec), m	0.78	0.80	0.78	0.79
SEA STATE, m	−0.12	−0.18	−0.05	−0.14
TOTAL, m	0.08	0.19	−0.09	−0.20
DISTANCE FROM LASER, Km	−0.44	0.25	1.57	2.39

B. THE EFFECT OF SEA STATE ON ALTIMETER MEASUREMENTS

by

R. Kolenkiewicz

OBJECTIVE

The primary objective of this effort is to determine the effects of sea state on altimeter height measurements using Seasat data. A secondary objective is to study the characteristics of short period (3 day) variations in sea surface topography due to non-tidal sources.

BACKGROUND

The existence of a sea state dependent bias on altimeter measurements has been known at least since the publication in 1971 of results showing such an effect in nanosecond radar measurements from a tower (Yaplee, et al., 1971). The magnitude of the observed effect was on the order of 5% of the $H_{1/3}$ value, or 20% of the rms wave height. Such effects, amounting typically to 10-20 cm, were largely ignored by the GEOS-3 project--with reasonable justification considering the GEOS-3 altimeter noise level of 70 cm at the 10 pps data rate. For Seasat, with noise at the sub -10 cm level, sea state bias effects were totally ignored in the JPL geophysical data processing, even though a number of effects of smaller magnitude were included.

RECENT ACCOMPLISHMENTS

The existence and importance of sea state bias has been demonstrated by two recent developments. First, the Seasat calibration results (Kolenkiewicz and Martin, 1979) have been found to be much more consistent for the four Seasat calibration passes having laser support than they are without a sea state bias correction. Second, Jackson (1979), has theoretically derived a sea state bias correction which is approximately the product of height skewness and rms wave-height. This formula is consistent with that used for correcting the Seasat calibration passes in the vicinity of Bermuda.

Because the Seasat orbit almost exactly repeated during the last 30 days of the satellite's lifetime, a large data set (10 passes) is available for each groundtrack with a common geoid. Differences between overlapping passes are due to orbit errors, propagation errors, tidal errors, sea state bias effects, and temporal sea surface height effects (current movements, etc.). The four Seasat calibration passes have been differenced, using October 22, 1978 as the reference pass (Martin and Kolenkiewicz, 1979). A sample is shown in Figure 6B-1 with a linear trend having been removed from the differences. Also shown in Figure 6B-1 is the computed sea state bias difference based on Jackson's formula. North of Bermuda, there are numerous eddies in the vicinity of the Gulf Stream boundary, and the pass-to-pass differences are dominated by eddy movement. South of Bermuda, the sea surface topography is more stable and the differences are reasonably well explained as being due to differing sea states.

SIGNIFICANCE

Sea state bias is an effect which must be taken into account if 10 cm altimetry is to be obtained from radar altimeters. The large Seasat data set from overlapping tracks is a unique data set for verifying sea state bias formulas.

FUTURE EMPHASIS

Seasat data from the overlapping track period, and including tropospheric propagation corrections from the SMMR data, will be differenced using one pass for each track as a reference. The differences will then be compared with the $H_{1/3}$ differences.

REFERENCES AND PUBLICATIONS

Yaplee, B. S., A Shapiro, D. L. Hammond, B. D. Au, and E. A. Uliana, "Nanosecond Radar Observations of the Ocean Surface from a Stable Platform" IEEE Trans. Geoscience Elect., GE-9, 170-174, 1971.

Kolenkiewicz, R., and C. F. Martin, "Preliminary Determination of the Seasat Altimeter Height Bias," presented at the 1979 Spring Meeting of the American Geophysical Union, Washington, D.C.; EOS Transactions, American Geophysical Union, Vol. 60, No. 18, May 1979.

Jackson, F. C., "The Reflection of Impulses from a Nonlinear Random Sea," GSFC X-946-79-10, March 1979.

Martin, C. F. and R. Kolenkiewicz, "Utilizing Seasat Data to Determine Sea State Bias Effects on Altimeter Data," presented at the 1979 Fall Meeting of the American Geophysical Union, San Francisco, CA; EOS Transactions, American Geophysical Union, Vol. 60, No. 46, November 13, 1979.

Figure 6B-1. Seasat Height Differences

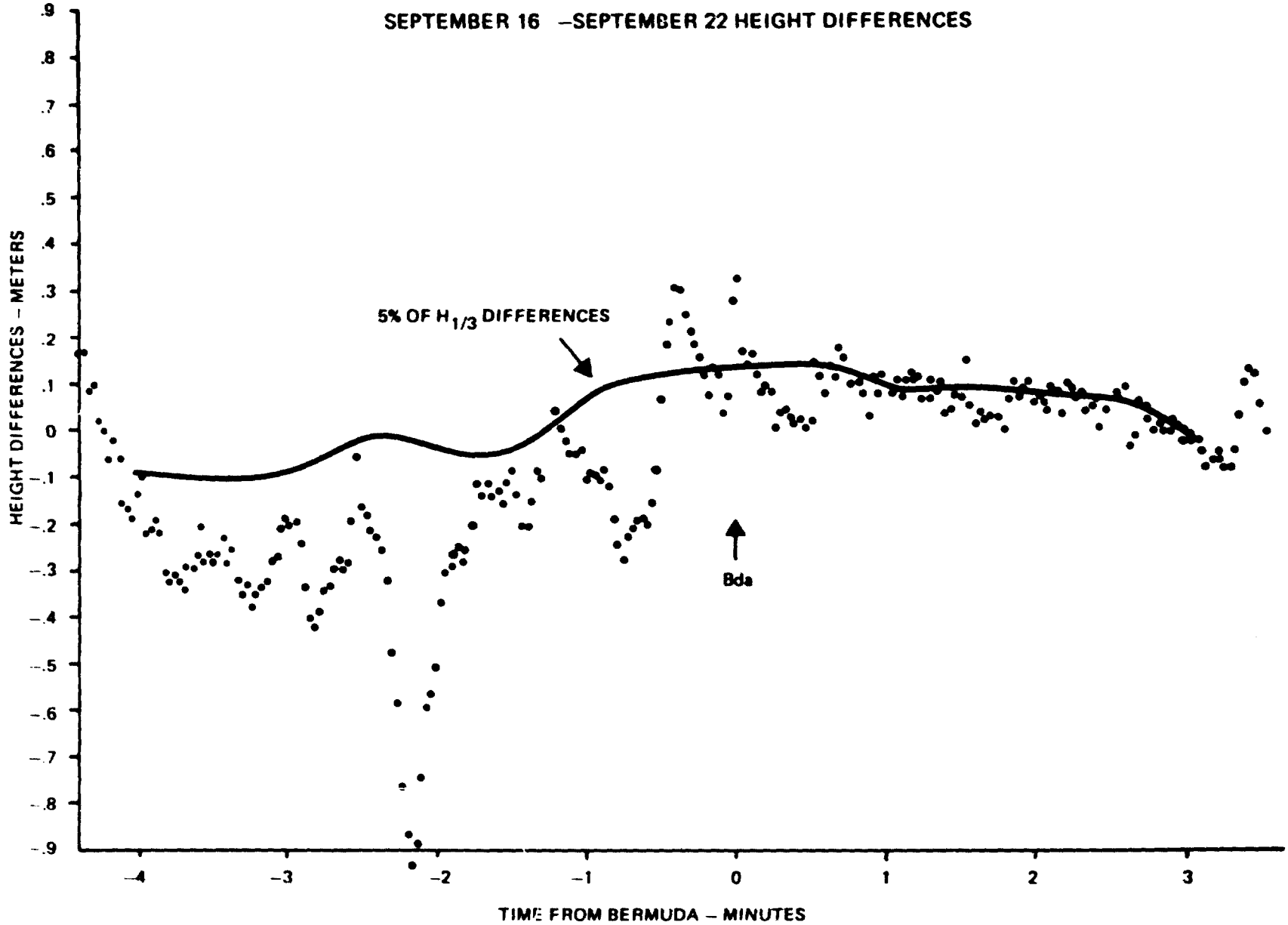

181
9-9

C. MEAN SEA SURFACE COMPUTATION USING GEOS-3 ALTIMETER DATA

by

J. G. Marsh

OBJECTIVE

The objective of this work is to compute a global mean sea surface (the geoid) using a combination of satellite altimeter data and precision orbital data based upon laser and Unified S-Band observations. This surface will form the basis for subsequent dynamical ocean processes analyses as well as analyses of geophysical problems such as mantle convection.

BACKGROUND

The GEOS-3 radar altimeter experiment conducted during the period of 1975-1978 has provided a homogeneous grid of altimeter data over the oceans with a resolution in most areas of a fraction of a degree (Figure 6C-1). The precision of these data is on the order of 30 to 50 cm. Since GEOS-3 did not have an onboard memory system for the altimeter data, the passes are usually limited to lengths of a few thousand kilometers.

During the time period of July to October 1978 the Seasat radar altimeter experiment also provided a global set of altimeter data. The precision of the Seasat data is better than 10 cm. Also, since Seasat had an onboard data storage system, the data were recorded in the form of long unbroken passes spanning the world's oceans. In the present Seasat data analyses an 18-day set of data covering the time period of July 28 to August 15 has been used. This set of data provided a grid spacing of about 1.5° at the equator.

Techniques have been developed for combining the GEOS-3 and Seasat altimeter data with precision ephemeris data based upon laser and Unified S-Band tracking observations so that the individual profiles can be used to calculate contour maps of the ocean surface with respect to the center of mass reference ellipsoid.

RECENT ACCOMPLISHMENTS

The mean sea surface computation technique employed for GEOS-3 consisted of first of all, the establishment of a reference grid of passes based upon laser and Unified S-Band orbital solutions, and secondly the adjustment of tilts and biases for the remaining passes in order to minimize the crossover residuals in a least squares sense (Marsh, et al., 1979a). For this reference grid we have computed orbits for 45, 5-day arcs of GEOS-3 data using the GEM 10B gravity model. These arcs were specially selected to have good global data coverage by the laser and S-Band stations and also to provide orbits which assure global coverage by the altimeter data.

In order to analyze in detail the regional variations in orbit error as well as the characteristics of the altimeter data we have divided the earth into sixteen regions and computed the crossover statistics for the passes in each region.

The regions are shown in Figure 6C-2. The number of crossovers and passes, the rms and mean crossover differences and an estimated timing bias on the altimeter data are presented for each region in the Table. The 1975 data are separated from the 1976 data since earlier analyses had indicated that the 1975 orbits were more accurate than the latter orbits. The crossover differences contain not only orbit error in each orbit but also any other time dependent unmodeled effects such as tidal model errors or height variations resulting from ocean circulation processes for example. The dominant contributor to the rms difference is orbit error with the rms oceanographic effects being probably on the order of 30 cm. Of course the orbit error reflects the sum of the errors in both orbits, thus to obtain the uncertainty in a single orbit we should divide by $\sqrt{2}$. In 1975 the rms differences range from 1 to 2 meters, with the best agreement usually noted for areas in the North Atlantic (e.g., XG7, XG8, N9) and poorest agreement being in the southern oceans and in the western Pacific (e.g., XG1, XG4, N1). This regional variation is attributed to gravity model error and the lack of precision tracking data in these more remote areas. Similar trends are noted in the 1976 data however the overall rms differences are larger since in general the 1976 orbits are not as accurate as the 1975 orbits. Our initial inspections of the mean values led us to suspect that the systematic nature of the values could be attributed to an error in the altimeter time tags. Timing bias solutions for each of the regions revealed a systematically negative trend in the results. Due to the large sample size and the global distribution of the data, the timing errors are believed to be statistically significant. The source of this discrepancy is not known as of this time. To some extent such a timing error will be averaged out in the computation of a mean sea surface using ascending and descending passes however it may corrupt long wavelength studies such as the estimation of J_2 and J_4 coefficients from the altimeter data.

Figure 6C-3 presents a contour map of the mean sea surface based upon a combination of the reference grid and the remaining altimeter data. The surface has been oriented with respect to the center-of-mass of the earth and scaled through the use of the reference orbits which were held fixed.

Comparisons of this surface with mean sea surfaces based upon altimeter data but using different adjustment techniques, Brace, 1977; Rapp, 1978 along global profiles have indicated agreement usually on the order of 2-3 meters or better.

Figure 6C-4 presents a preliminary contour map of the mean sea surface topography in the N. Atlantic Ocean based upon the 18-day set of Seasat altimeter data, Marsh, et al., 1979b. The surface computation technique employed was similar to that

used for the GEOS-3 data however, since the data were continuous and accurate orbit data could be computed for every pass of altimeter data, tilts and biases were not adjusted for a subset of the passes. Prior to surface computation analyses with the Seasat data, a timing bias analysis was also performed. The results of these analyses indicated that a timing correction of 68.5 m.s. was necessary (Tapley, et al., 1979).

SIGNIFICANCE

Using radar altimetry and precise orbital data, techniques have been developed and utilized for the computation of mean sea surfaces on a global as well as a regional scale. These mean sea surfaces form a basic reference surface which will be applied to investigations of dynamic ocean processes as well as geophysical analyses in ocean areas.

FUTURE EMPHASIS

During the next year a significant amount of additional Seasat and GEOS-3 altimeter data will become available. These data will be used to extend and enhance the present results. Also computations will be carried out for sub-regions as a function of time in an attempt to reveal time dependent phenomena.

REFERENCES AND PUBLICATIONS

Marsh, J.G., Martin, T.V., McCarthy, J.J., Chovitz, P.S., "Mean Sea Surface Computation Using GEOS-3 Altimeter Data," Marine Geodesy, Vol. 3, pp. 181-200, 1979a.

Marsh, J.G., Williamson, R.G., Martin, T.V., "Seasat Orbit and Altimeter Data Analyses," EOS Transactions, AGU, Vol. 60, No. 46, p. 806, 1979b.

Tapley, B.D., Schutz, R.E., Marsh, J.G., Townsend, W.F., Born, G.H., editors, "Accuracy Assessment of the Seasat Orbit and Altimeter Height Measurement," Seasat Orbit Accuracy Assessment and Bias Calibration Workshop Report, June 11-16, 1979, University of Texas, Austin.

Brace, K., "Preliminary Ocean Area Geoid from GEOS-3 Satellite Radar Altimetry," Defense Mapping Agency Aerospace Center, St. Louis, Missouri, 1977.

Rapp, R.H., "GEOS-3 Data Processing for the Recovery of Geoid Undulations and Gravity Anomalies," J. Geophys. Res., 84, 3784-3792, 1979.

TABLE 6C-1. SUMMARY OF GEOS-3 ALTIMETER CROSSOVER DIFFERENCES AND TIMING ERROR ESTIMATES

	1975					1976				
AREA	NO. OF CROSSOVERS	NO. OF PASSES	RMS (m)	MEAN (m)	TIMING BIAS (m.s)	NO. OF CROSSOVERS	NO. OF PASSES	RMS (m)	MEAN (m)	TIMING BIAS (m.s)
XG1	187	41	1.97	0.28	- 7.1	584	94	1.44	-0.88	-22.3
XG3	368	89	1.89	1.19	-42.0	27	14	1.62	-1.04	-23.8
XG4	313	54	1.90	-1.21	-54.5	2	3	--	--	--
XG5	561	97	1.48	-0.32	9.2	13	11	2.25	-0.49	-34.2
XG6	--	--	--	--	--	305	76	1.06	-0.44	40.1
XG7	1058	79	1.12	0.09	1.9	182	31	1.14	-0.66	-13.3
XG8	1207	92	1.12	-0.41	-13.5	511	54	1.42	-0.88	-17.8
N1	244	58	1.70	0.41	12.3	21	13	1.45	-0.81	-18.3
N2	429	81	1.78	-0.56	-30.6	--	--	--	--	--
N3	213	103	1.53	0.07	- 5.9	22	12	3.33	-2.23	-47.0
N4	31	18	1.62	0.45	-15.2	330	71	1.47	0.11	- 5.9
N5	18	12	1.02	0.44	-32.4	114	47	1.50	-0.30	-31.8
N6	57	22	1.21	-0.30	11.6	38	23	1.70	-0.34	-68.2
N7	36	31	0.94	-0.48	-14.5	17	18	2.82	-2.64	-63.2
N8	19	14	1.19	-0.60	-20.3	52	24	2.36	-1.36	-36.1
N9	102	34	1.19	-0.03	- 1.1	4	5	--	--	--

OVERALL TIMING BIAS ESTIMATES: 1975 -9.2 ± 0.5 m.s.

1976 -18.7 ± 0.6 m.s.

TRUE TIME = OBSERVATION TIME + Δt

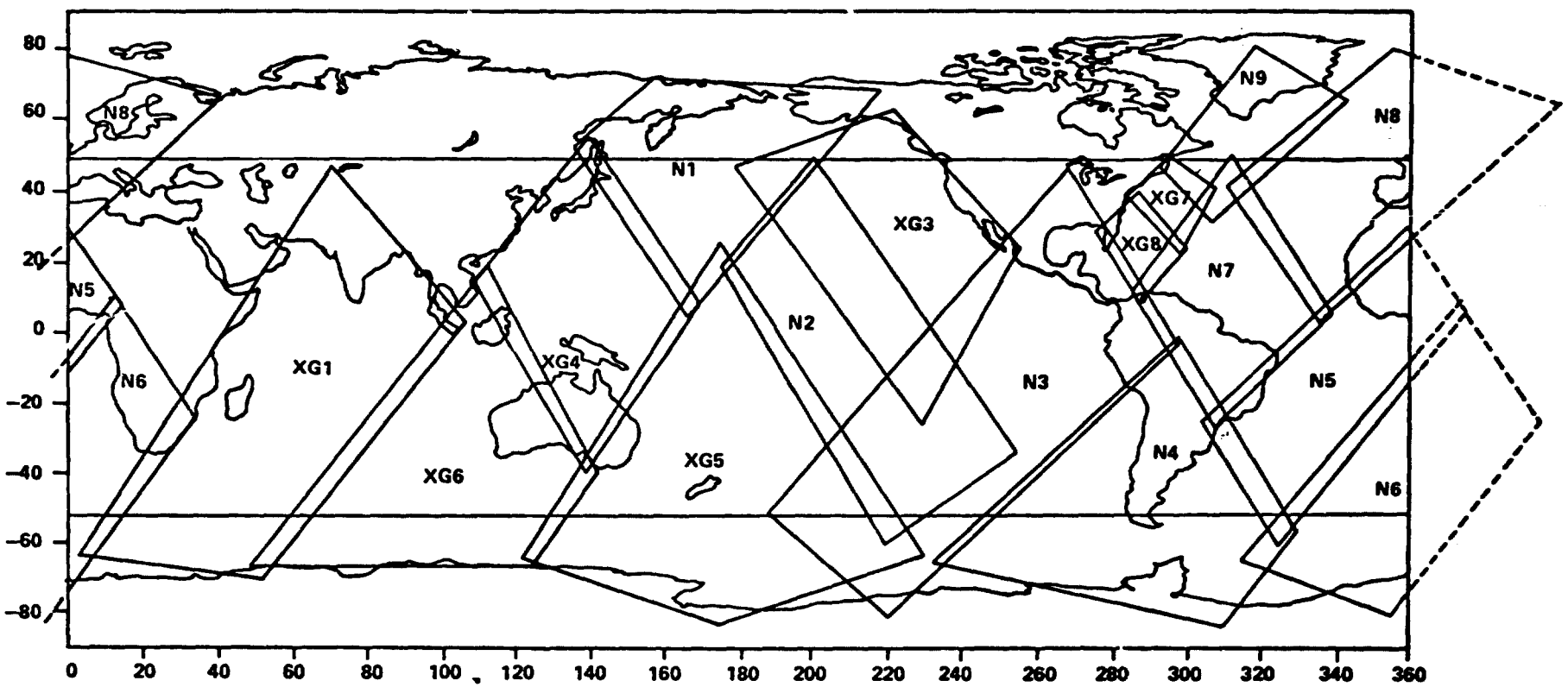

Figure 6C-1. GEOS-3 Altimeter Investigation Areas

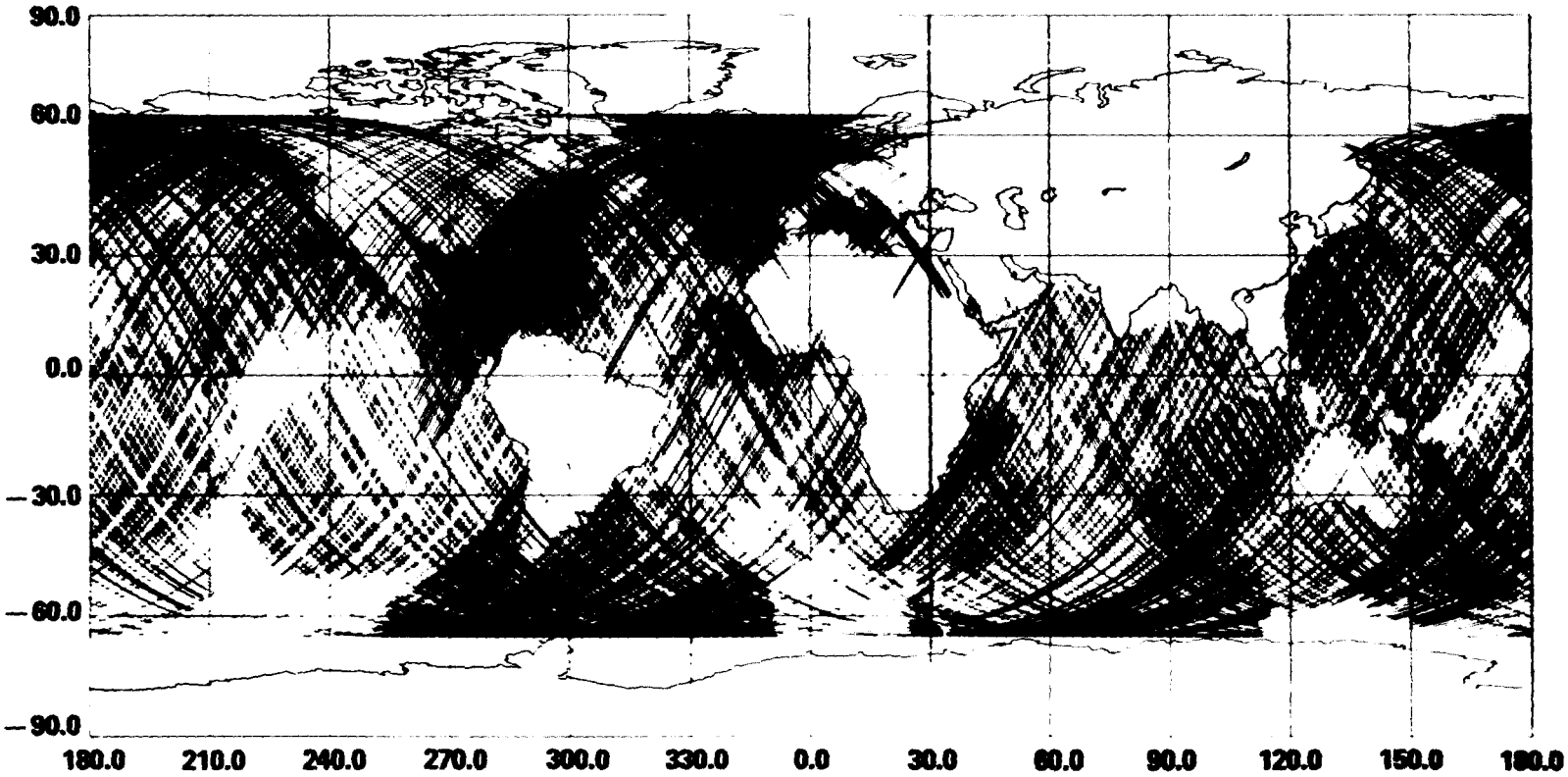

Figure 6C-2. GEOS-3 Altimeter Data Available at GSFC
January 1978

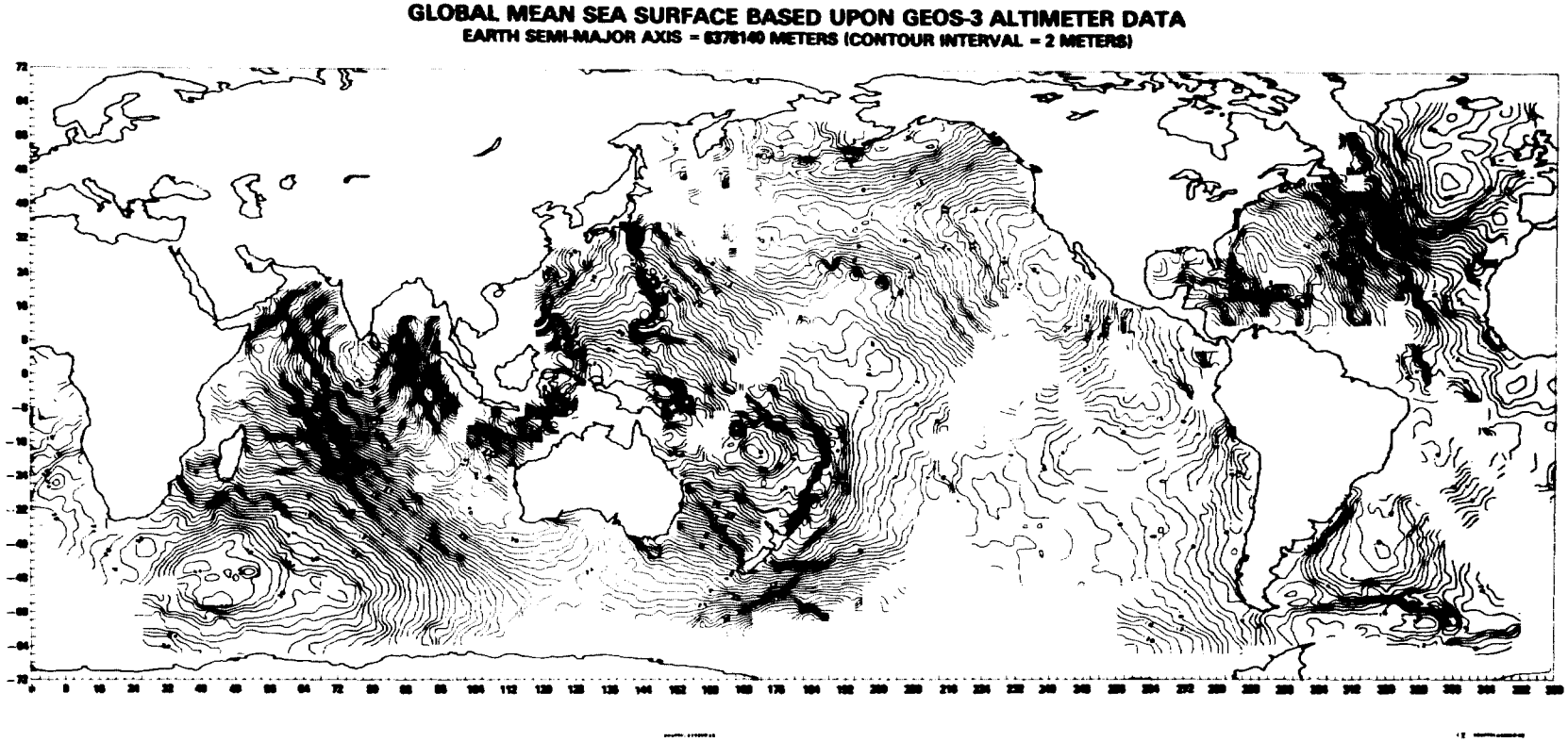
GLOBAL MEAN SEA SURFACE BASED UPON GEOS-3 ALTIMETER DATA
EARTH SEMI-MAJOR AXIS = 6378140 METERS (CONTOUR INTERVAL = 2 METERS)

Figure 6C-3

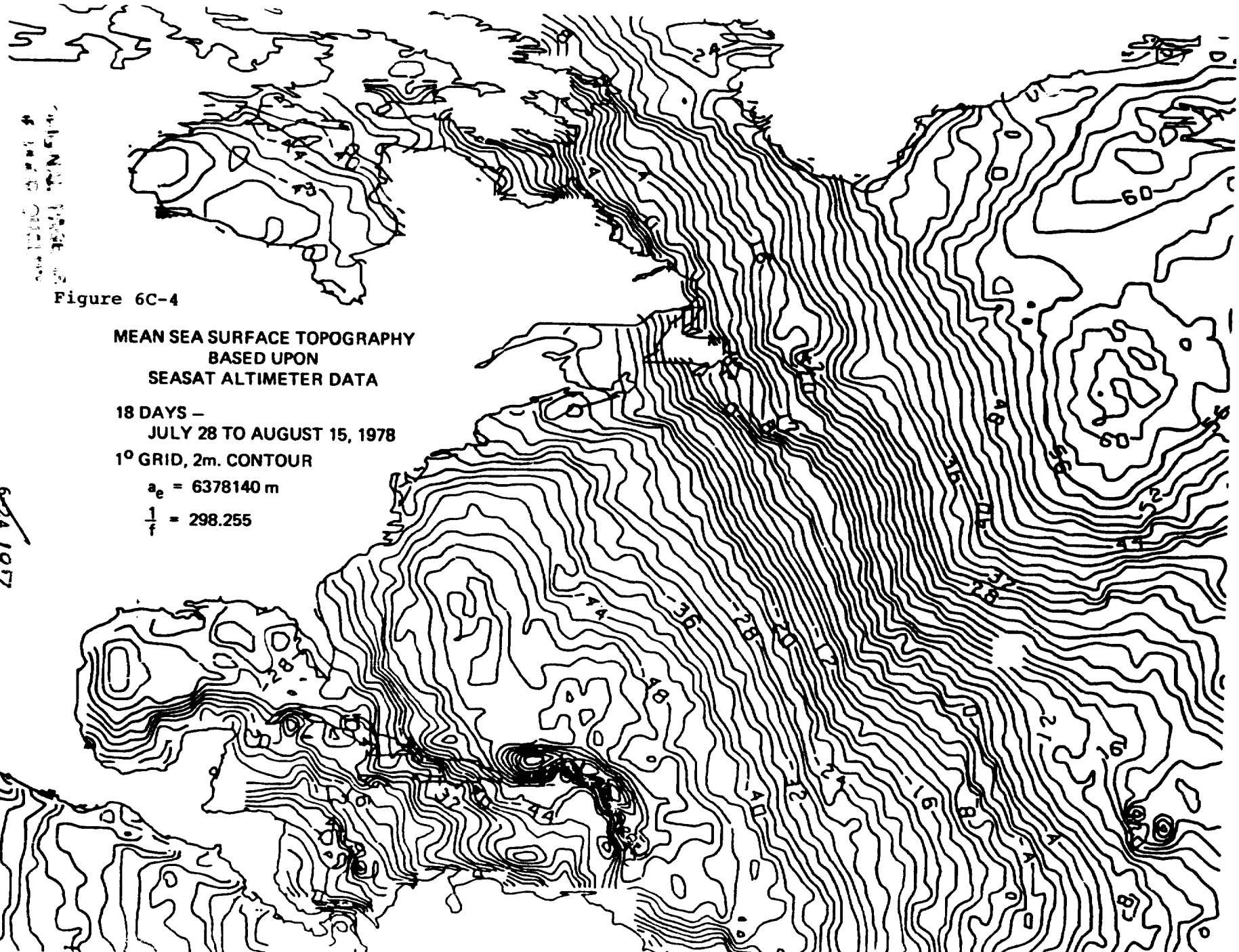

Figure 6C-4

MEAN SEA SURFACE TOPOGRAPHY
BASED UPON
SEASAT ALTIMETER DATA

18 DAYS –
JULY 28 TO AUGUST 15, 1978

1° GRID, 2m. CONTOUR

a_e = 6378140 m

$\frac{1}{f}$ = 298.255

D. OCEAN CIRCULATION

by

R.E. Cheney

OBJECTIVES

The overall goal of the oceans program is to gain a better understanding of meso-scale circulation through remote sensing techniques. Present studies focus on satellite altimetry data gathered by Seasat in the western North Atlantic. Dynamic topography associated with ocean currents is obtained by differencing the altimeter heights with a gravimetric geoid model. The value of this technique can be evaluated by comparison with independent oceanographic observations, which include trajectories of satellite-tracked drifting buoys used to monitor the movements of Gulf Stream rings.

BACKGROUND

Approximately 1000 orbits of altimetry data were obtained by Seasat between July and October 1978. The altimeter measured the radial distance from the satellite to the sea surface based on the travel time of very short pulse (3nsec) microwave signals. Accuracy was on the order of 10 cm. When combined with independent orbit computations, the data can be expressed as sea surface heights with respect to the center of the Earth. Geoid models can then be used to determine the deviation of the instantaneous sea surface from an equipotential surface. In this way it is possible to solve for geostrophic ocean currents, which are associated with sea surface slopes.

The western North Atlantic was used as a testing ground for this new technique primarily because of the availability of an accurate gravimetric geoid model for this area (Marsh and Chang, 1978). It is also a region of large amplitude (1-2 m) ocean signals associated with the Gulf Stream and rings formed by the Stream. In a cooperative project with the Naval Oceanographic Office and the Coast Guard, satellite-tracked buoys were parachuted into five different cold rings in the Sargasso Sea. Their trajectories provided valuable surface truth for the altimeter.

RECENT ACCOMPLISHMENTS

Analyses of numerous Seasat passes have shown that the altimeter/geoid technique can be used to accurately detect Gulf Stream features (Cheney and Marsh, 1980). A series of eight profiles obtained at 3-day intervals along the same track is shown in Figure 6D-1. The Gulf Stream is clearly apparent as a 130-165 cm step near 37^{o}N, and a cold ring is evident at 33.5^{o}N. Tracking data from one of the surface drifters indicated that Seasat flew directly over the ring during the first pass on September 17, and a 45 cm depression was observed in the altimeter profile. During the next three weeks the ring moved 100 km west of the ground track. Figure 6D-1 shows that the sea surface depression associated with the ring gradually disappeared from the altimeter profile as the ring moved out from under the satellite's footprint, a dramatic demonstration of the altimeter's capabilities.

Although Seasat failed in October 1978 after only two drifters had been deployed, the remaining three buoys were launched as originally planned to learn more about the movements of cold rings. An example of a surface buoy's ability to follow a cold ring for long periods of time is shown in Figure 6D-2. In 8½ months the buoy completed 63 loops about the ring center with an average period of four days. The ring itself moved in a complicated fashion, usually drifting slowly westward a few km/day, but occasionally surging forward at 20 km/day.

SIGNIFICANCE

Work completed thus far provides a high degree of confidence in the Seasat data as well as in the geoid model, and demonstrates the wide variety of problems which can be attacked with this unique data set. For example, significant variation in the height of the Gulf Stream observed in the altimetry suggests dramatic changes in transport. The Seasat data provides a means of examining the time and space scales of this variability. It should also be possible to determine the number and distributions of Gulf Stream rings during this time by constructing sea surface topographic maps. Problems such as these have never been adequately resolved, primarily due to the spatial limitations inherent in standard oceanographic methods.

FUTURE EMPHASIS

The complete Seasat altimeter data set should be available by spring 1980. Subsequent emphasis will be on the development of techniques to extract the desired oceanographic information. Many of the results will be descriptive in nature but with the advantage of statistics obtained from repeated samplings over three months. An example would be determined of the mean current field together with the distribution of eddy kinetic energy for the western North Atlantic. We also hope to look at areas such as the

6-29 99

Southern Ocean, the Kuroshio, and the Equatorial Current. Where possible, comparisons will be made with documented oceanographic observations and historical data.

REFERENCES AND PUBLICATIONS

Campbell, W.J., R.E. Cheney, J.G. Marsh and N.M. Mognard, "Ocean Eddy Structure by Satellite Radar Altimetry Required for Iceberg Towing," to appear in Cold Regions Science and Technology, 1979.

Cheney, R.E. and J.G. Marsh, "A Preliminary Look at Seasat Altimetry in the Gulf Stream Region," Gulfstream, 5 (2), NOAA National Weather Service publication, 1979.

Cheney, R.E. and J.G. Marsh, "Seasat Altimetry Observations of Dynamics Ocean Currents in the Gulf Stream Region," submitted to Journal of Geophysical Research, 1980.

Cheney, R.E., P.L. Richardson and B.P. Blumenthal, "Air Deployment of Satellite Tracked Drifters," submitted to Journal of Geophysical Research, 1980.

Marsh, J.G. and E.S. Chang, "5' Detailed Gravimetric Geoid in the Northwestern Atlantic Ocean," Marine Geodesy, 1 (3), 253-261.

6-27-200

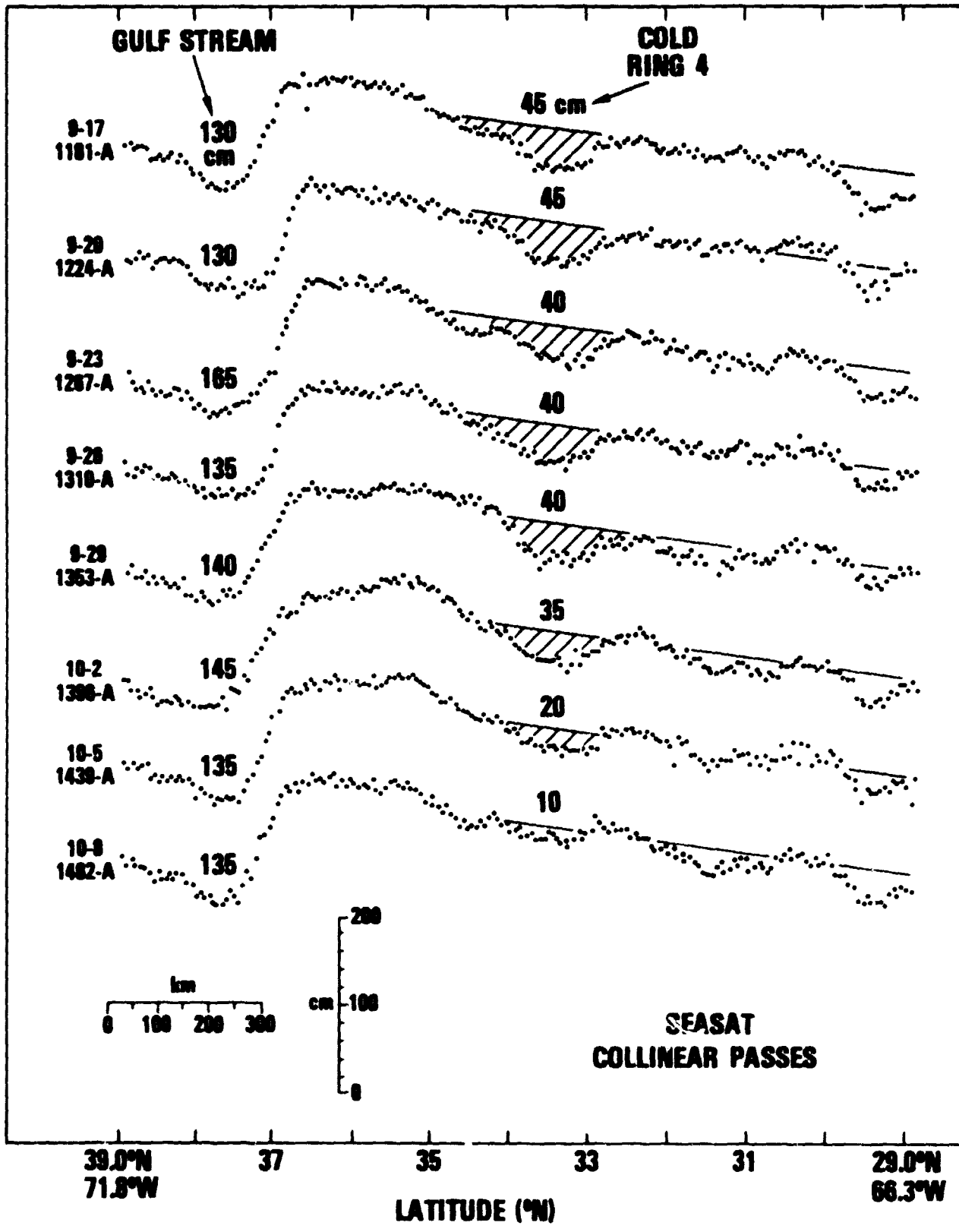

FIGURE 6D-1 Altimeter residuals for 8 collinear passes obtained over a 3-week period.

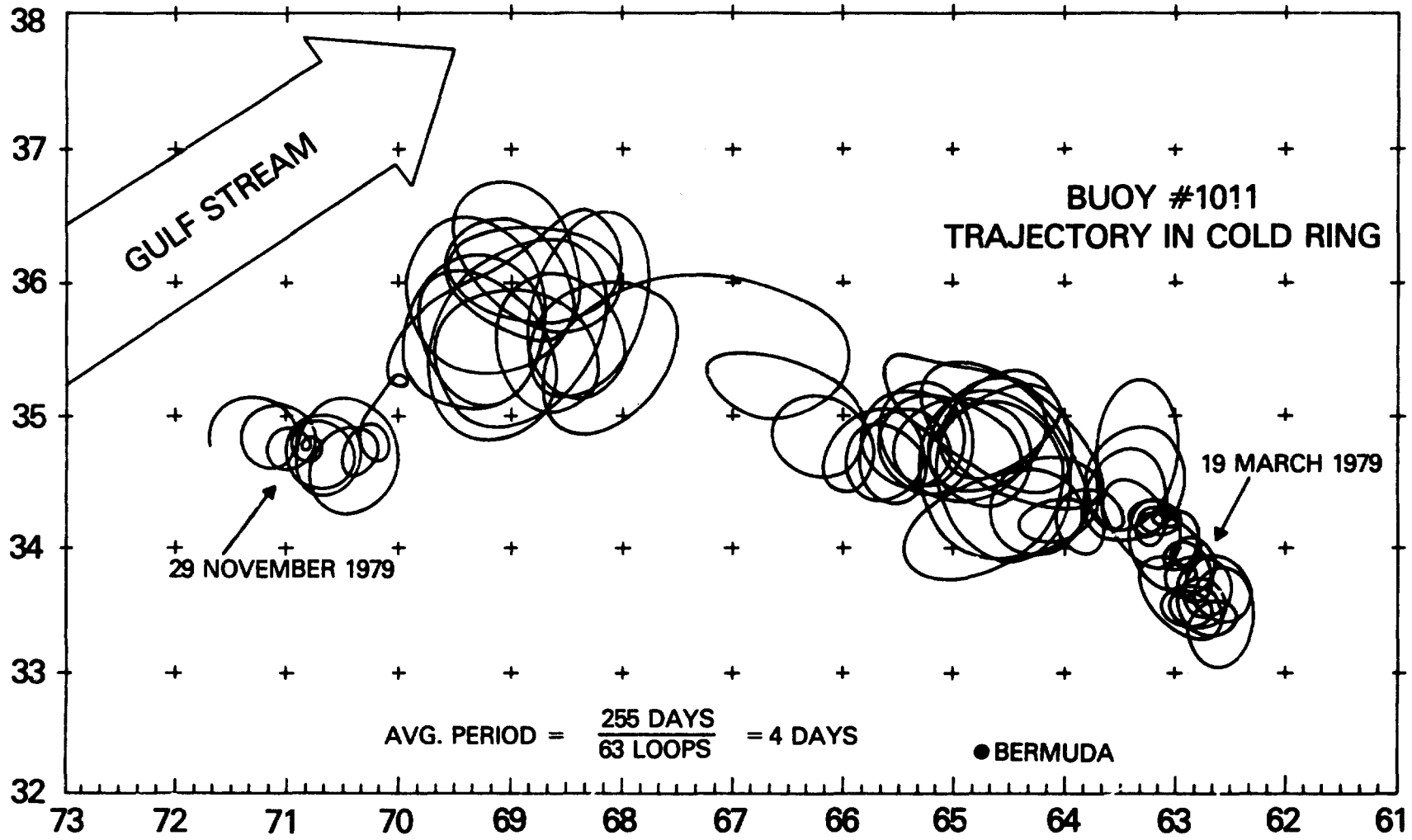

FIGURE 6D-2 8 1/2 month trajectory of a surface buoy in a cold Gulf Stream ring.

E. STARLETTE ORBIT ANALYSES FOR OCEAN TIDAL STUDIES

by

T. L. Felsentreger and J. G. Marsh

OBJECTIVE

The objective of this work is to obtain more accurate orbital data for the Starlette satellite and to use these data for the computation of ocean tidal information.

BACKGROUND

Analyses have been carried out over the past several years at GSFC for the solution of ocean tidal parameters from precision satellite orbit data, e.g., Felsentreger, Marsh & Agreen (1976); Felsentreger, et al., (1978; 1979). These analyses have been limited by the accuracy of the orbital elements which we were able to compute with existing programs and modeling techniques, and also by the arc lengths of data available. Many of the geodetic satellites are being continuously observed by the laser systems so that arc lengths of several years are now possible. Furthermore, computer program development and data availability now permit significant improvments to be made in the accuracy of orbit computations. During the past year, such efforts have been concentrated on a 4-year set of Starlette satellite data.

The Starlette satellite launched in 1975 by the French Space Agency, Centre National d'Etudes Spatiales has proven to be a valuable complement to the U.S. geodetic satellites for earth and ocean tidal analyses. This small dense passive satellite, equipped with laser cube corner reflectors is not significantly perturbed by drag and solar radiation pressure and thus is an excellent satellite for studying the perturbations due to earth and ocean tides. The satellite has been observed by the GSFC, SAO and European laser systems since launch and thus we have accumulated a long record of data. Previous analyses indicated that orbit computations based upon the GEM-10B gravity model produced more accurate results than those obtainable with the previous GEM-10 gravity model. This improvement is primarily attributed to two factors. First of all, the GEM-10B solution contained a significant amount of altimeter data over the ocean areas which were not previously covered by ground tracking stations or surface gravity data. Secondly, the GEM-10B model contained a complete set of spherical harmonic coefficients to degree and order 36. Recent analyses have indicated that coefficients even out to degree 45 produce along track orbit perturbations of a few meters. Even though these coefficients were not included in the GEM-10B model a portion of the effect was aliased into the (36,36) model.

RECENT ACCOMPLISHMENTS

In an attempt to more fully account for these subtle higher degree coefficients above degree 40 a new analysis of the Starlette laser tracking data recorded during the time period of 1975 to 1978 has been undertaken. Thirteen different laser stations have provided observational data during this time period. These data have been used to compute the best fitting orbits over 5-day arcs using the Geodyn Program in order to edit the data and to consequently select a subset of orbital arcs which can be used as input for the adjustment of the gravity model, particularly the higher degree coefficients. The overall rms fits for the 5-day arcs are typically about 2 meters, however, the GSFC data, e.g., San Diego, usually fits to about the meter level while the SAO data rms is usually about 3 meters. A set of these 5-day arcs has been selected and the normal equations are being combined with other orbit perturbation data for the solution of a more accurate gravity model for Starlette.

SIGNIFICANCE

(The significance of pursuing work in the earth and ocean tide area has been clearly outlined in a recent written communication from Lambeck (1979). Some of this information is presented verbatim below.)

The Earth's tides are reflected in numerous geophysical observations. Locally, they result in changes in gravity, stress, and tilt of the crust and in variations in height. Globally the tides cause periodic changes in the Earth's rotation and introduce perturbations in the motions of close Earth satellites. Thus apart from any intrinsic interest that the tidal phenomena may have, the tides must be known and understood as they are a major source of perturbation in geophysical measurements. This is particularly true in orbit analysis where the tidal forces can cause quite large perturbations in the motion of close satellites.

Tidal perturbations include contributions from solid, oceanic and atmospheric tides with their relative importance being roughly of the order 100:10:1. Since the fluid tidal effects cannot be separated from those of the solid tide, the usual procedure is to adopt nominal solid earth tide parameters and to solve for the ocean tide parameters. Numerical models of the ocean tides are based on solutions of the Laplace tidal equations. To obtain significant solutions, realistic assumptions about the energy dissipation mechanism have to be made. A frequent assumption is that dissipation is by bottom friction and that it is limited to shallow seas but it is usually found that a more global dissipation mechanism must be introduced, such as a virtual internal friction coefficient or an eddy viscosity coefficient. The alternative approach has been to permit flow across the boundaries of the ocean, implying that the dissipation occurs either at or near the boundary in shallow seas.

The satellite observations provide a direct measure of the rate of dissipation in the oceans, once the significance of the solid Earth as an energy sink has been discounted.

That is, the rate of energy dissipation is a function of only the amplitude and phase of the single harmonic in the tide that has the same degree and order as the tide-raising potential. This estimate is independent of any assumption about the nature of the energy dissipation mechanism or mechanisms, the distribution of this mechanism in the oceans and the interactions between the solid and ocean tides. It should therefore provide an additional observation to be satisfied by any solution of the Laplace tide equations.

Another area where the satellite results may provide useful information is in the comparison of the ocean tide response as a function of frequency. Observations of the age of the tide suggest a frequency dependence of at least local tidal dissipation. Also, the few available ocean tide models suggest that the lag angles as a function of frequency may elucidate this question further.

A further area where the tidal phenomena is of geophysical interest concerns the tidal acceleration of the Moon, for those components in the ocean tide potential that cause the periodic perturbations in the satellite motion also cause the secular acceleration of the Moon in its orbit, and an important part of the secular acceleration $\dot{n}$ of the Earth's spin.

Energy dissipation in the Earth-Moon system has three potential sinks: (i) the oceans, which is the primary sink, (ii) the solid Earth, and (iii) the Moon. Numerical tide models provide an estimate of (i) that is dependent on assumptions made about the dissipation mechanisms. The satellite observations provide a measure of the sum of (i) and (ii). Astronomical observations of the lunar acceleration provide a measure of the sum of (i), (ii) and (iii). Hence, a separation of the energy sinks is possible in principle but the generally good agreement between the three independent estimates points to the dominance of the oceans as the energy sink.

The Moon solid+ocean tide perturbation in inclination seldom exceeds 0".3 with a period of 10-12 days. The ocean contribution is about 10 percent of this and to obtain significant results requires that 10-12 day perturbations can be determined with a precision of better than 0".003. Clearly this can only be achieved if the tracking data is of great precision and well distributed along the orbit.

FUTURE EMPHASIS

It is anticipated that tidal parameter recovery will proceed using two techniques. The first technique will be based upon the analysis of the long-term evolution of the mean orbital elements, and secondly an attempt will be made to solve for the tidal parameters directly from the tracking data using the Geodyn program.

The recovered tidal parameters will be compared with tidal models based upon numerical integration of the Laplace tidal equations and also from the analyses of satellite altimeter data.

REFERENCES AND PUBLICATIONS

Felsentreger, T.L., J.G. Marsh, and R.W. Agreen, "Analyses of the Solid Earth and Ocean Tidal Perturbations on the Orbits of the GEOS-1 and GEOS-2 Satellites," J. Geophys. Res., 81, 2557-2563, 1976.

Felsentreger, T.L., J.G. Marsh, and R.G. Williamson, "Tidal Perturbations on the Satellite 1967-92A," J. Geophys. Res., 83, 1837-1842, 1978.

Felsentreger, T.L., J.G. Marsh, and R.G. Williamson, "M_2 Ocean Tide Parameters and the Deceleration of the Moon's Mean Longitude from Satellite Orbit Data," J. Geophys. Res., 84, 4675-4679, 1979.

Lambeck, K., The Australian National University, Canberra, Australia (private communication), 1979.

CHAPTER 7

LAND RESOURCES

edited by

Darrel Williams

OVERVIEW

The availability of accurate and timely land cover and land use information is central to the management, utilization, and conservation of our land resources. Repetitive and synoptic views of our Earth's surface provided by remote sensor systems such as the Landsat multispectral scanner represent a unique land resources data collection system capable of providing information on current and changing land use/land cover patterns. The common goal of the land resources research activities at Goddard is to evaluate and improve remote sensing systems and analysis techniques to provide the information required for intelligent resource management decisions.

Six Division scientists and two Resident Research Associates (RRA's) are involved in land resources research activities on a regular basis. They are investigating remote sensing applications for a variety of land use/land cover categories, including forested areas, rural areas disturbed by strip mining activities, and urban areas. The objective of the forestry-related activities is to investigate the use of remotely sensed data to detect and assess the areal extent and severity of natural or man-induced disturbances of forest land. The objective of the surface mine project is to evaluate new remote sensing techniques and sensor packages for the monitoring of surface mines in the eastern United States by the Environmental Protection Agency. The primary thrust of the urban area delineation investigations, which are being conducted in conjunction with the Bureau of Census, is to develop procedures using Landsat MSS data to detect changes from non-urban to urban land cover.

Two other investigations are being conducted independent of any specfic discipline or land use/land cover category. One area of activity is the development and evaluation of algorithms to reduce or eliminate the effect of topographic variability upon multispectral sensor response. The other area of research is concerned with determining both the sources and degree of autocorrelation or redundancy in Landsat data.

Despite the diversity of land resources applications under investigation, our research activities share several common hallmarks. One such hallmark is the detection of change from one land use/land cover category to another. Other common features include the integration of Landsat data with ancillary data (i.e., terrain data, soils information, census survey data, etc.) and the development of automated methods to assess the accuracy of information derived from remotely sensed data. Our research projects also involve the study of both present and future satellite missions. Landsat MSS data, Seasat Synthetic Aperature Radar (SAR) data,

and aircraft MSS and multilinear array (MLA) data are being utilized to quantify the advantages and limitations of existing remote sensing systems and analysis techniques. Given this type of background experience, we will be in a better position to provide intelligent input relative to the sensor and mission parameters required from future satellite missions if improved land resources management information is to be acquired from space.

N80-20763

A. REMOTE MONITORING OF FOREST COVER CONDITIONS

by

D. Williams, S. Wharton, and R. Nelson

OBJECTIVE

The objective of this research is to investigate, develop and test analysis techniques which will facilitate the use of existing and proposed satellite sensor systems to detect, monitor, and assess the areal extent and severity of forest disturbances.

BACKGROUND

Forest disturbances result from both natural phenomena and the impact of man on the environment. Natural forest disturbances include insect and disease infestation, drought, flood, fire, windthrow and ice storms. Disturbances caused by man's intervention may include typical forest management practices (i.e., selective timber harvest, clearcuts and controlled burns, cattle grazing, etc.), recreational activities, urban expansion, right-of-way development and changing land use patterns. These events often have a widespread and catastrophic impact upon forest land productivity by reducing the rate of tree growth or causing tree mortality. For example, the annual loss due to insect infestations has been estimated to exceed 5 billion board feet. These losses, coupled with increased worldwide demand for wood and wood fiber products, illustrates that forest managers need timely information regarding changes in the condition of forest stands. However, current survey techniques consisting of ground measurements and low altitude aerial surveillance and photography are often found to be inadequate. Federal, state, and private forestry organizations have requested assistance in the research and development of techniques to facilitate the use of satellite remotely sensed data for monitoring forest cover conditions.

Research has been conducted at Goddard over the past few years in cooperation with the Forest Pest Management Division of the Pennsylvania Bureau of Forestry to determine the feasibility of using Landsat MSS data to detect deciduous forest stands which have been defoliated by the gypsy moth caterpillar during their late June/early July feeding cycle. A multitemporal, geometrically-corrected, and map-registered Landsat data set depicting both non-defoliated (July 19, 1976) and defoliated (June 27, 1977) forest cover conditions was created for a test site in central Pennsylvania. Preliminary analyses of this data set indicated that areas of heavy defoliation could be detected and classified. However, complications were encountered because certain non-forest cover types, such as cropland, were spectrally similar to defoliated forest lands. This spectral similarity resulted in the classification of some non-forest areas as heavy defoliation, i.e., an error of commission. The effect of topographic variability upon scene reflectance was also evident in the

misclassification (confusion) of shaded areas of healthy forest and fully illuminated areas of moderate defoliation. Research activities during the past year have been primarily directed towards the development and evaluation of techniques to solve or reduce these problems.

RECENT ACCOMPLISHMENTS

A hierarchial classification procedure has been successfully developed to eliminate potential errors of commission between non-forest cover types and areas of defoliation. The technique involves the classification of the non-defoliated Landsat data set into two simple categories; forest and non-forest. These classification results are then applied to the defoliated Landsat data set to remove or "mask" all non-forest pixels from the image. This eliminates the possibility of incorrectly mapping non-forested areas as defoliation since only areas of forest cover remain in the data set. The binary mask has been found to be an easily applied and effective technique because of the unique spectral response of the forested areas in this region. Similar techniques could also be utilized to selectively eliminate other land use/land cover categories.

Efforts have also been initiated to develop an accurate, cost-effective technique for assessing the severity of defoliation using Landsat digital data. The three officially recognized categories of defoliation are: light,0-30% leaf canopy removed; moderate, 31-60% leaf canopy removed; and heavy, 61-100% leaf canopy removed. Since defoliation causes a reduction in leaf canopy biomass, several MSS band ratioing techniques, which have been successfully utilized to estimate cropland and rangeland standing green biomass, were investigated relative to this forestry problem. These techniques are collectively referred to as "Vegetative Index" (VI) ratios. The six different VI ratios which were evaluated for estimating the severity of defoliation are summarized in Table 7A-1. Preliminary analyses of the results indicate that the VI ratios yield thematic maps similar to those derived from the more conventional approach of training field selection, signature extraction, and maximum likelihood classification. The ratio techniques are less time consuming (people and machine) than the typical classification scenerio and offer a simple technology to transfer to user agencies. In addition, recent laboratory studies have shown that band ratioing tends to reduce the effect of topographic variability upon scene illumination. Quantitative analyses of the VI thematic maps are currently underway to determine: (a) which VI ratio agrees most closely with available ground estimates, (b) how well the VI results compare with conventional classification results, and (c) whether the ratio approaches reduce the errors of commission between shaded areas of healthy forest and fully illuminated areas of moderate defoliation.

SIGNIFICANCE

The forest/non forest binary mask technique eliminates the potential for errors of commission between two spectrally similar, yet unrelated cover types such as defoliated forest land and cropland.

If this major obstacle were not resolved, the user community would find Landsat data to be unsatisfactory for monitoring forest cover conditions. The techniq . can also be used by other disciplines to remove confusing or unwanted land cover categories. Additional computer processing costs can be reduced because fewer pixels must be processed.

Vegetative Indexes have been evaluated for estimating standing green biomass in cropland and rangeland situations, but their application to related disciplines has been lacking. The work initiated at Goddard may lead to the quantification of the utility of VI ratios for estimating forest leaf canopy biomass, to the detection of forests under stress, and to the development of ratio techniques specifically for monitoring forestry related problems.

The informal cooperation between Goddard and the Pennsylvania Forest Pest Management group has lead to the initiation of a three year Applications Pilot Test (APT) project. The objective of the APT is to develop and transfer remote sensing technology to the Pennsylvania agency so they can conduct annual surveys of defoliation damage using Landsat MSS data.

As a result of this work, Goddard has also been asked to participate in the AgRISTARS/Renewable Resources research activities by conducting research for the remote monitoring of natural or man-induced forest disturbances in addition to insect related damage.

FUTURE EMPHASIS

The quantitative analysis of the VI classification results will be completed and the best approaches will be evaluated further and refined for forestry applications. In conjunction with this effort, a quantitative, ground-based technique to evaluate forest leaf canopy biomass is being developed in order to calibrate the Landsat derived results.

Digital terrain data will be acquired and merged with the central Pennsylvania multitemporal data set to facilitate the development and evaluation of techniques to reduce the influence of topographic variability upon scene reflectance. Additional information concerning related research is presented in Section D of this chapter.

Future research efforts will also include the analysis of Landsat-D Thematic Mapper simulator data to determine the added utility of better spectral, spatial, and radiometric resolution for monitoring forest cover conditions.

PUBLICATIONS

Williams, D.L., M.L. Stauffer, and K.C., Leung, "A Forester's Look at the Application of Image Manipulation Techniques to Multitempor' Landsat Data," presented at the Fifth Annual Symposium on Machine Processing of Remotely Sensed Data, Purdue University, West Lafayette, Indiana, June 27-29, 1979.

Williams, D.L. and M.L. Stauffer, "What Can the Forestry Community Expect from Landsat-D Thematic Mapper Data?," presented at the Symposium on Remote Sensing of Natural Resources, University of Idaho, Moscow, Idaho, September 10-14, 1979.

Williams, D.L. and L.D. Miller, "Monitoring Forestry Canopy Alteration Around the World with Digital Analysis of Landsat Imagery," presented at the ISP/IUFRO International Symposium on Remote Sensing Observation and Inventory of Earth Resources and the Endangered Environment, Freiburg, West Germany, July, 1978, and published in color as a NASA information brochure in August, 1979.

TABLE 7A - 1 VEGETATIVE INDEX RATIOS

Ratio Vegetative Index (RVI)	MSS7/MSS5
Difference Vegetation Index (DVI)	2.4 X MSS7 - MSS5
Transformed Vegetative Index (TVI)	$\sqrt{\frac{MSS7 - MSS5}{MSS7 + MSS5} + 0.5}$
Green Vegetation Index (GVI)	-0.29 X MSS4 - 0.56 X MSS5 + 0.60 X MSS6 + 0.49 X MSS7
Perpendicular Vegetative Index (PVI)	$\sqrt{(SOIL5 - MSS5)^2 + (SOIL7 - MSS7)^2}$ Where SOIL5 = 0.85 X MSS5 + 0.35 X MSS7 SOIL7 = 0.35 X MSS5 + 0.15 X MSS7
Linear Vegetative Index (LVI)	-2.58 X MSS4 - 7.28 X MSS5 + 0.88 X MSS6 + 3.59 X MSS7

B. SURFACE MINE MONITORING

by

J. R. Irons

OBJECTIVE

The purpose of the surface mine monitoring project is the evaluation of new remote-sensing techniques and sensor packages for the monitoring of surface mines in the eastern United States. The project addresses the impact of the increased spatial resolution and additional spectral bands provided by potential new sensors on monitoring capabilities. The evaluation will result in recommendations to the Environmental Protection Agency (EPA) for operational monitoring procedures.

BACKGROUND

The EPA's Environmental Monitoring and Support Laboratory (EMSL) is conducting a comparative study of remote-sensing techniques for the monitoring of eastern, midwestern, and western surface mines. The current project at GSFC was funded by the EMSL as a part of this overall study. The EPA hopes to develop rapid, cost-effective, remote-sensing techniques to meet the monitoring requirements set forth in the Federal Surface Mining Control and Reclamation Act of 1977 (Public Law 95-87).

Remotely sensed data were acquired by a variety of sensors over three central Pennsylvania study areas during 1978 and 1979. The areas are located on the Appalachian Plateau and contain an excellent cross section of abandoned, reclaimed, and active mines. The study areas are representative of the regions affected by surface mining within the Appalachian bituminous coal fields. The data sources utilized in the study of the areas are: EPA's airborne 11-channel, Daedalus 1260 Multispectral Scanner; the airborne Thematic Mapper Simulator (TMS) multispectral scanner; the Landsat MSS; high-altitude color and color infrared aerial photography, and low-altitude color and color infrared aerial photography.

RECENT ACCOMPLISHMENTS

A spectral band selection study was recently completed. The study objective was to determine the most useful spectral bands for discriminating among the land-cover types commonly associated with surface mines. To meet this objective, stepwise linear discriminant analysis was applied to Daedalus Scanner data collected over the Clarion County, Pennsylvania study area on May 17, 1979.

The first step in the data analysis was the delineation of training areas representing land-cover types associated with surface mines.

The represented categories included: deciduous forest, coniferous forest, row crops, pasture, bare soil, graded mine spoil, ungraded mine spoil, revegetated mine spoil (forbes and legumes), revegetated mine spoil (trees), and exposed coal. Several training areas located across the study area were delineated for each land cover category. From the training areas a random sample of 50 picture elements were chosen to represent each category.

The multispectral data corresponding to the randomly sampled picture elements were input to a stepwise linear discriminant computer program. The program computed a sequence of linear classification functions, and the data channels used in deriving the functions were added to the analysis in a stepwise manner. At each step, the channel which could contribute the most to the discrimination of the land-cover types was added for the derivation of a classification function.

Due to data preprocessing problems, only the data channels corresponding to the following nine spectral bands were subjected to analysis: 0.45-0.50um, 0.50-0.55um, 0.55-0.60um, 0.60-0.65um, 0.65-0.69um, 0.70-0.79um, 0.80-0.89um, 0.92-1.10um, and 8-14um. On the basis of the stepwise linear discriminant analysis five spectral bands were chosen in the following order as the most useful of the available bands for discriminating among the land cover types: 0.60-0.65um, 0.92-1.10um, 0.80-0.89um, 8-14um, and 0.50-0.55um.

SIGNIFICANCE

The results of the spectral band selection study provide guidance for the design and utilization of future remote sensing systems. In particular, the selected bands can be compared to the bands sensed by the proposed Landsat-D Thematic Mapper (TM). Table 7B-1 list TM bands which approximate the Daedalus scanner bands selected by the study. The TM appears to have the required spectral sensitivity for the effective remote sensing of Eastern surface Mines.

FUTURE EMPHASIS

Future efforts will concentrate on a comparison of results obtained from the analysis of the data acquired by the different sensors under study. Area measurements for the land cover categories will be compared to ground reference data. The ground reference data consists of photointerpreted, field checked, and planimetered low altitude aerial photography. The accuracy of the area inventories derived from the various data types will allow EPA to choose the remote sensing systems and analysis techniques best suited to EPA's surface mine monitoring requirements.

Results obtained with TMS data will be of particular interest. The data will be resampled to a 30 meter-by-30 meter resolution to more closely simulate the expected data from the TM. The analysis results will indicate whether or not a proposed satellite system can provide information in sufficient detail and accuracy for operational mine monitoring.

Table 7B-1

Spectral Band Comparison

Selected Daedalus Scanner Spectral Bands (μm)	Analagous TM Spectral Bands (μm)
0.60-0.65	0.63-0.69; TM3
0.92-1.10	none
0.80-0.89	0.76-00.90; TM4
8 -14	10.4 -12.5; TM7
0.50-0.55	0.52-0.60; TM2

C. NASA-CENSUS APPLICATION PILOT TEST (APT) AND URBAN AREA DELINEATION STUDIES

by

D. Toll and S. Wharton

OBJECTIVES

The overall objective is to develop and evaluate remote sensing technology to delineate and periodically update urban areas in the United States and to transfer that technology. The primary objective is to develop procedures using Landsat MSS data for accurately detecting changes from non-urban to urban land cover. Other objectives include: (1) integration of Census statistics with Landsat derived results tailored to Census geographer requirements, (2) assessment of the cost effectiveness, accuracy, timeliness and increased capability of using Landsat technology operationally, and (3) training of Census Bureau personnel.

BACKGROUND

The Census Application Pilot Test (APT) is beginning the fourth year of a six year program to develop procedures using satellite data to replace or enhance the use of aerial photography and ground site visits for delineating approximately 300 Standard Metropolitan Statistical Areas (SMSA) prior to each census. During the first two years of the APT three different approaches were evaluated. First, routine Landsat image enhancements and classification maps were used to delineate five selected SMSA's (Seattle, Austin, Richmond, Boston, and Orlando). This approach proved to be as accurate (in terms of location of boundary) as conventional census procedures. In the second approach, multitemporal Landsat imagery were used to detect changes in urban expansion. As a result of evaluation by Census Bureau geographers, they recommended that this approach be the primary area of further development. The third approach involved the investigation of methods of incorporating Census statistics with Landsat results. Census concluded this approach improved upon the information display system available and should be pursued in conjunction with the change detection approach. In summary, Census geographers have requested a redirection in APT activities to investigate change detection procedures more thoroughly, while maintaining the option of data integration within an information system context.

RECENT ACCOMPLISHMENTS

At the beginning of 1979 we started an intensive effort to develop procedures for accurately detecting changes in land cover in the urban fringe zone. The first step was a review of the change detection literature. This was followed by a critical evalution of selected papers. A systematic plan was then developed to improve upon our capabilities to monitor urban expansion. This plan includes preprocessing steps to remove adverse effects from spatial misregistration, ground cover heterogeneity and sun angle differences. Processing steps were also evaluated for detecting changes with raw, transformed, and classified data sets. Landsat MSS data were used in all analyses.

Although much of the change detection work is ongoing, there have been a number of accomplishments during 1979. Precision scene to map registration within one pixel's accuracy was obtained for portions of 15 Landsat MSS scenes. Digital Image Rectification System (DIRS) software was used to register a master Landsat scene to USGS 7½' topographic maps, followed by scene to scene registration techniques for the remaining scenes. Several of these scenes were selected from coverage during a given year to study: (1) the optimum time of year for change detection and (2) the allowable deviation from anniversary date selection. The remaining scenes were selected from several years of Landsat coverage to monitor the dynamic spectral changes which occur from non-urban to urban land cover. Preliminary analysis of data for Denver, Colorado have shown late summer is the best time of year for detecting changes in the urban fringe zone. However, additional work is being done to further investigate the temporal aspects of land cover change.

Preprocessing functions have been implemented to remove adverse effects in multitemporal data resulting from atmospheric haze and solar elevation differences. This includes a dark object subtraction routine which references on clear water bodies, in addition to procedures for standardizing the mean and variance (i.e., histogram matching). Effects from varying terrain and different solar elevations are being evaluated with theoretical non-Lambertian and Lambertian models. Other preprocessing functions to remove the "salt and pepper" effect in the urban fringe are being evaluated. One particularly useful approach finds the vector with the least amount of variation and averages in that direction only, thus maintaining important urban boundaries.

Previous investigations of dimensionality reduction schemes have shown that principal component transformations improve the non-urban to urban separation while reducing the number of vectors in the data set. Two of the most promising dimensionality reduction techniques (projection pursuit and principal component analyses) are currently being further evaluated.

Several change detection approaches have been devised and implemented. These include: (1) techniques to combine one dates digital values with anothers prior to thresholding significant spectral changes from non-changes (e.g., image differencing and image ratioing); (2) classification of one date at a time, followed by the comparison of two or more classified dates to detect land cover change (e.g., classification differencing), (3) regression of one dates digital values against another by band, followed by the examination of residuals for spectral changes, and (4) obtaining signatures of multitemporal land cover change from two or more data sets (e.g., multitemporal classification).

There are several ramifications and combinations which can be derived from these change detection approaches. For example, with the image differencing approach, emphasis was placed on the development of techniques to threshold change from non-change with the use of univariate and multivariate t-tests which yield error rates. This procedure is followed by zeroing out the non-change pixels and performing a classification on the change pixels using the differenced and/or the raw data (usually always the last date). The major goal will be to design a change detection system compatible with Census Bureau requirements.

A plan was developed to obtain an accuracy assessment of the change detection approaches. This included the development of procedures for design data analysis, and data display. As a reference data set we used photointerpretation with field checks. Preliminary results have shown a success in detecting urban expansion (less than 25% omission and commission error rates).

A more complex procedure of detecting urban expansion is being evaluated in the context of a Geographic Information System (GIS). After a survey of available GIS software systems, a system from Environmental Systems Research Institute was purchased for use at GSFC (purchased jointly with ERRSAC) and merged with VICAR (image processing) software. This system will be used to evaluate a change information system at a test site near Denver, Colorado. Topographic, thematic, and remotely sensed data were gathered and digitized. The digitized information will be used in conjunction with Landsat data to indicate the areas of change.

In addition to Landsat MSS data, other types of remotely sensed data are in the process of being evaluated. This includes ongoing work on evaluating the shuttle payloads, particularly the Large Format Camera, for monitoring urban expansion. Additionally, Landsat Thematic Mapper simulator data were obtained for Denver, Colorado and Washington, D.C. for comparison with MSS capabilities.

Preliminary investigation of the utility of SEASAT Synthetic Aperature Radar (SAR) data for assessing urban area delineation capabilities was completed. Conclusions derived from this study were that SEASAT SAR imagery can be used to delineate urban areas and to determine the extent of change from non-urban to urban land cover. Furthermore, it was concluded that newly constructed single family residential areas were readily visible as were most older residential areas within the city. Remaining categories could not be precisely separated according to the USGS land use/land cover classification system. The separate categories of recreation and parks, cemetaries and undeveloped land could not be identified but were detectable as a combined group of "open space". Institutions and schools were mistaken for open space due to the low return of their grounds. Commericial and Services activities were identifiable in certain instances. Small shopping centers and commercial blocks in residential areas were not identifiable, but the contact between the core central business district and the fringe transition zone and adjacent inner city residential land cover was visible.

The SAR data were next density sliced in an attempt to define spectral signatures or signature ranges for urban land cover categories. Six system/land cover classes were found by creating the most homogenous, specific, and meaningful land cover classes possible. These classes did not correspond to any of the traditional land cover classes, but they did make the extent of urban built up land more apparent. It is believed that reducing the amount of image noise by smoothing or averaging the data before density slicing will increase the amount and type of information obtainable from the SAR imagery.

SIGNIFICANCE

We are investigating procedures which show vast potential for upgrading the Census Bureau techniques for delineating urban areas. Not only is significant progress being made in providing an operational system for the Census Bureau, but we are also advancing the state of the art in change detection methodology.

FUTURE EMPHASIS

Work will continue through FY81 on evaluating change detection procedures on a regional basis. At the end of this time there will be a go/no-go decision point for the implementation of a full scale technology transfer phase. Background and results of the project are being compiled to be included in the 2nd Edition (1981) of the Manual of Remote Sensing.

REFERENCES AND PUBLICATIONS

Davis, J.B. and S.Z. Friedman, 1979. Assessing Urbanized Area Maps Through the Integration of Landsat and Conventional Data, American Society of Photogrammetry, Washington, D.C. p 776-791.

Henderson, F.M., Wharton, S.W., and D.L. Toll, 1980. Preliminary Results of Mapping Urban Land Cover with SEASAT SAR Imagery, submitted to proceedings of the American Society of Photogrammetry, 46th Annual Meeting, St. Louis, Missouri.

Knapp, E.M., Justice, C.O. and K. Ingram, 1979. The Integration of Landsat and Ancillary Data for Urban Area Residential Development Suitability Analysis, paper given to Urban and Regional Information Systems Association, Proceedings, San Diego, California.

McKinney, 1979. Cartographic Considerations for the Intergration of Landsat Digital Imagery with Existing Spatial Data, Fourth International Symposium on Computer Assisted Cartography, Reston, VA, November, 1979.

D43

N80-20766

D. IMPROVEMENT IN CLASSIFICATION ACCURACY OF LANDSAT MSS DATA IN AREAS OF MOUNTAINOUS TERRAIN

by

C. Justice, B. Holben, S. Wharton

OBJECTIVES

The objectives are:

(1) To eliminate the topographic effect on multispectral data.
(2) To improve discrimination of cover types by integrating "a priori" terrain data.

BACKGROUND

In an effort to realize the potential of remotely sensed data for Earth Resources applications, research is being undertaken to increase our understanding of the spectral properties of natural surfaces and to examine the applications of such data to many parts of the world. Large areas of the Earth's surface are composed of rugged and mountainous terrain, areas which are often inaccessible and rich in natural resources. Existing environmental data bases for such areas are often poor. For effective regional planning and resource management, there is a need for accurate and up-to-date inventories of land cover and careful monitoring of resource exploitation. Remotely sensed satellite data have considerable potential for providing environmental information for such areas. However, recent studies have revealed problems particular to the interpretation of multispectral data in areas of rugged and mountainous terrain. Two distinct approaches to improving classification accuracy are currently being examined in the Earth Resources Branch. The first approach is to use "a priori" terrain information to provide improved discrimination of surface cover types. The second approach is to develop and test algorithms to eliminate the topographic effect on multispectral sensor response.

RECENT ACCOMPLISHMENTS

The first approach is to use the digital terrain data to improve classification accuracy. This is achieved by an "a priori" understanding of the relationship between the cover type distribution and selected terrain variables e.g. elevation, slope angle, aspect, distance from watershed. To date this approach has involved integration of the Landsat and digital terrain data, accuracy assessment of the terrain data and selection of preliminary training sites for the classification procedure.

The second approach to date, has involved examination of two models to simulate the topographic effect. The authors collected hand-held radiometric data of a uniform sand surface oriented at a complete range of slope angles and aspects for several solar elevations.

These measured radiances were used to test the following models.

Lambertian Model:

$L = L_n * \cos i$

Non-Lambertian Model:

$L = Ln\ (\cos^{k} i * \cos^{k-1} e)$

Where: L = Radiance
Ln = Radiance when i = e=0
i = Incidence Angle
e = Exitance Angle
K = Minnaert Constant

The "K" value is derived by linearizing the equation.

$$\log (L * \cos e) = \log Ln + K * \log (\cos i * \cos e)$$

If log (L* cos e) is plotted against log (cos i * cos e) then "K" is the slope of the regression line.

The non-Lambertian model produced the overall highest statistical correlations with the field spectra, although consideration of exitance angle, implicit in the model, was shown to be less important for aspects away from solar azimuth, e.g., 90 . In these cases, the Lambertian model also yielded high correlations with the field spectra. The results of the analysis demonstrated that the Lambertian model was less suitable for simulating the spectral response at high solar elevations.

When the two models were applied to normalize the field measured data, the non-Lambertian model was found to be consistently superior to the Lambertian model at reducing the "topographic effect", confirming the results of the correlation analysis. The remaining variation in the normalized radiance values were thought to be largely due to a diffuse light component which was not addressed by the present model.

Detailed examination of the empirical constant "K" revealed that "K" was not a constant value for cover types varying only as a function of phase angle and wavelength but varied considerably with surface geometry, i.e., slope and aspect. The non-Lambertian model as used by Smith et al (1979) was improved by deriving the empirical value "K" for each aspect. The "K" values generally decreased with azpect, away from solar azimuth. The non-Lambertian model was more sensitive to variations in the "K" value at those aspects near to solar azimuth.

SIGNIFICANCE

The intention of the study was to examine the radiance simulation models for possible application to eliminating the topographic effect on Landsat data. As both the models reduce the radiance values to represent radiances from a flat surface with the sun directly overhead, they also have a potential application for reducing sun angle differences between multitemporal data sets. For application to Land-

sat data, both models require information concerning surface geometry. Such data is available for the United States in the form of digital terrain data provided by the USGS. Registration of the digital terrain data to the Landsat data and calculation of slope and aspect have been demonstrated. Digital elevation data with an improved resolution of 30m ground spacing are being made available in the form of Digital Elevation Model (DEM) Tapes by the Digital Application Group at USGS Reston.

The Lambertian model requires only slope and aspect data for any given Landsat pixel but as shown in this study is only effective for a restricted range of slopes and aspects. The non-Lambertian model is effective over a wider range of slopes and aspects but requires radiance information for specific cover types to calculate the empirical "K" value. Calculating "K" values for each cover type and each aspect is not a practical procedure and the authors suggest the following alternative possibilities, which will be the subject of a future study. Sytinskaya (1943) showed that "K" values for vegetated surfaces were substantially lower than for non-vegetated surfaces. It may be that a two or three level stratification of the Landsat data, based on a ratioed radiance transformation could be used to derive "K" values which would provide an improvement over the Lambertian model. Also, it may be possible to use the non-Lambertian model only for those aspects where the Lambertian model is ineffective and where the non-Lambertian model is sensitive to "K".

FUTURE EMPHASIS

As a result of this study the authors believe there to be three main areas that require further research: first, the contribution of diffuse light to the "topographic effect" from both skylight and terrain scattering; second, examination of the application of the models to normalizing multi-temporal data, specifically to examine the cause of the differences between the normalized radiance values at different solar elevations; third, the application of the models to Landsat data, using surface geometry derived from digital terrain data. Two publications are currently in press regarding examination of the difuse contribution to the topographic effect and the effectiveness of ratioing adjacent channels to remove the topographic induced variations.

REFERENCES

Holben, B.N. and C.O. Justice, 1979. Evaluation and modeling of the topographic effect on the spectral response from nadir pointing sensors. NASA/GSFC T.M. 80305, 19 pp.
(Submitted to Photogrammetric Engineering and Remote Sensing)

Justice, C.O., 1978. An examination of the relationship between selected ground properties and Landsat MSS data in an area of complex terrain in southern Italy. Proc. American Society of Photogrammetry, Fall Meeting, Albuquerque, New Mexico, pp. 303-328.

Smith, J.A., Tseu Lie Lin and K.J. Ranson, 1979. The Lambertian assumption and Landsat data. Paper accepted for publishing by Photogrammetric Engineering and Remote Sensing.

Sytinskaya, N.N., 1949. Determination of the degree of smoothness of planets by photometric methods. Uchenye Zapiski, L.G.U. No. 116. (59-311-41: Translated 1959) - NASA NG3-81360, 18 pp.

E. SOURCES OF VARIATIONS IN LANDSAT AUTOCORRELATION*

by

M. L. Labovitz

OBJECTIVES

The assumption of stochastic independence of observations underlies most statistical procedures used in analyzing remotely sensed data (i.e., classification, discrimination, trend determinations, etc.). Analyses using data which neglects this property can lead to fallacious results, for example overly optimistic estimates of classification accuracies. The objectives of this research is stated in the form of the following questions.

1. Does Landsat data depart from the independence assumption?

2. Can one general model representing these departures be developed?

3. Are these departures affected by ancillary properties of the data (e.g., cloud cover, satellite, location)?

BACKGROUND

That adjacent pixels of Landsat data are highly autocorrelated (non-independent) has been demonstrated recently by several researchers. It is now commonly assumed that pixel sequences follow a Markovian model. However, Craig (1979) recently demonstrated that the Markovian assumption is an incomplete model and that such sequences are, in fact, best described (in the notation of Box and Jenkins, 1970) as an ARIMA (1,0,1) process (Auto-Regressive Integrated Moving Average). Because this represents a considerable departure from the simple Markovian assumption and because it has strong implications for data analysis, data interpretation, and data compression it is important that it be evaluated critically. In addition, exploiting this knowledge to improve classifiers requires that precise estimates of the parameters of the model be available. Finally, it is critical that the various factors which might change the parameters of the model be examined for their actual effect. Thus the objectives given above may be restated more specifically as (1) to determine whether the ARIMA (1,0,1) model is consisntly superior to others; (2) to estimate the effects of various possible sources of variation on the values of the parameters ϕ_1 and θ_1 of this model.

*Research conducted in cooperation with R.G. Craig, Department of Geology, Kent State University.

RECENT ACCOMPLISHMENTS

This year an experiment was conducted which considered five factors which could conceivably be suspected of influencing the degree of autocorrelation of Landsat data. These factors are:

1. Satellite - e.g., data from Landsat 1 might not follow the same model as data from Landsat 3.

2. Scanner - there are six detectors per channel on each satellite and their individual electromechanical properties might differentially effect the model.

3. Channel - in particular the unequal sensitivity of silicon photodiodes (MSS channel 7) as opposed to photomultiplier tubes (MSS channels 4, 5 and 6).

4. Cloud Cover - Craig (1976) detected some evidence that this especially effects the MA (1) parameter.

5. Location - many factors are confounded under this term For example, land cover, land use and physiographic characteristics.

The particular levels of each factor which were analyzed are as follows:

1. Satellite - Landsat 1 and Landsat 2.
2. Scanner - numbers 3 and 6 (chosen randomly).
3. Channel - MSS 4 and MSS 7 (least correlated).
4. Cloud Cover - 0% and 10% (most commonly used).
5. Location - Richmond, VA and Denver, CO (representing diverse physiographic regions).

SIGNIFICANCE

The ARIMA (1,0,1) model is substantiated as the most appropriate model for Landsat data. This model is given by

$$X(t) = \phi_1 X(t-1) + a(t) + \theta_1 a(t-1),$$

where: θ_1 and ϕ_1 are parameters;

$X(t)$ is the gray scale value of location t;

$a(t)$ is a noise term associated with location t.

These two parameters, θ_1 and ϕ_1, completely characterize the form and amount of redundancy in the Landsat data. Of the 5 factors already mentioned, only location had a significant affect on the value of ϕ_1 (Table 7E-1, factor 1), while θ_1 was largely affected by changes in cloud cover (Table 7E-1, factors 2, 3). This finding (1) eliminates certain of the factors from future studies; (2) gives us direction as to where and how to look for the efficient measurement and removal of redundancy in Landsat data. Removal of the redundancy would yield a data set which meets the assumptions made in may multivariate statistical procedures used here at Goddard.

FUTURE EMPHASIS

Future work should be guided by the knowledge that the ARIMA (1,0,1) model is indeed appropriate. Evidently no electromechanical properties of the satellite contribute to the autocorrelation problem. Research should be directed towards ascertaining the variables which contribute to the location effect. We are specifically attracted to the possibility that terrain characteristics may induce much of the structure observed. Research in this area would allow us to characterize land cover classes based upon the value of ϕ_1 and θ_1. Secondly by filtering the data with the appropriate model, we can perform classifications upon an independent set of observations. Further, since there is redundancy in adjacent pixels, compression schemes utilizing the ARIMA (1,0,1) model should be developed based on knowledge of the relationship between location and the amount of redundancy.

REFERENCES AND PUBLICATION

Craig, R.G., 1979. Autocorrelation in Landsat data, in Proceedings 13th International Symposium on Remote Sensing of Earth Resources, Ann Arbor, Michigan.

Craig, R.G., and M.L. Labovitz, 1980. Sources of Variation in Landsat Autocorrelation, in 14th International Symposium on Remote Sensing of Earth Resources, San Jose, Costa Rica.

Table 7E-1. Significant sources of variation (SOV) in analysis of variance

Factor 1

SOV	F Ratio, f*	P(F >f*)
Location	22.295	4.453×10^{-5}

Factor 2

SOV	F Ratio, f*	P(F >f*)
clouds	56.364	1.24×10^{-8}
location-channel	15.856	3.54×10^{-4}
satellite-channel	12.757	0.001
location-cloud-scanner	7.556	0.0097
location-cloud-satellite	8.156	0.007

Factor 3

SOV	F Ratio, f*	P(F >f*)
cloud-channel	6.001	0.0198

CHAPTER 8

AGRICULTURE

edited by

D. W. Deering

OVERVIEW

The agricultural remote sensing program is directed toward providing a rational basis for the definition of future remote sensor systems with emphasis on defining satellite sensor requirements for agriculture information needs. Additionally, the agriculture research is concerned with developing techniques to enable the most effective use of current (e.g. Landsat MSS) and approved (e.g. Landsat-D Thematic Mapper) satellite data. The approach being used to attain these objectives is to develop a fundamental quantitative understanding of the relationships between spectral responses and vegetation scene factors and how they are ultimately related to important agronomic production parameters, including crop biomass and plant stress, and final crop yield.

The current research emphasis is on developing a quantitative understanding of nine basic physical and remote sensing attributes, which are known to be or which are potentially important for the detection, measurement and monitoring of agricultural crops. The identification of useful spectral bands for the assessment of crop status (including canopy cover, herbaceous biomass and plant stresses) and for crop type discrimination continue to be significant activities. These studies involve the use of narrow band, multi-channel spectrometers and radiometers for determining optimal band locations and bandwidths, as well as fixed-band portable radiometers used in more extensive studies for quantifying the sensitivities of selected spectral regions to the measured agronomic variables. Radiometric sensitivity limits that will allow the detection of significant variations in scene parameters are also being studied.

Sun elevation (time of day effects) and off-nadir viewing effects on the capabilities for remote crop assessment are receiving increased emphasis. The preliminary studies have shown that changing sun/target/view angle effects can be substantial. Because future satellite systems may enable data acquisition at various times of the day and at off-nadir viewing angles, it is desirable to investigate potential enhanced capabilities, and it is imperative to understand the undesirable effects and develop techniques to correct for them. Consequently, the anisotrophic irradiance (sky) and radiance (scene) effects are being studied to develop proper mathematical models to describe these effects. Spatial resolution requirements will be confounded with off-nadir viewing and will receive increased emphasis in relation to both off-nadir pointing sensors as well as nadir-pointing, higher resolution sensors (e.g. Landsat MSS vs TM).

The polarization of radiant energy by the vegetation canopy is affected by both leaf orientation and leaf water status and thus may become a potent tool for assessment of stress and for plant type discrimination--this is now under investigation. New techniques for remotely sensing crop canopy temperature, which is useful for inferring soil moisture conditions and crop yield, are being developed through studies of the thermal relationships in plant canopies. For both thermal and visible/near infrared data the required frequency of data acquisition for adequate measurement or monitoring of various important crop parameters must be determined in order to optimally or even adequately define satellite sensor and system requirements. Field measurements are being taken with high temporal resolution, which will help define these requirements.

The agriculture remote sensing studies include experiments conducted under controlled laboratory and greenhouse conditions, in specially designed small field plots and in large "commercial" fields. The field studies reported herein relied on cooperation and technical support from the Beltsville Agricultural Research Center/USDA/SEA in Maryland and the Water Conservation Laboratory/USDA/SEA in Phoenix, Arizona.

A. REMOTE SENSING OF LEAF WATER CONTENT IN THE NEAR INFRARED

by

Compton J. Tucker

OBJECTIVES

The purpose of the study was to simulate the spectral effects associated with leaf dehydration by use of a leaf radiation model, in order to identify the potentially most useful spectral bands for water stress remote sensing.

BACKGROUND

The limitation of soil water availability to plants is a common environmental occurrence. This limitation of soil water availability to plants is referred to as water stress and/or drought stress. Water or drought stress, as used herein, refers to the combination of abiotic conditions which in turn produce serious internal plant water deficits which limit photosynthesis and restrict plant growth. Although relatively little can be done once drought injury occurs, different agricultural management practices offer the possibility of reducing drought related injury. Present techniques for accurate ground-based evaluation of the severity of drought stress (i.e., soil moisture, etc.) are time consuming and restricted in spatial extent which limit their agricultural applicability.

RECENT ACCOMPLISHMENTS/RESULTS

A stochastic leaf radiation model was used to predict leaf spectral reflectance as a function of leaf water content for a dicot leaf (Figure 8A-1; Table 8A-1). Simulated spectral reflectances, corresponding to different leaf water contents or equivalent water thicknesses, were analyzed to quantify reflectance differences between different equivalent water thicknesses (Figure 8A-2). Simulation results coupled with consideration of atmospheric transmission properties and the incident solar spectral irradiance at the earth's surface resulted in the conclusion that the 1.55-1.75μm region was the best suited wavelength interval for satellite-platform remote sensing of plant canopy water status in the 0.7-2.5μm region of the spectrum (Figure 8A-3)

CONCLUSIONS/SIGNIFICANCE

1. Simulated spectral reflectances using different leaf water contents resulted in different reflectance changes in the 0.7-2.5μm region of the spectrum.

2. Consideration of the solar spectral irradiance and atmospheric transmission characteristics resulted in the conclusion that the 1.55-1.75μm spectral interval was the best suited band in the 0.7-2.5μm region for monitoring plant canopy water status from space platforms.

3. The 1.48-1.75um spectral interval was the best suited band for ground-based monitoring of plant canopy water status. The 1.50-1.63μm region showed the greatest spectral radiance changes with simulated leaf dehydration.

FUTURE EMPHASIS

This simulation study is complete and has been accepted for publication. These findings can be tested when Landsat-D's thematic mapper goes into operation in 1982.

PUBLICATIONS

Tucker, C.J. 1980. Remote Sensing of leaf water content in the near infrared Remote Sensing of Environment (in press).

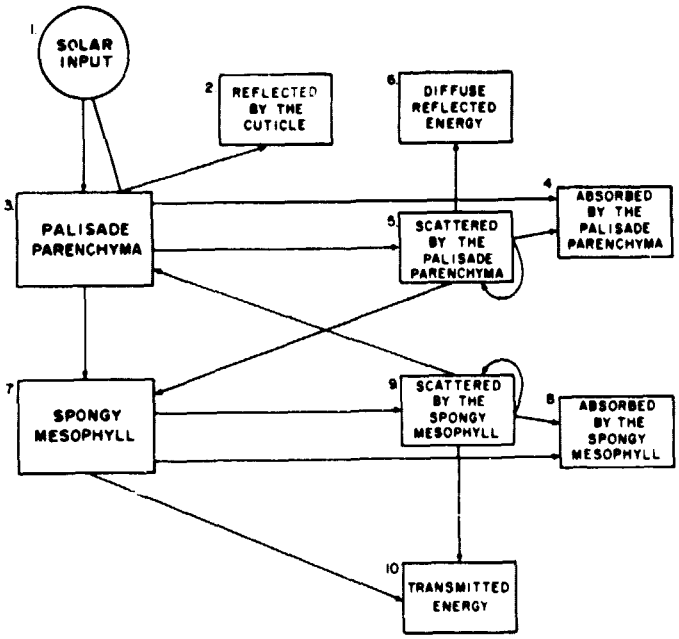

Figure 8A-1. Compartment model of a dicot leaf optical system. The arrows between compartments represent the flow(s) and their direction. The processes or leaf cellular aggregates are indicated within each compartment. The model treats a dicot leaf as a leaf optical system which was represented as a Markov process with a unique transition matrix of probabilities at each 0.01 μm interval between 0.40-2.50 μm. Probabilities were calculated at every wavelength interval based upon leaf thickness, structure, pigment composition, and water content. The model, driven by absorption and scattering mechanisms, gives accurate estimations of measured values for dicot leaf spectral absoption, spectral reflection, and spectral transmission at 0.01 μm intervals between 0.40 and 2.50 μm.

Table 8A-1. Leaf simulation output for an equivalent water thickness of 0.018 cm and the extinction coefficients of liquid water at selected wavelengths.

Wavelength (μm)	Extinction of H_2O	Absorptance (%)	Reflectance (%)	Transmissance (%)
0.70	0.00	28.22	38.81	32.85
0.77	0.03	0.17	51.87	47.36
0.90	0.06	0.39	51.77	47.25
0.97	0.46	3.01	50.58	45.89
1.22	1.00	6.34	49.06	44.16
1.47	26.0	65.99	19.88	14.13
1.60	5.56	35.37	35.37	29.21
1.97	110.0	89.18	6.90	3.92
2.15	20.8	60.41	22.81	16.78
2.50	73.2	85.30	9.18	5.51

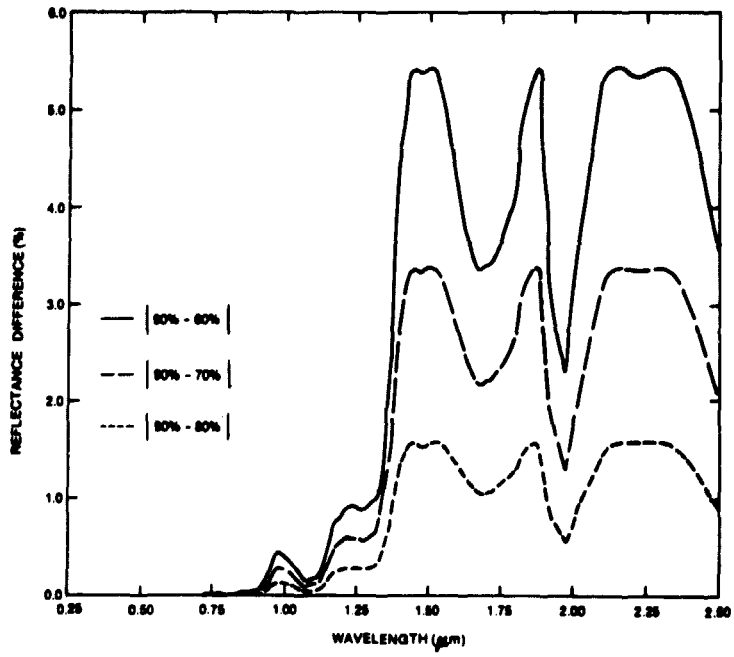

Figure 8A-2. Simulated spectral reflectance differences between equivalent water thicknesses of 0.018, 0.016, 0.014, and 0.012 cm. The greater the reflectance difference, the more apparent spectrally the change in equivalent water thickness.

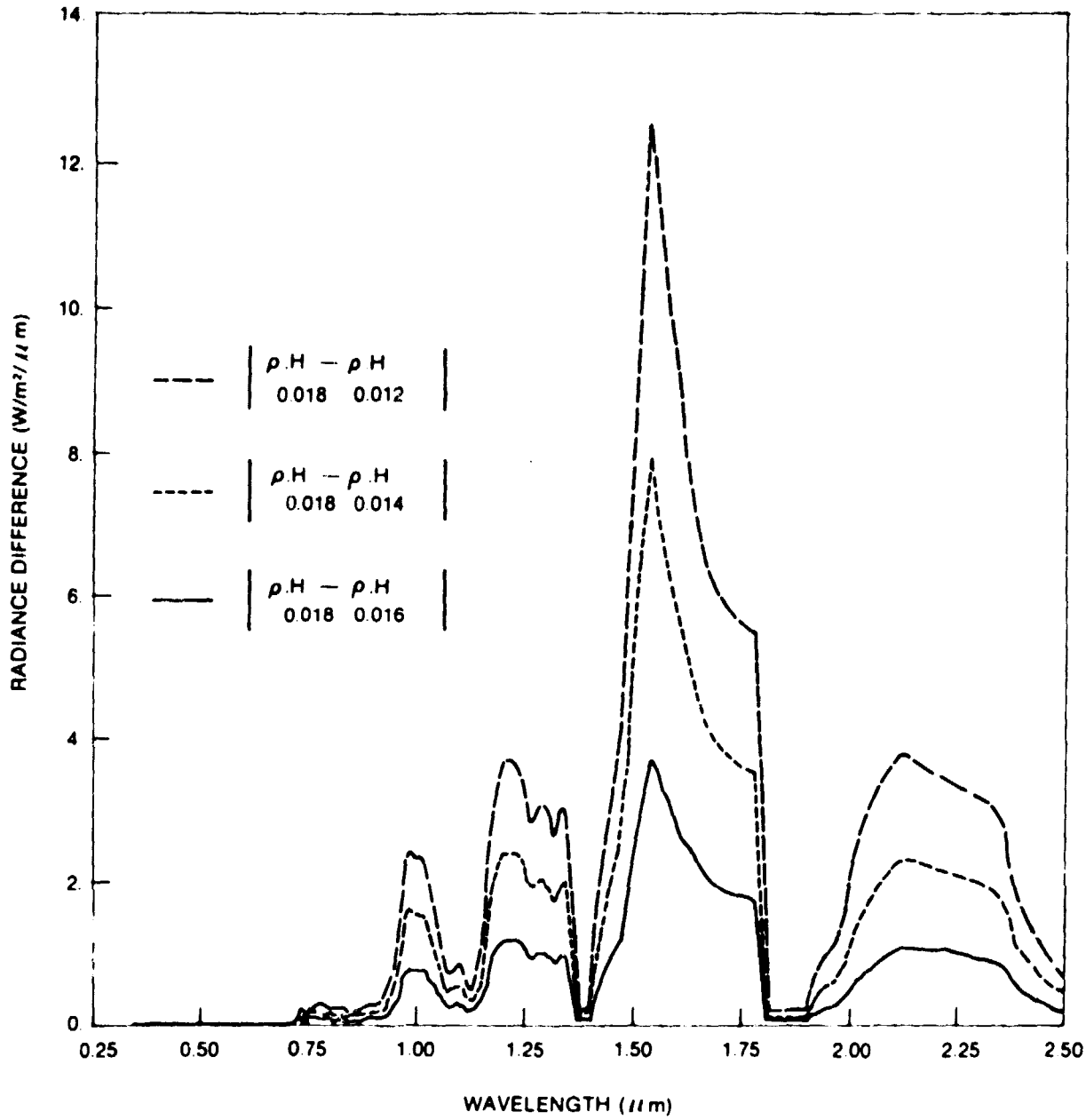

Figure 8A-3. Spectral Radiance differences between equivalent water thicknesses of 0.018, 0.016, 0.0104, and 0.012 cm. The spectral radiance difference resulted from multiplying the simulated spectral reflectance differences (Figure 1) by solar spectral irradiance function. The greater the radiance difference the more detectable the change in equivalent water thickness. Note the superiority of the 1.50-1.75 μm region when the spectral reflectance-spectral irradiance product is considered.

B. PLANT STRESS AND RELATIONSHIPS TO SPECTRAL RESPONSES

by

J. B. Schutt

OBJECTIVES

The goals of our cooperative efforts with the Plant Stress Laboratory, of the Beltsville Agricultural Research Center/SEA are to establish the spectral responses of leaves and plant canopies to environmental factors which give rise to stress, and determine the most suitable wavelengths for decoupling these responses for remote sensing applications.

BACKGROUND

The relative positions of spectral reflectance curves taken from plants or plant canopies is a measure of the responses of individual leaves to water availability; atmospheric pollutants; senescence, both induced and natural; growth stage; and soil type. Only the spectral confounding of age and water status has been recognized in the literature, where results from the correlation of spectral response with water status has relied upon dry and turgid leaf weights - on E-M dash quantities unavailable in remote sensing. To better understand canopy spectra and elucidate how spectra can be decoupled on a leaf by leaf basis, laboratory spectra are being collected on plants grown regulated in growth chambers, greenhouses, and in the field.

RECENT ACCOMPLISHMENTS

Cotton Leaf Age and Water Stress

Near-IR reflectances (0.8-2.5) were measured for the first and fourth leaves on cotton plants grown in chambers. Data for the first leaves, L1, (24-26 days old) and fourth leaves, L4, (15 days old) which were evaluated individually and in combination, showed 1.45 to be the most significant wavelength for estimating water content. The r^2 values were 0.4, 0.88 and 0.85 for L1 and L4, individually and in combination, respectively. By taking the ratio of 1.65 to 1 , the results given in the same order were 0.93, 0.81, and 0.63, respectively. These results indicate that relating water status to spectral response is dependent upon leaf age.

Preliminary results obtained by comparing the near-IR reflectance curves of cotton plants grown in a chamber, greenhouse and in the field show that field cotton has the lowest reflectance over the regions from 0.8 to 1.3u and 1.92 to 2.5u, with greenhouse and growth chamber spectra with higher reflectances in respective order. The reflectance levels from 1.42-1.92u (1.55-1.75u) were found to be independent of lighting conditions.

Tomato Plant Stress from O_3 and SO_2

Spectral response curves were recorded in the near ultraviolet region (uv) (0.25 to 0.36u) and near IR region (0.8 to 2.5u), for tomato leaves which were subjected to O_3, SO_2 and their combination. Although

insufficient data were collected to attempt a separation by treatment, it was determined that incipient effects were detectable in the near-IR, but greater consistency in detectability was found in the near-UV because of the lower sensitivity to leaf structure and plant moisture variations. Results showed that visible damage appeared first at the upper surface of a leaf, while incipient damage was first detected at the under surface. By ratioing the reflectance values of the lower surface to the upper surface for UV data, an early damage index could be calculated.

Polarization Response and Plant Stress

Monodirectional and integrated reflectance measurements provide only a single spectral data source. By taking polarization data, data acquisition (scene information) from a single scene may be quadrupled. Stokes vector components are obtained, as well as the degree of polarization. We began such an endeavor through the acquisition of field data, but the variability introduced by the inability to make simultaneous measurements required that laboratory measurements be undertaken. The representative, but preliminary, results (Figure 8B-1) show that differences are observable in the polarization responses resh (80% moisture) and dehydrated (35% moisture) cotton leaves for essentially depolarized incident light at six wavelengths.

SIGNIFICANCE

These investigations have shown that the interpretation of spectral curves, apart from compositional variations requires a consideration of leaf age, water status, and illumination history. In addition, in the case of tomato leaves, the effects of O_3 and SO_2 are observable most reliably in the UV region. Finally, polarization spectra show promise for the assessment of water status.

FUTURE EMPHASIS

Continued laboratory investigations are required to assess the feasibility of separating effects resulting from the degenerate behavior of reflectance spectra toward environmental conditions Polarization data require further laboratory experimentation and verification. These data will be collected in the field to check their dependence upon atmospheric variability. In addition, prospects for processing polarization data independently of a reference plate will be pursued.

PUBLICATION

Schutt, J.B., Rowland, R.A. Fleming, A.L., "The Use of Near Infrared Reflectances for the estimation of Leaf Water Content in Cotton Leaves". (Accepted for publication in the Agronomy Journal.)

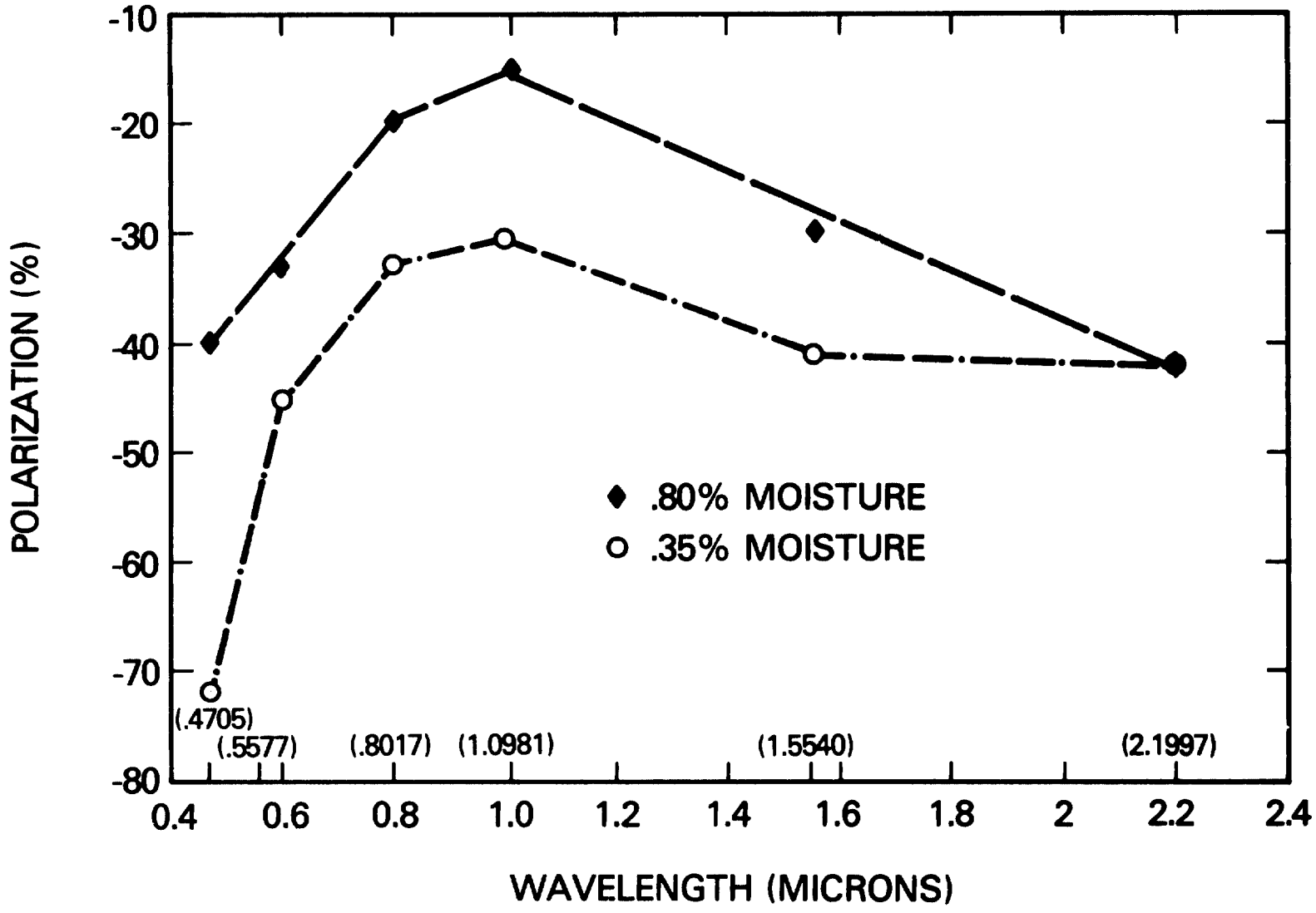

Figure 8B-1. Polarization response at six wavelengths for two cotton leaf moisture contents.

C. MONITORING DROUGHT IN COLORADO WITH LANDSAT MSS

by

C. J. Tucker and D. W. Deering

OBJECTIVES

The primary project objectives were:

I. To develop an operational capability for monitoring drought impact using Landsat data.

II. To develop system specifications and procedures for using Landsat products, for use by state agencies.

III. To compare Landsat data taken state-wide in 1973 (a wet year), 1976 and 1977 (dry years), and 1978 (a normal year).

IV. To evaluate project results by analyzing drought impact (recovery) in Colorado for 1978.

BACKGROUND

The Federation of Rocky Mountain States (FRMS) submitted a proposal to the Economic Development Administration of the Department of Commerce to develop quantitative methods for calculating a drought index. The technique was to use Landsat images as the primary data input. The FRMS soon became defunct and the original proposal was dropped.

During 1977, Colorado State University (CSU), with the cooperation of the Colorado Department of Agriculture, NASA Headquarters, and the NASA/Goddard Space Flight Center (GSFC), made a preliminary evaluation of the use of Landsat to monitor drought impact. The results were sufficiently promising to attract the attention of the Governor of Colorado and the Colorado Drought Council. With their support and the support of the CDA, Dr. Gene Maxwell of CSU prepared a new proposal for NASA and the project was funded. The study addressed certain technical questions which had to be answered before any federal, regional or state agency could commit programs and budgets to routinely use Landsat for monitoring drought impact.

It was determined at the outset that one of the best indications of drought in Colorado and much of the western United States is the "condition" of natural rangelands. A shortage of precipitation might be seen first in the form of reduced primary production in the grasslands and shrublands. Hence, a major effort was directed at the use of spectral vegetation indicies for monitoring standing crop biomass in these regions.

Total water demand in the western states is closely related to the demand of irrigated agriculture. Under a prolonged severe deficit, affecting urban and industrial users, the allocation of water resources will require an accurate measure of the agricultural water demand. Therefore, the mapping of irrigated agriculture, by crop type, was given a high priority.

A third project emphasis was placed on operational factors which would affect a commitment to use Landsat data on a routine basis for collecting drought or other related information. These factors include

(a) probability of cloud cover (image availability)
(b) identification of optimum image dates and the need for multiple date analysis
(c) use of the least expensive data product capable of providing the required information
(d) operating with a minimum of ground control or ground truth data

RECENT ACCOMPLISHMENTS

Optical and digital analyses of Landsat MSS data clearly showed the transition from predrought to drought to recovery conditions for the years of 1973, 1976, and 1978. Quantitative analyses of rangeland and hay production in selected localities have produced results similar to those shown in Table 8C-1.

Table 8C-1. Changes in green biomass (wet weights) from 1973 to 1976 to 1978 showing the transition from predrought to drought to recovery.

Weston Quad (South-Central Colorado) Shrubland

Area--------- 4,112 Hectares

Year	Biomass (kg)	% Change
1973	35×10^6	-
1976	20×10^6	-43%
1978	58×10^6	+66%

Earl Quad (South-Central Colorado) Grassland and Hay

Area--------- 20,817 Hectares

Year	Biomass (kg)	% Change
1973	228×10^6	-
1976	64×10^6	-72%
1978	122×10^6	-25%

Mapping of crop types in 1978 for selected quads in 5 counties produced acreage accuracies which were between 80 and 90% for most crops, when an optimum image date was available. These results are without post processing, for areas of 100% cultivated land.

The results of specific technical studies within the scope of the project are summarized as follows:

1. The primary production of standing crop biomass can be measured under conditions found in Colorado, using a single vegetation index formed from Landsat Bands 5 and 7. Of six indicies analyzed,

7/5 and (7-5)/(7+5) performed the best.

Although increased accuracy can undoubtedly be achieved by adjusting index values for different vegetation types, acceptable results for monitoring of drought impact can be obtained by using a single set of universal values to relate indices to biomass levels. This has been demonstrated for several rangeland, hay and even crop communities in Colorado and one semiarid location in Australia.

2. The dominant irrigated agricultural crops in Colorado (corn, sugar beets, alfalfa, beans, potatoes and barley) can be mapped with sufficient accuracy to estimate irrigated crop water demand.

The procedure used are quasi-unsupervised and utilize prior knowledge of relative positions occupied by these crops in spectral space. Ground truth can be limited to the identification of crop type for a few selected fields, by a county extension agent, on demand, as needed.

Boundary problems and false identification in non-cultivated areas will limit the accuracy of raw classification results, even under the best of circumstances. Post processing using readily available ASCS field statistics can greatly improve the accuracy. If ASCS photography is too outdated, RBV images can be used in their place, with reduced improvement.

Selection of image dates is critical and two or more dates may be needed under certain circumstances.

3. Actual water use of all crops can be monitored to the extent that water use is related to crop type and above ground biomass production. Rough estimates of water use appear feasible even without crop identification.

4. Cloud cover maps (frequency of cloud free days) have been generated for Colorado for the months of May through September. These maps, along with crop growth calendars, can be used to estimate the probability of obtaining images on required dates from one or two satellites.

5. Standard FCC products obtained from NASA/GSFC, EROS Data Center and the USDA (Salt Lake City) prior to and during the project lacked adequate quality control for reliable drought monitoring use. Good FCC's can be generated with minimal laboratory equipment if competent and motivated personnel are available.

6. Special optical products (contrast stretched and/or transformed) can significantly improve the quantity of information extracted by photointerpretation. However, these products should be specially generated for each application. Furthermore, the total cost may approach that of digital processing, and the results do not.

SIGNIFICANCE

An operational capability to monitor drought impact using Landsat data has been developed. This capability has been demonstrated for the semiarid climate of Colorado and could probably be extended to

other climates. Key components of the monitoring system include:

A. Annual statewide monitoring using FCC prints prepared from 70mm or 23cm Black and White transparencies.

B. Quantitative assessment of forage production on rangeland and certain hay fields using level slicing or graymapping of a single vegetation index formed from MSS bands 5 and 7. No ground truth calibration is required if current MSS calibrations are maintained.

C. Water use and water demand estimates from the mapping of irrigated crop types using a maximum likelihood algorithm. Signature development employs a quasi-unsupervised series of data analyses. Post processing of classification results using known field boundaries is used to improve the accuracy of acreage estimates.

This operational capability is supported by cloud cover statistics which show a high probability of obtaining the required imagery. Successful operation of the system will require careful selection of image dates according to crop and natural vegetation growth patterns. Two image dates may be required in some locations and will produce improved results at all locations. Step by step procedures have been developed for operating such a system.

FUTURE EMPHASIS

The technical aspects of this study using Landsat MSS data have been completed. CSU has made recommendations for follow-on studies which include the evaluation of various methods for distributing vegetation index data in a digital format to interested users. Three journal articles are currently in preparation describing the significant results of the project.

D. EFFECTS OF WHEAT IRRIGATION FREQUENCY ON REFLECTANCE IN SELECTED SPECTRAL BANDS

by

E. W. Chappelle, F.W. Wood and W. W. Newcomb

OBJECTIVES

The objective of these studies was to assess the capabilities of selected spectral bands for the determination of vegetational water status. In addition, it was felt necessary to determine what agronomic parameter best reflected changes in crop water status.

BACKGROUND

The remote sensing of crop water status is important from both the standpoints of the physiological state was well as providing the necessary information for irrigation scheduling in arid regions. Studies of crop water relationships have been the subject of investigations of a number of experimenters. They have, however, been making use of only a limited number of spectral bands. The effects of water content in vegetation permeates so many aspects of the plants physiology that the investigation of the potential utility of a number of bands greater than those used in the past appeared warranted.

RECENT ACCOMPLISHMENTS

Experiments were conducted at the SEA/USDA Water Conservation Lab in Phoenix, Arizona in the Spring of 1979 in conjunction with water stress studies conducted by Drs. Ray Jackson and Paul Pinter. Our experiments involved spectral observations of different phenological grow stages, with each stage being irrigated at a different frequency.

The measurements taken for the experiments to be reported here were made in April, 1979 on wheat crops which had been planted in November, December, and February. The vegetation cover of the February planting was so heterogeneous as to render replicate sampling impractical. The data to be discussed here will deal principally with the November and December planting dates.

Spectral measurements were made with a multispectral radiometer (Barnes) with a range of 400 to 2500 nm and with a resolution of 10 nm between 400 and 1000 nm that falls off to 25 nm beyond thes end points. The crop spectral measurements were made at 10 ft. from the plot border at a height of 10 ft., giving an FOV of 2.5 x 5 ft. The spectral data were analyzed on the basis of their relationships to the weight of plant water per unit area, and a stress factor, which is defined as the difference between the vegetation canopy temperature (T_c) and the ambient air temperature (T_a).

The data from the November and December planting dates were pooled for statistical analysis; consequently, ignoring the effects of differences in phenological stages. Future experiments will be

designed so that it will be possible to evaluate the effect of response to water treatment as a function of growth stage in a more rigorous statistical manner.

The relationships between reflectance at 15 selected spectral bands (Figure 8I-1) and the two plant water stress indicator variables are provided in Table 8D-1. The slopes of the regression lines provide information concerning the relative sensitivity of the bands. The bands at 1425 and 1940 nm were observed to be highly sensitive to crop water treatment, as expected, considering the high extinction coefficients of water in these bands. These bands, however, will be of little use in satellite applications. The significant bands which appear to be useful bands for the evaluation of water status are 870, 985, and 2200. The chlorophyll band at 670 nm is observed to be relatively insensitive to water conditions, as compared to 870 nm. The significance of the bands at 985 and 2200 nm remain to be explained. However, 2200 nm is a polymer vibrational band; i.e., it may be influenced by the concentrations of starches and carbohydrates.

The 1200 nm band showed a very low correlation between reflectance and both water content and T_c-T_a. This was true only in the case of the November and December planting dates. However, for the February planting date, where the canopy cover was very sparse, the 1200 nm reflectance was highly correlated with water content ($r = 0.81$) and very highly correlated with T_c-T_a ($r^2 = 0.99$). By pooling the data for the November and December planting dates and plotting 1200/870 against water content, a correlation of 0.9 was observed. The explanation of the full significance of the 1200 nm band and the ratio of 1200/870 will require additional study.

Operational remote sensing methods for plant water status or stress measurement will most likely require techniques that will "adjust" for differences in growth stage or phenology of a crop. The factors involved include adjustments for different crop biomass, exposed soil background, and plant maturation. D.W. Deering has proposed a prototype three-band plant water status or stress index (SI), which may enable some normalization for these growth stage effects. The SI, in the preliminary configuration, is a ratio of a shortwave infrared radiance measurement (in the region of 1.55 to 1.75μm) to a "vegetation index," such as the simple photographic infrared/red ratio or the Normalized Difference (ND) parameter.

A simple test of the SI for its relationship to percentage plant water content, using the Phoenix, Arizona wheat canopy data, (Figure 8D-1) revealed a very close relationship ($r^2 = 0.97$). Consequently, further study of this and other special "adjustor" indices is warranted.

SIGNIFICANCE

On the basis of the preliminary study data described here, the most useful spectral bands for the evaluation of crop water status appear to be 870, 985, and 2200 nm. A spectral band at 1200 nm and the ratio of 1200/870 would appear to be significant, but further work will be required for a satisfactory understanding. A special water stress index ratio appears promising for an operational satellite remote sensing tool.

FUTURE EMPHASIS

Further, more intensive studies with a different experimental approach are planned for the spring and summer 1980.

Table 8D-1. Reflectance relationships in fifteen spectral bands to plant water content and stress degrees (canopy temperature minus ambient air temperature).

Wavelength	Reflectance vs Plant Water/M^2		Reflectance vs T-Canopy T-Ambient	
	Slope	r	Slope	r
400	-0.61	.81	0.32	.79
560	-1.41	.83	0.19	.78
670	-2.38	.93	1.68	.83
720	-3.27	.61	0.40	.41
870	5.47	.94	-2.77	.71
985	2.84	.82	-1.68	.86
1220	0.36	0	-0.48	.45
1275	0.109	.08	-0.48	.47
1425	-3.68	.89	1.69	.83
1660	-2.78	.87	1.00	.65
1774	-2.98	.90	1.11	.71
1780	-3.13	.83	1.24	.68
1940	-3.61	.86	1.71	.84
2220	-4.49	.92	1.84	.78
2250	-4.16	.91	1.74	.79

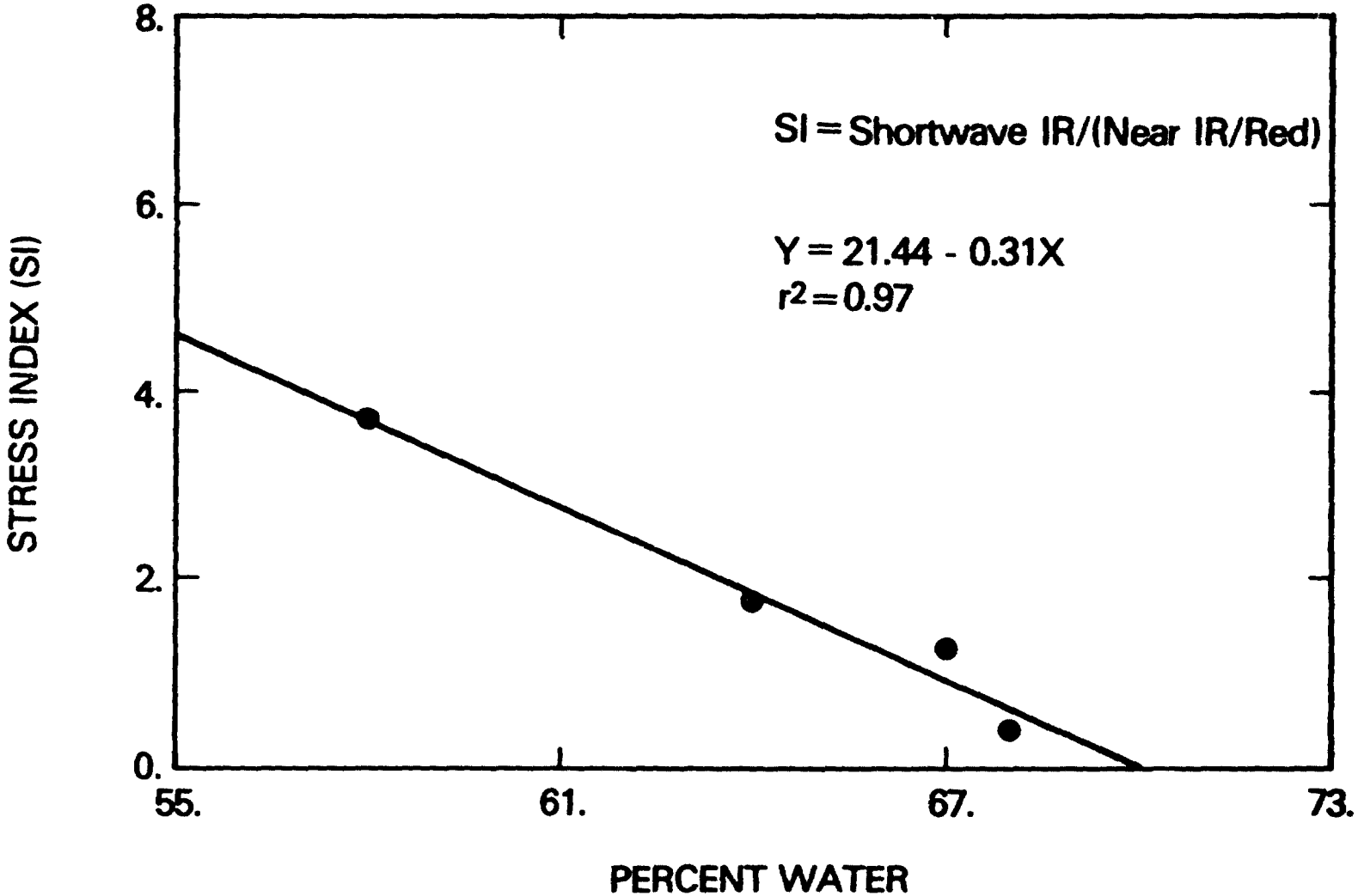

Figure 8D-1. Relationship between the prototype "water stress index" (SI) and percentage plant water content for four water treatments on wheat for the December planting data. For these data the wavelengths used were: SWIR = 1660 nm, near IR = 870 nm and red = 670 nm.

E. OFF-NADIR VIEWING EFFECTS ON SPECTRAL ASSESSMENT OF GREEN BIOMASS

by

D. W. Deering

OBJECTIVES

The objective of this experiment was to evaluate under highly controlled plant conditions the magnitude of the differences in spectral response and spectral measurement sensitivity to herbaceous green biomass at nadir and at selected off-nadir sensor viewing angles. The research reported herein is an initial experiment of a more comprehensive study, which has the objective of evaluating sun elevation and sensor view angle effects on remote sensing of vegetation--particularly on the capabilities for measuring important agronomic variables.

BACKGROUND

Pointable satellite sensors, which are being designed for future earth observation missions, will potentially enable temporal resolutions of one to three days with a single satellite sensor. Off-nadir viewing at several different look angles and at least two (opposite) pointing directions will be required, however, and the effects on classification, mensuration and ground parameter estimation using off-nadir spectral data are not known. Certain remote sensing applications may actually be improved via an off-nadir view (e.g., vegetation classification, biomass assessment in areas of sparse ground cover, etc.), whereas other application capabilities may deteriorate (e.g., acreage assessment).

The anisotropic characteristics of the vegetation, atmospheric path radiance differences at different look angles, etc. will cause spectral measurements obtained at various off-nadir angles and directions to be different even when there is no change in the status of the ground target. The nature and causes of these variations must be understood if off-nadir viewing from satellite sensors is to be used to increase temporal resolution. Sun elevation considerations will be very important in developing this understanding.

The interactions of red and near infrared radiation with green plant material have been studied for several years and are fairly well understood. Techniques have been developed to determine the amount of green plant material or green biomass on the ground with remote sensors that utilize both the red and infrared spectral regions. It is not known, however, how this determination is affected when the sensor "looks" at the vegetative scene in an off-vertical or off-nadir pointing mode. It is hypothesized that with sparse or low density plant cover conditions, such as occur early in the crop growth cycle and on rangelands of arid and semi-arid regions,

that an off-nadir view will enhance the spectral measurement sensitivity to the status (e.g., cover, biomass, moisture condition, etc.) of the vegetation. This enhancement should be possible by decreasing the soil background ("noise") affecting the spectral response and correspondingly increasing the amount of plant material in the view of the sensors.

In studies of vegetation one of the most difficult tasks is to vary one factor while holding all other factors constant to study the independent effects of the first factor. Often it is physically impossible to do so because of the biological interactions (either at the physiological or plant community levels) under normal or field conditions. In this study, artificially created vegetation scenes using greenhouse grown wheat plants were assembled in 0.75m X 0.75m wooden flats or "plots." The wheat plants were planted in small (5cm.) peat pots at a density of 12 plants per pot, and were all grown under essentially identical conditions. On the day before the spectral measurements were taken, the wheat canopies were assembled in the wooden flats by uniformly spacing 0, 36, 68, 100, 132, 164, and 196 wheat pots within a matrix of bare soil pots of the same size. Three replicates were made of each wheat biomass level.

Spectral measurements were taken on each of the plots with a two-channel, red (0.64-0.69um) and photographic infrared (0.79-0.83um) portable radiometer, which was affixed to a specially designed angular measurement and support device. The spectral measurements were taken on March 29, 1979 near solar noon (54^{o} sun elevation) to minimize the sun angle variation during the measurement period. The sensor angular measurement positions were restricted to a 0^{o}-50^{o} range, because side-to-side pointing on future satellites will be less than 50^{o} off-nadir because of excessive geometric distortions and severe atmospheric effects at larger angles.

RECENT ACCOMPLISHMENTS

The red and near-infrared spectral radiances were found to be highly correlated with the wheat green biomass on a dry weight basis for the nadir (0^{o}o) view and for all five off-nadir view angles examined. Linear regression analyses of red band data yielded coefficients of determination (r^2) of about 0.90 for 0^{o}-30^{o} view angles, and 0.76 and 0.80 for 40^{o} and 50^{o} view angles, respectively. The reduced linear correlation at the larger view angles is the result of increased red energy absorption by the greater amount of plant material "seen" by the sensor at the lower biomass levels. This effect conforms to the hypotheses stated above, and results in a more pronounced curvilinear relationship (Figure 8E-1, top) at the 40^{o} and 50^{o} off-nadir view angles. The anomalously high radiances at 30^{o} is unexplained at this time.

Infrared radiance relationships to wheat green biomass were linear for all view angles with the coefficients of determination (r^2) for the relationship being greater than 0.95 in all cases. The infrared radiances were observed to be markedly greater for the

30°-50° view angles than for the 0°-20° view angles for all but the lowest biomass situation (Figure 8E-1, bottom). This enhancement of the infrared response also conforms to the hypothesis stated above, as numerous studies have shown higher infrared reflectance for greater quantities of green plant material viewed by a sensor. In this case, however, the greater quantity of biomass viewed by the sensor results from off-nadir viewing of the sensor rather than from increasing the quantity of biomass per unit area on the ground.

The ratio of the near-infrared radiance to the red radiance is frequently used as an index to the quantity of herbaceous green biomass, and is typically a more sensitive and consistent estimator of the status of the vegetation than is either spectral band used independently. The infrared/red ratio parameter was found to be very highly linearly related (Figure 8E-2) to the quantitiy of dry green biomass for all view angles (r^2 - 0.96). However, the slope, and hence the capability for use as an estimator of green biomass, progressively increased from 0° to the 50° view angle (b = 0.006 to 0.012, respectively).

SIGNIFICANCE

Off-nadir pointing of remote sensors decreased the red radiance and increased the infrared radiance in a situation of sparse ground cover and low levels of green biomass by increasing the proportion of the measured spectral response that was affected by interaction with the plant material component of the vegetation scene. The magnitude of the spectral radiance value changes with changes in off-nadir viewing angle indicate that from 0°-20° no significant radiometric adjustments will be necessary, but at larger view angles, adjustment-to-nadir algorithms may be necessary for many applications.

The infrared/red ratio vegetation index exhibited enhanced sensitivity to the green biomass in low biomass situations. These results reveal the potential for improving vegetation status determination, particularly biomass estimation, in sparse ground cover and low biomass situations through off-nadir pointing of remote sensors. This study did not, however, consider possible atmospheric degradation that may result from off-nadir pointing from satellite altitudes.

FUTURE EMPHASIS

The greenhouse wheat experiment will be followed by a field plot experiment with wheat, corn and soybeans during the 1980 growing season to verify these results under natural conditions. Additionally, row direction effects and sun elevation influences on the spectral measurements taken in an off-nadir pointing will be examined.

PUBLICATIONS

Deering, D. W., "Off-Nadir Viewing Effects On Spectral Assessment of Green Biomass," submitted to Remote Sensing of Environment.

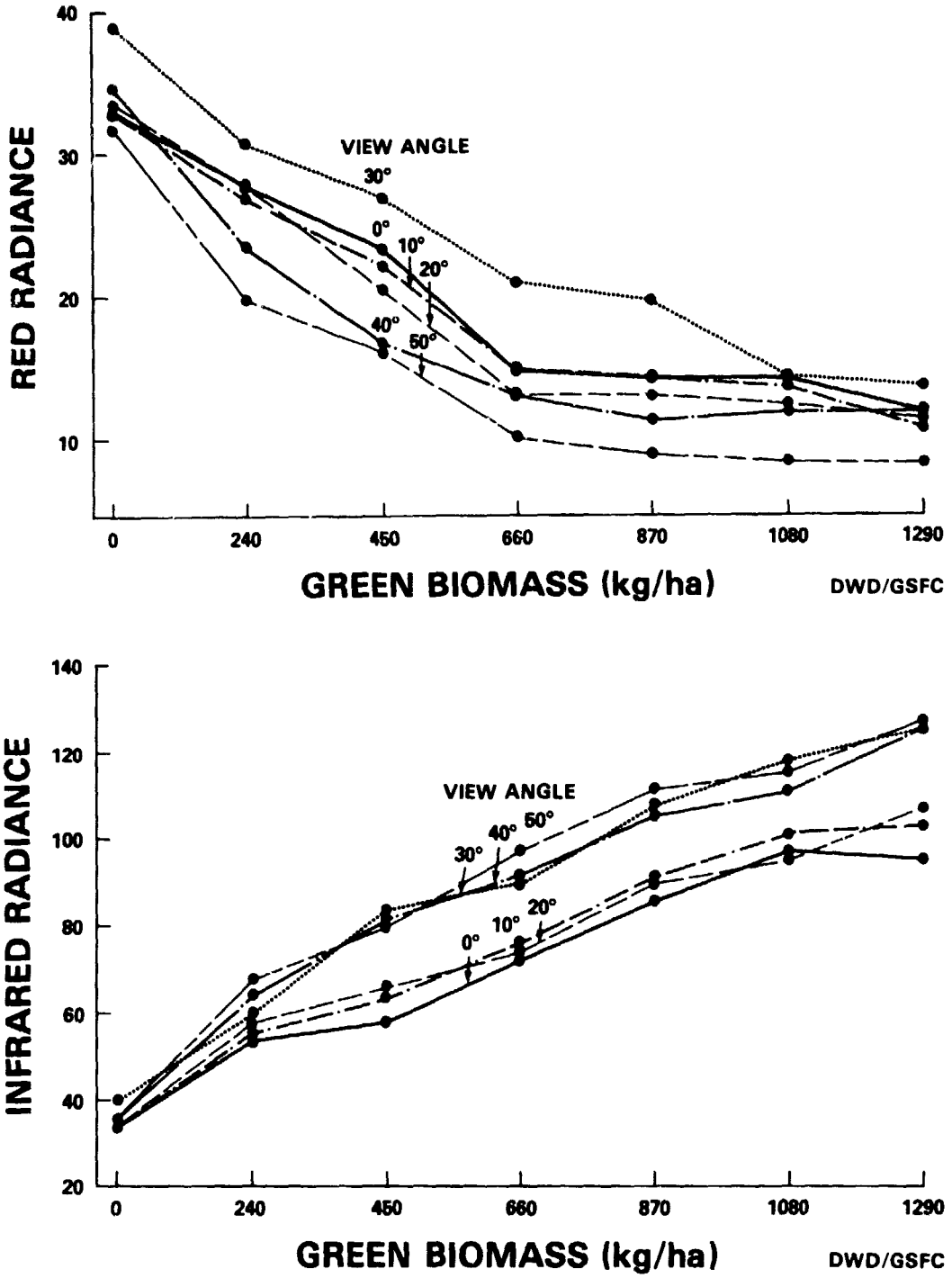

Figure 8E-1. Sensor view angle effects on red (top) and infrared (bottom) spectral radiance relationship to wheat green biomass (dry weight).

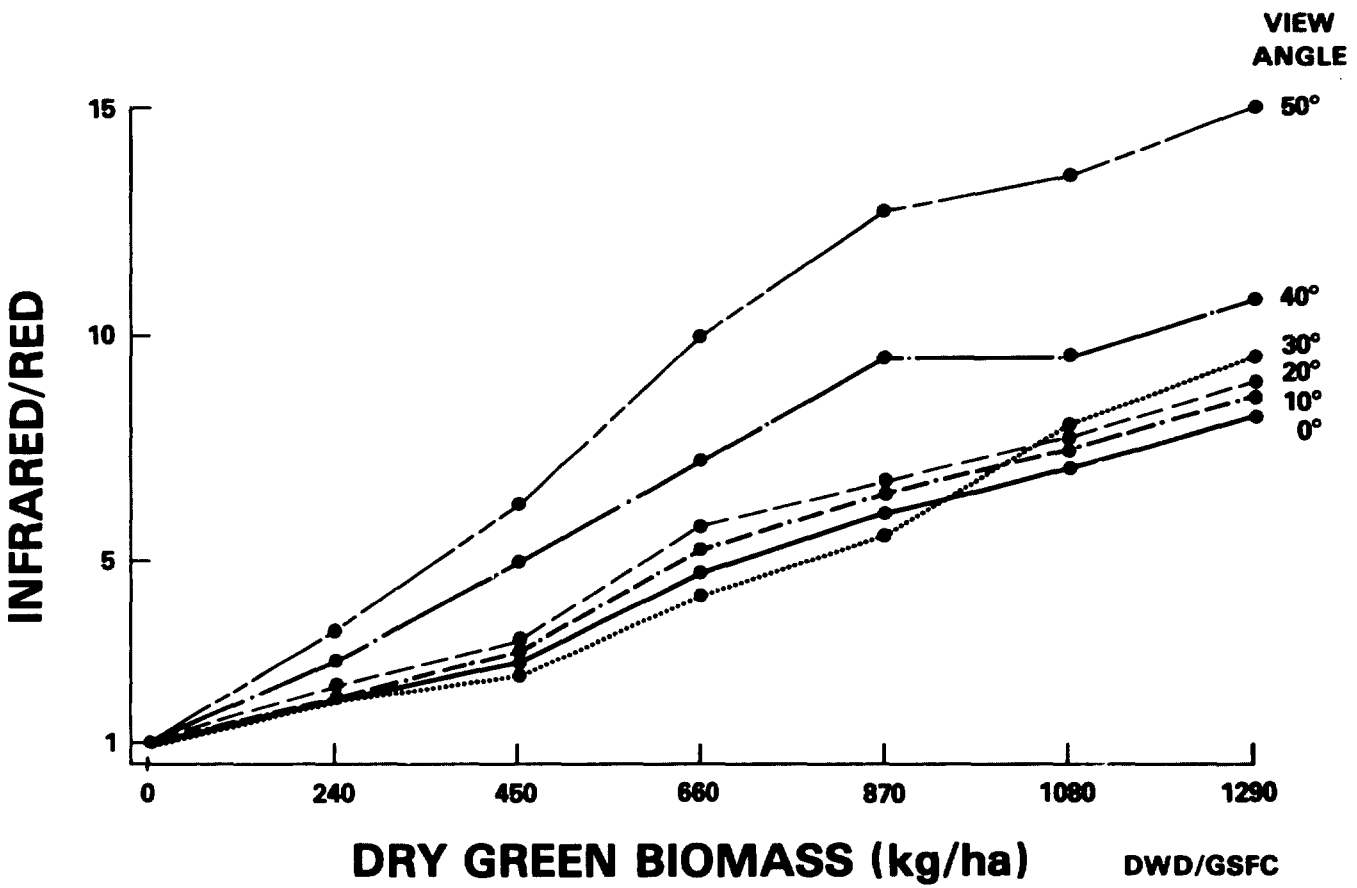

Figure 8E-2. Sensor view angle effects on infrared/red spectral ratio sensitivity to herbaceous green biomass (dry weight) of wheat.

F. THERMAL ANISOTROPY OF VEGETATION CANOPIES

by

D. S. Kimes

OBJECTIVES

The objectives of the study are to develop a quantitative understanding (mathematical modeling) of the anistropic behavior of vegetation canopies in the thermal infrared spectral region. The model needs to relate, in physically based manner, sensor response as a function of view angle to the vertical temperature profile and geometric structure of the vegetation canopy.

BACKGROUND

A new aspect of current work in remote sensing is the investigation of the angular distribution of both reflected and emitted radiation, with the hope that specific directional measurements may provide superior information for inferring various vegetation characteristics such as plant water stress, and plant yield. In the thermal infrared region, although individual canopy elements approximate isotropic radiators, the radiation from the canopy may also be anisotropic, because of canopy geometry-induced variations in energy flow (Kimes, 1979c; Kimes et al., 1979c). These spatial variations in energy flow affect the surface temperature distribution within the canopy, so that as sensor view angle varies, the relative proportions of surface elements of different temperature that present themselves to direct view by the sensor also vary. The result is an angular variability or anistropic behavior in sensor response that is a function of both canopy geometry and the vertical canopy temperature profile.

RECENT ACCOMPLISHMENTS

A deterministic model was developed to quantify these anistropic relationships. The canopy was abstracted into an arbitrary number (n) of horizontally infinite layers and the following equation was derived.

$$L(\theta,\phi) = \pi^{-1} \cdot \sum_{i=1}^{n} \left[\left(\prod_{k=0}^{i-1} PGAP_k(\theta,\phi) \right) \cdot PHIT_i(\theta,\phi) \cdot \epsilon_i \cdot \sigma \cdot T_i^4 \right] \quad (1)$$

where

$L(\theta,\phi)$ = Thermal infrared radiance ($W \cdot M^{-2} \cdot SR^{-1}$) of a canopy view angle (θ,ϕ) where θ and ϕ are the inclination and aximuth angles respectively

n = Number of discrete layers in the canopy system including the ground

$PGAP_k(\theta,\phi)$ = Probability of gap in the direction θ,ϕ for layer k. By convention $PGAP_o(\theta,\phi)=1.0$ for all θ and ϕ.

$PHIT_i(\theta,\phi)$ = Probability of hit in the direction θ,ϕ for layer i and $PGAP_k(\theta,\phi) = 1\text{-}PHIT_i(\theta,\phi)$ for i=k. By convention $PHIT_n(\theta,\phi) = 1.0$ for all θ and ϕ where n denotes the ground.

ε_i = Mean component emisivity in layer i

T_i = Mean component surface temperature in layer i (^oK)

σ = Stefan-Boltzmann constant ($W \cdot M^{-2} \cdot {}^oK^4$).

The underlying assumptions and justification of the above formula are presented by Kimes (1979b). The PGAP and PHIT terms describe the geometric structure of the vegetation canopy. Specifically, the PGAP term is the probability that a vegetation cap occurs in a particular layer and at a particular view angle. The PHIT term is the converse of PGAP as described above. Both, terms can be derived from mathematical models of vegetation structure (Kimes, 1979b).

Field studies were conducted at Phoenix, AZ, on irrigated wheat fields to measure the anistropic sensor response for wheat canopies of various geometric structures and to document the predictive capabilities of equation 1 (Kimes, et al. 1979a, Kimes et al. 1979b). Figure 1 shows the measured sensor response (effective radiant temperature, ERT) versus view angle for five wheat plots during noon 18 May 1979. The thermal infrared sensor response to emissions from vegetation canopies may deviate significantly from that expected for a Lambertain surface. For a wheat canopy of leaf area index 1.5 (plot 4B, Figure 8F-1), for example, we observed a response differential as great as 13 C, when going from a viewing zenith angle of 0 degrees to one of 80 degrees. However, this phenomenon can be accurately quantified as a function of vegetation canopy geometry and the vertical temperature distribution of the canopy components by equation 1. Canopy geometry parameters (PGAP, PHIT) and canopy temperature profiles were measured and the theoretical response of the sensor predicted by equation 1. The root-mean square deviations between theoretically predicted and measured canopy temperatures for all plots and measurement periods was less than 1.1 C, for all sensor view angles. (Figure 8F-2).

SIGNIFICANCE

To date, this investigations has demonstrated that the anistropic behavior of vegetation canopies can be accurately quantified using deterministic techniques based on physical principles. This quantitative understanding of the phenomena serves as a sound base for making intelligent, remote sensing inferences from thermal infrared measurements of vegetation canopies.

FUTURE EMPHASIS

For accurate inferences of vegetation characteristics, it is well established that temperature profiles of vegetation canopies need to be determined uniquely rather than single composite canopy temperatures (soil + vegetation) (Kimes, 1979a; Kimes et at, 1979a). Knowledge of temperature profiles of vegetation and substrate are also important in geologic, hydrolic and forestry applications (Kimes 1979b). Using multiple sensor view angles with apriori

information of the geometric structure of vegetation, unique temperatur distributions may be derived from equation 1. This approach could point the way toward a technique for the unambiguous separation of soil and canopy layer temperatures from a series of off-nadir composite sensor measurements.

REFERENCES AND PUBLICATIONS

Kimes, D.S. (1979a), Effects of vegetation canopy structure on remotely sensed canopy temperatures. Remote Sens. of Environ., (Submitted), NASA TM 80331.

Kimes, D.S. (1979b), A thermal vegetation canopy model of sensor response, Ph.D. Dissertation, Colorado State University, Fort Collins, CO.

Kimes, D.S., Idso, S.B., Pinter, P.J., Jr., Jackson, R.D., and Reginato, R.J. (1979a), Complexities of nadir-looking radiometric temperature measurements of plant canopies, Appl. Optics, (Submitted).

Kimes, D.S., Idso, S.B., Pinter, P.J., Jr., Reginato, R.J., and Jackson, R.D. (1979b), View Angle Effects in The Radiometric Measurement of Plant Canopy Temperatures, Remote Sens. of Environ., (Submitted).

Kimes, D.S., Smith, J.A., and Ranson, K.J. (1979c), Terrain feature canopy modeling, Final Rept., U.S. Army Res. Office. Grant No. DAAG 29-78-G-0045.

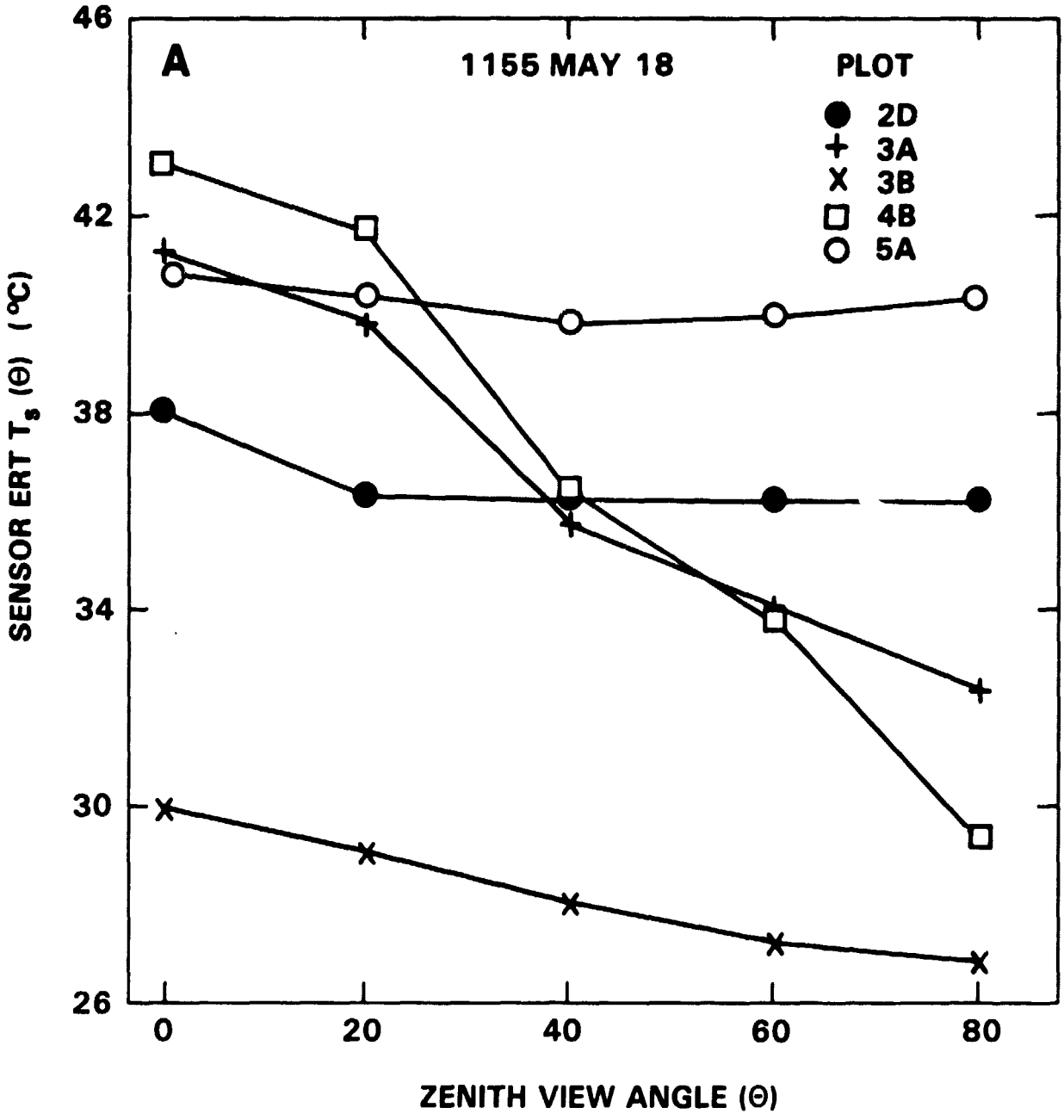

Figure 8F-1. Measured sensor response T_S (θ) versus sensor view angle (θ) for five wheat plots during the noon measurement period of 18 May, 1979 (from Kimes et al., 1979a).

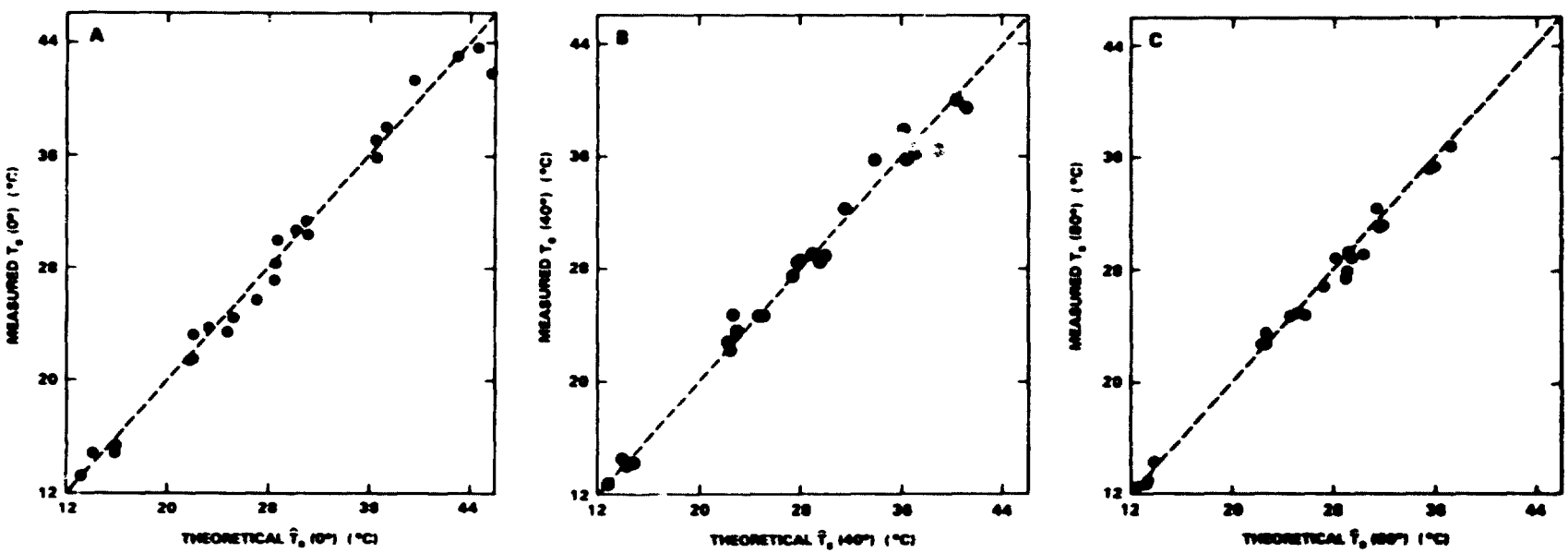

Figure 8Γ-2. Measured sensor response T_S (θ) versus the theoretical $\hat{T}_S$ (θ) for sensor view angles (θ) equal to 0^o (A), 40^o (B), and 80^o (C). T_S (θ) is based on a derivation of equation 1 (from Kimes et al., 1979b).

G. TIME OF DAY EFFECTS ON WHEAT REFLECTANCE IN FIFTEEN SELECTED BANDS

by

E. W. Chappelle, F. W. Wood and W. W. Newcomb

OBJECTIVES

The goal of this study was to determine the magnitude and nature of time of day influences on reflectance of a wheat canopy in fifteen selected spectral bands over a moderate range of sun elevations.

BACKGROUND

It has been established that radiometric measurements of vegetation are affected by changes in sun elevation. In ground investigations it is frequently very difficult or impossible to collect the required quantity of field spectra during a period of time in which there is no change in sun elevation. Valuable information for possible data correction or for defining sampling period limits could be obtained from an experiment to determine the nature of the reflectance variations in different regions of the spectrum that are associated with changes in sun angle.

RECENT ACCOMPLISHMENTS

This preliminary study was conducted in conjunction with a water stress experiment conducted at the SEA/USDA Water Conservation Lab in Phoenix, Arizona in April 1979. Spectral measurements were taken on a $BaSO_4$ standard panel and a 3-month old wheat plot using a multispectral reflectometer. Fifteen wavelengths (400, 560, 670, 720, 870, 985, 1220, 1275, 1425, 1660, 1774, 1780, 1940, 2220, and 2250 nm) were monitored at seven different times of the day from approximately 10 a.m. until after 4 p.m. The measurements were taken from a height of 10 ft., resulting in a FOV of 2.5 x 5 ft. The measured reflectances were normalized relative to a $BaSO_4$ panel at each different time period.

Examination of six representative spectral bands (Figure 8G-1) reveals that the reflectance values were not symmetrical about solar noon for low sun angles (48° at 10:08 and 47° at 15:00). For high sun angles (58° at 11 to 64° at 1:00) the curves show little effect due to a change in sun elevation. Low sun angles (below 50°) measurement anomalies may result in part from confounding effects of time of day and engineering hardware characteristics of the reflectometer that was being used.

The absorption bands (e.g. 670 nm) showed little reflectance variation (range 2-4% reflectance) with time of day, but the assymetry about solar noon, which is more apparent in the "reflective" bands (e.g., 870 nm), can also be seen in the absorption bands.

These data indicate that there likely exists a differential influence on reflectance in different spectral bands which must not be ignored in analysis of multispectral data taken at different times of the day. The time of day effects may be due to changes in the composition of incoming light, shadow effects, canopy, geometry, chlorophyll fluctuations, moisture changes, and etc.

SIGNIFICANCE

For proper analysis of radiometric measurements taken outside a nominal solar noon window (in this case, at sun angles less than 50^{o}) the time of day and instrument characteristics must be understood.

FUTURE EMPHASIS

Experiments are being designed to quantify the effects of time of day and sun angle on radiometric measurements and to try to explain the causes of reflectance assymetry about solar noon. Before these experiments are conducted, a study will be made to determine the sensitivity of the radiometer to sun angle changes.

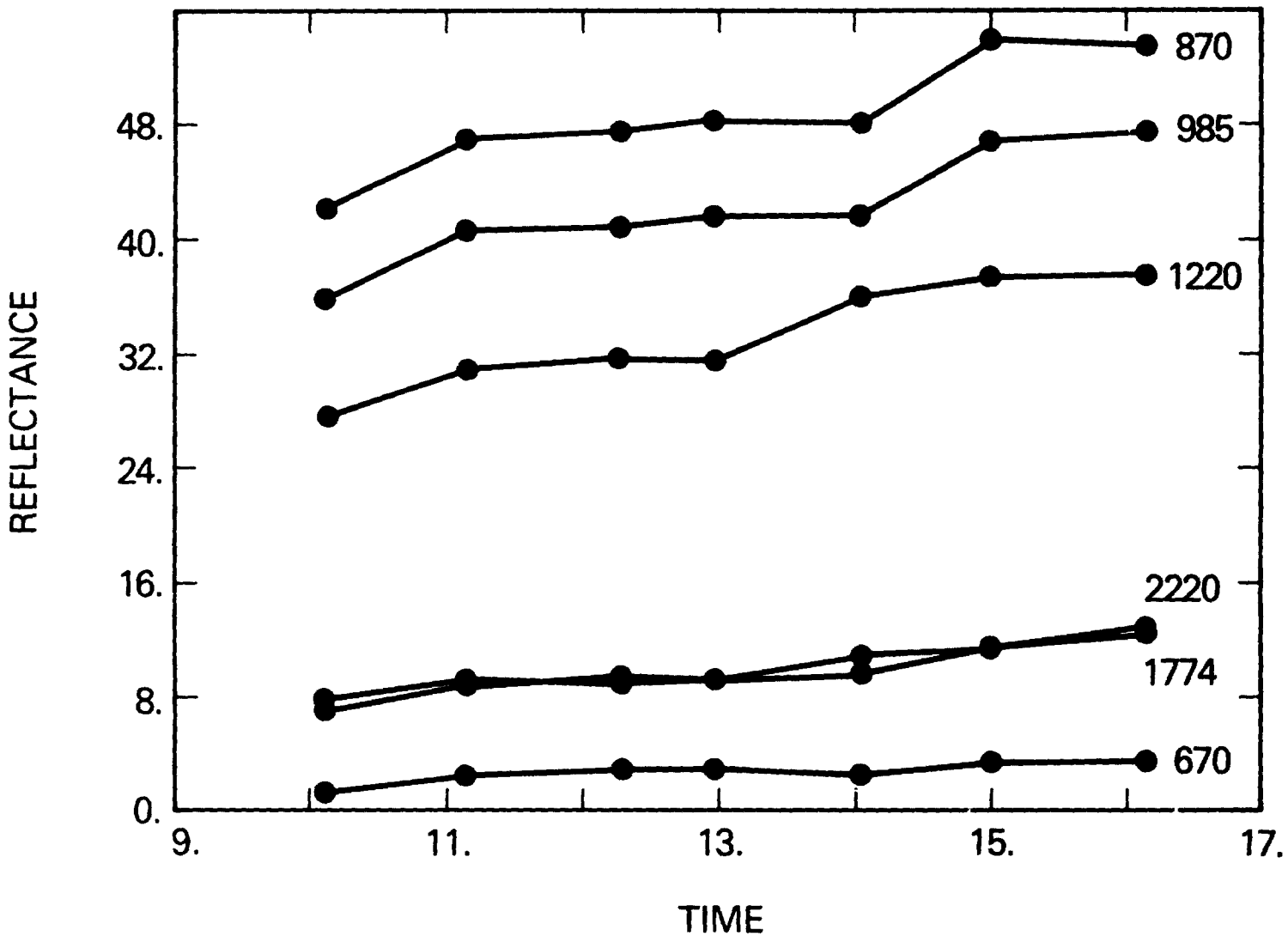

Figure 8G-1. Reflectance variations of six representative spectral bands for a 3-month old wheat canopy at seven times during a day.

H. ASSESSING SOYBEAN LEAF AREA AND LEAF BIOMASS BY SPECTRAL MEASUREMENTS

by

B.N. Holben, C.J. Tucker, C. Fan

OBJECTIVES

The objective of this study was to establish the basic relationship of red and photographic infrared spectral data to green leaf area index for a soybean canopy.

BACKGROUND

Red and photographic infrared spectral radiances have been correlated with soybean total leaf area index, green leaf area index, chlorotic leaf area index, green leaf biomass, chlorotic leaf biomass, and total biomass. The most significant correlations were found to exist between the ir/red radiance ratio data and green leaf index and/or green leaf biomass(r^2 = 0.85 and 0.86, respectively). These findings demonstrate that remote sensing data can supply information basic to soybean canopy growth, development, and status by non-destructive determination of the green leaf area index or green leaf biomass.

RECENT ACCOMPLISHMENTS

A soybean (Glycine max(L.)Merr.) field on an Elinsboro sandy loam soil located on the USDA Beltsville Agricultural Research Center, in Maryland was selected for study. Sixty circular 0.25 m^2 plots were used with four plots being sampled per week for fifteen weeks. The soybeans were planted on May 20, 1978, and had a row spacing of 76 cm and 5 cm within the row. The crop emerged in early June and reached 100% canopy cover in early August. The first freeze occured on October 11, 1978.

Each week four pairs of red(0.63-0.69μm) and photographic infrared (0.775-0.825μm) spectral data were collected for each of the four plots measured with a hand-held radiometer similar to Pearson et al. (1976). Concurrent agronomic data pertaining to crop development, estimated canopy cover, number of leaves, and plant height were recorded before each of the 0.25m^2 plots were harvested All of the above ground vegetation was immediately harvested and the total wet biomass determined. Subsequently, the total wet biomass was stratified into wet green leaf biomass, wet chlorotic leaf biomass, and wet stem biomass. The wet green and wet chlorotic leaf biomasses were immediately run through an automatic leaf area meter to determine the green leaf area and chlorotic leaf area. The wet biomass fractions were then force air dried at 60°C for 48 hours before the dry green leaf biomass, dry chlorotic leaf biomass, and dry stem biomass determinations were made. The stem biomass determinations included reproductive organs.

The spectral radiance data were collected at approximately one week intervals and were collected in direct sunlight under cloudless or partly cloudy skies between the hours of 1030-1430 EDT. Atmospheric conditions varied from very clear with low humidity, to hazy with high humidity. A solar irradiance reading was taken from a $BaSO_4$ panel prior to measuring each plot with the hand-held radimeter. Radiance data were used in the analysis because the two bands in question (0.63-0.69 and 0.775-0.825μm) are close together in a spectral sense and atmospheric transmission characteristics are similar for both bandwidths.

The radiance data were used to form the ir/red radiance ratio and the normalized difference of (ir-red)/ir+red). All radiance data were averaged for each plot (i.e., the mean of the four observations) and the averaged values used thereafter in the statistical analysis. The data analysis correlated and regressed the red radiance, the photographic ir radiance, ir/red radiance ratio, and the normalized difference (ND) with respect to the various plant canopy variables measured (Table 8H-1; Figure 8H-1).

CONCLUSIONS/SIGNIFICANCE

1. The ir/red radiance ratio was found to be linearly and highly correlated with soybean green leaf area index, green wet leaf biomass, and green dry leaf biomass.

2. The normalized difference was exponetially related to the green leaf area index, green wet leaf biomass, and green dry leaf biomass. The asymptotic nature of this relationship prohibits the use of the normalized difference for estimating these plant canopy variables in high leaf density vegetation canopies.

3. Estimated crop cover and the red radiance individually were poor choices to evaluate crop canopy condition for high green leaf biomass situations.

4. Spectral estimation of the projected green or photosynthetically active leaf area of plant canopies by use of red and photographic infrared spectral data can provide a crucial input to primary productivity models.

REFERENCES

Holben, B.N., C.J. Tucker, and C.J. Fan, 1980. Assessing soybean leaf area and leaf biomass by spectral measurements. Photogram. Engr. and Remote Sensing (in press).

FUTURE EMPHASIS

This project has been completed and a manuscript has been accepted for publication.

Table 8H-1. Linear Correlation Coefficients between the four Spectral variables and the Plan Canopy variables. The sample sizes are noted in parenthesis.

Canopy Variable	Red	IR	IR/Red	ND
Green LAI (52)	−0.75	0.75	0.92	0.81
Green Wet Leaf Biomass (60)	−0.67	0.79	0.93	0.82
Green Dry Leaf Biomass (60)	−0.68	0.75	0.92	0.83
Chlorotic LAI (40)	0.02	−0.14	−0.30	0.07
Chlorotic Wet Leaf Biomass (42)	0.01	−0.12	−0.29	0.07
Chlorotic Dry Leaf Biomass (40)	0.03	−0.20	−0.34	0.05
Total LAI (40)	−0.84	0.85	0.89	0.84
Total Wet Leaf Biomass (42)	−0.82	0.85	0.90	0.82
Total Dry Leaf Biomass (40)	−0.84	0.82	0.88	0.83
Wet Stem Biomass (60)	−0.32	0.00	0.05	0.35
Dry Stem Biomass (40)	0.55	−0.74	−0.74	−0.54
Total Wet Biomass (60)	−0.73	0.31	0.65	0.71
Total Dry Biomass (60)	−0.58	−0.14	0.26	0.36
Estimated Crop Cover (60)	−0.93	0.48	0.79	0.87

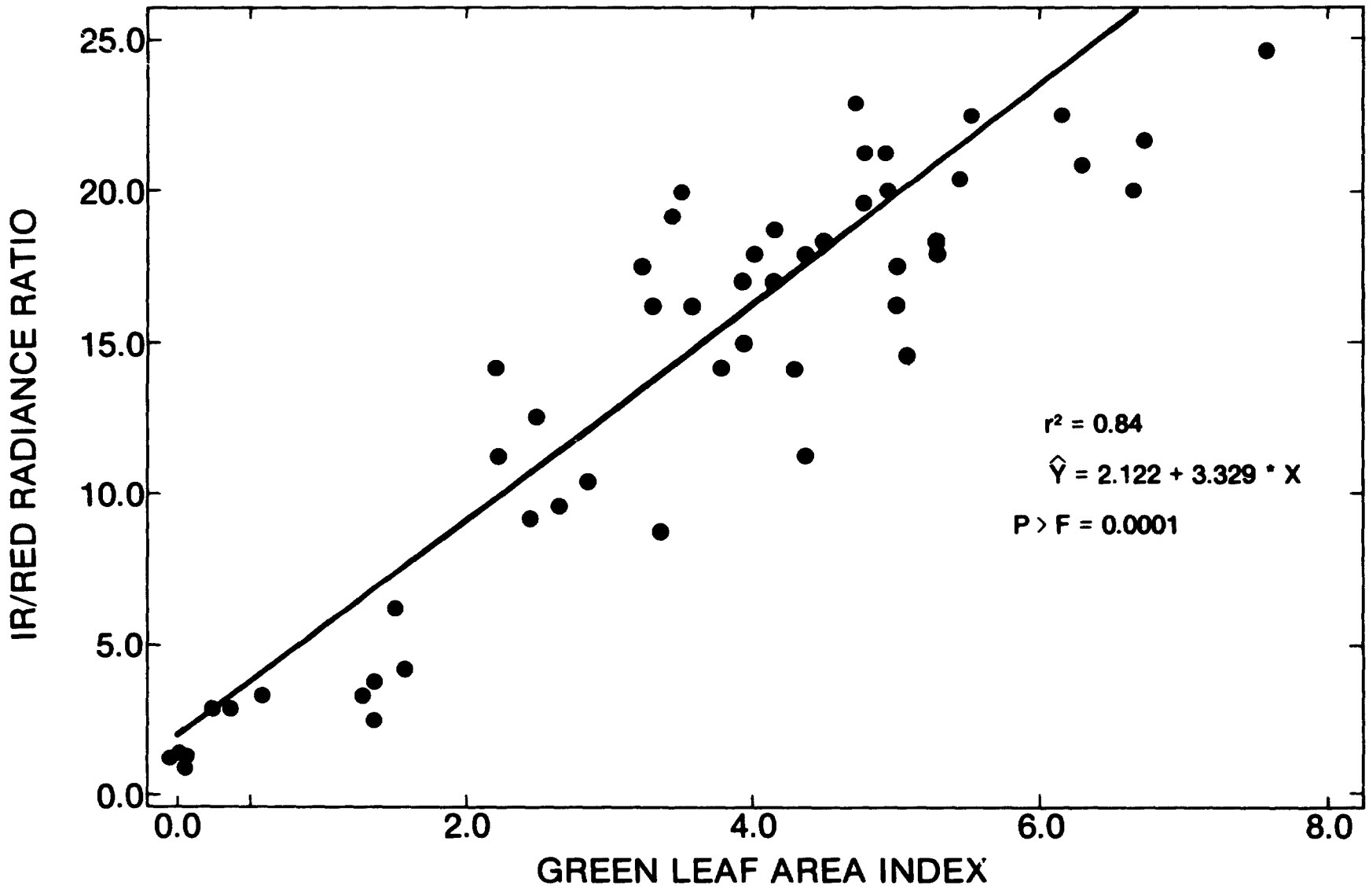

Figure 8H-1. Relationship between soybean green leaf area index and the infrared/red radiance ratio.

D5

I. RELATIVE SENSITIVITY OF FIFTEEN SPECTRAL BANDS TO CHANGES IN SOYBEAN CANOPY COVER FOR WET AND DRY SOILS

by

E.W. Chappelle, R. Bell, F.W. Wood, D.W. Deering, M. Labovitz

OBJECTIVES

The objectives of the study were 1) to test the validity of a "principal factor" routine, which will be used further to determine the informational bands for vegetation remote sensing, and 2) to evaluate the relative sensitivities of the eleven spectral bands to canopy cover changes under wet and dry soil conditions.

BACKGROUND

The spectral bands that have been most frequently and intensively studied in agricultural remote sensing have been the various bands in the red and the photographic infrared regions. It is expected that additional spectral regions may have additional utility for vegetation assessment, and consequently, studies are needed to identify those positions and optimal bandwidths for specific uses. The multispectral reflectometer used in this study measures reflectance from 400 nm to 2500 nm in 350 discrete bands, and thus provides considerable versatility in band selection for a variety of uses. Representative spectra for soybeans, corn, and soil using this instrument are presented in Figure 8I-1. Fifteen "critical bands," which were selected on the basis of their being either maxima or minima, are superimposed on these spectra.

For this experiment, which was designed to provide a model for developing algorithms for the statistical selection of informational bands and to evaluate the sensitivity of the selected bands to canopy cover and soil surface moisture, a simple experimental design was desired. In order to prevent the concommitant plan status changes accompanying normal growth-related changes in canopy cover, an artificial situation was created whereby the ratio of soil to vegetation was varied in regular increments at a fixed stage of plant growth (an all-green canopy with 100 percent canopy cover).

Using a 6 x 6 m soybean plot with a 1.5 x 3 m bare soil corner, the ratio of soil to vegetation was changed by varying the position of the spectral reflectometer over the plot. Spectral measurements were made with the bare soil portion under dry and water saturated conditions. Eleven spectral bands were subjectively chosen for analysis. The correlation values (r or r^2) for the critical bands relative to canopy cover were all greater than 0.9 for the dry soil and, with the exception of 1660 and 1700 nm, were greater than 0.9 for the wet soil situation.

RECENT ACCOMPLISHMENTS

The principal factor analysis was performed on the simulated canopy data using a varimax rotation to retain independence of the factors. Two factors accounted for 94.4 percent of the total variance. The first factor related negatively to canopy cover

(or biomass), with the bands at 400, 560, 670, 720, 1425, 1660, 1774, 1940, and 2220 nm, being strongly loaded on this factor with correlation values (r^2) exceeding 0.82. A cutoff point occurred between 720 and 870 nm and also between 1275 and 1425, delineating the bands which fell strongly into the second factor. The second factor is positively related to cover (or biomass) and is considered a reflectance factor.

The factor analysis algorithm correctly defined the point of strong chlorophyll absorption at 670 nm and of high reflectance at 870 nm. The factor analysis results also indicate a strong reflectance peak at 1275 nm followed by strong (water) absorption 1425nm. Because all variables that are correlated highly with the same factor provide redundant information, those highly correlated variables not at points of change could be dropped. In this simulated canopy cover experiment, the bands containing the maximum information occur at 670, 720, 870, 1275, and 1425 nm.

The sensitivity of the eleven different bands to change in canopy cover and the effect of soil moisture on sensitivity are revealed by their regression slopes (Figure 8I-2). The comparison of slopes for dry soil and wet soil reveal that the spectral band sensitivity to canopy cover change is greater for wet soil than for dry soil in the 870-1275 nm region and reversed in the remaining bands except the isobestic band (720 nm), which only changes sign. The ratios of the wet and dry slopes (Figure 8I-3) reveal that the bands whose sensitivity to canopy cover changes are least affected by water are 720, 870, 990, 1220 nm. Of these four bands, the 0.87 and 0.99 nm bands were the most sensitive to changes in canopy cover.

SIGNIFICANCE

The experimental results indicate the potential impact of surface soil moisture changes on the interpretation of spectral data as applied to the assessment of vegetatational status and thus points out the necessity for either an accurate determination of surface soil moisture or the development of techniques for elimination of its effects. Any analysist of crop spectra must, at least, recognize that these effects exist.

The factor analysis approach has been validated by the test results.

FUTURE EMPHASIS

In future spectral band selection experiments the soil surface moisture will be measured in studies to determine the quantitative relationships between vegetation parameters and spectral reflectance. Factor analysis techniques will be used for analysis of the multi-spectral reflectometer data to determine the possible existence of additional information bands for specific vegetation parameter assessment.

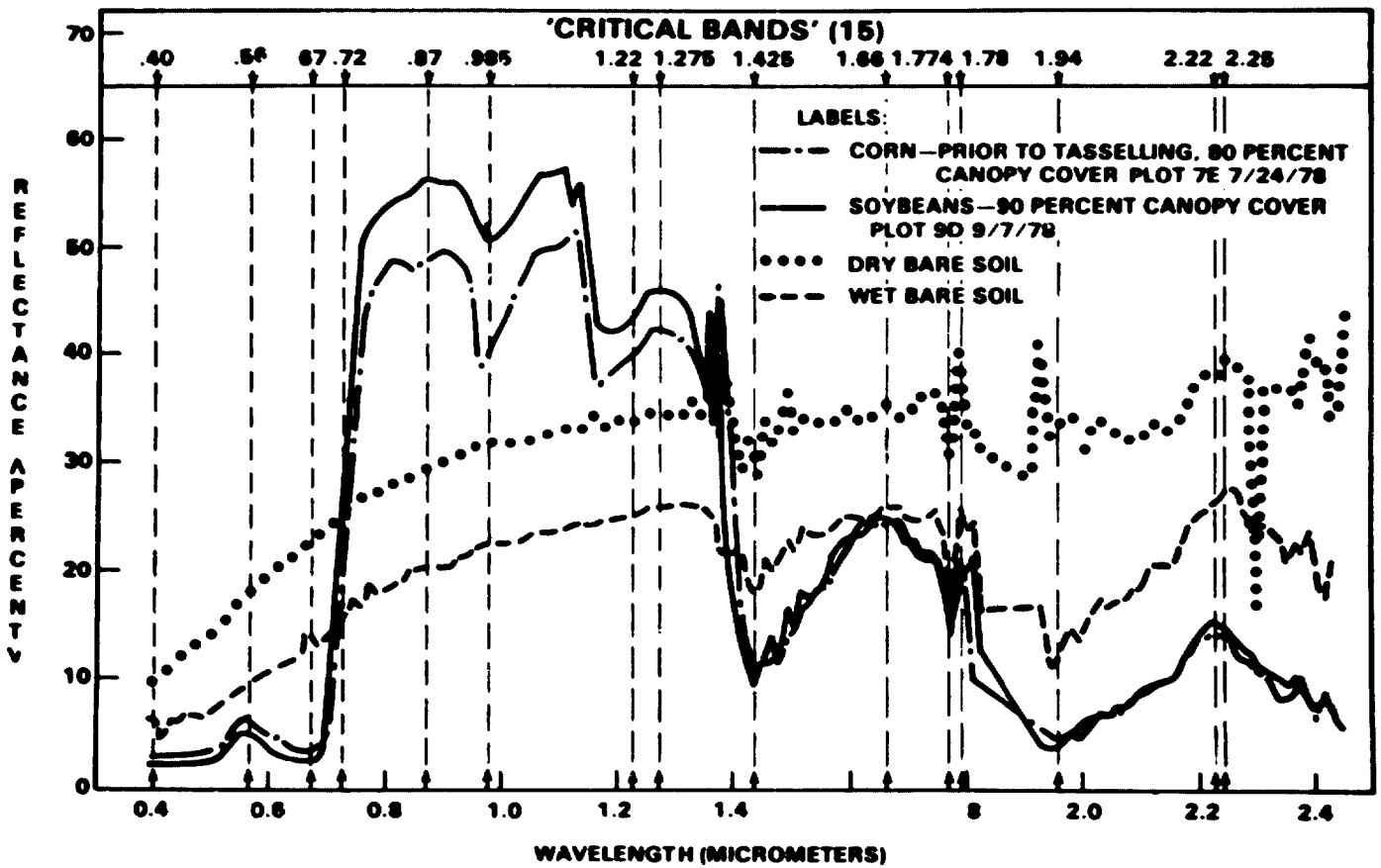

Figure 8I-1. Spectral responses obtained with the Barnes multispectral reflectometer and "critical bands" selected for preliminary analysis.

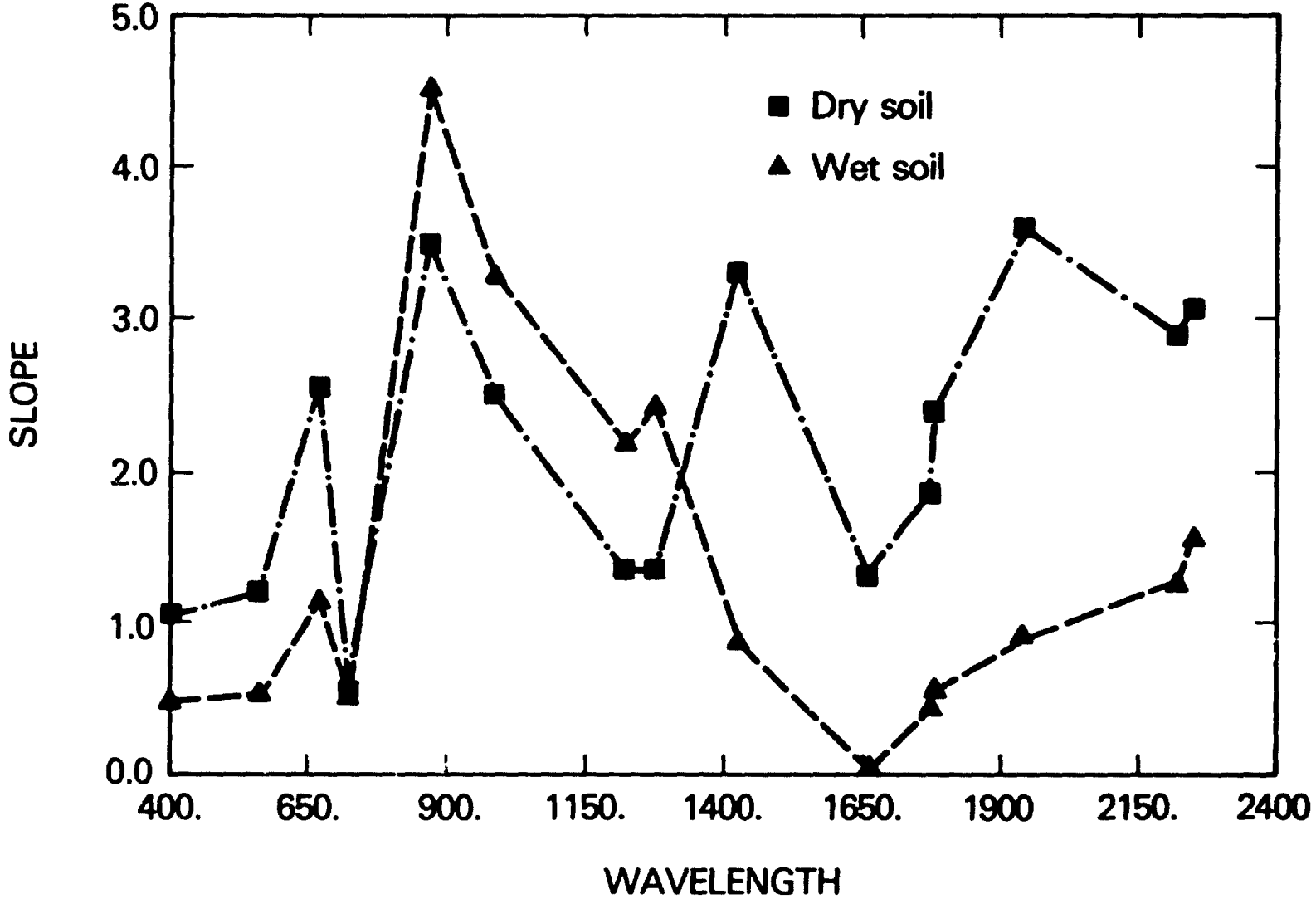

Figure 8I-2. Regression slopes for the relationships between soybean canopy cover and spectral reflectance under wet and dry soil conditions.

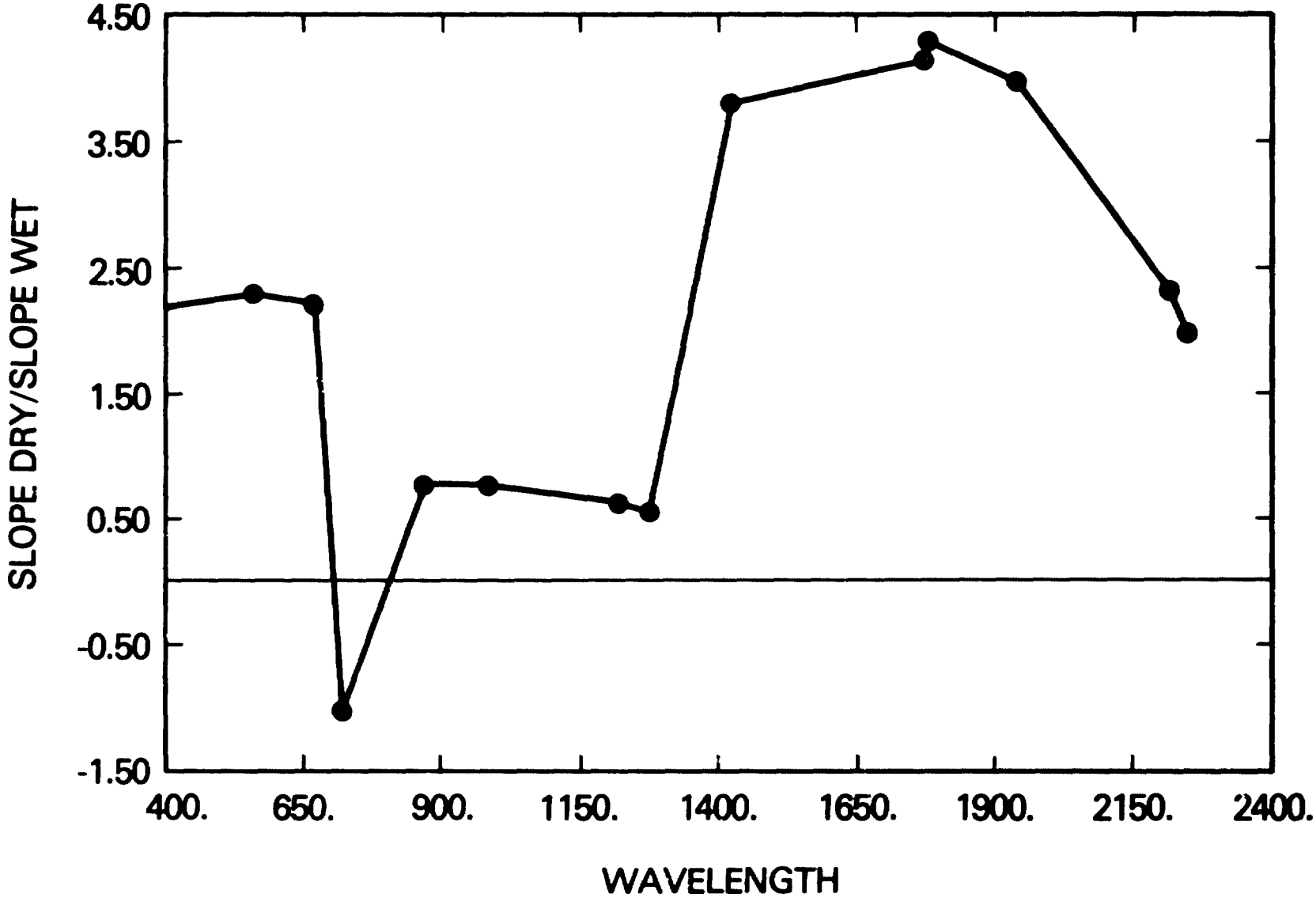

Figure 8I-3. Ratios of regression slopes for soybean canopy cover vs spectral reflectance relationships for selected spectral bands.

J. RADIOMETRIC RESOLUTION FOR MONITORING VEGETATION: HOW MANY BITS ARE NEEDED?

by

C. J. Tucker

OBJECTIVES

The work described herein was undertaken to explore and quantify the relationship between the number of quantizing levels of a satellite remote sensing system and the ability of that system to resolve spectral information related to physiological condition from vegetated surfaces. The approach was taken where in situ collected reflectance data, computed radiance data for the orbital altitude of the sensor system in question, and simulated digital count satellite scanner system output for 16, 32, 64, 128, 256, and 512 quantizing levels were evaluated. These relationship(s) were quantified statistically by regressing the spectral variables against sampled plant canopy biological data. Comparison of coefficients of determination (r^2 values) then allowed for quantifying the improvement(s)/degradation(s) resulting from the different quantizing levels.

The research described in this report addressed the specific question of how many quantizing levels or number of bits were required for earth resource satellite missions which monitor vegetation resources. To accomplish this end, Landsat-D Thematic Mapper bands TM3(0.63-0.69μm) and TM4 (0.76-0.90μm) were selected for detailed radiometric resolution study. TM3 was selected because it receives spectral radiances which are very low in energy as a result of chlorophyll absorption in the 0.63-0.69μm region. TM4 was selected because it receives spectral radiances which are very high in energy as a result of the high levels of foliar spectral reflectance characteristic of green vegetation. These two bands represented the two extremes in the 0.40-2.50μm spectral region for remote sensing of vegetation missions.

Three in situ collected data sets were originally used for this study. They included a September, 1971 grassland data set; an April, 1978 winter wheat data set; and May, 1978 data set. The three data sets were selected because they represented a range of different reflectance values and also represented data from a natural ecological scene (the grassland data) and agricultural scenes (the winter wheat data). For the sake of brevity, however, only the 1971 grassland data will be discussed herein. Extremely similar experimental results were also found for the winter wheat data sets.

BACKGROUND

Satellite sensor bands receive spectral radiances according to their spectral configuration. The in situ data used for this analysis were spectral reflectance data and thus conversions were made to express the spectral reflectance data as spectral

radiance data. To accomplish this, an atmospheric transmission model was used where each of the spectral reflectances were illuminated by a computed spectral irradiance value at sea level. The resulting spectral radiance then was passed directly overhead to a 706 km orbital altitude (Figure 8J-1). Data input values to the atmospheric model included the reflectances of TM3 and TM4(i.e., the reflectance data; Table 8J-1), twelve solar zenith angles, and a horizontal visibility at sea level of 27 km.

The atmospheric radiative transfer model which was used for this analysis was based on the Turner and Spencer (1972) model. This simulation program calculated the spectral path radiance and the total spectral radiance at any altitude in the earth's atmosphere according to a modified 2-stream radiative-transfer function. The path radiance was a function of the solar zenith angle, the nadir view angle, the azimuth angle between the vertical solar plane and the vertical view plane, the horizontal visibility at sea level, the surface background spectral reflectance, and the target spectral reflectance. The horizontal visibility at sea level was a surrogate for the atmospheric aerosol concentration. The atmosphere was treated as being plan-parallel, horizontally homogeneous, and nonabsorbing which was bounded by a spatially uniform Lambertian surface.

After the reflectance data were converted into radiances and passed directly overhead to 706 km, they were "remotely sensed" by a computer program which converted the radiances into digital count output values for 16, 32, 64, 128, 256, and 512 quantizing levels (i.e., 4,5,6,7 8, and 9 bits). This was done for TM3 by using the saturation target reflectance value of 53% for a solar zenith angle of 22° and a clear rural atmosphere horizontal visibility of 27 km. The saturation target reflectance value of 75% was used for TM4 with the identical atmospheric conditions. Ten percent was added to each maximum saturation to bring each value exactly in line with the Mapper specifications for TM3 and TM4.

RECENT ACCOMPLISHMENTS

Results of the analysis demonstrated that solar zenith angle had an effect on $QE\Delta\rho$ (Figure 8J-2), that 256 quantizing levels gave a 1-3% improvement per channel over 64 quantizing levels (Figure 8J-3), and the 256 quantizing levels gave a 1% improvement per channel over 128 quantizing levels. No improvements were found for 256 vs 512 quantizing levels.

CONCLUSION/SIGNIFICANCE

1. The solar zenith angle was found to have an influence upon the noise equivalent change in reflectance.

2. Quantizing levels had a decided effect upon the ability to resolve spectral radiances which were highly related to plant canopy vegetational status.

3. TM3 and TM4 showed a per channel improvement of 1-3% for 256 levels vs 64 levels. A slight (approximately 1%) improvement resulted from 256 levels vs. 128 levels. No improvements were found for 512 vs 256 levels.

4. The TM4/TM3 ratio and the normalized difference showed a 1-2% improvement for 256 levels vs. 64 levels. No improvements were found for 256 levels vs. 128 levels for these linear combinations.

5. Either 128 or 256 quantizing levels appear optimum for orbital monitoring of terrestrial vegetation for TM3 and TM4 bands or similar sensor bands. However, the data rate for 256 quantizing levels is 12.5% higher than the data rate for 128 quantizing levels, other parameters being identical.

6. The radiometric resolution of the Thematic Mapper was found to be closely matched to the scene dynamic radiance range for targets without incorporating variable gain control in the instrument.

FUTURE EMPHASIS

The project was completed and has been submitted to journal. The results of this study can be confirmed by analysis of thematic mapper on SPOT imagery when these future satellite systems are launched.

REFERENCES

Tucker, C.J. 1980. Radiometric Resolution for monitoring vegetation: How many bits are needed? Submitted to the International Journal of Remote Sensing.

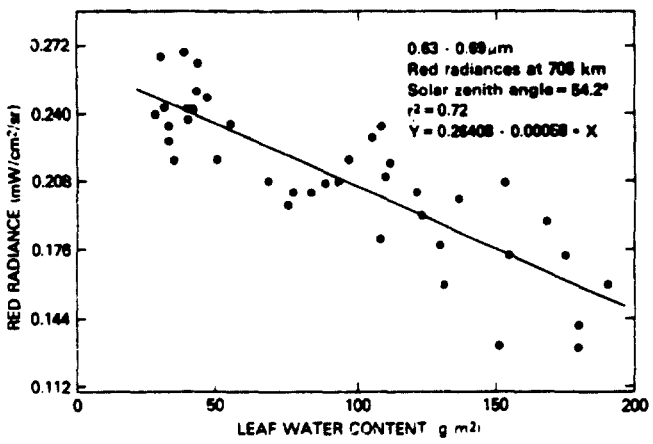

A

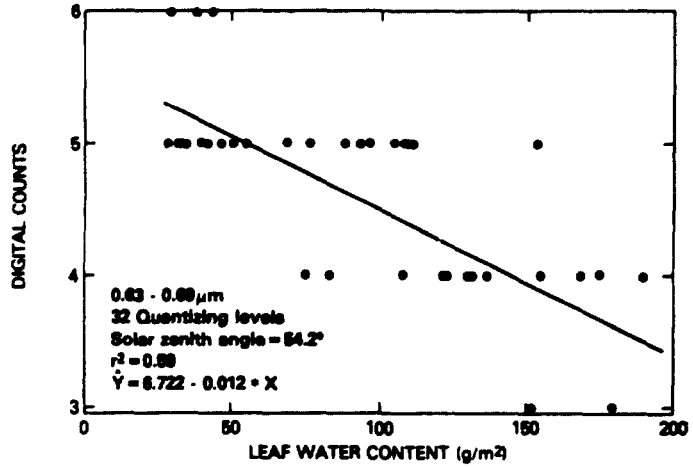

C

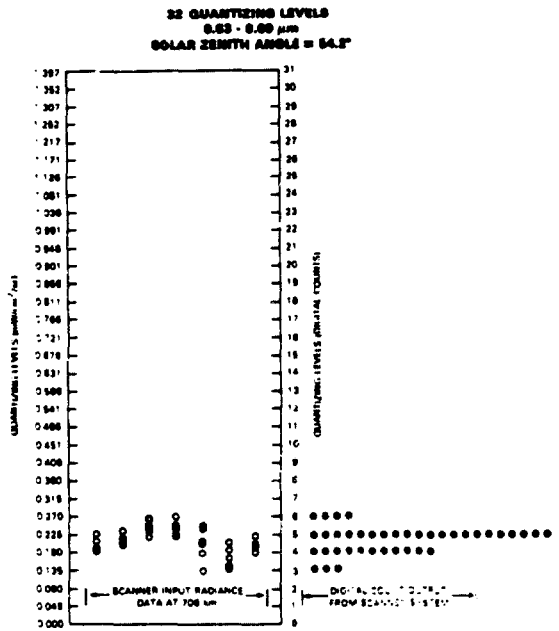

B

Figure 8J-1. Conversion of TM3 (0.63-0.69μm) radiance data at 706 km into digital count data for TM3 with 32 quantizing levels. (A) represented the radiance data presented to the satellite band, (B) showed the quantizing levels (in energy units and the associated digital count values) and digital count output for the data in question, and (C) plotted the digital count output from (B) against the leaf water content. The degrading effect of quantizing at 32 levels was apparent by comparing (A) to (C).

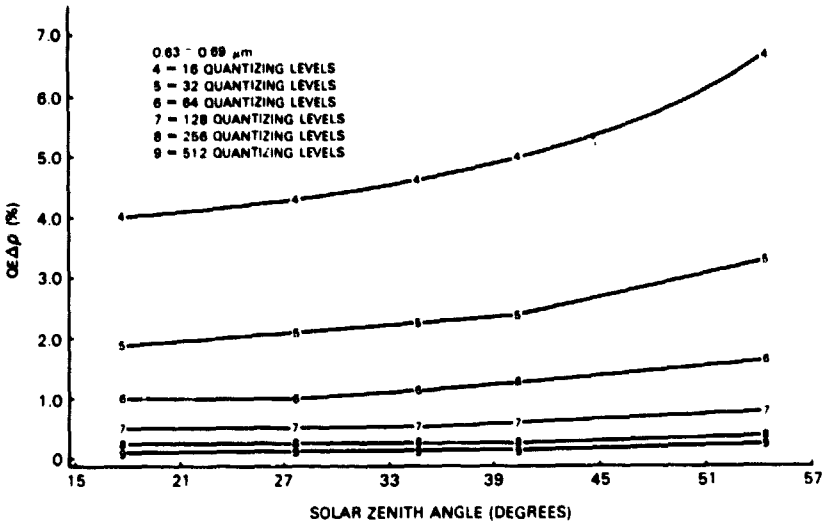

A

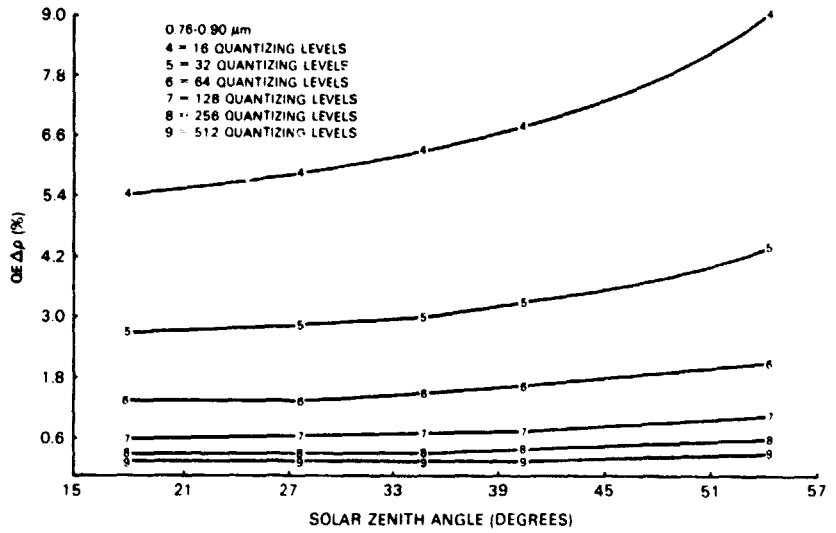

B

Figure 8J-2. The noise equivalent change in reflectance (NEΔρ) for (A) TM3 and (B) TM4 as a function of solar zenith angle and number of quantizing levels for a clear rural atmosphere (horizontal visibility at sea level equaled 27 km).

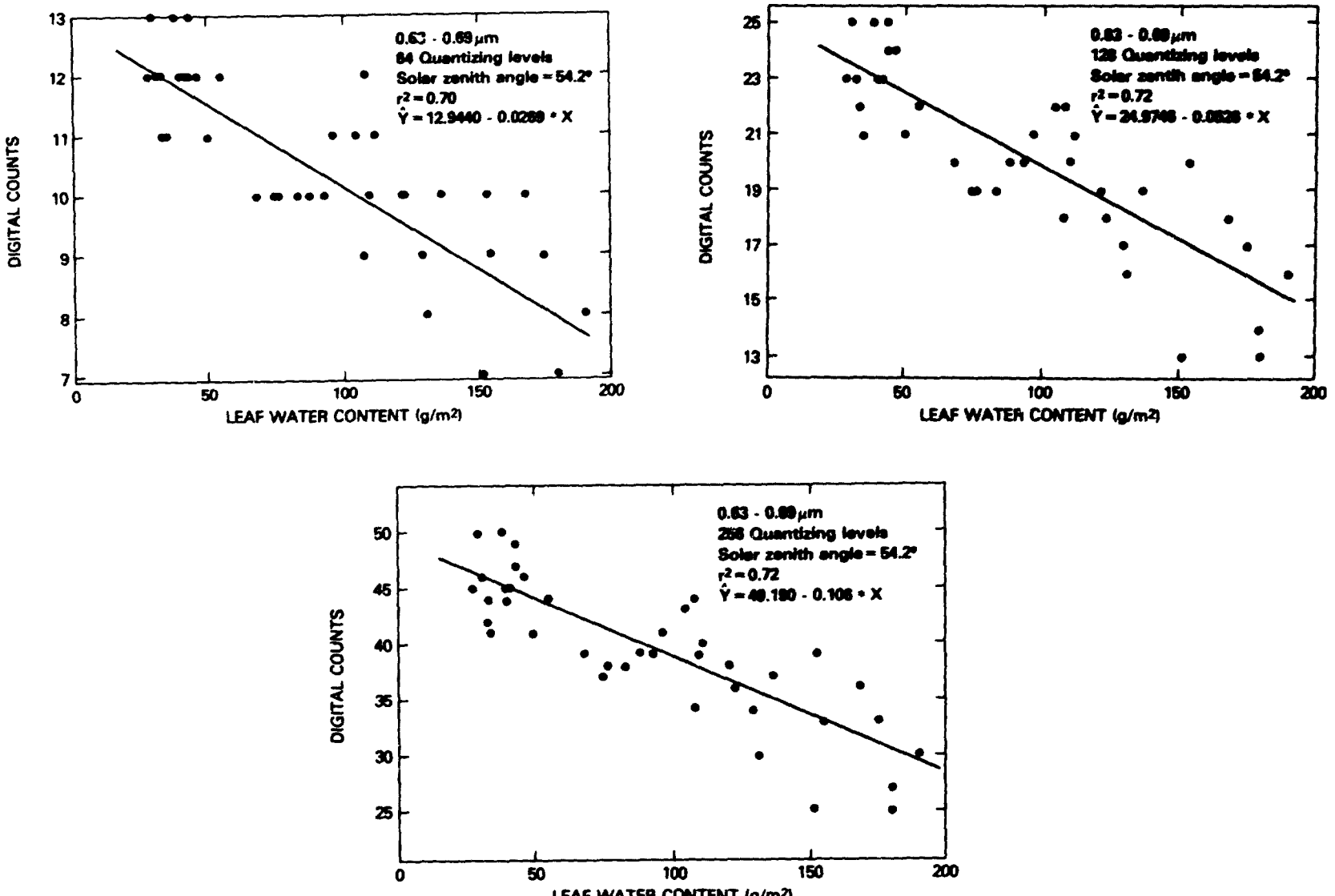

Figure 8J-3. TM3 digital count output plotted against the leaf water content for the September, 1971 data for (A) 64 quantizing levels, (B) 128 quantizing levels, and (C) 256 quantizing levels. Note the 2% improvement between 64 and 256 quantizing levels. Similar regression results were found for TM4.

Table 8J-1. Coefficient of Determination (r^2) Values Resulting from the Regressions Between the Spectral Variables for Five Solar Zenith Angles and Leaf Water Content for the September, 1971 Data. TM3=0.63-0.69 μm, TM4=0.76-0.90 μm, ND = (TM4-TM3)/(TM4+TM3), and RATIO = TM4/TM3.

SPECTRAL VARIABLE	SOLAR ZENITH ANGLE (DEGREES)	NUMBER OF QUANTIZING LEVELS						RADIANCES AT 706 KM	INPUT REFLECTANCES
		16	32	64	128	256	512		
TM3	54.2	0.50	0.59	0.70	0.71	0.72	0.72	0.72	0.72
TM3	40.27	0.50	0.69	0.72	0.71	0.72	0.72	0.72	0.72
TM3	34.62	0.60	0.70	0.71	0.72	0.72	0.72	0.72	0.72
TM3	27.68	0.59	0.66	0.71	0.72	0.72	0.72	0.72	0.72
TM3	17.65	0.49	0.68	0.68	0.71	0.72	0.72	0.72	0.72
TM4	54.2	0.67	0.60	0.74	0.77	0.76	0.76	0.76	0.76
TM4	40.27	0.41	0.72	0.75	0.76	0.76	0.76	0.76	0.76
TM4	34.62	0.68	0.77	0.78	0.75	0.76	0.76	0.76	0.76
TM4	27.68	0.71	0.66	0.74	0.76	0.77	0.76	0.76	0.76
TM4	17.65	0.48	0.67	0.76	0.76	0.77	0.76	0.76	0.76
ND	54.2	0.74	0.77	0.84	0.85	0.85	0.86	0.85	0.85
ND	40.27	0.61	0.81	0.86	0.85	0.85	0.85	0.85	0.85
ND	34.62	0.78	0.85	0.84	0.86	0.85	0.85	0.85	0.85
ND	27.68	0.77	0.79	0.84	0.85	0.85	0.86	0.85	0.85
ND	17.65	0.62	0.82	0.84	0.85	0.86	0.85	0.85	0.85
RATIO	54.2	0.70	0.76	0.81	0.82	0.82	0.82	0.82	0.82
RATIO	40.27	0.61	0.80	0.84	0.81	0.82	0.82	0.82	0.82
RATIO	34.62	0.76	0.82	0.80	0.83	0.82	0.82	0.82	0.82
RATIO	27.68	0.73	0.76	0.81	0.82	0.82	0.82	0.82	0.82
RATIO	17.65	0.58	0.78	0.80	0.82	0.83	0.82	0.82	0.82

K. THEMATIC MAPPER VERSUS MULTISPECTRAL SCANNER FOR CROP MONITORING

by

B.L. Markham and J.L. Barker

OBJECTIVES

The objective of this study was to compare the Multispectral Scanner (MSS) and the Thematic Mapper (TM) reflective bands for determining crop status as measured by percentage canopy cover. The effects of (1) spectral and radiometric differences between the sensors' bands and (2) atmospheric haze differences among bands on crop monitoring ability are being evaluated.

BACKGROUND

The Thematic Mapper to be carried on Landsat-D incorporates a number of engineering improvements over the Multispectral Scanners on earlier Landsats. These changes include additional spectral bands and increased spectral and radiometric resolution. These improvements are designed to increase the usefulness of the data for monitoring earth resources, particularly vegetated targets. Relatively little documentation of the expected improvement in crop monitoring capability resultant from these engineering changes is available. This study attempts to quantify the effect of these changes for corn and soybean crops and one measure of crop status (percentage canopy cover).

RECENT ACCOMPLISHMENTS

Field spectral reflectance and agronomic measurements of corn and soybean plots collected as part of the 1978 NASA-GSFC/USDA-BARC cooperative project were used for evaluation of MSS versus TM in this study. The narrow-band spectral reflectance measurements were converted to at-satellite-altitude radiances for selected atmospheric conditions and sun elevations using an atmospheric model, and were then integrated across the appropriate spectral intervals for each MSS and TM band, weighted by detector spectral response curves. These integrated radiances were combined in ratios and normalized differences and linearly regressed against percentage canopy cover for the growth portion and the senescence portion of the growing season. The coefficients of determination of the linear regressions provided the figure of merit for comparison of MSS and TM.

In comparing the TM bands with their MSS counterparts, TM2(.52-.60um)vs. MSS4 (.50-.60um); TM3(.63-.69um) vs. MSS5 (.60-.70um); TM4(.76-.90um) vs. MSS7 (.8-1.1um), the improved locations and decreased bandwidths of the TM bands resulted in no apparent improvement in performance over the MSS bands. For the growth stages of soybeans and corn, the "best" TM band ratios with MSS counterparts, which were TM4/TM2 for soybeans and TM4/TM3 for corn, had error levels comparable to their MSS counterparts, MSS7/MSS4 and MSS7/MSS5, respectively (Table 8K-1).

For the senescence stage the results are similar, although normalized differences appear more linearly correlated with canopy cover than ratios and the apparent "best" band combinations are different.

The added value of the "new" TM bands - TM1(.45-.52um), TM5(1.55-1.75um) and TM6(2.08-2.35um) for canopy cover measurements appears limited, although the results are conflicting. For soybeans, the "best" ratios involving these bands had higher predicted errors in estimating canopy cover than other bands. For growing corn, however, ratios of TM4 to TM5 and TM6 show higher correlations than other bands, as does the ratio of MSS7/MSS6. The reason for the apparent better performance of these ratios for corn has not been resolved, although it may be a result of larger amounts of noise in the corn data. What the "new" TM bands may provide, especially TM5 and TM6 by covering a different region of the spectrum, is a means to obtain additional independent measures of canopy cover or plant canopy status.

The radiometric sensitivities of the two sensors' bands were simulated by introducing quantization noise to the spectral data. The simulated at-satellite radiances were rounded to 3, 4, 5, 6, 7 and 8 bit levels, and the appropriate band combinations were calculated and regressed with percentage canopy cover. Using the percentage uncorrelated variance in the regressions ($100(1-R^2)$) as a figure of merit, a general increase in uncorrelated variance (error) with decreased bit rate was observed (e.g., the points in Fig. 8K-1). However, without some form of a best fit curve, quantitative evaluation of the effect of a given change in radiometric sensitivity was not possible, due to the scatter of the points. Therefore, a curve of the form:

$$\text{PERCENT ERROR} = (100 - I) \cdot e^{(-A \cdot \text{Bit Rate})} + I$$

where I is the percentage error without rounding, and A is the least squares fitting constant, was fit to the data. From these curves, the predicted error levels for bit rates equivalent to the radiometric sensitivities of the previously determined "best" TM and MSS band combinations were extracted and compared, where the radiometric sensitivities (NeL) for a given bit rate were given by the quantization step size divided by the $\sqrt{12}$.

For the growing soybean data set, most appropriate for this analysis because of the high R^2 values of the "best" TM and MSS combinations (Table 8K-1), for both the best TM and MSS ratio, the introduction of quantization noise equivalent to sensor noise levels increased the expected error from its limiting value (error without rounding) by less than 1% (Figure 8K-1).

The indicated improvement resultant from the increased radiometric sensitivity of the TM bands over the MSS bands is .5% (from 1.8 to 1.3% error) while only .1% error change is indicated with further radiometric sensitivity improvement. These results suggest that both the MSS and TM are on the shoulder of the radiometric performance curve for canopy cover measurements for soybeans, such that although approximate doubling of radiometric sensitivity of the TM over the MSS increased performance .5%, further doubling of radiometric sensitivity would increase performance only .05%.

SIGNIFICANCE

The expected performance improvements of the TM over the MSS due to improve spectral and radiometric characteristics were not conclusively evident in this study, though potential improved utility was apparent. The spectral performance improvements are expected to be realized more fully for other measures of crop status and the radiometric improvements more useful for crops growing under poorer illumination conditions than the summer, mid-latitude corn and soybean conditions evaluated.

FUTURE EMPHASIS

Although this study is complete, except for evaluation of the atmospheric simulations and a final report, investigations of the improved utility of TM versus MSS will continue as part of the Landsat-D assessment work.

Table 8K-1. Average* Percent Uncorrelated Variance ($100(1-R^2)$)
In Linear Regressions of Spectral Transformations and Canopy Cover

			Soybeans				Corn			
			Growth (N=9)		Senescence (N=9)		Growth (N=10)		Senescence (N=8)	
Sensor	Band A	Band B	RATIO[1]	ND[2]	RATIO	ND	RATIO	ND	RATIO	ND
	4	2	.8	3.1	17.5	7.0	32.6	29.9	2.3	1.7
	4	1	1.8	7.6	13.8	7.0	46.3	39.3	2.5	3.2
TM	4	3	1.9	3.9	15.4	4.0	29.1	29.7	2.5	1.6
	2	3	3.0	2.4	5.7	6.3	30.5	29.6	1.0	.7
	4	6	3.3	5.6	14.6	5.4	13.0	19.6	2.1	3.3
	4	5	6.7	7.7	11.7	4.6	14.1	14.9	2.5	1.6
	7	4	.8	4.0	16.2	7.2	37.1	33.4	2.2	1.8
	6	4	.9	2.2	15.7	8.9	47.6	43.2	2.2	2.3
MSS	7	5	1.5	3.4	15.7	4.4	28.1	28.5	2.4	1.2
	6	5	1.5	1.6	15.0	5.6	33.5	32.2	1.9	1.2
	7	6	3.9	5.3	62.2	62.2	12.3	13.0	3.8	4.3
	5	4	3.9	3.2	5.4	6.4	27.0	25.9	.5	.5

[1] RATIO=BAND A/BAND B

[2] $ND = \frac{(\text{BAND A}-\text{BAND B})}{(\text{BAND A}+\text{BAND B})}$

*Average of 3 field plots for soybeans, 2 field plots for corn

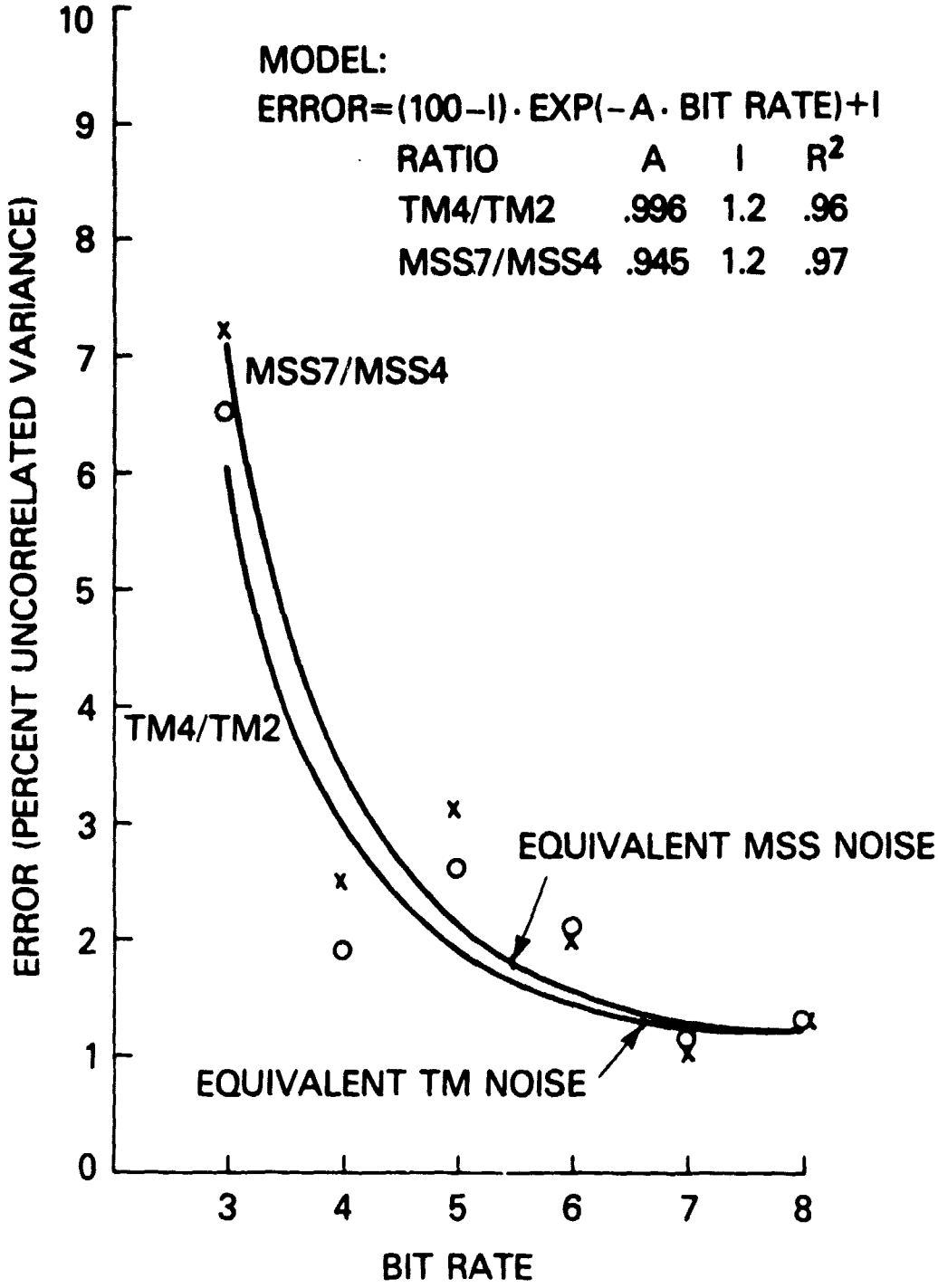

Figure 8K-1. TM Versus MSS Best Ratio Performance as Function of Quantizing Bit Rate (Growing Soybeans-20 KM Atmospheric Visibility)

L. SPECTRA OF ISOLATED VEGETATIONAL CONSTITUENTS

by

E. W. Chappelle and F. W. Wood

OBJECTIVE

The objective of the study is to identify the spectral bands and determine the spectral responses, as measured by a field spectometer, which relate to individual plant components.

BACKGROUND

Studies relating to reflectance of plant components are essential to the rational interpretation of spectral data collected on a vegetational scene. Such studies may yield important insight into the plant physiological factors and, hence, possibly to production factors, that affect spectral reflectance of crop canopies.

The major plant constituents are chlorophyll, beta-carotene, protein, starch, and carbohydrates. The laboratory spectra of these compounds, both absorption and reflective, have been well documented. There is, however, a paucity of information regarding the spectra of mixtures of these compounds. Also, the spectra of chlorophyll have been most often studied in organic solvents such benzene and chloroform which produces shifts in the maxima and minima of the points of absorption.

RECENT ACCOMPLISHMENTS

Using a non-laboratory field reflectometer with a relatively low resolution, preliminary spectral analyses have been conducted on purified chlorophyll a, beta-carotene, and dried wheat grains (Figure 8L-1). The spectra were compared to that of a soybean crop at a 100 percent canopy cover.

A striking difference is seen between the spectra of pure chlorophyll a and soybeans where the 560 nm band response of chlorophyll is much higher than that of soybeans. There is also no 985 nm absorption in chlorophyll as seen in soybeans. As would possibly be expected, chlorophyll shows no water absorption bands at 1240 and 1940 nm. There are other subtle differences between chlorophyll and soybeans that can be seen by examination of the spectra. Beta-carotene absorbs strongly throughout 560 and 670 nm. While the wheat grains do not show a characteristic chlorophyll absorption, the remainder of its spectra are similar to that of soybeans.

FUTURE EMPHASIS

Further spectra of pure plant components will be made as well as spectra on controlled mixtures of these pure components.

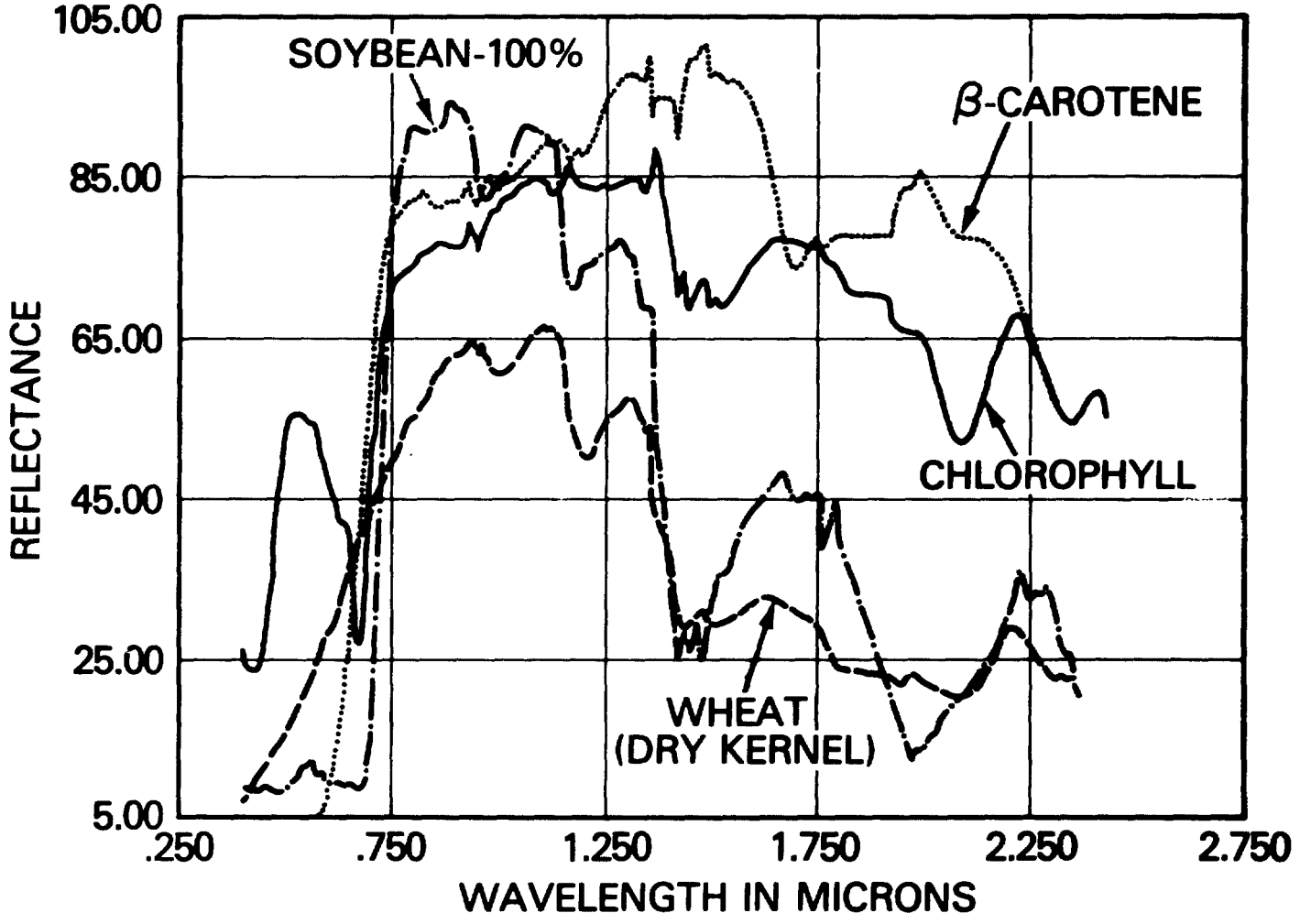

Figure 8L-1. Spectral reflectance of beta-carotene, chlorophyll a, and dried wheat kernals referenced to the field measured reflectance of a soybean canopy.

M. A SPECTRAL METHOD FOR DETERMINING THE PERCENTAGE OF GREEN HERBAGE MATERIAL IN CLIPPED SAMPLES

by

C. J. Tucker

OBJECTIVE

The objective of this experiment was to develop a spectral method for rapidly assessing the percentage of live herbage in clipped samples.

BACKGROUND

Green and brown biomass components are currently being performed via detailed and tedious hand sortings, which are extremely time-consuming and expensive.

RECENT ACCOMPLISHMENTS

A laboratory radiometric method for the rapid determination of green and brown vegetation precentages in clipped grass samples has been developed and tested (Figure 8M-1). The method uses red and photographic infrared radiance or reflectance differences between green and brown vegetation. Mixtures of green and brown material were found to have radiances or reflectances proportional to the percentage of green material present. This method may permit the use of rapid green/brown radiometric determinations to replace the tedious hand sorting now generally used. It may also have application in remote sensing of vegetation ground-truth work where the determination of dry green biomass in clipped samples is necessary.

CONCLUSION/SIGNIFICANCE

Red and photographic infrared spectral data were found to be highly correlated to the percentages of green and brown herbage material in clipped grass samples (Table 8M-1).

The red reflectance and radiance and the normalized difference were found to be most highly correlated to the percentage of green/brown herbage (Figure 8M-2).

Microwave drying of the grass samples prior to weighing and combining resulted in improved regression relationships.

FUTURE EMPHASIS

This technique is currently being tested by D.W. Deering for clipped herbage samples taken in a rangeland vegetation complex, and preliminary results are reported in the following article (N).

REFERENCES

Tucker, C.J. 1980. A spectral method for determining the percentage of green herbage material in clipped samples. Remote Sensing of Environment (in press).

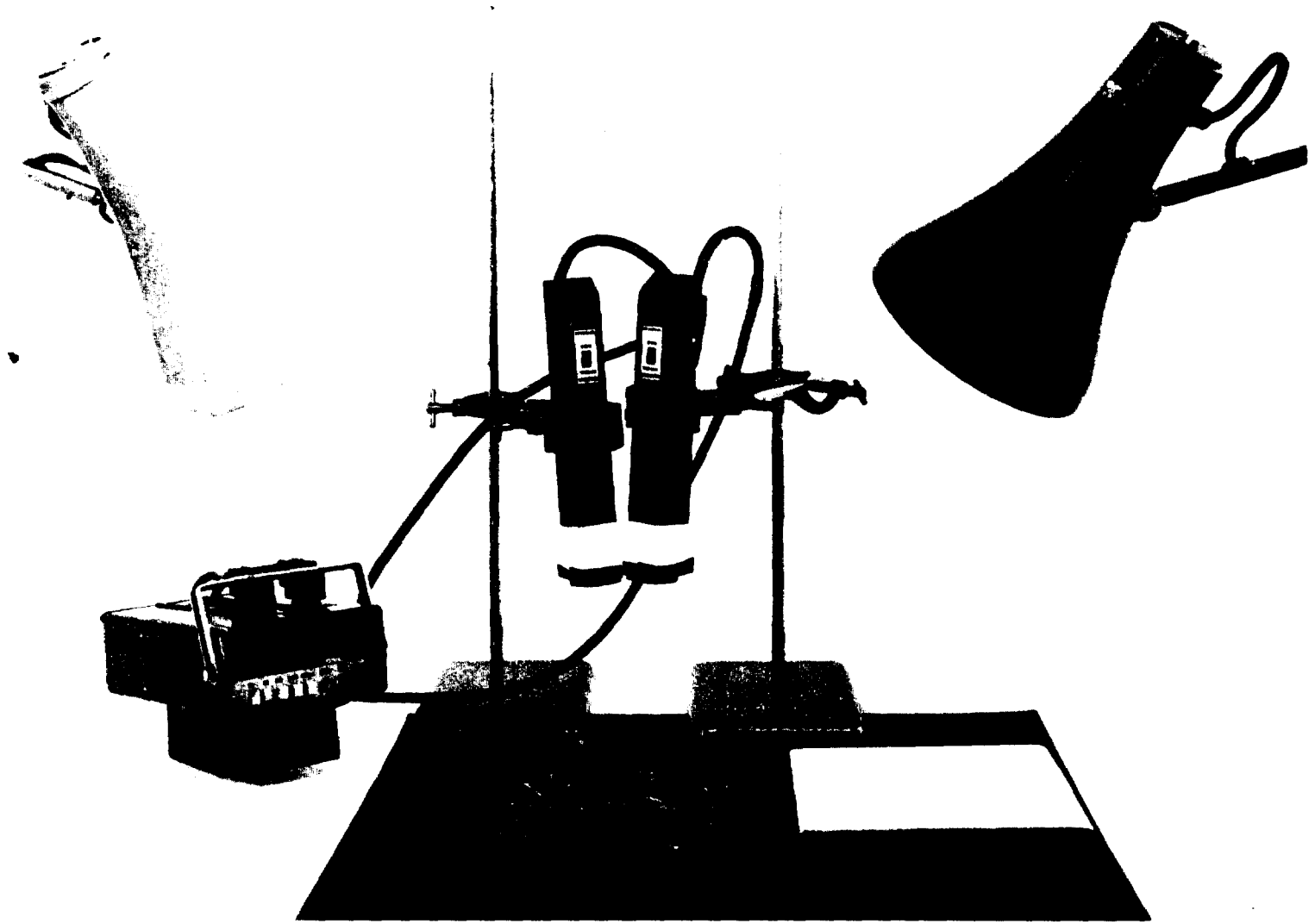

Figure 8M-1. Hand-held digital radiometer used as a green/brown estimation device. The instrument consists of a digital radiometer which measures radiances from laboratory samples through two filtered probes.

Table 8M-1. Coefficients of determination (r^2 values) between the four spectral variables and the percentage of green material in the various samples. RAD = radiance, RFL = reflectance, Red = 0.650-0.700μm, IR = 0.775-0.825μm, IR/Red = radiance or reflectance ratio, and the normalized difference (ND) = (IR-red/(IR + red).

Variable	RAD	RFL	RAD	RFL	RAD	RFL	RAD	RFL
	Wet R11		Wet R12		Wet R21		Wet R21	
Red	0.83	0.92	0.89	0.95	0.95	0.92	0.96	0.94
IR	0.67	0.08	0.76	0.89	0.81	0.92	0.92	0.93
IR/Red	0.91	0.88	0.80	0.79	0.78	0.79	0.79	0.79
ND	0.96	0.93	0.90	0.91	0.93	0.95	0.96	0.95
	Dry R31		Dry R32		Dry R41		Dry R42	
Red	0.97	0.96	0.99	0.97	0.98	0.99	0.98	0.99
IR	0.02	0.02	0.04	0.43	0.72	0.54	0.78	0.65
Ir/Red	0.96	0.96	0.97	0.97	0.96	0.96	0.94	0.94
ND	0.98	0.97	0.99	0.99	0.99	0.99	0.99	0.99

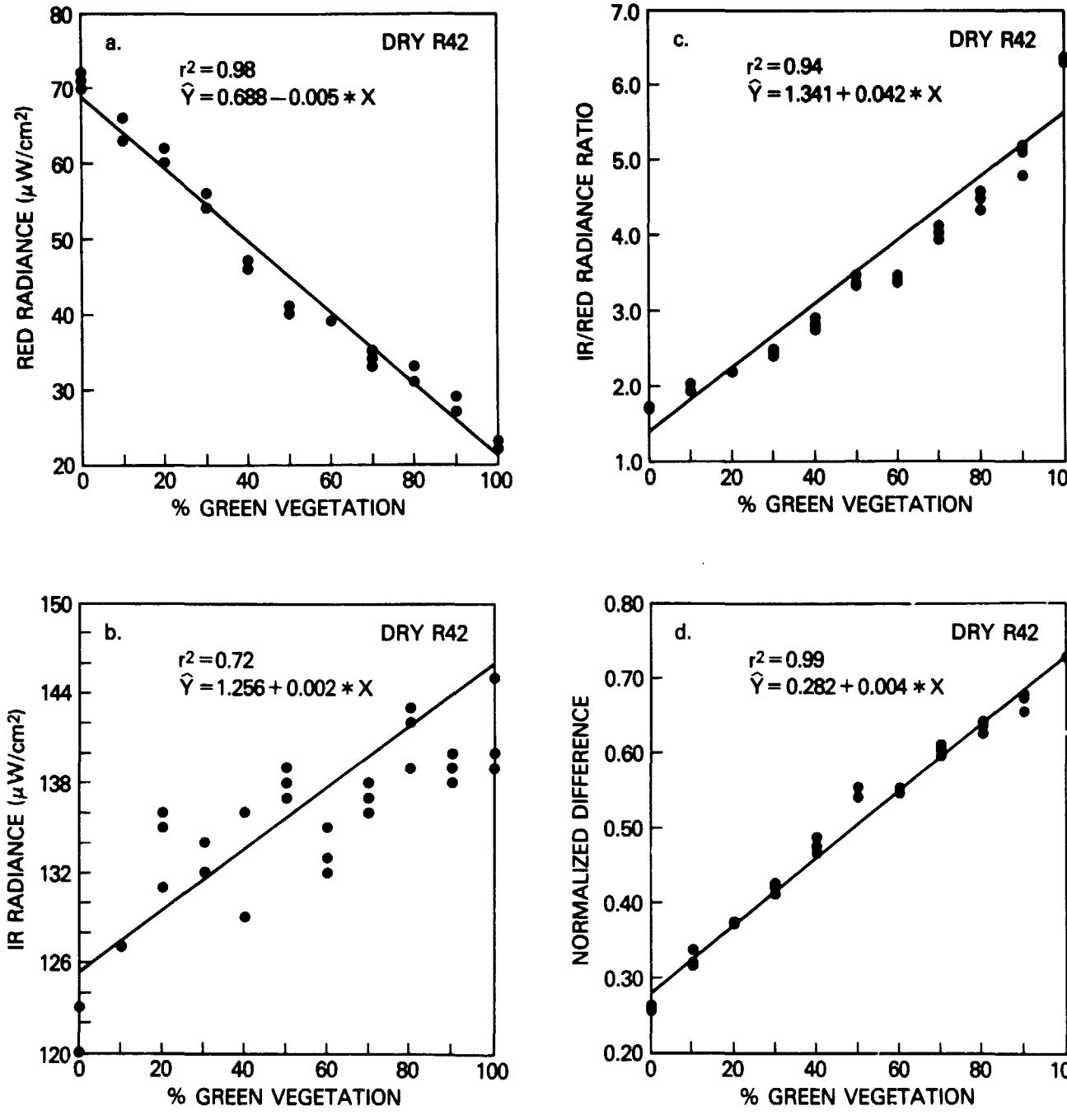

Figure 8M-2. Spectral data plotted against the percentage of green material in the 20-g clipped sample using microwave-dried PRG. (a) Red radiance, (b) IR radiance, (c) IR/red radiance ratio, (d) Normalized difference.

D58

N80-20781

N. EVALUATION OF A SPECTRAL METHOD FOR PERCENTAGE GREEN DETERMINATION USING CLIPPED RANGELAND FORAGE SAMPLES

by

D. W. Deering

OBJECTIVE

The objective of this study was to evaluate, using rangeland forage samples, a spectral "laboratory" method for determining the percentage of green herbage material in clipped samples that had previously been reported for a somewhat artificial, monospecies sample set.

BACKGROUND

Very encouraging results were reported from an experiment to develop a laboratory radiometric technique for the rapid determination of green and brown proportions of vegetation in clipped grass samples (see article no. 8M by C.J. Tucker). It was hoped that a spectral assessment technique could be developed to replace the tedious, time-consuming, hand sorting method that is generally used.

The determination of the quantity of green plant material or green biomass and the proportions of green and brown in field samples has long been an important activity in vegetation analysis for resource management and scientific investigations. More recently, it has become necessary in quantitative remote sensing investigations in agriculture, rangelands, forestry, and other vegetation-oriented disciplines. Frequently, the difficulties involved in originally acquiring and subsequently analyzing the herbage samples discourage and prevent the collection of such quantitative ground truth. Therefore, a simple, rapid and accurate method for the determination of the percentage green herbage and, subsequently, the dry green biomass in clipped herbage samples would be a valuable tool.

The same type of two-channel radiometer with red (0.64-0.69 μm) and photographic infrared (0.79-0.83μm) spectral bands was used in this study and in the study by Tucker. A similar approach to sample preparation (including chopping and mixing) and spectral measurements was used (including a black background, use of 150W bulbs, $BaSO_4$ reflectance panel, remixing, three replicates/sample) for both experiments. The clipped rangeland herbage samples were oven-dried, therefore, no fresh or "wet" sample analyses were possible. However, Tucker reported the best results with oven-dried samples so this should not be held as a detriment to the experiment.

The experiment by Tucker used fresh green perennial ryegrass, which was manually combined with dead brown grass hay of the same species to create the desired green/brown proportions. The 42 rangeland forage samples were collected as ground truth for a rangeland remote

sensing investigation in West Texas in April 1979 over a wide variety of vegetation/soil types (range sites). The species composition, the proportion of green to brown and the proportion of leaf to stem components in the samples varied enormously. Yet this is the "real world" situation in natural vegetation sampling and, consequently, constitutes a rigorous but important test of the method.

RECENT ACCOMPLISHMENTS

The red and photographic infrared radiances were converted into reflectances to adjust the data for significant light source variations between sample readings. The individual red and infrared reflectance measurements were linearly related to the percentage green vegetation in the clipped rangeland forage samples (Figure 8N-1), but the results of the correlation analysis revealed that a large amount of the variability in spectral response was not directly related to the percentage green vegetation. Coefficients of determination (r^2) were 0.32 and 0.48 for the red and infrared, respectively.

The infrared/red ratio and the Normalized Difference or ND (Infrared-Red)/(Infrared+Red) parameter have frequently been used as green vegetation indices, and Tucker reported that these two vegetation indices, particularly ND, were very highly correlated with the percentage of green herbage. The infrared/red ratio relationship to percentage green range herbage in the current experiment was considerably improved (r^2 = 0.69) over the individual red and infrared reflectance relationships, but the ND parameter exhibited the highest correlation (r^2 = 0.75; Figure 8N-2).

Two observations concerning the range forage sample data are significant. First, despite the greater variability in the range forage sample analysis, a very high correlation was exhibited with the ND parameter. Second, and possibly most important, the ND vs. percentage green vegetation regression equations were almost identical in both studies (Y = 0.226 + 0.004 X for range samples; Y = 0.282 + 0.004 X for ryegrass samples).

SIGNIFICANCE

The aforementioned results lead to the suggestion that it may be feasible to determine a "universal" regression equation estimator and develop a standardized technique for laboratory radiometric analysis of percentage green herbage for clipped and dried ("preserved") herbage samples from a wide variety of vegetation types.

FUTURE EMPHASIS

The spectral method of percentage green herbage determination will be further tested on additional rangeland forage samples as well as agricultural crop field samples. An attempt will be made to develop standardized laboratory techniques and a "universal" regression estimator.

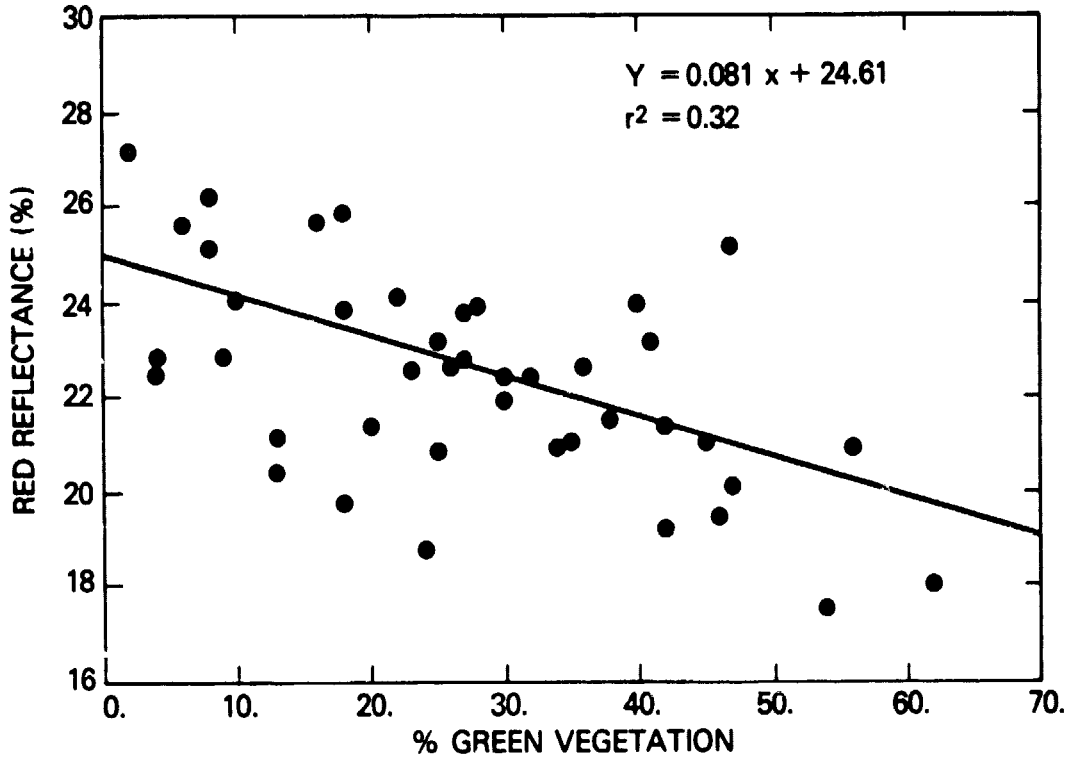

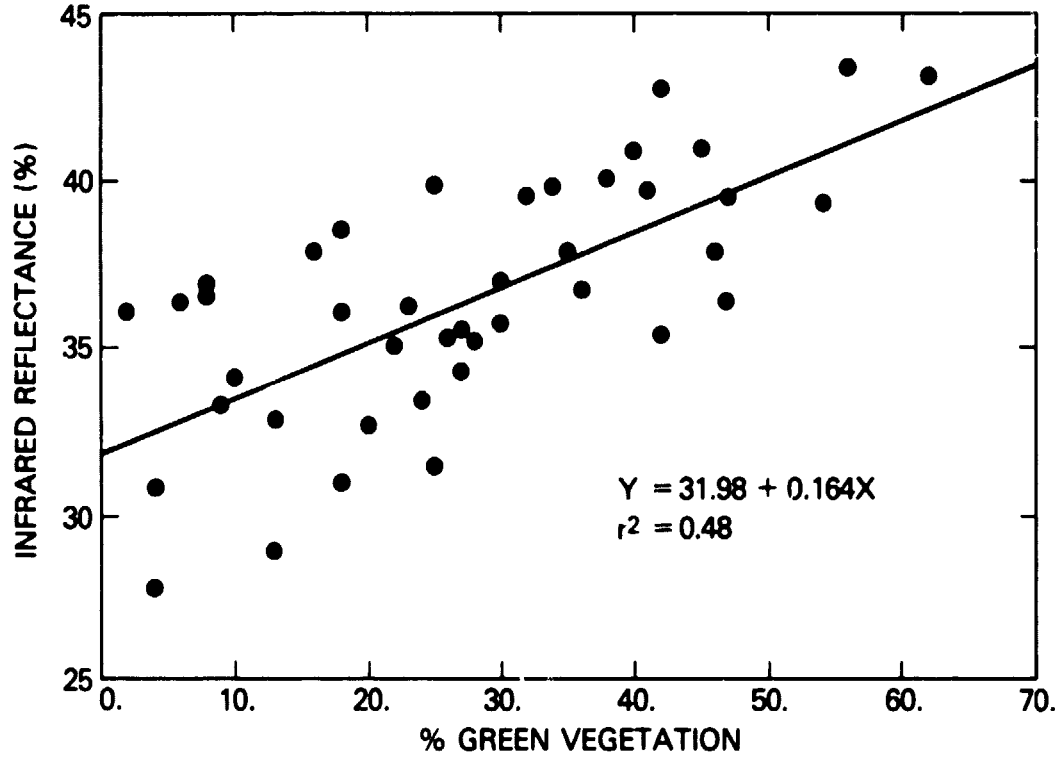

Figure 8N-1. Red and photographic infrared reflectance vs. the percentage green vegetation in rangeland forage samples from a diverse selection of range sites in West Texas.

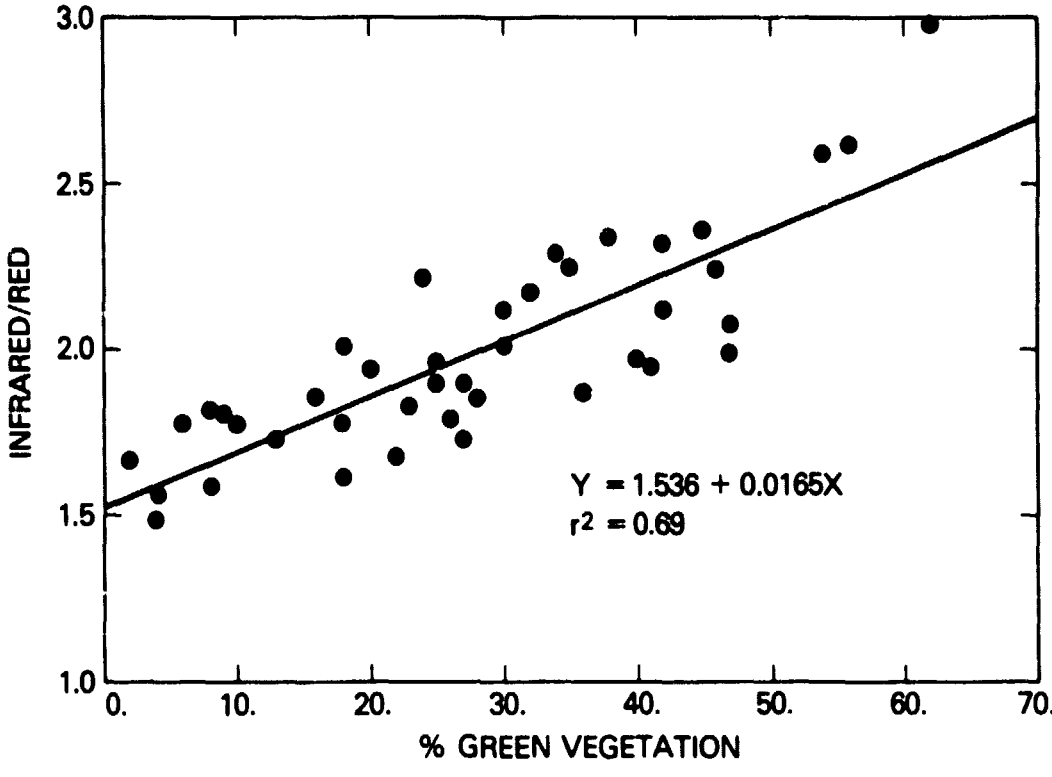

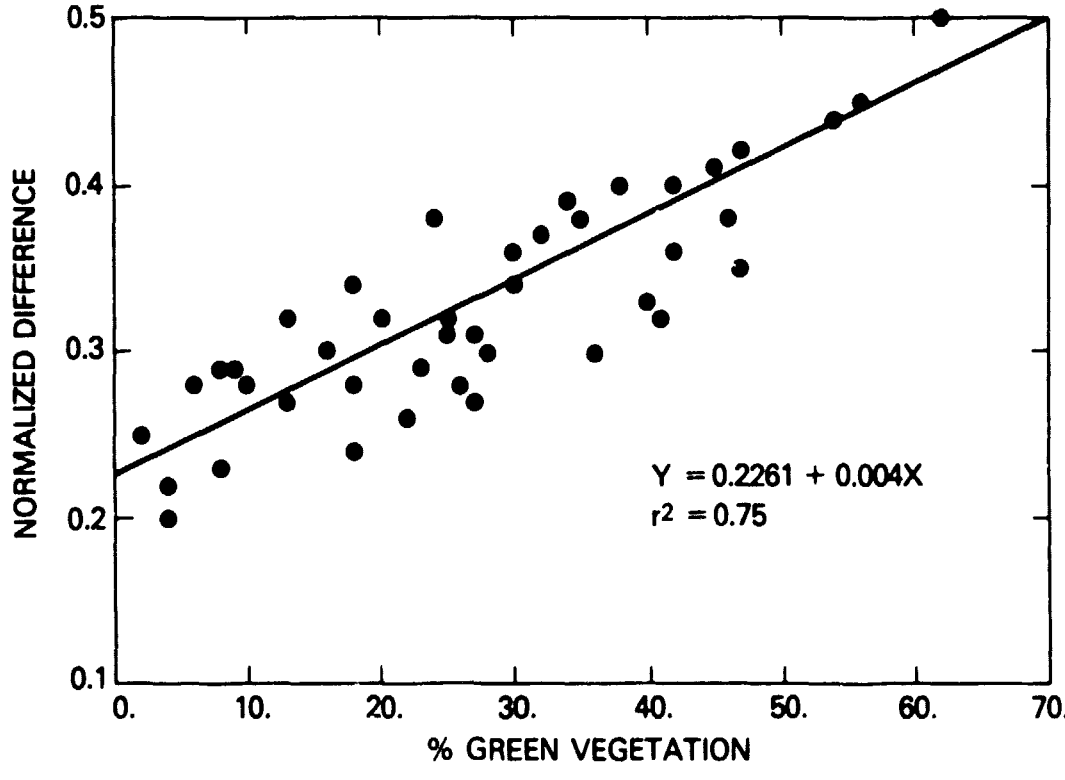

Figure 8N-2. Infrared/red ratio and Normalized Difference (IR-Red)/(IR+Red) parameters vs. the percentage green vegetation in rangeland forage samples from a diverse selection of range sites in West Texas.

N80-20782

A. LANDSAT-D ASSESSMENT SYSTEM

by

D. Williams, D. Deering, K. Meehan, and J. Tucker

OBJECTIVE

The objective of the Landsat-D Assessment System (LAS) is to provide a facility and capability to perform analyses that will quantify the engineering and technological advantages afforded by the Landsat-D system, and, in particular, the Thematic Mapper (TM).

BACKGROUND

The four major objectives of the Landsat-D project are: (a) to assess the capability of the TM to provide improved information for Earth Resources management, (b) to provide a transition for both domestic and foreign users from MSS data to the higher resolution and data rate of the TM, (c) to provide system level feasibility demonstrations in concert with user agencies, and (d) to encourage continued foreign participation in the program. Within the total project framework is a ground segment component, referred to as the LAS, to ensure that these major objectives are achieved. LAS activities will include: (a) data quality tests to define and validate output products relative to user applications, (b) TM versus MSS performance evaluation tests to quantify the advantages of the TM improved spatial, spectral, and radiometric resolution in comparison to the MSS, (c) data systems applications tests to demonstrate the ability of the Landsat-D system to provide useful results in a timely manner, and (d) operational sensors and data system studies to determine what might be the appropriate characteristics for an operational system.

Investigations relative to these LAS activities will be conducted in five Investigator Working Groups, referred to as Landsat-D Discipline Experiment Teams (DET). There will be one DET for each of the following major discipline areas:

- o Agriculture, including crop identification, acreage, condition, yield assessment
- o Forest and Rangeland, including plant community differentiation, biomass estimation, range condition and trend
- o Water Resources, including inland water resources and wetlands, observation, inventory management and modeling
- o Geology, including mineral and petroleum exploration
- o Land Resources and Environmental Studies, including land use and coastal zone inventory, planning and modeling and other investigations or situations dealing with environmental problems or concerns.

Non-NASA DET membership will be decided based upon an evaluation of proposals to be solicited by an Announcement of Opportunity (AO). Successful proposers will be appointed to membership on one experiment team only. Two NASA scientists will be appointed to each team, and at least one of these scientists will be from Goddard. In addition to conducting data use investigations, the NASA appointees will serve as executive secretary and coordinator on day to day team matters and will act as liaison with major NASA projects and ongoing NASA-sponsored research efforts.

Until formal DET membership is definitized, an internal DET advisory group has been appointed to assist the Landsat-D Project Scientist in defining and/or reviewing the LAS facility layout, software requirements, data formats, etc. and to conduct pre-launch investigations using aircraft-acquired TM simulator (TMS) data. Four Earth Resources Branch discipline scientists were appointed to this internal advisory group to represent the agriculture, forest and rangeland, geology, and land resources disciplines.

RECENT ACCOMPLISHMENTS

Through extensive interactions with Information Extraction Division personnel, the functional requirements of the LAS software system and user interface were determined by reviewing the applications capabilities and system structure of several image processing systems familiar to Goddard scientists. These systems were analyzed for strengths that might be incorporated into the LAS, as well as weaknesses that must be avoided. In a parallel effort, typical LAS user scenarios were compiled by discipline to ensure that the man/machine interfaces needed for effective application of the LAS software were considered. The Information Extraction Division summarized the resulting information in an internal white paper entitled, "LAS Functional Requirements Document." They have begun the development and implementation of LAS software based upon these inputs.

The majority of the remaining LAS activities and accomplishments were related to the acquisition and preliminary analysis of TMS data, and associated aerial photography and ground truth data. It is the intent of the discipline scientists to utilize these data to quantitatively assess the incremental improvement afforded to the various disciplines by the improved spectral, spatial and radiometric resolution of the TM versus the MSS. During 1979, TMS data were collected over: a forested area in eastern North Carolina (June 14, November 20); agricultural and rangeland areas in Colorado (June 20) and western Texas (April 11*, June 22, September 21); geological areas of interest in central Utah (August 28) and western Montana (August 29); urbanized areas surrounding Washington, D.C. (June 14) and Denver, Colorado (June 20); and areas of surface mining activity in central Pennsylvania (June 14).

Site visits, for the collection of ground truth, were conducted at or near the time of TMS data acquisition for the western Texas, western Montana, and central Pennsylvania study areas. Ground sampling

* The TMS scanner was inoperable at this time and the Bendix MSS scanner was substituted for the TMS.

activities were particularly extensive on the western Texas study area during all three overflights, which were spaced out over the growing season and scheduled to closely coincide with Landsat overpass. The vegetation status was documented on twenty-two vegetation/soil strata by GSFC and Texas A&M researchers, and these data have been analytically summarized for comparison with aircraft and satellite data.

The timely analysis of TMS data by Goddard scientists has been hampered by the inordinately slow processing turnaround at the Johnson Space Center for converting aircraft scanner data from analog to digital format. The only TMS data which were received in time to permit preliminary analysis during 1979 were those collected over the eastern North Carolina forested study area in June. Five of the eight TMS channels (i.e., those corresponding to the first five Landsat-D TM bands) were operational at the time of this overflight, but scene illumination was deteriorated by the presence of thin cirrus clouds above the aircraft. As a result, analysis of these data has been limited to qualitative comparisons of TMS 30-meter spatial resolution, with MSS 80-meter resolution and U-2 aerial photography having 1-2 meters spatial resolution (Fig. 9A-1).

Two studies were conducted during 1979 using spectral data collected in situ, as well as simulated spectral reflectance data, rather than TMS data. One of these studies addressed the number of radiometric quantizing levels required for satellite monitoring of vegetation resources, while the other was initiated to investigate the ability to remotely sense leaf water content in the near infrared portion of the electromagnetic spectrum. Conclusions drawn from these studies indicate that the Landsat-D TM radiometric configuration closely matches scene dynamic radiance ranges without incorporating variable gain control in the instrument, and that TM band 5 (1.55-1.75μm) should be ideal for the remote sensing of plant canopy water status. Both of these investigations are documented in greater detail in Chapter 8, Sections A and J.

SIGNIFICANCE

These pre-launch activities are providing us and the Landsat-D Project Scientist with valuable information relative to what the remote sensing user community might expect from TM data. This experience will facilitate the planning of post-launch research activities to achieve the four major Landsat-D project objectives summarized in the BACKGROUND. Also, our discipline/user oriented inputs relative to the functional requirements of the LAS software system and user interface should result in improved processing capabilities for LAS users.

FUTURE EMPHASIS

The emphasis of future activities will include: (a) continued interaction with Information Extraction Division personnel to evaluate and refine LAS system and software requirements, (b) detailed processing and analysis of the TMS and ground truth data which has been collected, and (c) continued support of the Landsat-D Project Scientist in evaluating potential changes in mission parameters, etc.

PUBLICATIONS

Tucker, C. J., "Remote Sensing of Leaf Water Content in the Near Infrared," Remote Sensing of Environment, 1980 (in press)

Tucker, C. J., "Radiometric Resolution for Monitoring Vegetation: How Many Bits are Needed?" preprint of a manuscript submitted to International Journal of Remote Sensing, 1980.

Williams, D. L, and V. V. Salomonson, "Data Acquisition and Projected Applications of the Observations from Landsat-D." Proceedings of the ASP-ACSM Fall Convention, Sioux Falls, South Dakota, 1979, 14 pp.

Williams, D. L. and M. L. Stauffer, "What Can the Forest Community Expect from Landsat-D Thematic Mapper Data?" Proceedings of the Symposium on Remote Sensing of Natural Resources, University of Idaho, Moscow, Idaho, 1979.

COMPARISON OF U-2 AERIAL PHOTOGRAPHY WITH TM SIMULATOR AND LANDSAT-2 MSS COMPOSITE IMAGES

	U-2	TMS	MSS
DATE:	4/18/79	8/14/78	7/3/79
WAVELENGTH:	0.51 - 0.90 μm	0.52 - 0.60 μm 0.63 - 0.69 μm 0.76 - 0.90 μm	0.50 - 0.60 μm 0.60 - 0.70 μm 0.80 - 1.10 μm
APPROXIMATE GROUND RESOLUTION:	2 METERS	30 METERS	80 METERS

6 KILOMETERS

6 KILOMETERS

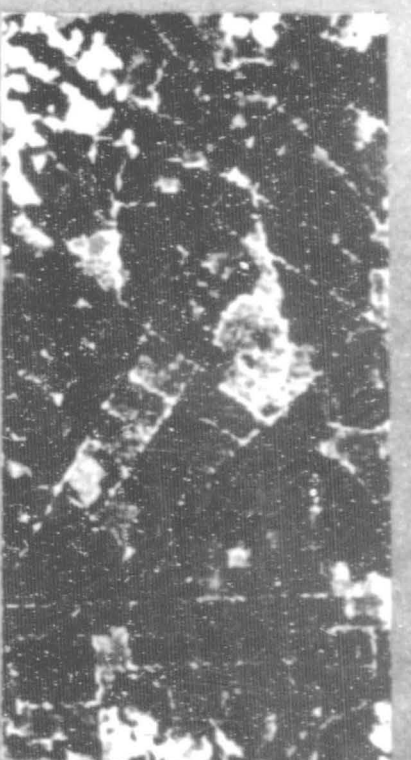

6 KILOMETERS

D60

B. MULTISPECTRAL LINEAR ARRAY SENSOR DEVELOPMENT

by

C. C. Schnetzler

OBJECTIVE

The objective of the program is to conceptually design a multispectral linear array (MLA) sensor for spacecraft flight in the mid-1980's. This sensor will provide new and unique Earth survey research capabilities beyond those possible with current sensor systems, and will be an engineering test of the new MLA technology.

BACKGROUND

Electromechanical scanners, such as the MSS on Landsat 1, 2, and 3, and the TM, which will fly on Landsat-D, are representative of NASA's present remote sensing capabilities from space platforms. However, these types of sensors have reach a plateau of development where any additional improvement in performance will be extremely costly. The next generation of satellite sensors will probably use linear arrays, each composed of a large number of solid state detectors in the push-broom mode, i.e., a mode where the forward motion of the satellite sweeps the array of detectors, which are oriented perpendicular to the ground track, across the scene. Advantages to such a mode include the elimination of complex mechanical scan mechanisms; increased geometric fidelity, both across track and between bands; and higher sensitivity due to longer dwell time of each detector. A clear disadvantage is the need for calibration of a much larger number of detectors.

Early in calendar year 1978 GSFC was asked by NASA Headquarters to work on a potential new start for an MLA sensor which would be ready for spaceflight by the mid 1980's.

ACCOMPLISHMENTS

Over 1979, the emphasis has been on defining the required sensor parameters from the scientific researchers' point of view and from this, developing a phase A systems specifications and design. On the science side, a Science Working Group, composed of remote sensing researchers in diverse fields, held three meetings to advise GSFC on desired specification. These systems specs were then presented at a MRS Workshop held in Colorado State University, attended by approximately 70 scientists. Input from this group was used to define the optimum sensor parameters for multidisciplinary use. Compared to the TM, the sensor is designed to provide improved temporal, spectral and spatial resolution. Across track pointing of up to $\pm 40^{\circ}$ will provide 1 to 2 day frequency of observation. Along track pointing of $\pm 60^{\circ}$ will allow atmospheric measurements to be made so that corrections can be made to the scene radiometry. Additionally, along track pointing will enable the requisition of stereo images. Spatial resolutions of the Sensor will be 15 meters with a swath width of 30 kms. Filter wheels over each of four silicon arrays will allow an inflight choice among five spectral bands per array. Bands as narrow as 20 nm can achieve NE$\Delta\rho$ of approximately 0.5%.

Two six month "proof-of-concept" studies were performed in 1979 - one on the utility of bi-directional measurement from a high pointing angle sensor and the other on techniques of atmospheric correction. The report on these studies is due at the end of January, 1980.

SIGNIFICANCE

A "new start" presentation was made by the study team to NASA Headquarters (Code E) in late summer, 1979. Although the decision was made not to proceed in 1980, the work done in 1978 and '79 will form the starting point for future deliberations about linear array sensors.

FUTURE EMPHASIS

No funding was received for continuing this sensor definition work in 1980.

PUBLICATIONS

"Multispectral Resource Sampler Advisory Group Meeting Summary Report of February 26, 1979 meeting." ORI report dated March, 1979.

"Multispectral Resource Sampler Workshop Summary Report." ORI dated June, 1979.

"MRS Literature Survey of Atmospheric Corrections." ORI report.

"MRS Literature Survey of Bidirectional Reflectance." ORI report.

"A Bibliography/Studies Related to Determination of Spatial Resolution Requirements For Optical Sensors." Texas A & M report dated August, 1979.

"Multispectral Resource Sampler: An Experimental Satellite Sensor For the Mid-1980's," Schnetzler, C.C. and L.L. Thompson, Proceeding SPIE Technical Symposium, Huntsville, AL, May 22-24, 1979, Vol. 183.

D-1

C. LINEAR ARRAY PUSHBROOM RADIOMETER DATA ANALYSIS

by

J. Irons and S. Wharton

OBJECTIVE

The main purpose of this effort was to evaluate and demonstrate the utility of data acquired by a linear array instrument for remote sensing applications.

BACKGROUND

The Earth Observations Systems Division, Code 940, of GSFC has designed and built a linear array radiometer. The instrument, christened LAPR for Linear Array Pushbroom Radiometer, was designed as an aircraft multispectral sensor for the remote sensing of earth resources. Instead of a scanning mirror, the LAPR employs linear arrays of photodiodes to view a swath perpendicular to the flight path. The radiometer was built with three Reticon arrays containing 512 silicon photodiodes each. A seperate set of optics focus radiant energy on each array, and these optics provide for a 60 degree total-field-of view, or "scan angle", across the flight path. Each photodiode has an instantaneous-field-of-view of 2.54 milliradians, and the photodiodes are sensitive to energy within the wavelength range of 450 to 900 nm. The optics were designed so that optical filters mounted in front of the arrays can be easily interchanged.

The LAPR acquires one channel of data per array. The continuous electric signal from each photodiode is sampled, quantized to eight-bit digital data (zero to 255 counts), and the digital data are recorded on magnetic tape aboard the aircraft. Thus, the LAPR generates three-band digital imagery.

LAPR data must undergo several preprocessing steps before analysis. First, the data from each photodiode are calibrated by a gain factor and a dark-level factor. The gain factors were derived from test data taken while the LAPR was mounted on an integrating sphere. Dark-level factors are computed from dark-level readings taken immediately preceeding and following data acquisition.

The data is also geometrically corrected for aircraft roll. A gyroscope was mounted on the platform aircraft and roll angle is recorded as header information for each scan line. The data is roll corrected by shifting pixels in the appropriate direction along each scan line.

The data are then corrected for channel misregistration. The optics for each array are not perfectly aligned, resulting in a slight geographic offset from channel to channel. Up to now, the channels have been visually registered using the interactive display capabilities of the Image-100 analysis system to shift the imagery a few pixels. A more accurate registration can

be achieved by resampling the data using ground control points.

RECENT ACCOMPLISHMENTS

The LAPR was flown over several study areas during 1979 in support of ongoing research conducted by the Earth Resources Branch. False color imagery and thematic maps were generated from the data acquired on several of the flights. Table 9C-1 lists information pertaining to these flights. The imagery and maps qualitatively demonstrate LAPR data utility. Vertical stripping due to raw data miscalibration is not visually evident in any of the imagery. Qualitative comparisons of the thematic maps to aerial photography indicate accurate delineations of land cover categories.

The calibration of the raw LAPR data was also investigated. Following the data acquisition flights, the instrument was again mounted on the integrating sphere and test data were acquired for several levels of radiance. The previously determined gain and dark level correction factors were applied to the test data and the calibrated test data were analyzed. Preliminary analyses showed that at a given radiance level the calibration did not produce equal digital values across the array. Either the correction factors never adequately calibrated the LAPR data, or the response of the photodiodes drifted over time.

SIGNIFICANCE

The LAPR provides the Earth Resources Branch with a flexible, readily available, aircraft multispectral sensor for remote sensing research. The ability to change spectral filters permits the evaluation and selection of optimum spectral bands for particular applications. The aircraft platform can be flown at different altitudes, at various times during the day, and on different dates. These capabilities allow research on the effects of resolution, sun angle, and season on remotely sensed data.

More importantly, the LAPR demonstrates linear array technology for remote sensing. The instrument can be used to simulate proposed spacecraft linear array systems such as the Multispectral Resource Sampler (MRS). Filters corresponding to spectral bands planned for the MRS can be mounted on the LAPR, and some of the problems and characteristics of MRS data can then be anticipated by the collection and analysis of LAPR data.

FUTURE EMPHASIS

(1) The LAPR will continue to acquire data in support of research projects conducted by the Earth Resources Branch. Data analyses will concentrate on an evaluation of calibration procedures and results.

(2) A new aircraft mount is under development for the LAPR. The mount will permit off-nadir pointing of the instrument in order to simulate the pointing capabilities proposed for the MRS.

(3) Division personnel will interact with Code 940 in the design of a new linear array radiometer. The new instrument is designed around four Westinghouse photodiode arrays. The radiometer will provide a higher signal-to-noise ratio, finer resolution, and one more data channel than the current LAPR.

TABLE 9C-1

LAPR FLIGHT CHARACTERISTICS

Supporting Project	Study Area Location	Flight Date	Flight Time	ALTITUDE (meters-above mean-datum)	Resolution at Nadir (m)	FILTER BANDWIDTHS (nm) Array 1	Array 2	Array 3
Surface Mine Monitoring	Clarion Co. Penn.	5/17/79	1200	3000	7.5	802.5-847.5	577.5-622.5	462.5-507.5
Census APT	Laurel, Prince Georges, Co. Maryland	8/17/79	1200	2900	7.2	802.5-847.5	577.5-622.5	537.5-582.5
Forestry	Cubmerland Co., Penn.	6/27/79	1000	2900	7.2	802.5-847.5	577.5-622.5	462.5-507.5

D-22

D. THE SPACEBORNE LASER RANGING SYSTEM

by

W.D. Kahn

OBJECTIVES

The Spaceborne Laser Ranging System is a proposed short pulse laser on board an orbiting spacecraft. It measures the distances between the spacecraft and many laser retroreflectors deployed on the Earth's surface. The precision of these range measurements is assumed to be + 2 cm.

It is the objective of this study to assess the Spaceborne Laser Ranging System's capability to detect and monitor very small crustal movements which are on the order of 0.3 to 0.5 cm/yr in central California. Furthermore, an orbiting pulsed laser system could be used to provide continuous monitoring of crustal deformation in California as well as many other areas of the world and has the potential to provide an almost real-time system for detecting percursory ground motions before large earthquakes.

BACKGROUND

The concept of the Spaceborne Laser Ranging System was developed as a technique for monitoring from space, frequently and over long time periods, the relative positions of a large number of geodetic reference points. The Spaceborne Laser Ranging System consists of an orbiting spacecraft carrying a pulsed laser ranging measuring system which measures the range between the spacecraft and laser retroreflector arrays on the ground. By distributing these retroreflectors over regions of seismic activity and crustal deformations associated with tectonic plate boundary motion, earthquake zones, and ground motion due to fluid withdrawal, mountain building or volcanic activity, this spaceborne technique conceptually would permit the monitoring of whole regions with a high density of points in a relatively short period of time, creating the impression of obtaining a geodetic "snapshot" of the area. Such measurement sets can be compared with other measurement sets obtained at appropriate intervals and the observed displacements used to develop regional maps of strain and strain-rate.

RECENT ACCOMPLISHMENTS

A series of simulations have been performed of a survey of the state of California using a Spaceborne Laser Ranging System. In the simulations, approximately 150 laser targets were distributed

over California at a separation of 50 km. The simulations provided estimates of the precision with which baseline distance can be determined in the presence of noise and bias of the laser system; perturbations of the spacecraft motion and errors in the refraction correction.

The orbit of the satellite is assumed to be circular at 1000 km and 50° inclination to the equator. A medium inclination orbit was chosen because it provides ground tracks across California in almost orthogonal directions (southwest to northeast and northwest to southeast). The distribution of satellite ground tracks obtained provided a strong geometric distribution of range measurements. In contrast, a polar orbit provides only north to south and south to north tracks and these provide strong geodetic ties in the north-south direction, but only weak control in the east-west direction.

The simulations have been conducted over survey intervals of 1, 3, and 6 days, respectively, assuming 50% cloud cover that for the 6 day observation period reduces the number of successfully observed tracks over the area from 36 to 18. For all the simulations, the data on the observed tracks are assumed to be taken at the rate of 10 pps with a noise of 2 cm and a bias of 0.3 cm. The effect of errors in the gravity field on the motion of the satellite were accounted for by adopting the GEM-10 covariance model of the gravity field derived from satellite tracking and surface gravity data. The effects of solar radiation pressure and air drag on the satellite were assumed to be in error by a constant percentage in the estimation of their effect on the solutions.

Figure 9D-1 shows the baseline precision as a function of the baseline length. This measure of precision for a 50 km baseline is about 0.3 cm and increases to 1 cm for a 1200 km baseline. For baseline lengths up to 300 km, the precision is primarily dependent on system noise, but for longer baselines, say from 400 km to 1200 km, the uncertainty in the geopotential becomes the dominant error source. For a system noise of 3 cm, the noise curve in Figure 9D-1 will be shifted upward by a factor of 1.5 for baselines less than 400 km and then the unadjusted parameters, predominantly the uncertainty in the Earth's gravity field, dominate the precision for longer baselines.

From the knowledge of the precision with which baseline determinations can be made, the elongation rate precision can be calculated. In Figure 9D-2 the elongation rate precision is given for a 50 km baseline as a function of the measurement program period T. For the calculation of elongation rate precision, a survey period T_S of six days was assumed and an interval between surveys, the resurvey period, T_R of 6, 14 and 30 days was chosen.

As can be seen from the figure, the Spaceborne Laser Ranging System has the capability of determining elongation rates to a precision of better than 1×10^{-8} strain per year over a 2½ to 3 year period T. Furthermore, an order of magnitude improvement in the elongation rate precision can be achieved over a five year period by making continuous measurements over about a week every other month. The figure also shows that little improvement in the elongation rate determinations is achieved by increasing the measurement frequency (i. ., decreasing the resurvey period T_R). This means power for the laser system can be conserved and thus the system's lifetime extended without degrading the measurement precision. Finally, Figure 9D-2 shows that elongation rate measurements to better than 1×10^{-9} per year may be possible within a decade or less of measurements.

SIGNIFICANCE

It is shown that the concept of a Spaceborne Laser Ranging System has the capability to (a) determine baselines to a precision of less than 1 cm over distances of up to 100 km; and (b) determine the elongation rate to a precision of better than 1 part in 10^8 per year during a period of 2 years. Such a system could provide a capability to observe the precursory geodetic motions believed to occur before large earthquakes. Indeed, established on a global scale, with survey areas around all major seismic zones, the Spaceborne Laser Ranging System could provide the first real probability for "capturing" a magnitude 7.5, and above, earthquake.

In addition, general geodetic survey work can be performed accurately and very rapidly with minimal incumbrance by the terrain.

FUTURE EMPHASIS

The future studies are to be expanded to determine the requirements for a global crustal monitoring system using a "free flyer." Such studies will include optimization of orbit attitude and inclination. Tracking geometry, data precision, sampling rates, and data processing techniques will be considered in arriving at a feasible mission for a "free flyer" to monitor crustal movements on a global scale.

REFERENCES AND PUBLICATIONS

Kahn, W.D., F.O. Vonbun, D.E. Smith, T.S. Englar, B.P. Gibbs, "Performance Analysis of the Spaceborne Laser Ranging System," NASA Technical Memorandum 80330, October 1979; to be published in Bulletin Geodesique).

Vonbun, F.O., W.D. Kahn, P.D. Argentiero and D.W. Koch, "Spaceborne Earth Applications Ranging System (SPEAR)." Journal of Spacecraft and Rockets, Vo. 14, No. 8, August 1977, pp. 492-495.

Smith, D.E., "Spaceborne Ranging System." Proceedings of the Ninth Geodesy/Solid Earth and Ocean Physics (GEOP) Research Conference. October 2-5, 1978; Department of Geodetic Science Report No. 280, The Ohio State University, pp. 59-64.

Smith, D.E., B.D. Tapley. "The Report From the Workshop on the Spaceborne Geodynamics Ranging System." IASOM TR 79-2 Institute for Advanced Study in Orbital Mechanics, The University of Texas at Austin, Austin, Texas, March 1979.

Mueller, I.I., B.H.W. Van Gelder and M. Kumar. "Error Analysis for the Proposed Close Grid Geodynamic Satellite Measurement System (CLOGEOS)." Department of Geodetic Science Report No. 230, The Ohio State University, September 1975.

Fitzmaurice, M.W. "NASA Ground Based and Space-Based Laser Systems." NASA Technical Report 1149, January 1978.

Cohen, S.C. and G.R. Cook. "Determining Crustal Strain Rates with a Spaceborne Geodynamics Ranging System Data; Manuscripta Geodetica, Vol. 4 (1979), 245-260.

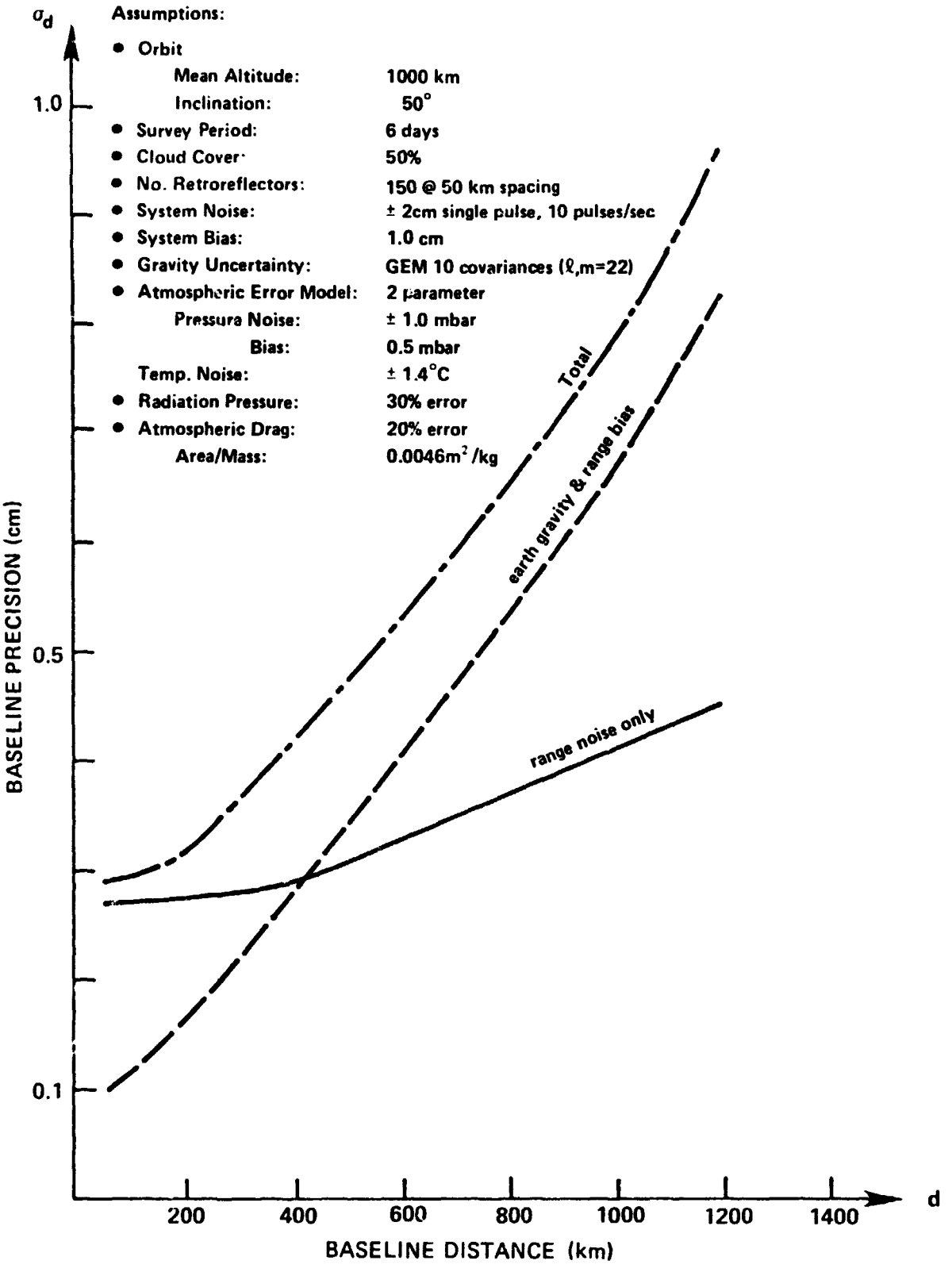

Figure 9D-1 . Baseline Precision vs Baseline Distance

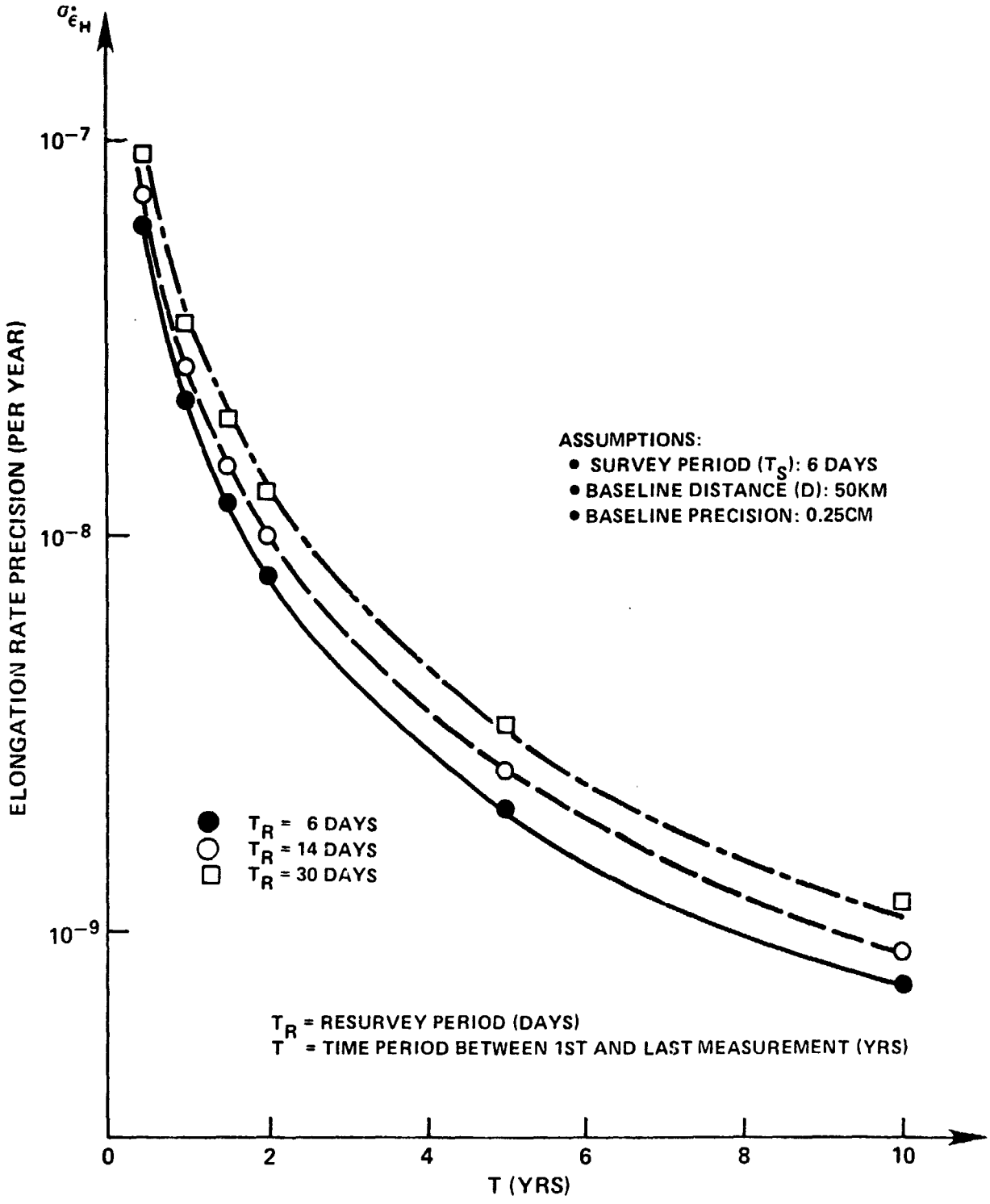

Figure 9D-2. Elongation Rate Precision vs Total Measurement Periods.

ACRONYMS AND ABBREVIATIONS

AGIS	Automated Geographic Information System
AgRISTARS	Agriculture and Resources Inventory Surveys Through Aerospace Remote Sensing
AGU	American Geophysical Union
ALTKAL	Linear Filter for Altimeter Data
AMI	Agricultural Management Information
AO	Announcement of Opportunity
APL	Applied Physics Laboratory
APT	Applications Pilot Test
ARC	Appalachian Regional Commission
ARIES	Astronomical Radio Interferometric Earth Survey
ARIMA	Auto Regressive Integrated Moving Average
ASCS	Agricultural Stabilization and Conservation Service
ASVT	Applications Systems Verification Test
ATS	Applications Technology Satellite
BARC	Beltsville Agriculture Research Center
BE-C	Beacon Explorer Satellite
BMD	Biomedical Computer Program
CCT	Computer Compatible Tape
CDA	Colorado Department of Agriculture
CRIB	Computer Resource Information Bank
CSU	Colorado State University
DCP	Data Collection Platform
DEM	Digital Elevation Model
DET	Discipline Experiment Teams
DIRS	Digital Image Rectification System
DSN	Deep Space Network
ECOOE	East Coast Onshore-Offshore Experiment
EMSL	Environmental Monitoring and Support Laboratory
EPA	Environmental Protection Agency
ERODYN	Error Analysis Companion to GEODYN
ESAD	Earth Survey Applications Division
ESRI	Environmental Systems Research Institute
FCC	False Color Composite
FOV	Field of View
FRMS	Federation of Rocky Mountain States
GEM	Goddard Earth Model
GEODYN	Geodynamics Orbit Determination and Parameter Estimation Program
GIS	Geographic Information System
GM	Gravitational Mass of the Earth
GOES	Geosynchronous Operational Environmental Satellite
GRAVSAT	Dedicated Gravity Field Satellite
GSFC	Goddard Space Flight Center

ha	Hectare
HCMM	Heat Capacity Mapping Mission
HO	Haystack Observatory
IAU	International Astronomical Union
IBIS	Image Based Information System
IFOV	Instantaneous Field of View
ILS	International Latitude Service
IPMS	International Polar Motion Service
IR	Infrared
ITI	Information Theory Inference
JHU	Johns Hopkins University
JPL	Jet Propulsion Laboratory
kg	kilogram
LAGEOS	Laser Geodynamics Satellite
LAI	Leaf Area Index
LAPR	Linear Array Pushbroom Radiometer
LAS	Landsat-D Assessment System
LED	Laser Earth Dynamics
LURE	Lunar Ranging Experiment
MA	Moving Average
MAGSAT	Magnetic Field Satellite
MERIT	Monitoring of Earth Rotation and Intercomparison of Techniques
MLA	Multispectral Linear Array
Moho	Mohorovcic Discontinuity
MRS	Multispectral Resource Sampler
MSDS	Multispectral Scanner and Data System
MSS	Multispectral Scanner
mybp	million years before present
ND	Normalized Difference
NGS	National Geodetic Survey
nm	nanometer
NRAO	National Radio Astronomy Observatory
nsec	nanosecond
OVRO	Owens Valley Radio Observatory
PCA	Point of Closest Approach
PGAP	Probability of Gap
PGS	Preliminary Gravity Field Solution
PHIT	Probability of Hit
POGO	Polar Orbiting Geophysical Observatory
PPME	Pacific Plate Motion Experiment
PRG	Perennial Ryegrass
RASS	Rock Analysis Storage System
RRA	Resident Research Associate
r^2	coefficient of determination
SACC	Science and Applications Computing Center
SAFE	San Andreas Fault Experiment

SAO	Smithsonian Astrophysical Observatory
SAR	Synthetic Aperature Radar
SAS	Statistical Analysis System
SEA	Science and Education Administration
SLR	Satellite Laser Ranging
SMMR	Scanning Multifrequency Microwave Radiometer
SMSA	Standard Metropolitan Statistical Area
SOLVE	Computer Program for Gravity Field Solutions
SOV	Sources of Variation
SST	Satellite-to-Satellite Tracking
STALAS	Stationary Laser Tracking Station, Greenbelt, MD.
SWIR	Short Wave Infrared
Ta	Ambient Air Temperature
Tc	Crop Canopy Temperature
TM	Thematic Mapper
TMS	Thematic Mapper Simulator
USDA	U.S. Department of Agriculture
USGS	U.S. Geological Survey
UV	Ultraviolet
VEPCO	Virginia Electric Power Company
VI	Vegetative Index
VLBI	Very Long Baseline Interferometer
WATSTORE	Water Resources Storage System